UNIVERSIDADE DE LISBOA
INSTITUTO SUPERIOR TÉCNICO

Modeling water fate in different agro-ecosystems for improving land management practices

Lucian Simionesei

Supervisor: Doctor Ramiro Joaquim de Jesus Neves
Co-Supervisor: Doctor Tiago Cunha Brito Ramos

Thesis approved in public session to obtain the PhD Degree in Environmental Engineering

Jury final classification: Pass with Distinction

2024

UNIVERSIDADE DE LISBOA

INSTITUTO SUPERIOR TÉCNICO

Modeling water fate in different agro-ecosystems for improving land management practices

Lucian Simionesei

Supervisor: Doctor Ramiro Joaquim de Jesus Neves

Co-Supervisor: Doctor Tiago Cunha Brito Ramos

Thesis approved in public session to obtain the PhD Degree in Environmental Engineering

Jury final classification: Pass with Distinction

Jury
Chairperson: Doctor José Manuel de Saldanha Gonçalves Matos, Instituto Superior Técnico, Universidade de Lisboa
Members of the Committee:
Doctor Ramiro Joaquim de Jesus Neves, Instituto Superior Técnico, Universidade de Lisboa
Doctor Luís Leopoldo de Sousa e Silva, Escola de Ciências e Tecnologia, Universidade de Évora
Doctor José Manuel Monteiro Gonçalves, Escola Superior Agrária de Coimbra, Instituto Politécnico de Coimbra
Doctor Paula Cristina Santana Paredes, Instituto Superior de Agronomia, Universidade de Lisboa

2024

ABSTRACT

This thesis addresses the global concern of sustainable water management in agriculture, particularly in Mediterranean agro-ecosystems, where water scarcity is a growing issue due to population growth and climate change. The primary focus was the development of a Decision Support System (DSS) called IrrigaSys, based on the MOHID-Land model, to optimize irrigation water management at the plot scale. The key objectives were to create a user-friendly DSS framework, calibrate the MOHID-Land model for various crops, assess the impact of remote sensing data assimilation, and demonstrate the DSS's effectiveness in improving irrigation schedules and water use efficiency.

The DSS integrates various components, including meteorological data, the MOHID-Land model for soil water balance, and a user-friendly interface, accessible through web and mobile platforms. It also incorporates Sentinel-2 imagery of Normalized Difference Vegetation Index (NDVI). IrrigaSys has been successfully deployed in collaboration with stakeholders in southern Portugal, supporting over 100 plots for five years.

The calibration of the MOHID-Land model for maize, pasture, and vineyard crops demonstrated its accuracy in simulating soil water dynamics and crop growth. Additionally, the thesis explored the use of remote sensing data, to enhance model accuracy. While remote sensing data assimilation improves model estimates, it also highlights the importance of complementing this information with local crop datasets. This thesis introduces a novel approach to optimize irrigation management using the MOHID Land Irrigation Module and concludes with a chapter that conducts a post-evaluation of IrrigaSys employing a multicriteria analysis (MCA) approach.

In summary, this research contributes significantly to sustainable water management in agriculture. The development of IrrigaSys, the calibration of the MOHID-Land model, and the utilization of remote sensing data offer valuable tools and insights for enhanced irrigation practices. This integrated approach empowers farmers, improves water productivity, and advances informed decision-making for water resource management, providing a pathway for more sustainable and efficient agricultural practices.

Keywords: Irrigation scheduling, MOHID-Land, Decision support system, Soil water balance, remote sensing

RESUMO

Esta tese tem com tema a preocupação global da gestão sustentável da água na agricultura, particularmente em agro-ecossistemas mediterrânicos, onde a escassez de água é uma questão crescente devido ao crescimento populacional e às mudanças climáticas. O foco principal foi o desenvolvimento de um Sistema de Suporte à Decisão (DSS), chamado IrrigaSys, com base no modelo MOHID-Land, para otimizar a gestão da água de rega à escala da parcela. Os principais objetivos foram criar uma estrutura DSS fácil de utilizar, calibrar o modelo MOHID-Land para várias culturas, avaliar o impacto de dados de deteção remota, e demonstrar a eficiência do DSS na melhoria da gestão de rega e na eficiência do uso da água.

O DSS integra vários componentes, incluindo dados meteorológicos, o modelo MOHID-Land para o balanço de água no solo e uma interface de utilizador amigável, acessível através de plataformas web e móveis. Também incorpora imagens do Índice de Vegetação(NDVI).

A calibração do modelo MOHID-Land para culturas de milho, pastagem e vinha demonstrou a sua precisão na simulação da dinâmica da água no solo e no crescimento das culturas. Além disso, a tese explorou o uso da deteção remota, para melhorar a precisão do modelo. A tese introduz uma nova abordagem para otimizar a gestão da rega usando o módulo de rega MOHID Land e conclui com um capitulo que faz uma avaliação ao IrrigaSys utilizando uma analise multicriterial (MCA).

Em resumo, esta tese contribui significativamente para a gestão sustentável da água na agricultura. O desenvolvimento do IrrigaSys, a calibração do modelo MOHID-Land e a utilização de dados de deteção remota oferecem ferramentas e conhecimentos valiosos para práticas de rega. Esta abordagem integrada capacita os agricultores, melhora a produtividade da água e promove a tomada de decisões informadas para a gestão dos recursos hídricos, proporcionando um caminho para práticas agrícolas mais sustentáveis e eficientes.

Palavras-chave: programação da rega, MOHID-Land, Sistemas de Apoio à Decisão, Balanço de Água no Solo, Deteção Remota.

ACKNOWLEDGMENTS

I would like to express my heartfelt gratitude to several individuals and groups who have been instrumental in the successful completion of this journey. Their unwavering support, guidance, and encouragement have been invaluable to me.

First and foremost, I extend my deepest appreciation to my supervisor, Dr. Ramiro Neves. Your insightful guidance, constructive feedback, and boundless knowledge have been pivotal in shaping this research. Your mentorship has not only enriched my academic understanding but also inspired my personal growth.

I am also indebted to my co-supervisor, Tiago Ramos, for his valuable contributions and support throughout this endeavor. Your expertise and collaborative spirit have played a significant role in the development of this work.

I extend my thanks to my colleague Ana Oliveira, her tenacity and determination were an inspiration to me. And Jorge Palma for his programming support that has added depth and diversity to my research journey.

To Hanaa Darouich, I extend my gratitude for her expertise and contributions, which greatly assisted me in concluding this thesis.

To my colleagues and ex-colleagues from Maretec, including Debora, Sara, Ligia, Marcos, Gonçalo, Paulo, Nuno, Vania, Cristina, Andreia, Carina, Hilda, Claudia, David, Eduardo, and countless others, I am truly grateful for the camaraderie, exchange of ideas, and shared experiences that have enriched my professional life.

A special note of gratitude goes to ARBVS, and particularly to José Nuncio and Margarida Cunha, for their valuable insights and contributions that have shaped the direction of my research.

To my family, whose unwavering love and support have been my foundation throughout this journey, I extend my deepest gratitude. Your belief in me has been my driving force. To my boyfriend, your patience, understanding, and encouragement have been a constant source of strength. Your presence in my life has made this journey all the more meaningful.

Last but not least, I want to acknowledge all my friends who have stood by me, offering laughter, companionship, and solace. Your presence has been a reminder of the importance of balance and connection.

In conclusion, the completion of this endeavor would not have been possible without the collective support of these incredible individuals and groups. My heartfelt thanks go out to

each and every one of you for your contributions to this journey of growth, learning, and accomplishment.

Thank You, Obrigado, Mulțumesc!

Contents

List of Figures

List of tables

1. Introduction

1.1 Background

The issue of freshwater use in agriculture has become a critical global concern due to the significant impact it has on the world's water resources. With agriculture being the largest user of freshwater, consuming more than two-thirds of total withdrawals (Gan et al., 2013), the increasing demand for food production, and a rapidly growing population, there are mounting challenges to meeting these demands sustainably.

An estimated 310 million hectares (ha) worldwide are irrigated compared to around 100 million ha in 1950 (Salmon et al., 2015). Meanwhile, agricultural production has grown between 2.5 and 3 times, thanks to significant increase in the yield of major crops. During that period, the world population increased by about the same factor, from 2.5 billion in 1950 to about 8 billion in 2023 and is expected to keep growing to 9.5 billion by 2050 ("FAO's Director-General on How to Feed the World in 2050," 2009).

The increase of evapotranspiration (ET) corresponds to an increase of the water demand of crops, can lead to an increase in the amount of freshwater that needs to be withdrawn for agricultural purposes in certain climates. As a result, farmers may have to use more water resources to irrigate their crops, which can put pressure on freshwater supplies, particularly in regions that are already water-stressed (Hatfield et al., 2011). At the same time the increase in temperatures and decrease in rainfall, caused by climate change, will make water a scarcer resource (Farré and Faci, 2009). Competition for water from different types of users, not related to agriculture, is also on the rise. This is even more obvious in arid and semi-arid areas.

In southern Europe, for example, increasing water demand and withdrawals have been building up the pressure on freshwater resources, with agriculture accounting for more than half of the total water abstraction, rising to more than 80% in some regions (Whytock, 2020). Aridity and droughts are becoming increasingly common in Southern Europe, which can have serious consequences for both the environment and the economy. To address this issue, there is a need for more sustainable water management practices, including the adoption of water-efficient irrigation systems and the promotion of more efficient use of water in agriculture. Additionally, policy measures such as water pricing, water rights allocation, and water-use restrictions may also help to conserve water resources and ensure their availability for future generations (Dige et al., 2013).

Irrigation plays a decisive role in increasing agricultural productivity and production stability in southern Europe, but erroneous irrigation practices drive unnecessary water

consumption and promote environmental degradation in regions ecologically sensitive to nutrients concentrations as well as soil degradation due to erosion and organic matter loss. Aware of these problems, the European Commission has given top priority to the protection of natural resources in the context of the Europe 2020 Strategy and Horizon Europe Strategy, including the sustainability of water resources (Comission, European, n.d.). Consequently, there has been a redirection of funding, moving away from stimulating production towards promoting Best Management Practices (BMP). In line with these strategic objectives, countries in southern Europe have implemented specific policy instruments aimed at maximizing the efficiency and effectiveness of irrigation water utilization. Taking Portugal as an example, particular policy measures like *Portaria n.502015*, n.d., and *Portaria n.542023, Measure 7.5* "Efficient Water Use", mandates the adoption of pressurized irrigation systems, the periodic inspection of irrigation systems, the precise quantification of irrigation pulses, and the definition of improved irrigation schedules resulting from the integration of data from meteorological stations, on soil water content status and crop water needs, i.e., based on the computation of the soil water balance at the plot scale. In mainland Portugal, individuals and entities engaged in agriculture may access economic support through adherence to specific eligibility criteria. Commitments, lasting five years, necessitate compliance of the measures enumerated before, to avoid administrative penalties. Optional commitments offer increased support for reused water usage. Support takes the form of annual non-repayable subsidies, contingent on varying factors. While accumulation of support is limited under certain interventions, non-compliance or irregularities may result in reductions or exclusions from support.

Better management tools are also required for integrating different physical and biochemical processes and simulating the different soil-water-atmosphere transfer systems across scales. The MOHID-Land model is a process-based distributed model developed at IST (Instituto Superior Técnico) (www.mohid.com), with the capability of simulating soil water dynamics, solute transport, and plant development at different scales (Brito et al., 2015, Epelde et al., 2016, Simionesei et al., 2016), being well suited to support irrigation optimization considering soil water moisture, but also crop development.

1.2 Context

IrrigaSys emerged from a long collaboration between MARETEC (Marine Environment and Technology Center) and the Water Irrigation Association (ARBVS). This collaboration began in 2009 with a research project called Aquapath-Soil (2009 – 2012). The aim of this

project was to provide support services for irrigation, utilizing satellite images, hydrological models, and meteorological data. Users could observe the project results through the website (http://www.agro-evapo.eu), accessing maps of Leaf Area Index (LAI) and animated maps of Actual Evapotranspiration (ET_a), or receive SMS notifications throughout the period with meteorological information and actual evapotranspiration data.

ET_a maps were generated by the MOHID LAND model and represented the evapotranspiration accumulated weekly throughout the growing period of maize, using LAI as input. Two models, SWAT and MOHID LAND, were used to calculate plant growth, actual evapotranspiration, and soil moisture by explicitly accounting for the water balance of the soil-plant-atmosphere system. The information provided in the SMS messages was obtained from the SWAT model running in forecast mode using meteorological data from the previous week and forecasts for the next week. The weather data included precipitation, temperature, relative humidity, wind speed, and solar radiation from the closest weather station to each field.

Continuing the Aquapath-Soil project, a partnership between ARBVS, DEIMOS, and MARETEC (IST) initiated the MyFarm (2012 – 2015) project effectively in 2012. Within this project, a remote irrigation support service was provided using prediction models and remote production control to approximately 50 farmers. These farmers received irrigation advice via SMS and satellite images (NDVI maps), covering about 120 plots (pivots and covers).

In 2013, MARETEC participated in a new research project called FIGARO (2013 – 2016). FIGARO, or "Flexible and Precision Irrigation Platform to Improve Farm Scale Water Productivity," was a European-wide research project co-funded by the European Commission under the 7th Framework Programme (FP7) for Research and Technological Development. FIGARO aimed to significantly reduce the use of fresh water on the farm level by developing a cost-effective precision irrigation management platform. The European-wide consortium developed a holistic and structured precision irrigation platform, offering farmers a flexible, crop-oriented management tool with a Decision Support System (DSS) module to optimize irrigation. The platform included comprehensive systems such as decision support systems, simulation and optimization models, user-friendly interface, multiple precision-technology sensors, as well as irrigation monitoring hardware and controls. While the platform was never implemented at full scale, it served as a model for IrrigaSys.

1.3 Working hypothesis

The hypothesis of this thesis is that irrigation water management at the plot scale can be improved using a process-based physical model with assimilation of data from external sources (e.g., remote sensing). Process-based physical models are complex tools, requiring well defined parameters to produce reliable estimates of the soil water balance. These include soil hydraulic parameters, crop growth parameters, and the inputs of the weather variables and crop coefficients needed for defining crop water requirements. Usually, farmers can provide little information about the characteristics of their plots for a correct implementation of process-based physical models. The recent technological advances at different levels (e.g., proximal and remote sensors) offer alternatives to such limitations. Therefore, this thesis aims to answer the following questions:

1. Can a process-based physical model like MOHID-Land be used for irrigation water management?
2. Can a decision support system (DSS) function with the MOHID-Land model as its core system?
3. Can remote sensing products be used for scaling up the DSS to plots with limited data availability?

1.4 Objectives for the thesis

The main objective of this thesis is to create a tool that will help farmers to improve water use efficiency at the plot scale.

Irrigation is essential for assuring agriculture productivity and enhancing farmers' economic competitiveness in the Mediterranean climate region. Inefficient practices often lead to soil salinization/sodification, nutrient leaching, runoff, and soil erosion, which impacts need to be mitigated. This thesis aims to develop a decision support system (DSS) for irrigation water management of annual and perennial crops in Mediterranean agro-ecosystem, contributing to the decision making process by optimizing irrigation schedules.

The specific objectives are:

- to develop a DSS built on the framework of the MOHID-Land model for improving irrigation water management at the plot scale.
- to calibrate the MOHID Land model for simulating soil water dynamics and crop growth in annual (pasture, maize) and perennial (grapevine) crops.

- to assess the impact of assimilation of leaf area index and crop coefficient data derived from remote sensing imagery on model simulations of soil water dynamics and crop growth.
- to demonstrate the capability of the MOHID-Land model in optimizing irrigation schedules, and improving irrigation water use and crop water productivity at the plot scale.
- to assess the influence of the DSS on the evolution of crop water use and irrigation scheduling within the Sorraia Valley irrigation district during 5 years of implementation.

1.5 Thesis structure

The thesis presents the following structure:

Chapter 1 - The introduction chapter presents the water issue around the world with a focus to Portugal. The chapter ends with the motivations for this work.

Chapter 2 - The bibliographic revision chapter, the main papers and books published on the subject are reviewed. The chapter addresses several topics such as decision support systems, and process-based models.

Chapter 3 - Presents the IrrigaSys DSS. This chapter further discusses the main strengths and limitations of IrrigaSys, with the latter being associated with difficulties in providing reliable estimates for all field plots based on limited data.

Chapter 4 - Describes MOHID-Land model calibration/validation procedures and results for three case studies: maize, pasture, and grapevine.

Chapter 5 – Shows the use of remote sense data as a way to improve the quality of the DSS, especially in the areas where other types of data cannot be collected.

Chapter 6 – Irrigation Scheduling chapter explains the MOHID Land Irrigation Module and highlighting its capabilities and functionalities.

Chapter 7 – Assesses, using multicriteria analysis, how farmers' performance compares with an optimized irrigation schedule provided by IrrigaSys

Chapter 8 – General Conclusions

1.6 Publications

Articles published in scientific magazines during the period of the thesis (2017-2023)

Modeling soil water dynamics and pasture growth in the Montado ecosystem using MOHID land
L Simionesei, TB Ramos, AR Oliveira, M Jongen, H Darouich, K Weber, V Proença, T Domingos, R Neves
Water 10 (4), 489

2018

This article is assessing MOHID-Land model's efficacy in simulating soil water dynamics and pasture growth in southern Portugal. The candidate contributed to setting up the model and was responsible for running the simulations. He also conducted the analysis of the results and wrote the paper.

Assessing the impact of LAI data assimilation on simulations of the soil water balance and maize development using MOHID-Land
TB Ramos, L Simionesei, AR Oliveira, H Darouich, R Neves
Water 10 (10), 1367

2018

This article is assessing the impact of Landsat 8-derived leaf area index (LAI) assimilation on MOHID-Land's simulations of soil water balance and maize state variables. The candidate contributed to setting up the model and was responsible for running the simulations. The candidate participated in the field experiment and processed the data. Additionally, he conducted the analysis of the results and contributed to the writing of the paper.

IrrigaSys: A web-based irrigation decision support system based on open source data and technology
L Simionesei, TB Ramos, J Palma, AR Oliveira, R Neves
Computers and Electronics in Agriculture 178, 105822

2020

This article is describing IrrigaSys, a plot-scale irrigation water management DSS utilizing online, open-source tools and meteorological data for soil water balance computation and irrigation scheduling. The candidate conceptualized the paper. He also contributed to setting up the model. Additionally, the candidate participated in the software development. He conducted the analysis of the results and wrote the paper.

Exploring the Use of Vegetation Indices for Validating Crop Transpiration Fluxes Computed with the MOHID-Land Model. Application to Vineyard
TB Ramos, L Simionesei, AR Oliveira, R Neves, H Darouich
Agronomy 11 (6), 1228

2021

This article is showing the validation of soil water balance simulations in an irrigated vineyard using MOHID-Land and Sentinel-2 NDVI data to enhance irrigation decision support. The candidate contributed to setting up the model and was responsible for running the simulations. He also participated in image acquisition. Additionally, the candidate conducted the analysis of the results.

Assessing the Impact of IrrigaSys Decision Support System on Farmers' Irrigation Practices in Southern Portugal: A Post Evaluation Study

H Darouich, L Simionesei, AR Oliveira, R Neves, TB Ramos

Agronomy 14 (1), 66

2023

This article is doing an postevaluation of farmer adherence to IrrigaSys DSS for irrigation scheduling in Southern Portugal using multicriteria analysis, highlighting its effectiveness in water conservation and economic returns over six years. The candidate contributed to data collection and software development. He also conducted the validation and analysis of the results. Additionally, the candidate contributed to writing the paper.

2. State of Art

This chapter aims to give a brief description and definition of models and decision support systems.

2.1 Models – general description

Models are defined as a usually miniature representation of something, a system of postulates, data, and inferences presented as a mathematical description of an entity or state of affairs (climate model), an example for imitation or emulation, or a description or analogy used to help visualize something (such as an atom) that cannot be directly observed. These are all definitions of how a model can be defined in just a few words. The word will be used during this thesis mostly with the definition of a representation of the natural world, a system of postulates, data, and inferences presented as a mathematical description of an entity or state of affairs. In our case the system we are dealing with is the soil-water-atmosphere nexus.

Simulation is a valuable method for comprehending diverse real and conceptual systems, offering insights into their inner workings. By creating computer programs that mimic the key aspects of a system, simulation models can take input data, run the underlying software, and generate output data for analysis. Simulation is an important tool that is expected to experience further growth in the future. It will continue to aid in the understanding of intricate human, human-environmental, and natural systems.

A **mathematical model** is a mathematical representation of reality, an abstract, simplified construct related to a part of reality and created for a particular purpose (Bender, 2000). As a contrast to a physical model that is a tangible representation or simulation of a system or phenomenon in the physical world. It is based on equations whose forms represent the qualitative behavior of the flows and storage and the parameters that dictate the quantitative behavior. Physical models have been largely replaced by mathematical ones, with the increase in the computers usage. They are cheaper to use and more flexible.

Irrigation scheduling models are used to determine the optimal timing and amount of water required for agricultural crops. These models take into account various factors such as weather conditions, soil moisture levels, crop type, and evapotranspiration rates.

Pereira et al. (2020) defines two types of irrigation scheduling models: water balance models and mechanistic soil water. Water balance models operate by solving the principle of mass conservation within a specified time interval, typically a day. The daily soil water balance is applied to the entire root zone. These models are not very demanding in terms of parameterization. When correctly calibrated, they offer high accuracy and are user-friendly for

irrigation scheduling. When coupled with or integrated into yield-water functions, these models can make predictions regarding crop yield based on water availability.

The daily soil water balance (Allen et al., 1998) applied to the entire root zone may be expressed by computing the soil water depletion at the end of every day ($D_{r,t}$, mm), which is given as:

$$D_{r,t} = D_{r,t-1} - (P_t - RO_t) - I_t - CR_t + ET_{a,t} + DP_t \quad \text{Equation 1}$$

where $D_{r,t-1}$ is the root zone depletion at the end of previous day t-1 (mm), P_t is precipitation (mm), RO_t is runoff (mm), I_t is the net irrigation depth (mm), CR_t is capillary rise from the shallow groundwater table (mm), $ET_{a,t}$ is the actual crop evapotranspiration (mm), and DP_t is deep percolation through the bottom of the root zone (mm), with all terms referring to day i.

Solving for the water balance Equation 1 necessitates having data on soil water content or the ability to estimate it from observed soil matric potential. These inputs are crucial for calculating the root zone depletion (Dr) on a daily basis. To facilitate this computation, a specialized algorithm is required, one that leverages knowledge of soil hydraulic properties, as well as information on field capacity (θ_{FC}, $m^3\,m^{-3}$) and wilting point (θ_{WP}, $m^3\,m^{-3}$) across various soil layers within the entire root zone.

Precipitation data is obtained through meteorological observations, while irrigation is artificially controlled and measurable. Estimating values for runoff (RO), deep percolation (DP), and capillary rise (CR) is not straightforward and necessitates the use of specific algorithms, as discussed by Liu et al. (2006) and Allen et al. (1998).

Deep percolation (DP) is considered to be the water lost after exceeding field capacity in the root zone following heavy rain or irrigation. The extent of water movement through capillary rise (CR) from the water table to the root zone relies on various factors, including soil composition, the depth of the water table, and the moisture level within the root zone. Typically, capillary rise is negligible when the water table lies more than approximately 1 meter beneath the lower boundary of the root zone. CR can be computed from parametric equations as a function of the water table depth, water content of the root zone, root density and soil characteristics (Liu et al., 2006). Runoff from the surface during precipitation can be estimated using standard procedures from hydrological texts.

Runoff, deep percolation and capillary rise cannot be just estimated when an accurate soil water balance is to be performed. Therefore, it is imperative to employ appropriate

computational methods. Actual evapotranspiration is estimated using FAO56 method (Allen et al., 1998) in most of the soil water balance models in use today.

$$ET_a = K_s K_c ET_0 \quad \text{Equation 2}$$

where K_S is the daily estimated value of stress coefficient, K_C is the crop coefficient and ET_0 is the reference evapotranspiration (mm). ET_0 is estimated by Penman–Monteith method:

$$ET_0 = \frac{0.408\Delta(R_n - G) + \gamma \frac{900}{T+273} u_2 (e_s - e_a)}{\Delta + \gamma(1 + 0.34u_2)} \quad \text{Equation 3}$$

where Δ represents the slope of the saturation vapor pressure-temperature relationship at mean air temperature (kPa $°C^{-1}$), γ is the psychometric constant (kPa $°C^{-1}$), T is mean daily air temperature (°C), R_n-G is the net balance of energy available at the surface (MJ m^{-2} d^{-1}), u_2 is wind speed (m s^{-1}), with measurements at 2 m height, (e_s-e_a) represents the vapor pressure deficit of air at the reference (weather measurement) height [kPa] .

Over the years, several soil water balance models have been developed, including AquaCrop (Raes et al., 2009), CROPWAT (Smith, 1989), ISAREG (Teixeira and Pereira, 1992), SIMDualKc (Rosa et al., 2012), DAISY (Boegh et al., 2009), SWB (Inthavong et al., 2011), WISE(Andales et al., 2014) etc..

In contrast, mechanistic models explicitly consider the time variable and compute water fluxes within and across the boundaries of the soil control volume. Mechanistic models are more demanding in terms of data requirements and utilize mechanistic approaches to replicate soil water processes. They often incorporate mechanistic sub-models to simulate aspects such as plant growth, crop yield prediction under the influence of various environmental factors, and the assessment of salt, chemical, and pollutant transport that can affect agricultural water usage and sustainability. Mechanistic methods for analyzing soil water balance typically employ the computation of variably saturated water movement, a process that is characterized by Richards' equation. The unsaturated soil hydraulic properties are often described with the van Genuchten-Mualem functional relationship (van Genuchten, 1980). When solving Richards' equation, various formulations can be used to specify boundary conditions. The upper boundary condition is established based on crop evapotranspiration flux and can be calculated using either the Penman-Monteith equation or the K_c-ET_0, FAO56 method, which involves the use of single or dual K_c values. These kinds of models often partition of actual evapotranspiration with reference to leaf area index (LAI) and they are also able to accurately compute percolation, capillary rise, and run-off. A common approach is coupling of these models with crop growth and yield models. One drawback of these models is that they can be challenging to

parameterize. There are several mechanistic models used as irrigation scheduling models such as HYDRUS-1D (Šimůnek and Hopmans, 2009), SWAP (Vazifedoust et al., 2008), SWB-2D (Annandale et al., 2003), RZWQM2 (Hanson et al., 1999). These models have in common the use of Richards equation, but they differ in how they handle upper boundary conditions. In some cases, crop evapotranspiration is calculated using Penman-Monteith equation, as in the case of SWAP. HYDRUS, on the other hand, uses the K_c-ET_0 approach from FAO56. Sometimes these models are integrated with crop growth and yield models, as seen in the case of SWAP and EPIC (Xu et al., 2013).

2.2 Decision Support System

2.2.1 Introduction

A decision support system (DSS) is generally defined as a computer-based tool or software that helps individuals or organizations make decisions by analyzing data and presenting information in a way that facilitates decision-making. DSSs are designed to assist with complex decision-making tasks that require analyzing large amounts of data from multiple sources, considering various factors and constraints, and weighing different options. These systems can be used in a variety of fields, including finance, healthcare, marketing, and operations management.

2.2.2 DSS application for managing irrigation

2.2.2.1 DSS structure

A DSS typically consists of four components: a database, a model/software, a user interface, and the output data.

The database component stores and manages the data that will be used in the decision-making process. That usually includes the input data like information about the soil, physical, chemical, or hydrologic characteristics. The details of information can take into account the spatial variability, or the vertical differences between soil's horizons. At a field/farm scale is provided by the farmer while at the regional/national scale it can come from a national database (eg. https://projects.iniav.pt/infosolo/) or continental one (eg. https://esdac.jrc.ec.europa.eu/content/europ.ean-soil-database-v20-vector-and-attribute-data). Information about crops is also included in those databases. This information is used to simulate growth, water requirements, and yield. The crops that are economically important, have been better studied and we can find easily information for different models and approaches. Another component of the database is the weather data. This data comes usually

at a daily timescale. Again, according to the spatial scale, we have different sources of information, meteorological stations at a farm/plot scale and national forecast systems at a regional scale.

The database is also where model simulation results are stored. Information like when and how much to irrigate, information about the soil and plant status, etc.

The model/software component includes the mathematical and analytical models that the system uses to analyze the data. There are several models to simulate crop growth and to estimate crop evapotranspiration. Rinaldi and He (2014) separate these models into three categories, depending on the hierarchy of the process and the scales involved: a) carbon- b) solar-, and c) water-driven. The carbon-driven, growth is based on the carbon assimilation by the leaves' photosynthetic process. The solar-driven it derives the biomass directly from intercepted solar radiation through a single synthetic coefficient (models like EPIC, CERES) (Basso et al., 2016; Neitsch et al., 2011; Williams et al., 1989). The last category, the water-driven highlights the strong connection between cumulative seasonal crop transpiration and biomass production when crops are adequately supplied with water. By normalizing for different climatic conditions, the approach divides crop transpiration by the atmospheric evaporative demand, resulting in the biomass water productivity (WP) slope. After normalization, crops are grouped into classes with similar WP, making the approach robust for water-limited environments.

The user interface component allows the user to interact with the system and input data. According to Loucks et al. (2005), it is an essential feature that permits easy meaningful data entry and display and control of the model. A friendly interface is very important for the end-users. To achieve a friendly user interface, designers should consider factors such as visual aesthetics, intuitive navigation, clear instructions, feedback mechanisms, and responsiveness across different devices. Regular user testing and feedback collection can help refine the interface and identify areas for improvement, ultimately leading to a more satisfying user experience.

Regarding the output data, the DSS can provide a wide range of information from simple alerts as SMS or more complex ones, in the shape of a report with graphs and tables. The information needs to be clear and well structured. The optimal format and level of detail and precision of the output data should depend on the needs and backgrounds of each individual involved in the decision making process.

2.2.2.2 DSS irrigation scheduling

In irrigation scheduling, Decision Support Systems (DSS) offer various criteria to help users determine the appropriate time and amount of irrigation water needed. These criteria can be selected and customized by users based on their specific requirements. Rinaldi and He (2014) divide the criteria commonly implemented in DSS as:

Soil Moisture Threshold: Users can set a desired soil water content threshold or a percentage of available water in a specific soil depth. Irrigation will be triggered when the soil moisture falls below this predetermined level.

ET Threshold: Users can fix an Evapotranspiration (ET) threshold, and the system will initiate irrigation when the cumulative daily Evapotranspiration minus effective rainfall reaches this predefined threshold.

Time Interval: Some schemes allow irrigation water availability only at fixed time intervals (e.g., every n days). Users can set these intervals to suit their irrigation needs.

Phenology-Based Irrigation: DSS can incorporate supplemental irrigation at critical crop stages, aligned with the phenological development of the crop.

DSS can provide the flexibility for users to choose among these criteria and also adjust the threshold levels according to their preferences and crop requirements. By offering a range of options, DSS enables more efficient and precise irrigation scheduling tailored to specific agricultural scenarios.

2.2.2.3 Examples of DSS

The literature shows a plethora of DSS, where the core engine is the most fundamental difference between systems. The simplest core engines rely on the estimation of evapotranspiration (ET) using water budget models, in which the total available water (TAW) refers to the soil water storage between field capacity (θ_{FC}) and the wilting point (θ_{WP}), with depletion being compared with the readily available water (RAW) for the effect of water stress on ET (e.g., Todorovic et al., 2016, Li et al., 2018, Abi Saab et al., 2019). Irrigation is then triggered based on weather forecast and a management allowed soil depletion (MAD) threshold that varies according to the sensitivity of crop phenological stages to water stress and economical goals.

More complex DSS engines are based on direct measurements of the soil water pressure head (h), soil moisture (θ) or plant stress using a wide variety of sensors (tensiometers, soil moisture probes, dendrometers, fruit gauges, tissue water content sensors, as well as measures of growth, sap flow and stomatal conductance). Sensor information can then feed the previous

simulation models (Todorovic et al., 2016, Abi Saab et al., 2019), decision modelling systems (Car, 2018), or machine learning algorithms (Navarro-Hellín et al., 2016, Goap et al., 2018, Nawandar and Satpute, 2019), which combined with weather forecasts provide farmers with optimized irrigation schedules for their agricultural fields. These DSS usually require continuous data acquisition in the soil-plant-atmosphere system to sense the soil moisture status or plant stress, and ideally the automation of irrigation controllers and systems to irrigate whenever the monitored parameters reach a certain threshold. Irrigation automation and increased communication options offered by telemetry/remote controllers further fasten the analysis and processing of field data in real time, assisting expert agronomists in supporting a greater number of fields, farms, and crops. The associated cost, sensor setup, and maintenance are the main obstacles in running these systems.

Other examples of web-based irrigation DSS are CIMIS (Eching et al., 2002), AIS (Vories et al., 2009), and TOPS-SIMS (Johnson and Trout, 2012) in use in the United States; IrriSatSMS (Hornbuckle et al., 2009) in Australia; IRRINET-IRRIFRAME (Mannini et al., 2013) and IRRISAT (Belfiore et al., 2022) in Italy; and SPIDER (Calera et al., 2017) in Spain. All of these DSS employ tipping-based approaches, relying on FAO56 procedures (Allen et al., 1998) to compute the soil water balance and estimate crop irrigation needs. Those incorporating remote sensing data further make use of preestablished relationships between canopy reflectance and crop transpiration to enhance the assessment of crop water requirements.

IRRINET is an expert system for irrigation scheduling developed by the CER (Emiliano-Romagnolo Canal Irrigation Consortium), IRRINET service is freely available on the Internet and provides 'irrigation advice' for the main water demanding crops. IRRINET system provides to farmers a day-by-day information on how much and when to irrigate crops, implementing a real-time irrigation scheduling. Climatic and meteorological data are gathered on a daily basis on the web-DB server from several acquisition and elaboration systems. Irrigation scheduling is determined by applying a mathematical model based on daily water balance of the soil-plant-atmosphere system. IRRINET model integrates water dynamics in the soil, crop growth, crop water requirements, and the contribution of the water table. The hourly calculations and empirical functions used in the model have been validated locally through extensive field trials over several decades (Mannini et al., 2013).

The California Irrigation Management Information System (CIMIS) is a network of 145 automated weather stations across California, providing free irrigation information and weather data to aid growers and landscape supervisors. The water budget method, using CIMIS

reference evapotranspiration values, involves three steps: determining initial soil water balance, subtracting daily crop water use until reaching a desired level, and applying irrigation to recharge the soil profile (https://cimis.water.ca.gov/).

SAPWAT integrates FAO guidelines for improved crop irrigation decision-making. It features a global CLIMWAT weather database, specialized South African weather stations, and a four-stage crop development curve. The program simplifies climate classification, calculates irrigation requirements, and considers factors like system efficiency. SAPWAT 4 is applicable at various scales, integrates economic analysis, and includes a rainwater harvesting module for small areas. Overall, it provides a user-friendly and comprehensive tool for efficient irrigation planning (https://sapwat.org.za).

The web-based decision support system called AQUAMAN that was developed to assist Australian peanut growers schedule irrigations, simulates the timing and depth of future irrigations by combining procedures from the food and agriculture organization (FAO) guidelines for irrigation scheduling (FAO-56) with those of the agricultural production systems simulator (APSIM) modeling framework (Chauhan et al., 2013).

CropIrri (Zhang and Feng, 2010) is a field crop irrigation management decision-making system based on the soil water balance model, crop phenology model, root growth model, crop water production function, and irrigation management model. The irrigation plan is made by predicting of soil water content in root zone and daily crop water requirement using historical and forecasting weather data, measured real time soil moisture data. The main function of CropIrri includes: real-time irrigation management decision-making support, simulation of soil water dynamics in the root zone, evaluation of the effect of certain irrigation plans on crop yield reduction, and database management.

The IrrigaSys (Simionesei et al., 2020), in use in Portugal, exhibits important differences from the aforementioned systems due to their increased complexity. The core engine of this system, the MOHID-Land model (Ramos et al., 2017), adopts a mechanistic approach wherein the Richards' equation is used for computing soil water storage and fluxes in the root zone, meaning that a full description of soil hydraulic functions is required, i.e., the soil water retention and soil hydraulic conductivity curves from saturation to oven dryness. Moreover, the model includes the simulation of crop growth, considering factors such as intercepted light, conversion of intercepted light into biomass, crop stress, and the number of heat units defining the crop season (Neitsch et al., 2011; Williams et al., 1989). The model further includes a

system dependent boundary condition based on soil pressure heads for irrigation scheduling (Ramos et al., 2017).

2.2.2.4 Conclusion

DSSs can help make more informed and data-driven decisions, improve efficiency, reduce costs, and increase productivity.

The utilization of DSS in agriculture management has experienced significant growth in the last decade, enabling quick evaluations of agricultural production systems globally and facilitating decision-making at both the farm and district levels. However, there are obstacles to the successful adoption of this technology in agriculture. Water management, particularly in irrigation practices, is a crucial area where DSS has been applied to address water scarcity issues, taking into account factors such as water availability, crop requirements, land size, irrigation systems, and crop productivity.

3. IrrigaSys: A web-based irrigation decision support system based on open-source data and technology

The material on which this chapter is based has been previously published in: Simionesei, L., Ramos, T.B., Palma, J., Oliveira, A.R., Neves, R., 2020. IrrigaSys: A web-based irrigation decision support system based on open-source data and technology. Computers and Electronics in Agriculture 178. https://doi.org/10.1016/j.compag.2020.105822

3.1 Introduction

Agriculture is by far the largest consumer of water, with about 70% of all freshwater withdrawals being used in irrigation (Water, 2020). In water scarce regions, irrigation is fundamental to fulfill crop water requirements, increase food outputs through higher yields, meet the growing food demand, ensure food stability, and increase prosperity of rural areas. However, inefficient practices often lead to increased nutrient leaching, enhanced runoff and soil erosion, salinity build-up in the rootzone, and the eutrophication of water bodies with associated biodiversity loss. Agricultural consumption of scarce water resources further faces an increasing competition from the multiple demands from different uses (urban consumption, industries, recreational), which makes it even more essential to improve water use efficiency in irrigated fields to cope with the increasing scarcity and contribute to the sustainability of agricultural systems.

The scientific community has invested considerable time and resources over the last two decades in the development of decision support systems (DSS) aimed at improving irrigation water management at the field and irrigation district scales. DSS are interactive software-based systems used to compile useful information from multiple raw data sources and provide optimized solutions to support farmers in the decision-making process. The architecture of these systems usually consists of a database for data repository, a core engine for computation of crop water requirements and irrigation scheduling, and a graphical interface for farmers' access to outputs (Rinaldi and He, 2014). The success of these systems has been gaining momentum with the development of online features and smartphone applications (Abi Saab et al., 2019; Goap et al., 2018; Nawandar and Satpute, 2019) offering continuous interaction between users and tools, increased operational flexibility, further allowing the update of data inputs in real-time. Nevertheless, DSS still fails in many regions of the world

due to a perceived gap between research and farming practices, farmers' mistrust in the embedded technology, and limited on-farm technology access (Car, 2018).

Despite the automation of sensors, models, and algorithms, human expertise and interaction with farmers are still fundamental for a proper setup of the DSS. This is also critical in IrrigaSys. Inputs on soils, crops, and irrigation systems are vital to the performance of DSS but need to be limited to a minimum regardless of the complexity of the models or algorithms used (Li et al., 2018; Yang et al., 2017). The success of a DSS is also associated with the reliability of predictions, which can only be validated in a small number of demonstrative case studies. These are fundamental to improve farmers' trust in the system, but cannot be scalable and available to every field supported by the DSS (Navarro-Hellín et al., 2016).

This chapter describes the IrrigaSys DSS developed to support irrigation water management in the Sorraia Valley irrigation district, southern Portugal. This irrigation district in Sorraia Valley, is part of one of the most important agricultural areas in the country. Water scarcity and inappropriate land management practices have been some of the most critical constraints to the sustainable production of maize and other agricultural crops (Cameira et al., 2003; Ramos et al., 2017). As a result, the government has established policy instrument *Portaria n.502015*, n.d. for improving irrigation efficiency in this and other irrigation areas, which amongst other actions has mandated the definition of improved irrigation schedules based on soil water content status and crop water needs. The specific objectives of this study are: (i) to present the IrrigaSys structure; (ii) to detail on the system implementation at the field plot scale; (iii) and to discuss the IrrigaSys strengths and weaknesses based on the experience gained from running the DSS over the last five years. This chapter consists of various Sections. After the current Introduction, Section 2 describes the structure of the IrrigaSys decision support system. Section 3 describes how IrrigaSys was implemented to support irrigation water management in the Sorraia Valley district. Section 4 discusses the main strengths and limitations of IrrigaSys. Finally, Section 5 presents the main conclusions. Results of this study may well contribute to the development of future DSS aimed at improving irrigation water management in water scarce regions.

3.2 System structure

The IrrigaSys service is composed of six main components (Figure 3.2-1): (i) an online platform for system administration, management, and visualization of outputs; (ii) a vadose zone model for computation of soil water dynamics and irrigation scheduling at the plot scale; (iii) a meteorological module for the hindcast and forecast of weather data; (iv) a Structured

Query Language (SQL) database for data repository and management of model inputs; (v) a remote sensing module for complementing system's outputs with satellite data; and (vi) several other dissemination platforms for facilitating users' access to the DSS. The following sections provide a detailed description of the individual components of IrrigaSys.

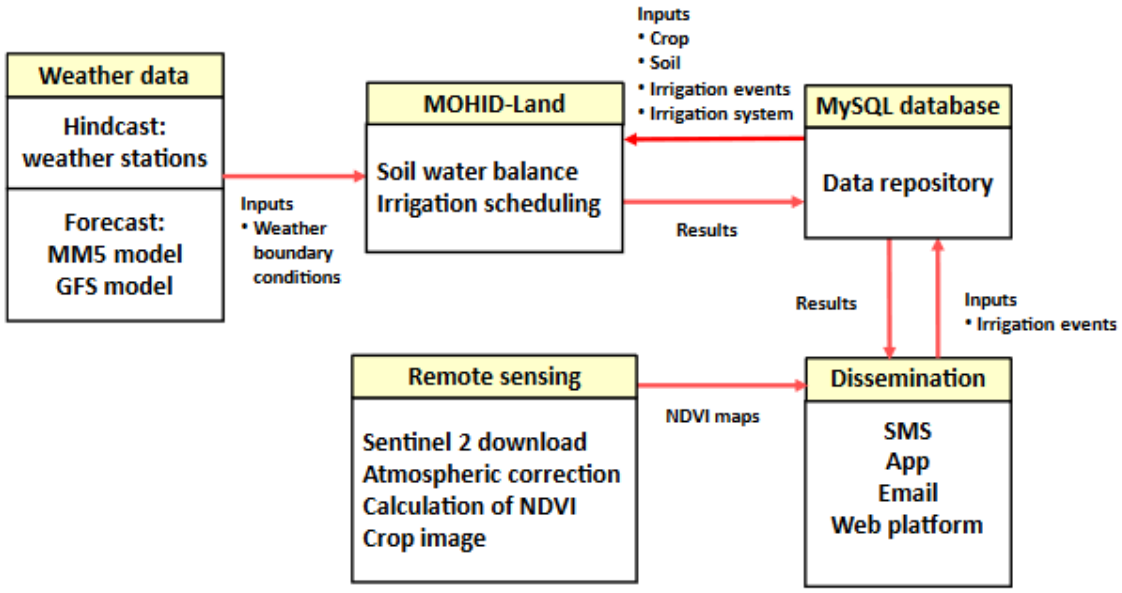

Figure 3.2-1 IrrigaSys conceptual scheme.

3.2.1 The online platform

IrrigaSys includes an online graphical interface (http://irrigasys.maretec.org/) to facilitate the system's administration, management, and visualization of outputs. The platform has three levels of access: administrator, manager, and regular user. The administrator level is available only to the system's developers, which are the ones authorized to add new clients to the system and configure field plot characteristics (soils, crops, irrigation systems). The manager level is available to the technicians managing the system and interacting with final users. Ideally, these technicians should be agronomists or irrigation managers. Every season, they are responsible for initiating the service provided by the DSS, activating plots and defining the sowing dates, crops, soil textures, and irrigation systems of every field plot served by the DSS. These plot characteristics are defined from the options menu created by the system's developers. Because IrrigaSys is not connected to controllers or field dataloggers and farmers may well deviate from irrigation schedules recommended by the system, the manager needs also to introduce actual irrigation events carried out by farmers in their respective plots, thus requiring close contact with IrrigaSys final users. The role of the irrigation manager is thus fundamental to the successful performance of the DSS. Finally, the user level is given to farmers, who can simply

visualize the DSS outputs for their plots. Farmers can also introduce irrigation events directly to the system through a smartphone application if they want to get more involved in the process.

3.2.2 The vadose zone model

The MOHID-Land model (Ramos et al., 2017) is the core engine of IrrigaSys and is used to compute soil water dynamics and irrigation scheduling at the field plot scale (Figure 3.2-3).

3.2.2.1 Introduction

This section describes the model, MOHID Land, that was chosen as the core model for the DSS. The next sections will give a description of the main processes and main equations used.

The chosen model, MOHID Land, serves as the central framework for the Decision Support System (DSS). MOHID Land is a comprehensive land surface model that specializes in simulating various hydrological, ecological, and environmental processes. It has been selected due to its versatility and robust capabilities in addressing complex interactions within terrestrial ecosystems.

MOHID Land encapsulates a multitude of critical processes that contribute to the accurate representation of land-atmosphere interactions and the behavior of terrestrial systems.

These processes likely include but are not limited to: **water cycle, energy balance, vegetation dynamics, soil processes.**

By integrating these core processes and equations, MOHID Land serves as a comprehensive tool within the Decision Support System, enabling a better understanding of land-related phenomena and aiding in informed decision-making for environmental management and resource planning.

3.2.2.2 MOHID Land model description

MOHID-Land is an open-source, physically based, distributed model using a finite-volume approach based on mass and momentum balance equations (Trancoso et al., 2009). The model is capable of integrating different physical and chemical processes across different scales (plot, field, and catchment scales) depending on the specifications of the simulation domain (Bernard-Jannin et al., 2016; Brito et al., 2015; Epelde et al., 2016; Simionesei et al., 2016). MOHID-Land includes different modules for simulating soil water dynamics, solute and particle matter transport, soil biochemical reactions, soil erosion, and crop growth at different scales (Trancoso et al., 2009). Figure 3.2-2 shows the conceptual scheme of MOHID-Land and the modules included in this thesis.

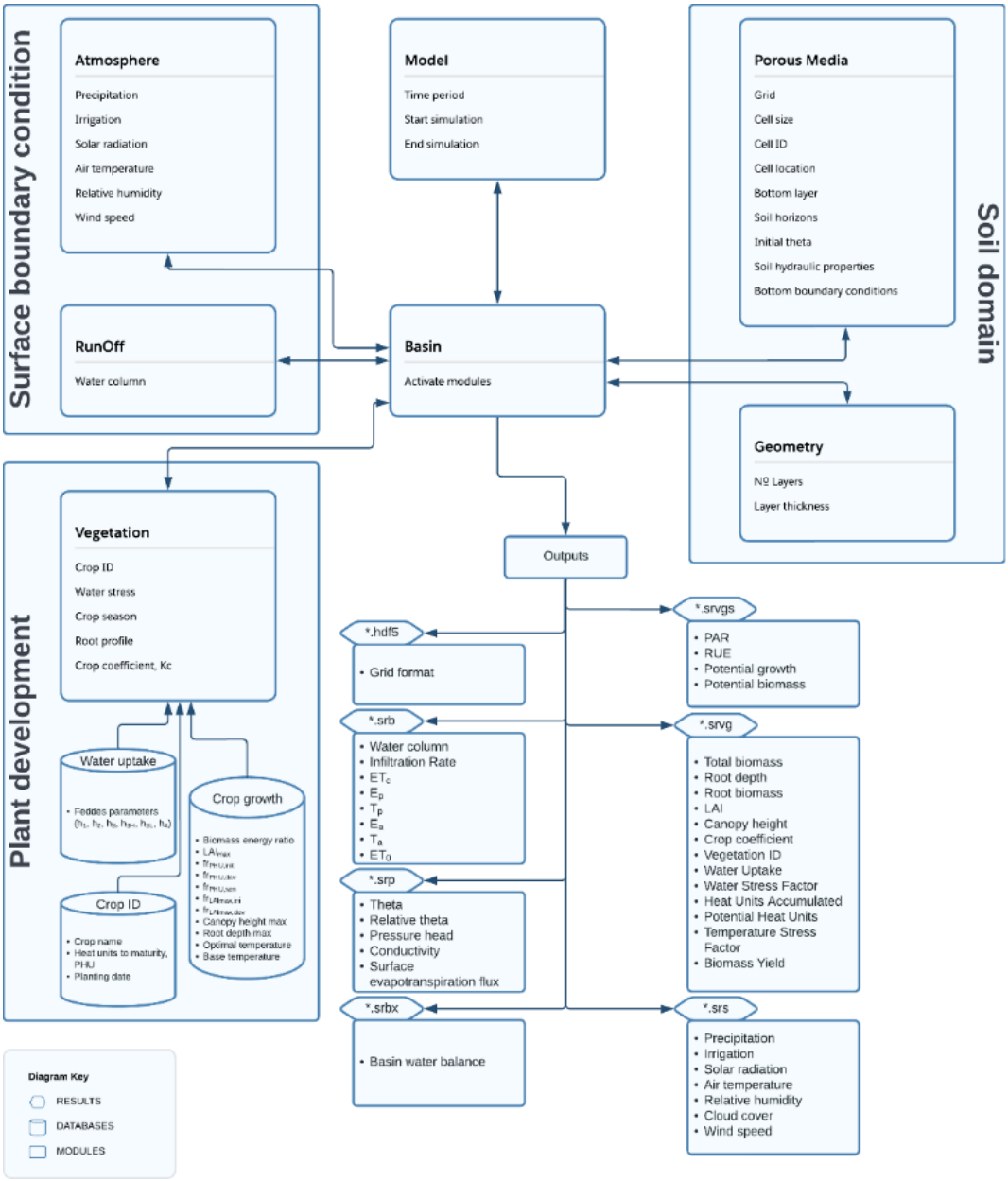

Figure 3.2-2 The structure of MOHID Land

The source code can be accessed at the MOHID code repository website (https://github.com/Mohid-Water-Modelling-System/Mohid). Below we give an overview of the main MOHID-Land processes that were included in this thesis (Figure 3.2-3).

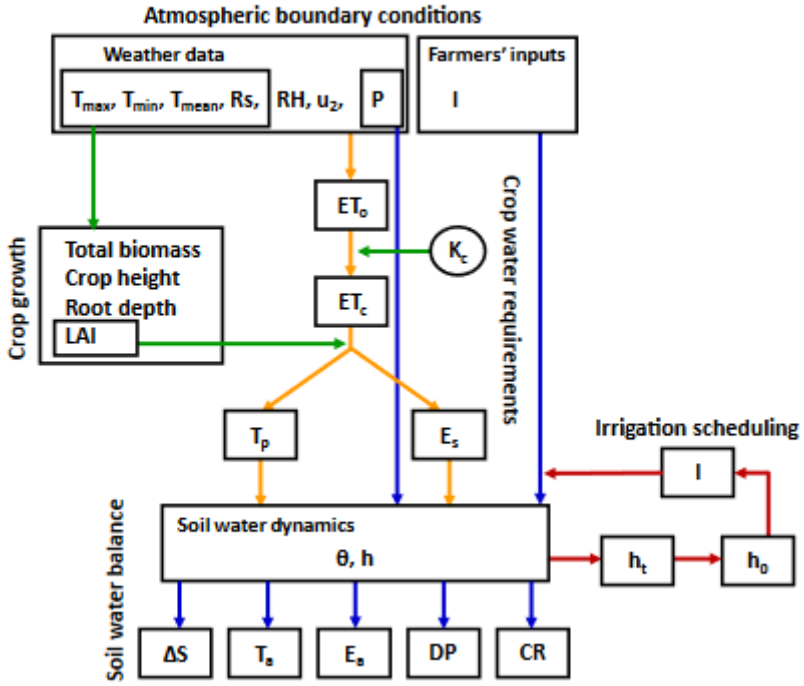

Figure 3.2-3 MOHID-Land conceptual scheme (Tmax, Tmin, and Tmean, maximum, minimum, and average surface temperature, respectively; Rs, solar radiation; RH, relative humidity; u2, wind speed; P, rainfall; I, irrigation; ETo, reference evapotranspiration; ETc, crop evapotranspiration; Kc, crop coefficient; Tp and Ta, potential and actual crop transpiration, respectively; Es and Ea, potential and actual soil evaporation, respectively; θ, soil water content; h, soil pressure head; ΔS, soil water storage variation; DP, deep percolation, CR, capillary rise; ht and h0, threshold and target soil pressure heads, respectively.

3.2.2.2.1 Water flow

Variably-saturated one-dimensional water flow is described using the Richards equation:

$$\frac{\partial \theta}{\partial t} = \frac{\partial}{\partial z}\left[K(h)\frac{\partial h}{\partial z} - K(h)\right] - S(z,t) \qquad \text{Equation 4}$$

where θ is the volumetric soil water content ($L^3\ L^{-3}$), t is time (T), z is the vertical space coordinate (L), h is the soil water pressure head (L), K is the hydraulic conductivity ($L\ T^{-1}$), and S is the sink term accounting for water uptake by plant roots ($L^3\ L^{-3}\ T^{-1}$). The unsaturated soil hydraulic properties were described using the van Genuchten-Mualem functional relationships (van Genuchten, 1980):

$$S_e(h) = \frac{\theta(h) - \theta_r}{\theta_s - \theta_r} = \frac{1}{(1+|\alpha h|^{\eta})^m} \qquad \text{Equation 5}$$

$$K(h) = K_{sat} S_e^l \left[1 - \left(1 - S_e^{1/m}\right)^m\right]^2$$

Equation 6

where S_e is the effective saturation ($L^3\ L^{-3}$), θ_r and θ_s denote the residual and saturated water contents ($L^3\ L^{-3}$), respectively, K_{sat} is the saturated hydraulic conductivity ($L\ T^{-1}$), α (L^{-1}) and η (−) are empirical shape parameters, $m = 1–1/\eta$, and l is a pore connectivity/tortuosity parameter (−).

3.2.2.2.2 Crop transpiration and soil evaporation rates

Crop evapotranspiration (ET_c, $L\ T^{-1}$) is determined from hourly/daily ET_0 values computed with the FAO Penman-Monteith method using the single crop coefficient approach (Allen et al., 1998):

$$ET_c = K_c ET_0 \qquad \text{Equation 7}$$

where K_c is a crop coefficient (−) incorporating crop characteristics and averaged effects of evaporation from the soil. ET_c was then partitioned into potential soil evaporation (E_p, $L\ T^{-1}$) and potential crop transpiration (T_p, $L\ T^{-1}$) as a function of LAI ($L^2\ L^{-2}$) (Ritchie, 1972):

$$T_p = ET_c\ (1 - e^{(-\lambda LAI)}) \qquad \text{Equation 8}$$

$$E_p = ET_c - T_p \qquad \text{Equation 9}$$

where λ is the extinction coefficient of radiation attenuation within the canopy (−). T_p values were used to compute the sink term (S) in Equation 4 using the macroscopic approach introduced by Feddes et al. (1978). In this approach, T_p is distributed over the root zone and may be diminished by the presence of depth-varying root zone stressors, namely water stress (Feddes and Zaradny, 1978; Šimůnek and Hopmans, 2009; Skaggs et al., 2006) as follows:

$$S(h,z,t) = \alpha(h,z,t)\ \ S_p = \alpha(h,z,t)\ \beta(z,t)\ T_p(t) \qquad \text{Equation 10}$$

where S and S_p are the actual and potential volumes of water removed from a unit volume of soil per unit of time ($L^3\ L^{-3}\ T^{-1}$), respectively, $\beta(z, t)$ is a normalized root distribution function (L−1). The actual transpiration rate (T_a, $L\ T^{-1}$) is thus obtained by integrating Equation 10 over the root domain, R (L), as follows:

$$T_a(t) = T_p(t) \int R\ \alpha(h,z,t)\ \beta(z,t)\ dz \qquad \text{Equation 11}$$

Root water uptake reductions due to water stress, $\alpha(h)$, are described using the piecewise linear model proposed by Feddes et al. (1978). The water uptake is at the

potential rate when the pressure head is between h_2 and h_3, dropped off linearly when $h > h_2$ or $h < h_3$, and becomes zero when $h < h_4$ or $h > h_1$. E_p values are limited by a pressure head threshold value in order to obtain the actual soil evaporation rate (E_a, L T^{-1}) (American Society of Civil Engineers (ASCE), n.d.).

3.2.2.2.3 Plant development

MOHID-Land includes a modified version of the EPIC model (Neitsch et al., 2011; Williams et al., 1989) for simulating crop growth. This model is based on the heat unit theory, which considers that all heat above the base temperature will accelerate crop growth and development. The total number of heat units for maize to reach maturity is calculated as:

$$PHU = \sum_{i=1}^{m} HU = \sum_{i=1}^{m} T_{av} - T_{base} \qquad when\ T_{av} - T_{base}$$ Equation 12

$$PHU = 0 \qquad when\ T_{av} \leq T_{base}$$

where PHU is the total heat units required for plant maturity (ºC) HU is the number of heat units accumulated on day i (ºC), i = 1 corresponds to the sowing date (−), m is the number of days required for plant maturity (−), T_{av} is the mean daily temperature (◦C), and T_{base} is the minimum temperature for plant growth (ºC). Accordingly, MOHID-Land integrated all sub-daily temperature data into daily averages when computing PHU and crop growth.

Crop growth is modelled by simulating light interception, conversion of intercepted light into biomass, and LAI development. Total biomass is calculated from the solar radiation intercepted by the crop leaf area using the Beer's law (Monsi, 1953):

$$\sum_{i=1}^{m} \Delta Bio_{act,i} = \sum_{i=1}^{m} \Delta Bio_i \ \ \gamma_i = \sum_{i=1}^{m} RUE \left(0.5\, PAR_{day,i}\left(1 - e^{(-\lambda LAI)}\right)\right) \gamma_i$$

Equation 13

where $\Delta Bio_{act,i}$ and ΔBio_i are the actual and potential increase in total plant biomass on day i (kg ha^{-1}), RUE is the radiation-use efficiency of the plant ((kg ha^{-1}) (MJ m^{-2})$^{-1}$), $PAR_{day,i}$ is the daily incident photosynthetically active radiation (MJ m^{-2}), λ is again the light extinction coefficient, and γ_i is the daily plant growth factor (0–1) which accounts for water and temperature stresses. RUE is estimated using the approach proposed by Stockle et al., 1992, while γ_i is computed as follows (Neitsch et al., 2011):

$$\gamma_i = 1 - max\ (w_{strs,i}, t_{strs,i})$$ Equation 14

where $w_{strs,i}$ and $t_{strs,i}$ are the water and temperature stresses for a given day i (−), respectively. Water stress ($w_{strs,i}$) is calculated as (Neitsch et al., 2011):

$$w_{strs,i} = 1 - \frac{T_{a\ cum,i-1}}{T_{p\ cum,i-s}} \quad \text{Equation 15}$$

where $T_{a\ cum}$ and $T_{p\ cum}$ are the cumulative T_a and T_p values on day i-1. The effect of water stress on crop growth is thus only reflected on the following day.

Note that although MOHID-Land computes hourly T_a (Equation 11) and T_p (Equation 8) values from hourly weather data, only cumulative daily values are considered when computing the effect of water stress on crop growth (Equation 15). Temperature stress is computed as temperature diverged from the optimal (T_{opt}, °C) using a sigmoidal function (Williams et al., 1989), similarly influencing crop development as water stress.

Leaf area index is computed as a function of heat units, crop stress, and development stage. During early crop stages (initial and crop development stages), the LAI added on day i is calculated as (Neitsch et al., 2011) :

$$\Delta LAI_{act,i} = \Delta LAI_i \ \sqrt{\gamma}_i = (fr_{LAImax,1} - fr_{LAImax,1-1}\ LAI_{max}\left((1 - e^{(5(LAI_{i-1} - LAI_{max}))}\right)\ \sqrt{\gamma_i} \quad \text{Equation 16}$$

where $\Delta LAI_{act,i}$ and ΔLAI_i are the actual and potential LAI increment added on day i ($m^2\ m^{-2}$), respectively, and $fr_{LAImax,i}$ and $fr_{LAImax,i-1}$ are the fraction of the plant's maximum LAI (LAI_{max}, $m^2\ m^{-2}$) on day i and i-1 (−), respectively. These fractions are calculated as (Neitsch et al., 2011):

$$fr_{LAImax,i} = \frac{fr_{PHU,i}}{fr_{PHU,i} + e^{(l_1 - l_2 fr_{PHU.i})}} \quad \text{Equation 17}$$

where $fr_{PHU,i}$ is the fraction of PHU accumulated up to day i (−), and l_1 and l_2 are shape coefficients (−). Once LAI_{max} is reached, LAI remains constant until senescence began ($fr_{PHU} > fr_{PHU,sen}$). Then:

$$LAI_{act,i} = LAI_i \ \sqrt{\gamma}_i = LAI_{max} \frac{(1 - fr_{PHU,1})}{(1 - sen)}\ \sqrt{\gamma_i} \quad \text{Equation 18}$$

where fr_{PHUsen} is the fraction of PHU at which senescence begins and LAI starts to decline (−).

The canopy height is computed as (Neitsch et al., 2011):

$$h_{c,i} = h_{c,max}\sqrt{fr_{LAImax,1}} \quad \text{Equation 19}$$

where $h_{c,i}$ is the canopy height for a given day i (m), and $h_{c,max}$ is the plant's maximum canopy height (m). Once maximum canopy height is reached, h_c remain constant until harvest. Root depth is also computed as a function of heat units, and increased linearly as follows (Neitsch et al., 2011):

$$z_{root,i} = 2.5\ fr_{PHU,i}\, Z_{root,max} \quad if\ fr_{PHU,i} \leq 0.4 \qquad \text{Equation 20}$$

$$z_{root,i} = Z_{root,max} \quad if\ fr_{PHU,i} > 0.4 \qquad \text{Equation 21}$$

where $Z_{root,I}$ is the root depth on a given day i (m), and $Z_{root,max}$ is the maximum root depth (m). Root depth is not affected by water stress as plants tend to expand their roots when water is a limiting factor.

Finally, yield (Y) is obtained from the product of the above-ground dry biomass (ABG biomass, kg ha^{-1}) and the actual harvest index (HI_{act}):

$$Y = ABG\ biomass \times HI_{act} \qquad \text{Equation 22}$$

The ABG biomass is obtained by subtracting root biomass from the total biomass, while HI_{act} was computed as (Neitsch et al., 2011):

$$HI_{act,i} = (HI - HI_{min}) \frac{\gamma_{w,i}}{\gamma_{w,i} + exp(6.13 - 0.833\,\gamma_{w,i})} + HI_{min} \qquad \text{Equation 23}$$

where HI is the potential harvest index on day i (−), HI_{min} is the minimum harvest index allowed (−), and γ_w is another water stress deficiency factor (0–1), computed this time as a function of the evapotranspiration deficit. HI is calculated as (Neitsch et al., 2011):

$$HI_i = HI_{opt} \frac{100\ fr_{PHU}}{fr_{PHU} + exp\,(11.1 - 10\ fr_{PHU}))} \qquad \text{Equation 24}$$

where HI_{opt} is the potential harvest index at crop maturity for ideal growing conditions (−). γ_w was computed as (Neitsch et al., 2011):

$$\gamma_{w,i} = 100 \frac{\sum_{i=1}^{m} ET_0}{\sum_{i=1}^{m} ET_c} \qquad \text{Equation 25}$$

where ET_a is the actual evapotranspiration (mm).

3.2.3 Weather hindcast and forecast

The atmospheric boundary conditions of the MOHID-Land model are defined using the hindcast and forecast weather data of IrrigaSys. For the hindcast period, the system is connected to a weather station network, downloading the data through an Application Programming Interface (API) written in Perl. Measured values of the maximum (T_{max}, ºC) and

minimum (T_{min}, ºC) surface air temperatures, minimum relative humidity (RH, %), wind speed (u_2, m s^{-1}), solar radiation (Rs, W m^{-2}), and rainfall (mm) are extracted daily from all meteorological stations in that network. The model then computes the ET_o rates for each plot using data collected from the closest station.

For the forecast period, the system follows a hierarchical structure to provide the forecast data for the seven incoming days. First, weather data is provided for the area by the MM5 mesoscale model (http://meteo.tecnico.ulisboa.pt), forced by the initial conditions from the NCEP (National Center for Environmental Prediction) Climate Forecast System Reanalysis, at a spatial resolution of 9 km. Daily values of average surface air temperature (T_{mean}, ºC), RH, u_2, Rs, and rainfall are then used to compute the model's atmospheric boundary conditions. When the MM5 option is not available, the same data is extracted from the Global Forecast System (GFS; https://www.nco.ncep.noaa.gov/pmb/products/gfs/) at a 30 km resolution.

3.2.4 Estimates of the soil water balance and irrigation scheduling

The soil water balance is given for the hindcast and forecast periods. First, the ET_c rates are computed from the product of the ET_o by the K_c value of each crop stage. These are then partitioned into T_p and E_p rates, and used for defining the atmospheric boundary conditions of the MOHID-Land model. The model further needs information on past irrigation events. Because the function of the DSS is to advise farmers and not manage irrigation plots, real irrigation events may well deviate from the service's recommendations. Therefore, IrrigaSys provides estimates of the soil water balance always from the sowing date to the current week (hindcast). This procedure is carried out every time the system runs, allowing to update it with newly acquired information whenever the system's irrigation manager is unable to introduce farmer's weekly irrigation data on time. For the forecast period, irrigation scheduling and the corresponding soil water balance are provided for a 7-day period using weather forecast data for the same period.

3.2.5 The database

IrrigaSys includes a relational database for data repository developed for the MySQL 8.0 (www.mysql.com) operating system. The database is divided into 13 tables, organized into six different groups (Figure 3.2-4). The first group is composed of 2 tables (USERS and COMPANIES) with personal information of farmers and agricultural companies (a farmer can manage one or more agricultural company) supported by the system:

- USERS stores the internet protocol addresses (ip_address), usernames (username), names (name, first_name, last_name), contact information (email, phone,

phone_alt), and passwords (password) of farmers registered in the system. The table contains also a series of attributes for managing their registration, namely a system for password issuing (activation_code, created_on, last login), encryption (salt), and retrieval (forgotten_password_code, forgotten_password_time, remember_code). Finally, the table further allows users' activation/deactivation (active).

- COMPANIES lists the company names (company, company_alias), their identification code (user_id), their value added tax identification number (vat), and their contact information (address, email, phone, phone_alt);

The second group includes 2 tables (PLOTS and SEASONS) with plot details:

- PLOTS provides the plots' names (name), geographical coordinates (latitude, longitude), and agricultural companies managing them (company_id);
- SEASONS contains information related to irrigation systems (irrigation_system_id), crops (crop_id) and respective sowing dates (sowing_date), soil textures (soil_texture_id), and initial soil water contents (initial_theta) of plots (plot_id) during each growing season (season_year). The table further includes the maximum amount of water allowed per crop and irrigation system (depth_max) as well as whether probes (probes) are used to monitor soil moisture. These are requirements to comply with the policy instrument (*Portaria n.502015*, n.d.) aimed at maximizing the effectiveness and efficiency of irrigation water use in Portugal, through which farmers are subsidized. This table also activates/deactivates (active) plots in the DSS (so that the model can start/stop computing the weekly water balance);

The third group covers 3 tables (IRRIGATION_SYSTEMS, SOIL_TEXTURES, and CROPS) describing the general options available for plot characterization:

- IRRIGATION_SYSTEMS characterizes the irrigation methods (name), namely the average debit (debit) and efficiency (efficiency);
- SOIL_TEXTURES lists the soil texture classes (name);
- CROPS lists the crops (name) and respective codes used in the MOHID-Land model (mohid_crop_id), the parameters related to the computation of the irrigation schedule h0 (target head) and ht (threshold_head), the crop coefficients for the initial (kc1), mid-season (kc2), and end-season stages (kc3), the PHU (phu), and the fraction of the PHU when those same stages are reached (respectively hu1, hu2, and hu3);

The fourth group includes 2 tables (GIVEN_IRRIGATION and METEO_STATIONS) with external information to the system:

- GIVEN_IRRIGATION compiles irrigation events (date) and amounts
- (irrigation) provided per plot and growing season by farmers (season_id), indicating also whether that data is given on a weekly or daily basis (data_type) and the necessary adjustments to be made during computation (modification_time);
- METEO_STATIONS stores information related to weathers stations connected to the DSS, including their identification (name), location (latitude, longitude), and whether they are active/inactive (active);

The fifth group (RESULTS) contains the main outputs of IrrigaSys:

- RESULTS stores information on weather hindcast and forecast (temperature_min, temperature_med, temperature_max, precipitation) as well as the soil water balance and irrigation scheduling (evtp_reference, evtp_crop, evtp_actual, crop_coefficients, irrigation, water_content, soil_saturation, field_capacity, deplfract_no_stress, root_depth) for each week (date_results) and growing season (season_id);

Finally, the sixth group contains 3 tables (GROUPS, USERS_GROUPS, and LOGIN_ATTEMPTS) with administrative functions:

- GROUPS lists the level of access for different users (name, description);
- USERS_GROUPS links each user (user_id) to the level of access (group_id);
- LOGIN_ATTEMPTS provides a counter for the number of unsuccessful logins (ip_address, login, time).

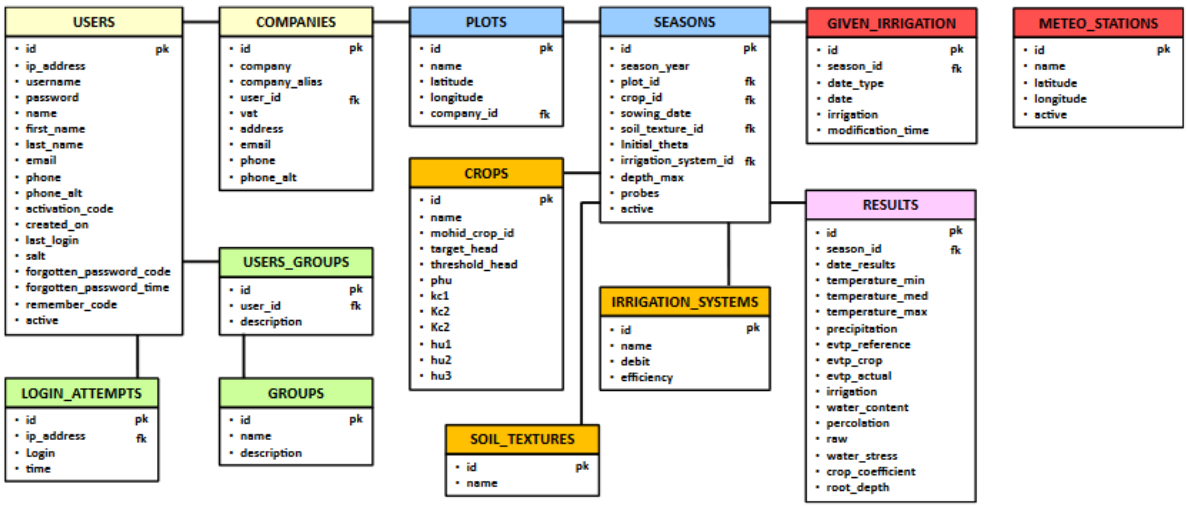

Figure 3.2-4 Structure and attributes of the IrrigaSys database (pk and fk correspond to primary and foreign keys, respectively).

3.2.6 Remote sensing products

Plot information is complemented with maps of the Normalized Difference Vegetation Index (NDVI) (Figure 3.2-5). The following procedures are carried out every week for the area under management using a script developed in Python:

1. Download of the latest Sentinel-2 image tiles having less than 10% cloud cover from the Copernicus Open Access Hub (Copernicus, 2022);
2. Atmospheric correction of the downloaded tiles using the Sen2cor software (ESA, 2020), which is a processor for Sentinel-2 Level 2A product generation and formatting, performing the atmospheric, terrain and cirrus correction of Top-Of-Atmosphere Level 1C input data, and creating Bottom-Of-Atmosphere corrected reflectance images;
3. Computation of the NDVI using the Sentinel-2 frequency bands 4 (Red) and 8 (NIR, Near Infra-Red) as follows:

$$NDVI = \frac{(NIR-Red)}{(NIR+Red)} \qquad \text{Equation 26}$$

4. Merge of all NDVI images, projection for the WGS84 reference system, and cropping for the border limits of the plots served by the DSS. IrrigaSys accesses then an open-source map server where the maps are published.

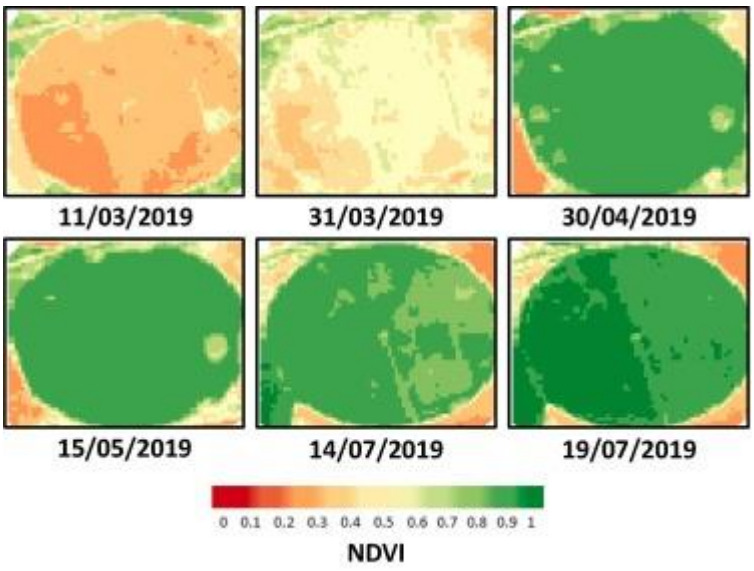

Figure 3.2-5 Crop homogeneity maps for a selected plot using the Normalized Difference Vegetation Index (NDVI).

3.2.7 System outputs

Results from IrrigaSys are disseminated using different platforms every week. The simplest way is through a Short Message Service (SMS) sent directly to farmers. Each programmable SMS identifies the plot and week number, and provides estimates of T_{max} (ºC), rainfall (mm), ET_c(mm), and recommended irrigation depth (mm) for that week.

Farmers can also access IrrigaSys results by logging in to an application developed for the Android mobile operating system (Figure 3.2-6a). The main menu presents three different buttons (Figure 3.2-6b). The first provides access to the plots managed by farmers (Figure 3.2-6c). Then, for each plot, the application shows the forecast for T_{max} and T_{min} (ºC), rainfall (mm), and ET_c (mm) as well as the evolution of the soil water content and the recommended irrigation schedule (mm) for the incoming 7 days. Also available is a pie graph showing the cumulative irrigation amount applied from the beginning of the growing season versus the maximum allowed for that crop and irrigation system by legislation (Figure 3.2-6d and e). The second button gives access to a menu where farmers can introduce irrigation events directly into the system (i.e., without going through the system's irrigation manager). Information can be provided on a weekly or daily basis (Figure 3.2-6f). Finally, the last button sends users to a configuration menu. This application is available for download from the "Google Store".

Figure 3.2-6 Smart phone application for accessing the IrrigaSys results. a) login menu; b) main menu; c) menu with registered plots; d) and e) menu with the weather forecast, evolution of soil water contents, and cumulative irrigation amounts; and f) menu for providing past irrigation events to feed the system.

Each farmer also receives a weekly email with reports for all respective plots in a pdf format. The report is divided in five parts. The first identifies the farmer, the plot, the crop, the sowing date, the irrigation system, and the date of the report. The second presents the water balance for the previous and incoming week as well as the same pie graph described earlier with the cumulative irrigation amounts versus the threshold limit given by legislation. The third component consists of two graphs, one giving the evolution of the soil water content from the sowing date to the present date, and another with the rainfall and irrigation events registered in the system during the same period. The fourth component details the estimates of the soil water balance as well as the forecast of T_{max} and T_{min} (ºC), rainfall (mm), ET_o (mm), and Et_c (mm) for the incoming 7 days. Finally, the fifth component presents the NDVI map calculated from the most recent cloud-free Sentinel-2 image. The IrrigaSys results can further be accessed through an online platform (Figure 3.2-7), which naturally includes all previous information. The farmers have direct access to the latest weather forecast, the soil water balance, the NDVI map as well as to a repository with all issued reports for each plot.

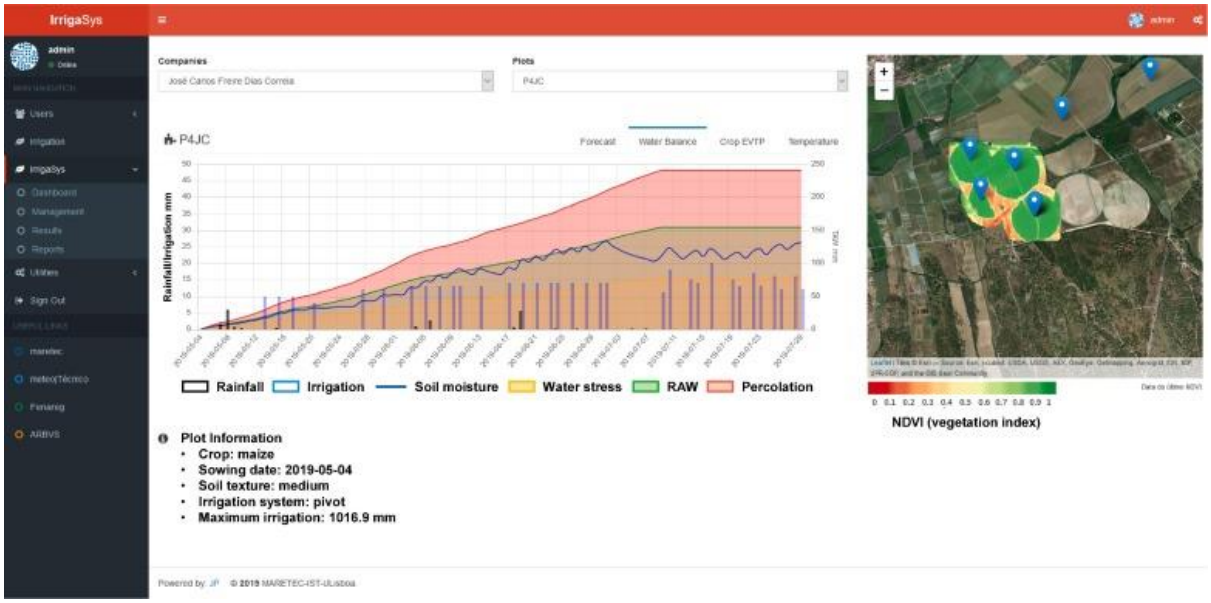

Figure 3.2-7 The IrrigaSys online platform. Results menu.

3.3 Implementation

3.3.1 Study area

The IrrigaSys DSS has been supporting irrigation water management in the Sorraia Valley irrigation district, in southern Portugal, for the last five years (38.95 N, 8.54 W). The climate in the region is semi-arid to dry sub-humid, with hot dry summers and mild winters with irregular rainfall. The mean annual rainfall is close to 500 mm, varying from 200 to 900

mm along the years. The annual surface air temperature averages 15 ºC, ranging from ~9 ºC in January to ~22 ºC in July, while the mean annual reference evapotranspiration is close to 900 mm. The dominant soils are Fluvisols, Planosols, Cambisols, Luvisols, and Regosols. Rice (Oryza sativa L.) and maize (Zea mays L.) are the main crops in the region, occupying respectively 32.0–40.2% and 21.4–38.4% of the total irrigated area from 2007 to 2018. The previous crops obviously influence the choice of the irrigation method, with surface, sprinkler (centre pivot), and drip systems covering 7713, 6985, and 4383 ha, respectively (total area: 19,332 ha) (ARBVS, 2019). Water access is on demand.

Over the last 5 years, IrrigaSys has provided service to 30 farmers, managing 103 plots with an area varying from 0.03 to 75 ha (total area of 2080 ha). The crops included maize, tomato (Solanum lycopersicum L.), potato (Solanum tuberosum L.), peanut (Arachis hypogaea L.), bell pepper (Capsicum annuum L.), sunflower (Helianthus annuus L.), and vineyard (Vitis vinifera L.). Only pressure irrigation systems were supported by IrrigaSys.

3.3.2 System setup and requirements

The IrrigaSys DSS was developed in close cooperation with the local Water Board (Associação de Regantes e Beneficiarios do Vale do Sorraia, ARBVS), complementing the services already provided to their associates to ensure the compliance with legislation requirements for funding management practices aimed at improving irrigation water use efficiency (*Portaria n.502015*, n.d.). Farmers did not adhere directly to the system. It was ARBVS that made sure they would join the system, organizing workshops, and maintaining close contact with their associates during the irrigation season to collect the information needed to run the system and comply with legislation. Over the years, the number of associates and plots that received the service varied between 133 in 2017 and 101 in 2022 (Table 3.3-1). The measure started in 2015 and ended in 2020. It was extended in the next two years ,and it was replaced in 2023 by a new legislation (“Portaria n.542023,” n.d.).

Table 3.3-1IrrigaSys parcels that received counseling between 2017 and 2022

Year	Number of parcels
2017	133
2018	128
2019	132
2020	110
2021	100
2022	101

The implementation of IrrigaSys requires a substantial amount of information. Nevertheless, farmers are only required to provide a few simple basic inputs, which include the plot location, the crop and respective sowing date, the irrigation system, and the soil texture data. Similar requirements can be found in other DSS (Li et al., 2018; Yang et al., 2017). This information needs to be provided at the beginning of each growing season, and most is transferable from one season to the other. Farmers are also required to provide the daily/weekly irrigation inputs, which without it IrrigaSys cannot give reliable estimates of the soil water balance.

IrrigaSys selects then predefined MOHID-Land files from the options available in the database. The soil domain is always defined by a vertical grid discretized into 11 grid cells, with 1 m wide, 1 m long, and varying thickness from 0.05 m at the surface to 0.5 m at the bottom. Each grid cell then defines a control volume where the state variables (e.g. soil water contents) are computed in the center of the cells and fluxes (and related variables) on the faces. The surface boundary conditions are the T_p and E_p rates as well as rainfall and irrigation amounts. The bottom boundary condition is always set to free drainage. The soil hydraulic parameters of the Mualem-van Genuchten model (van Genuchten, 1980) are the main variables characterizing soils in the pre-defined MOHID-Land files. These are derived for each soil horizon using the texture data provided by farmers and the pedotransfer functions (PTFs) in Ramos et al. (2013). Exceptions are the plots where the MOHID-Land model has been implemented with more detail following previous studies (Ramos et al., 2017), which naturally adopt the locally calibrated/validated soil hydraulic parameters instead. For the initial conditions, all plots are set to field capacity.

IrrigaSys is connected to a network of ten weather stations (www.meteoagri.com), which provide the necessary data for computing the model surface boundary conditions for the hindcast period. Plots are associated to a specific weather station based on plot location. This weather network was already part of the service provided by ARBVS to their farmers' associates and needed only to be connected to IrrigaSys. The K_c values for the initial, mid-season, and end-season stages listed in Allen et al. (1998) are used to estimate crop water requirements. Gross irrigation needs are then computed from the net irrigation requirements and standard irrigation efficiency values characterizing irrigation systems. On the other hand, T_p reductions due to water stress are parametrized according to Wesseling et al. (1991)

database. The default values of the EPIC model for different crops are further considered for modeling crop development (Neitsch et al., 2011). Exceptions are again crops (maize, pasture, and vineyard) previously simulated by the MOHID-Land model in the region (Ramos et al., 2017) which calibrated/validated parameters serve as reference for all plots with the same characteristics. Finally, the NDVI maps are produced from the Sentinel-2 image tiles covering the Sorraia Valley region. Information is provided on a weekly basis, with the system maintaining the previous update when cloud cover is was above the threshold value (>10%).

3.3.3 System management

The IrrigaSys developers are the administrators of the system. The ARBVS technicians are granted the manager access level. They are responsible for setting up the plots in the system, activating it also at the beginning of each growing season. They further gather data related to irrigation events, every week, throughout the growing season, feeding directly the system with that information. By managing the system directly, the user's interface was built specifically to accommodate their requests and facilitate their job. This option came after previous unsuccessful DSS that were developed expecting farmers to contribute directly to the set up and management of the DSS. That never happened. In IrrigaSys, farmers are thus only given the user's access level.

The weekly gathering of irrigation data is the most extensive work needed for running IrrigaSys. This effort could obviously be minimized with automatic controllers and remote access to flowmeters installed in monitored fields, similarly to Abi Saab et al. (2019), but which option is not available. As this is fundamental for running the DSS, there are a set of rules in place to be followed when that information is not collected in due time. Most of these rules assume that the farmer has been conducting irrigation according to the DSS recommendations. As IrrigaSys always runs model simulations from the beginning of the growing season till the current date, the weekly water balance is then automatically updated whenever the missing real irrigation data is finally provided.

3.4 Discussion

IrrigaSys is a DSS developed in cooperation with irrigation managers and farmers to provide irrigation support on a weekly basis, accommodating their needs and requests in the best possible way. IrrigaSys is run on a demonstrative case located in the region, which serves to evaluate model performance on a weekly basis. However, the representativeness of this field is limited, with uncertainty associated to model predictions depending much on how well the

system is correctly configure in each agricultural field. The DSS requires a few basic inputs to run, but it is highly complex, demanding much more detailed soil, crop, and climate data than that given by farmers. Obviously, the more information is provided, the more reliable the outputs will be. As an example, in terms of soil characterization, the MOHID-Land model requires the complete description of soil hydraulic functions, i.e., the soil water retention and soil hydraulic conductivity curves from soil water content at saturation to oven dryness. These are fundamental for solving the non-linear partial differential equation used to simulate soil water dynamics. The direct determination of these properties in each plot would be ideal but highly utopic considering soil variability and the cost and time needed to perform such analyses. Instead, PTFs are used to indirectly estimate soil hydraulic parameters from soil texture data.

However, PTFs are also known to provide more robust estimates when additional soil data (e.g., dry bulk density, organic matter content) is used to complement soil texture (Van Looy et al., 2017). Thus, while more soil information should be provided by farmers, their knowledge on soil characteristics is usually limited to the texture class of the surface horizon and only a few know the soil particle distribution of their soils. Similar solutions were given in Todorovic et al., 2016, Li et al., 2018 and Abi Saab et al., 2019 to overcome the lack of soil hydraulic data. However, one should be aware that these DSS make use of much simpler simulation models for computing the soil water balance, with estimation errors associated to soil hydraulic data being likely smaller than in IrrigaSys.

Also, crop development plays here a fundamental role in the accurate computation of the soil water balance, where LAI values are decisive for the correct partition of ET_c rates into T_p and E_p. The accuracy of crop growth simulations depends much on a set of default parameters (Neitsch et al., 2011) that can hardly represent local conditions, much less season variability and the different sowing dates and crop varieties (with different cycles) that farmers adopt to cope with climate conditions. While IrrigaSys includes already a set of parameters calibrated/ validated locally for different crops, these are still insufficient to account for all possible variability. For this reason, farmers often contest IrrigaSys recommendations, particularly during the crop development and end-season stages, when the lengths of the crop stages in the system are misadjusted from reality. Hence, alternative options have been studied to better describe crop growth in the Sorraia Valley irrigation district. Ramos et al.(2018) analyzed the impact of assimilation of LAI data derived from Landsat 8 imagery on MOHID-Land

simulations. The main conclusion was that modeling vegetation growth at the plot scale could not depend solely on inputs from LAI data assimilation because estimates might diverge substantially from the reality, thus confirming the need to use a proper data set for calibration. Therefore, Simionesei et al. (2019a) used LAI data derived from the same satellite sensor for simply adjusting crop growth parameters and calibrating/validating the model (instead of assimilating it directly into the model), providing a more feasible solution for rapidly developing a large database of crop variability at the regional scale. The literature shows that crop parametrization in existing DSS is usually limited to basic variables as those used in water budget models (crop coefficient, duration of growing cycles, minimum and maximum root depth, optimum yield threshold) (Li et al., 2018, Abi Saab et al., 2019)), but examples can be found where more complex approaches were used. For example, Gu et al. (2020) modelled crop growth based on growing degree days using a large set of variables from different crop growth models.

One current limitation of IrrigaSys relies on not considering groundwater flow into the rootzone during the computation of the soil water balance. In the Sorraia Valley region, capillary rise plays a fundamental role in fulfilling crop water requirements in many agricultural plots (Cameira et al., 2003, Ramos et al., 2017), being thus essential its correct assessment for accurate irrigation scheduling. Solutions are still being analysed, which may include the remote monitoring of groundwater levels in existing piezometers or wells. The NDVI maps were added to IrrigaSys as farmers appreciated observing crop variability in their plots. Whether these maps were afterwards used for improving land management in their plots remains unknown. Nevertheless, the remote sensing module should be improved to also derive crop coefficients from vegetation indices, feeding the system with better and more reliable information on crop conditions. Finally, IrrigaSys outputs are nowadays accessed through a smartphone application developed in Android, but which is not available to all farmers since many use the iPhone Operation System (iOS) to which the application is not compatible.

3.5 Conclusions

IrrigaSys is a decision support system aimed at supporting irrigation water management at the field plot scale. The system provides optimized irrigation schedules as well as additional information (soil water balance, weather forecast for incoming days, satellite images) on a weekly basis to help farmers in the decision-making process. The system is highly complex but the data necessary to run it is minimal, and include the location of the agricultural field, the crop type, the sowing and harvest dates, the soil texture, and the characteristics of the irrigation

system in each plot as mandatory inputs. As the DSS is not remotely connected to sensors, information on applied daily/weekly irrigation depths is vital for the reliability of outputs.

IrrigaSys was developed using online, open source tools, having the flexibility to be implemented in any location in the world. However, the major strength results from the close cooperation between the academy and a local Water Board during its development, with many details being programmed based on irrigation managers suggestions, namely the decision rules to follow when irrigation data is not collected in due time to feed the system. On the other hand, the complexity of the DSS core engine as well as the inherent difficulties in calibrating/validating model parameters for all case scenarios constitutes a major weakness. Despite all these constraints, IrrigaSys has been performing reasonably well over the years, with some farmers considering the weekly information provided by the system before defining their irrigation scheduling. Nonetheless, their irrigation plans often deviate from the recommended ones. The crop development and end-season stages have always been the most conflicting stages, with outputs raising sometimes critics from farmers when misadjusted from reality. Critics are thus considered (and even welcomed) to help adjust model parameters to field conditions and reduce the uncertainty associated to model predictions. IrrigaSys needs thus to continue being developed to overcome such limitations and become a more trustworthy tool in irrigation water management.

4. Model calibration for three case studies: maize, pasture and grapevine

In this chapter, the calibration of the model for the main crops utilized in the Decision Support System (DSS), namely maize, pasture, and grapevine, is detailed. The outcomes of this calibration process have been documented in two scientific papers and a conference paper. The following succinctly presents the objectives of these articles/applications:

Chapter 4.1: This section focuses on modeling the dynamics of soil water and maize growth, taking into consideration the influence of shallow groundwater conditions. The study was conducted in the Sorraia Valley region of Portugal.

Chapter 4.2: In this part, the implementation of the MOHID Land model is discussed, specifically concerning the modeling of soil water dynamics and pasture growth.

Chapter 4.3: This section centers on the modeling of deficit irrigation in grapevine using the MOHID Land model.

These chapters collectively contribute to a deeper understanding of crop-specific interactions with soil and water dynamics, as well as how the MOHID Land model can effectively simulate these intricate processes for various crops.

4.1 Modelling soil water and maize growth dynamics influenced by shallow groundwater conditions in the Sorraia Valley region, Portugal

The material on which this chapter is based has been previously published in: Ramos, T.B., Simionesei, L., Jauch, E., Almeida, C., Neves, R., 2017. Modelling soil water and maize growth dynamics influenced by shallow groundwater conditions in the Sorraia Valley region, Portugal. Agricultural Water Management 185. https://doi.org/10.1016/j.agwat.2017.02.007

4.1.1 Introduction

In southern Europe, increasing water demand and withdrawals have been building up the pressure on fresh water resources, with agriculture accounting for more than half of the total water abstraction, rising to more than 80% in some regions (EEA, 2009). The problem has been enhanced by climate change, with climate projections showing a marked increase of summer temperatures and meteorological droughts (Kovats, 2014), and by economic development, with multiple economic activities (agriculture, energy production, industry, domestic use, tourism and recreation) competing for limited water resources. There is thus an immediate need for improving agricultural water management and for developing new strategies and management

options to address water use, performance, and productivity of agricultural systems (Todorovic et al., 2014).

Although irrigation plays a decisive role in increasing agricultural productivity and production stability in southern Europe, erroneous irrigation practices may also promote environmental degradation of an already ecologically sensitive region. Therefore, the European Commission has given top priority to the protection of natural resources in the context of the Europe 2020 Strategy, including the sustainability of water resources (European Commission, 2012, 2011). Following these policies, southern European countries have established specific policy instruments for maximizing the effectiveness and efficiency of irrigation water use. In this context, it seems essential the development of modern irrigation support tools to help farmers comply with legislation requirements and improve irrigation water management, including integrative modelling operational tools capable of simulating the full soil-water-atmosphere transfer system. These new modelling tools would not only help farmers improve irrigation water use at the plot scale but could also serve as support tools for evaluating the effectiveness of the policy instruments implemented.

The Sorraia Valley region, located in southern Portugal, is part of one of the most important agricultural areas in the country. Maize (Zea mays L.) is a leading crop in the region, occupying 25.6–44.9% of the total area irrigated during 2004–2014 (ARBVS, 2015). Water scarcity and inappropriate land management practices have been some of the most critical constraints to the sustainable production of maize and other agricultural crops. Over the last decade, agronomical research has focused on studying soil water flow and solute transport processes in the region to improve irrigation water management and optimize water use and water productivity. Some of the most relevant studies included the relationships between maize production and irrigation strategies (Paredes et al., 2014a), evaluation of economic impacts of various irrigation management strategies (Paredes et al., 2014b), and the assessment of nutrient (Cameira et al., 2007, 2003) and pesticide (Azevedo et al., 2000) fate while considering farmers' agricultural practices. However, while these studies included detailed field experiments and numerical modelling, and contributed in identifying the best management practices to be performed at the plot scale, most have only addressed part of the soil-water-atmosphere transfer system (mainly the root water uptake process) or included models that are currently not suitable to run as operational tools.

MOHID-Land is a physically-based mechanistic model developed at the Instituto Superior Técnico (Brito et al., 2015; Simionesei et al., 2016; Trancoso et al., 2009), capable of

simulating the full soil-water-atmosphere transfer system at the plot scale, including root water uptake, the influence of groundwater on the soil water balance, and crop development. Although conceptually different, MOHID-Land has embedded some of the approaches used by state-of-the-art models, such the HYDRUS software package (Šimůnek et al., 2016) and the SWAP model (Kroes and Van Dam, 2003), for describing physical processes at the plot scale. Recently, these reference models have been coupled with MODFLOW (Harbaugh et al., n.d.) and are today capable of combining processes in the vadose zone and groundwater (Twarakavi et al., 2008; Xu et al., 2012). They have also been coupled with the EPIC model (Neitsch et al., 2011; Williams et al., 1989) and can further simulate plant growth under different soil moisture, salinity, and temperature conditions (Han et al., 2015; Wang et al., 2015; Xu et al., 2015, 2013). Lately, the MOHID-Land model has been integrated in the FIGARO decision support system (DSS) for supporting irrigation water management in the Sorraia Valley region at the plot scale. The FIGARO DSS is a holistic and structured irrigation platform that offers farmers flexible, crop-tailored irrigation scheduling protocols for their specific fields. The FIGARO DSS is structured for data acquisition from monitoring devices (soil moisture sensors) and includes different forecasting meteorological and hydrological tools, enabling full decision support for end users at the plot scale (Linker et al., 2016). Nonetheless, a proper calibration/validation of the MOHID-Land model and the processes simulated at the plot scale were still missing, as well as the necessary developments for converting this model into an operational tool capable of optimizing irrigation scheduling and supporting irrigation water management practices.

Different soil-water balance models (Raes, 2002; Rosa et al., 2012; Vanuytrecht et al., 2014) are normally used for computing the irrigation scheduling for different crops, soils, and climate conditions. These models usually consider the soil domain simplistically, often defining it based on the notions of field capacity and the wilting point, with soil-water dynamics and irrigation scheduling being computed based on the soil-water storage capacity and atmospheric demands, as proposed by Allen et al. (1998), while other outputs such as percolation and capillary rise are defined using empirical or semi-empirical equations. Mechanistic models such as MOHID-Land are less commonly used for computing the irrigation scheduling as they require many parameters, including a full description of the soil hydraulic properties (i.e. the soil water retention and the unsaturated hydraulic conductivity curves), which measurements are complex and, thus, are not easily available for many regions of the world. Dabach et al. (2013) constitutes here a rare reference as these authors upgraded

the HYDRUS-1D model for computing irrigation scheduling by considering soil pressure heads, target thresholds, and crop evapotranspiration. Nonetheless, mechanistic models are usually considered to provide superior predictions of soil water contents than simpler soil water balance models, offering also larger capabilities in terms of irrigation water management. Hence, these models are today used, for example, for optimizing water saving practices in arid regions with shallow groundwater conditions (Ren et al., 2016; Xu et al., 2013) improving irrigation management with poor quality waters (Raij et al., 2016; Ramos et al., 2011); and quantifying the fate of agro-chemical contaminants in different ecosystems (Phogat et al., 2014; Ramos et al., 2012).

The main objective of this study was to use the MOHID-Land model for simulating soil-water flow and crop development in a plot with maize located in the Sorraia Valley region. The specific objectives were: (i) to predict soil water contents and fluxes, and the evolution of different crop growth parameters, including the leaf area index, canopy height, biomass, and yield during the 2014 and 2015 maize growing seasons; (ii) to compute the soil water balance while considering the effect of the groundwater table on soil water and maize growth dynamics; (iii) to implement a system-dependent boundary condition for automatically triggering irrigation when a certain threshold was reached at the root zone; and (iv) to optimize ' irrigation scheduling practices by analyzing different groundwater levels and threshold scenarios. The modelling approach will help us improve the model performance in the FIGARO DSS, and consequently irrigation water management practices at the plot scale, in the Sorraia Valley region.

4.1.2 Material and methods

4.1.2.1 Field experiment

This study was conducted at Herdade do Zambujeiro, located near Barrosa, Sorraia Valley, southern Portugal (38◦58′0.97′′N, 8◦44′46.63′′W), during the 2014 and 2015 growing seasons. The climate in the region is semi-arid to dry sub-humid, with hot dry summers and mild winters with irregular rainfall. Hourly weather data used in this study was taken from a meteorological station located nearby and included the average temperature (ºC), wind speed (m s^{-1}), relative humidity (%), global solar radiation (W m^{-2}), and precipitation (mm). These data were then used to determine the hourly reference evapotranspiration (ET_0, mm d^{-1}) using the FAO Penman-Monteith method (Allen et al., 1998) (Figure 4.1-1).

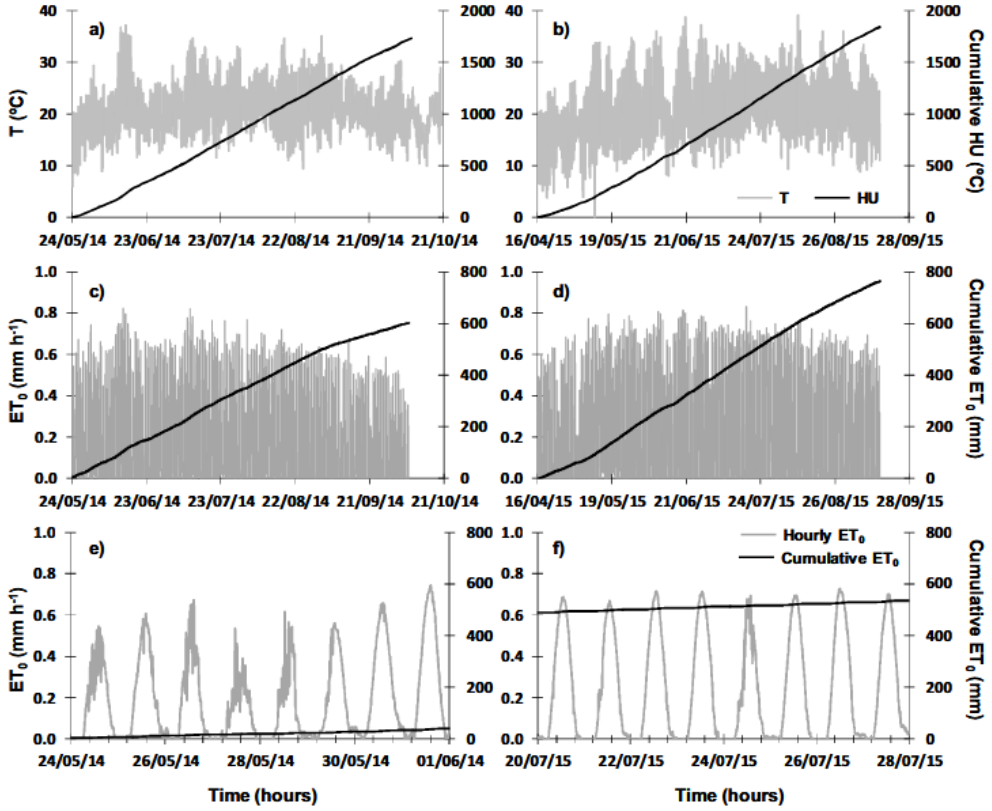

Figure 4.1-1 Hourly values of air temperature (T) and cumulative heat units (HU) during 2014 (a) and 2015 (b) crop seasons (top); hourly reference evapotranspiration (ET_0) during 2014 (c) and 2015 (d) crop seasons (middle); and hourly ET0 during a random week (detailed view) of 2014 (e) and 2015 (f) crop seasons (bottom).

The soil was classified as Haplic Fluvisol (IUSS Working Group WRB, 2014). The soil's main physical and chemical properties are presented in Table 4.1-1. The particle size distribution was obtained using the pipette method for particles having diameters <2µm (clay fraction) and between 2 and 20µm (silt), and by sieving for particles between 20 and 200µm (fine sand) and between 200 and 2000µm (coarse sand). These textural classes follow the Portuguese classification system (Gomes and Silva, 1962) and are based on international soil particle limits (Atterberg scale). The dry bulk density (pb, g cm^{-3}) was obtained by drying volumetric soil samples (100 cm^3) at 105 ºC for 48 h. The organic matter (OM, %) content was estimated from the organic carbon (OC, %) content determined by the Walkley–Black method, using the relation OM = 1.724 × OC (Nelson and Sommers, 1983). The soil water retention curve, θ(h), was determined on undisturbed soil samples (100 cm^3) using suction tables with sand for pressure heads above 10 kPa (Romano et al., 2002), and a pressure plate apparatus for pressure heads below 33 kPa (Dane and Topp, 2020). The saturated hydraulic conductivity (K_{sat}, cm d^{-1}) was determined on undisturbed soil samples (630 cm^3) using a constant-head method (Stolte, 1997).

Table 4.1-1 Main physical and chemical soil characteristics.

	Soil layers			
Depth (m)	0–0.2	0.2–0.4	0.4–0.6	0.6–0.8
Coarse sand, 2000–200 μm (%)	3.4	6.8	11.5	14.7
Fine sand, 200–20 μm (%)	44.6	47.8	53.6	48.4
Silt, 20–2 μm (%)	33.3	28.1	20.6	23.2
Clay, <2 μm (%)	18.8	17.3	14.3	13.7
Texture	Silty Loam	Loam	Loam	Loam
Bulk density ($g\,cm^{-3}$)	1.57	1.52	1.66	1.66
Organic matter (%)	1.73	0.96	0.57	0.59
van Genuchten-Mualem parameters:				
θ_r ($cm^3\,cm^{-3}$)	0.078	0.067	0.065	0.065
θ_s ($cm^3\,cm^{-3}$)	0.393	0.356	0.340	0.340
α (cm^{-1})	0.009	0.016	0.005	0.005
η (–)	1.75	1.31	1.80	1.80
ℓ (–)	−1.0	−1.0	−1.0	−1.0
K_s ($cm\,d^{-1}$)	500.3	22.6	0.7	0.7

θ_r, residual water content; θ_s, saturated water content; α and η, empirical shape parameters; ℓ, pore connectivity/tortuosity parameter; K_s, saturated hydraulic conductivity.

The field was cropped with maize hybrid P1574 (FAO 600) with a density of approximately 89,000 plants ha^{-1}. Management practices, including fertilization and irrigation, were performed according to the standard practices in the region and were decided by the farmer. During 2014, maize was sown on May 24 and harvested on October 8; the net rainfall reached 163 mm, while the net irrigation amounted 365 mm (Figure 4.1-2). During 2015, maize was sown on April 16 and harvested on September 20; the net rainfall reached only 12 mm, while the net irrigation summed 620 mm (Figure 4.1-2). The dates of the most relevant crop growth stages are presented in Table 4.1-1. Irrigation was applied with the farmer's stationary sprinkler system, wherein a Christiansen's coefficient of uniformity (CU, Christiansen, 1942) value of 71% was measured at the beginning of the 2014 growing season. Although this CU value can be considered 'low' (CU < 84%; (Keller and Bliesner, 1990)), maize crops always exhibited good homogeneity throughout the seasons due to the shallow depth of the groundwater table (Figure 4.1-1).

One SM1 capacitance probe (Adcon Telemetry, Klosterneuburg, Austria) and one ECH2O-5 capacitance probe (Decagon Devices, Pullman, WA) were installed at depths of 10, 30, and 50 cm to continuously measure soil water contents. TDR probes with waveguides from the Trase System (Soil Moisture Equipment Corp., Goleta, CA) were also installed at the same depths and locations to measure the soil water content every 15 days. TDR readings were used to calibrate the capacitance probes. One LEV1 level sensor (Adcon Telemetry, Klosterneuburg, Austria) was used to continuously monitor the groundwater level (Figure 4.1-2). One RG1

(Adcon Telemetry, Klosterneuburg, Austria) and two QMR101 (Vaisala, Helsinki, Finland) rain gauges were used to measure the amount of water applied per irrigation event (Figure 4.1-2).

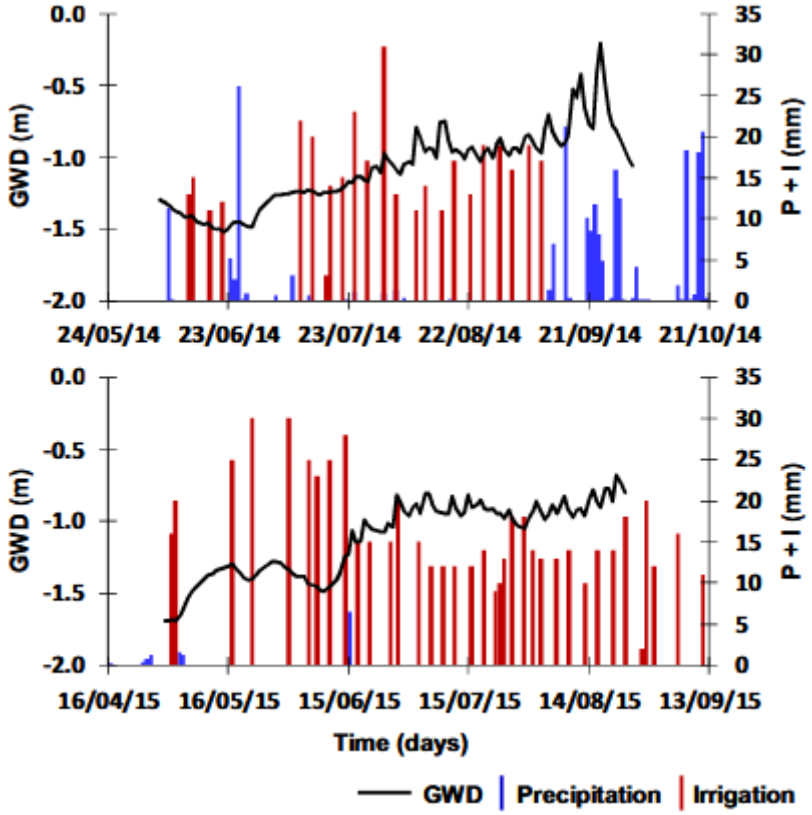

Figure 4.1-2 Daily values of precipitation, irrigation, and groundwater depth (GWD) during 2014 (top) and 2015 (bottom) crop seasons.

Table 4.1-2 Dates of crop growth stages.

Stage	2014		2015	
	Days	Date	Days	Date
Initial	31	24 May	37	16 Apr
Canopy development	30	24 Jun	32	23 May
Mid-season	52	24 Jul	53	24 Jun
Late season	27	14 Sep	26	16 Aug
Harvest	–	8 Oct	–	20 Sep

Leaf area index (LAI, m^2 m^{-2}), crop height, and the aboveground dry biomass were monitored every 15 days throughout each maize growing season by harvesting 3 random plants, every date. The same crop parameters were measured at the end of each crop season, but by harvesting all plants in a random area of 1.5 m^2 corresponding to approximately 12 plants). The length and width of crop leaves were measured in every harvested plant and then converted to LAI values as documented in Ramos et al. (2012a). The aboveground dry biomass was

determined by oven drying maize stems, leaves, and grain at 70 ºC to a constant weight. Maize yield was obtained from the grain's dry biomass measured at the end of each crop season.

4.1.2.2 Model setup, calibration and validation

The simulation period covered the full 2014 and 2015 growing seasons, being set from sowing to harvest in each year (Table 4.1-2). The soil profile was specified with 2 m depth, divided into four soil layers according to observations (Table 4.1-2). For depths below 0.8 m, the soil properties were assumed to be the same as those in the last observed layer. The soil domain was represented using an Arkawa C-grid type (Purser and Leslie, 1988), defined by one vertical column discretized into 100 grid cells with 1 m wide, 1 m long, and 0.02 m thickness each (i.e., 1 × 1 × 0.02 m^3) (Figure 4.1-3). Each grid cell then defined a control volume where the state variables (e.g. soil water contents) were computed in the center of the cells, and fluxes (and related variables) on the faces. Only vertical fluxes were possible with the specifications mentioned above (one-dimensional domain).

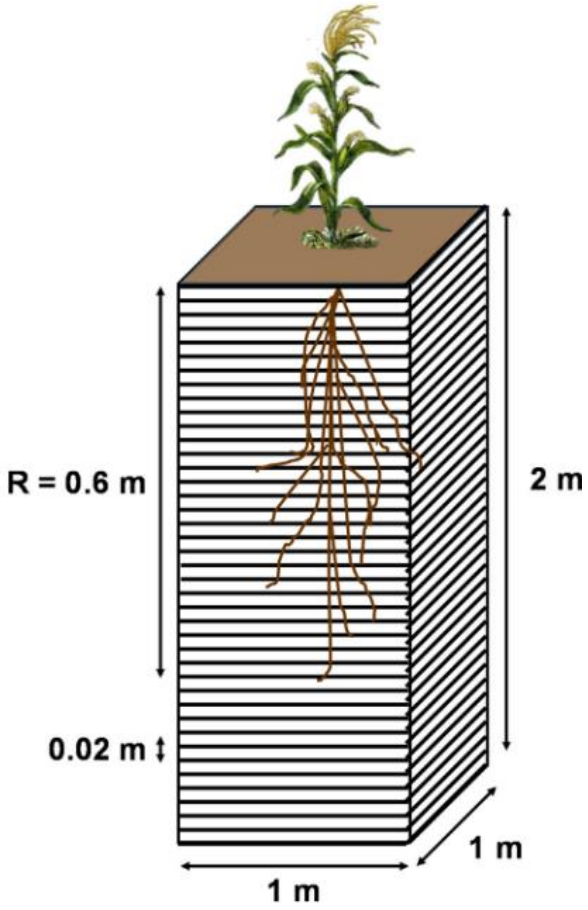

Figure 4.1-3 Soil domain discretization (R, root zone domain).

The upper boundary condition was determined by the actual evaporation and transpiration rates, and the irrigation and precipitation fluxes (Figure 4.1-2). ET_c values were

computed from hourly ET_0 values presented in Figure 4.1-1, using K_c values of 0.30, 1.20, and 0.35 for the initial, mid-season, and late season crop stages, respectively. These values were taken from Allen et al. (1998)) and correspond to standard K_c values for the Mediterranean region. The K_c value for the initial crop stage was then adjusted for the frequency of the wetting events (precipitation and irrigation) and average infiltration depths, while the K_c values for mid-season and late season crop stages were adjusted for local climate conditions taking into consideration crop height, wind speed, and minimum relative humidity averages for the periods under consideration (Allen et al., 1998). The following parameters of the Feddes et al. (1978) model were used to compute T_p reductions due to water stress: h_1 = -15, h_2 = -30, h_3 = -325 to -600, h_4 = -8000 cm (Wesseling et al., 1991). The bottom boundary condition was specified using the observed groundwater depth (GWD, Figure 4.1-1). The initial soil water content conditions were set to field capacity.

Datasets relative to 2014 and 2015 were used to calibrate and validate the model, respectively. The soil hydraulic parameters (Table 4.1-1) and the crop parameters (Table 4.1-3) were calibrated until deviations between the observed and simulated values were minimized. A trial-and-error procedure was adopted. First, the parameters of the van Genuchten-Mualem equations were determined with the RETC computer program (Van Genuchten et al., 1991) from soil hydraulic data ($\theta_{(h)}$ and K_{sat}) measured in different soil layers, and used in model simulations. The soil hydraulic parameters θ_s, α, η, and K_{sat} were then modified to reduce the deviations between the observed and simulated soil water contents. The parameter θ_r was not modified, following Šimůnek et al. (1998) and Jacques et al. (2002), who found that this parameter did not significantly influence soil moisture simulations. The connectivity/tortuosity parameter l was also not adjusted, being set to 1 following Schaap and Leij (2000a). Then, the crop parameters were calibrated by optimizing the default values of the EPIC model for maize (Neitsch et al., 2011) until deviations between the observed and simulated LAI, hc, and ABG biomass were minimized. Finally, the soil hydraulic parameters (θ_s, α, η, and K_{sat}) were again adjusted until the best fit between the simulated and observed soil water contents was reached. The model was considered calibrated when the statistical indicators obtained for the validation period (2015) were within the same range as those determined for the calibration period (2014).

Table 4.1-3 Optimized parameters of the crop growth model.

Optimized parameters of the crop growth model.

Crop parameter	Value
Optimal temperature for plant growth, T_{opt} (°C)	25.0
Minimum temperature for plant growth, T_{base} (°C)	8.0
Plant radiation-use efficiency, RUE [(kg ha^{-1}) (MJ m^{-2})$^{-1}$]	39.0
Total heat units required for plant maturity, PHU (°C)	1900
Fraction of PHU to reach the end of stage 1 (initial crop stage), $fr_{PHU,init}$ (−)	0.20
Fraction of PHU to reach the end of stage 2 (canopy development stage), $fr_{PHU,dev}$ (−)	0.43
Fraction of PHU after which LAI starts to decline, $fr_{PHU,sen}$ (−)	0.73
Maximum leaf area index, LAI_{max} (m^2 m^{-2})	6.5
Fraction of LAI_{max} at the end of stage 1 (initial crop stage), $fr_{LAImax,ini}$ (−)	0.05
Fraction of LAI_{max} at the end of stage 2 (canopy development stage), $fr_{LAImax,dev}$ (−)	0.95
Maximum canopy height, $h_{c,max}$ (m)	3.10
Maximum root depth, $Z_{root,max}$ (m)	0.6
Potential harvest index for the crop at maturity, HI_{opt} (−)	0.49
Minimum harvest index allowed, HI_{min} (−)	0.30

Model calibration and validation was performed by comparing field measured values of soil water contents, LAI, hc, and ABG biomass with the MOHID-Land simulations using various quantitative measures of the uncertainty, such as, the coefficient of determination (R^2), the root mean square error (RMSE), the ratio of the RMSE to the standard deviation of observed data (NRMSE), the percent bias (PBIAS), and the model efficiency (EF), respectively given by:

$$R^2 = \left\{ \frac{\sum_{i=1}^{n}(O_i-\bar{O})(P_i-\bar{P})}{\left[\sum_{i=1}^{n}(O_i-\bar{O})^2\right]^{0.5}\left[\sum_{i=1}^{n}(P_i-\bar{P})^2\right]^{0.5}} \right\}^2 \quad \text{Equation 27}$$

$$RMSE = \sqrt{\frac{\sum_{i=1}^{n}(O_i-P_i)}{n-1}} \quad \text{Equation 28}$$

$$NRMSE = \frac{RMSE}{\sqrt{\sum_{i=1}^{n}(O_i-\bar{O})}} \quad \text{Equation 29}$$

$$PBIAS = 100\frac{\sum_{i=1}^{n}(O_i-P_i)^2}{\sum_{i=1}^{n}O_i} \quad \text{Equation 30}$$

$$EF = 1 - \frac{\sum_{i=1}^{n}(O_i-P_i)^2}{\sum_{i=1}^{n}(O_i-\bar{O})^2} \quad \text{Equation 31}$$

where O_i and P_i are respectively the observed and model predicted values at time i, $\bar{O}$ and $\bar{P}$ are the respective mean values, and n is the number of observations. R^2 values close to 1 indicate that the model explains well the variance of observations. RMSE, NRMSE, and PBIAS values close to zero indicate small errors of estimate and good model predictions (Legates and McCabe, 1999; Moriasi et al., 2007; Wang et al., 2012) . Positive or negative PBIAS values refer to the occurrence of under- or over- estimation bias, respectively. Nash and Sutcliffe (Nash and Sutcliffe, 1970) modelling efficiency EF values close to 1 indicate that the residuals variance is much smaller than the observed data variance, hence the model predictions

are good; contrarily, when EF is very close to 0 or negative there is no gain in using the model, i.e., $\overline{O}$ is as good or better predictor than the model.

4.1.3 Results and discussion

4.1.3.1 Soil water contents

Figure 4.1-4 shows the daily averages of the soil water contents measured with capacitance probes at depths of 10, 30, and 50 cm during the 2014 and 2015 growing seasons, and compares these values with the MOHID-Land simulations. Soil water content measurements increased rapidly with irrigation or precipitation and then gradually decreased until the next irrigation/precipitation event because of water uptake and redistribution. Soil water content variations were expectably larger near the soil surface where root water uptake and soil evaporation were more pronounced. The bottom layers (>40 cm) also showed smaller water content variations due to their hydraulic characteristics (Table 4.1-1), mostly affected by continuous heavy ploughing practices over the years which resulted in some soil compaction.

Table 4.1-4 presents the statistical indicators used to evaluate the level of agreement between measured values and the MOHID-Land simulations. MOHID-Land performed reasonably well when simulating soil water contents during the 2014 calibration period. The value of R^2 was relatively high (0.73), showing that the model could explain the variability of the observed data. The errors of the estimates were quite small, resulting in a RMSE value of 0.018 $cm^3\ cm^{-3}$, and a NRMSE value of 0.061. The PBIAS value was 1.53%, indicating some overestimation of the measured data. The modelling efficiency EF was also high (0.70), indicating that the residual variance was much smaller than the measured data variance. The goodness-of-fit indicators obtained were thus within the range of values reported in the literature for water content simulations using different state-of-the-art transient vadose zone models (Han et al., 2015; Kröbel et al., 2010; Wang et al., 2014, 2015; Xu et al., 2015, 2013; Yu et al., 2006).

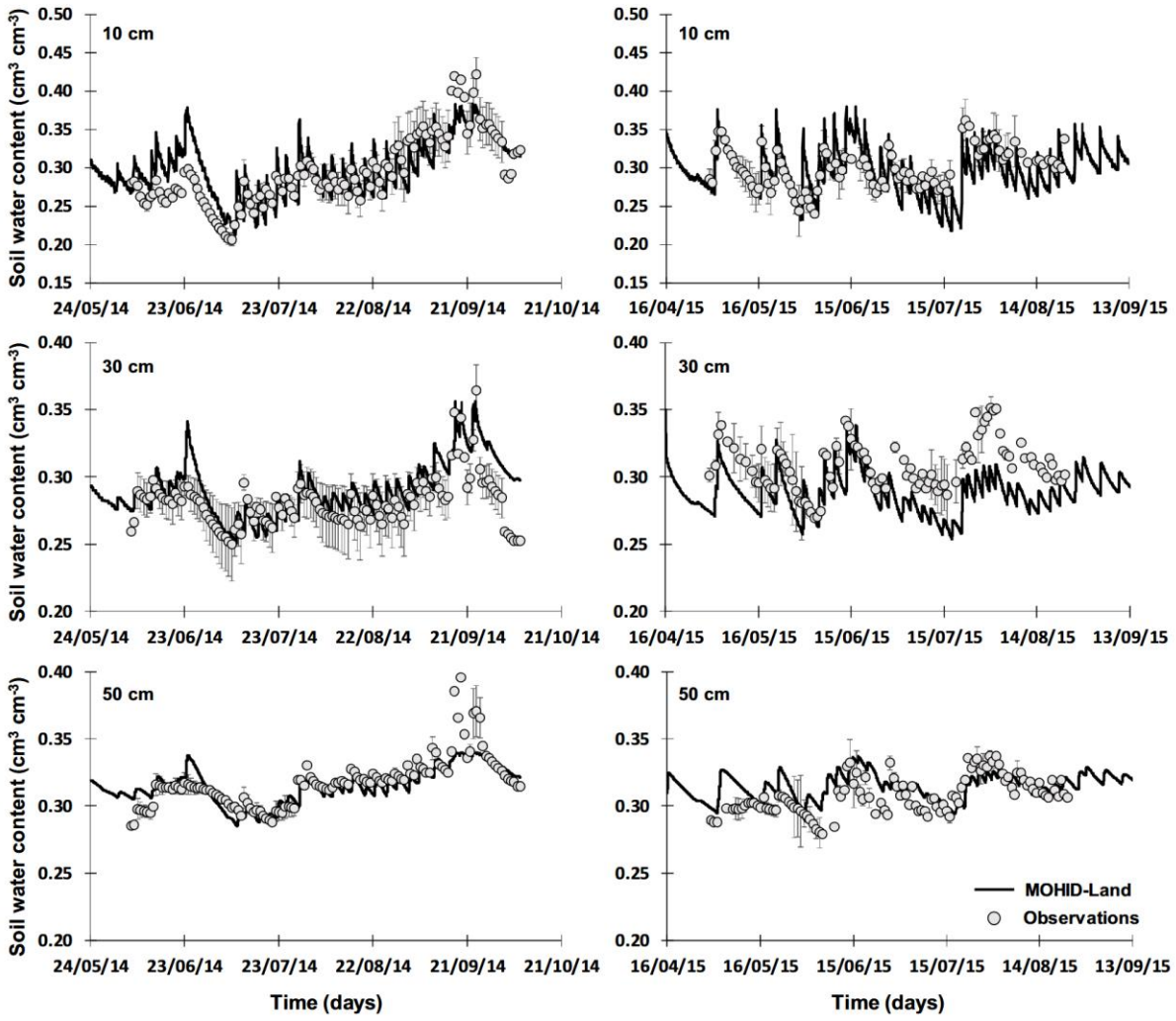

Figure 4.1-4 Measured and simulated soil water contents at depths of 10 (top), 30 (middle), and 50 cm (bottom) during 2014 (left) and 2015 (right) crop seasons. Vertical bars correspond to the standard deviation of measured data.

Similarly, the MOHID-Land model performed satisfactory when simulating soil water contents during the 2015 validation period. The errors of the estimates were very similar to those determined for the 2014 dataset, resulting in a RMSE value of 0.019 cm^3 cm^{-3}, and a NRMSE value of 0.063. The PBIAS value was 1.91%, this time indicating some underestimation of the measured data which was specially noticed at 30 cm depth (Figure 4.1-4). The R^2 value (0.37) and the modelling efficiency EF (0.11) were substantially reduced though Yet, the EF value can still be considered as acceptable. Ramos et al. (2012a) and Dabach et al. (2013) described how deviations between the measured and simulated water contents can be attributed to different causes, including errors related to field measurements, model inputs, and model structure. Most of those causes can also be considered here for explaining deviations observed in the 2015 dataset.

4.1.3.2 Crop growth

The LAI, h_c, and the aboveground biomass values estimated with the MOHID-Land model were also in agreement with the 2014 field observations (Figure 4.1-5). The RMSE values obtained by comparing simulated and measured LAI, h_c, and aboveground biomass values were 0.63 m^2 m^{-2}, 0.42 m, and 5128.3 kg ha^{-1}, respectively, whereas the NRMSE values were 0.16, 0.22, and 0.39 for the same crop growth parameters (Table 4.1-4). The R^2 values were higher than 0.93. The positive PBIAS values found for LAI (6.4%) and for the aboveground biomass (19.2%) showed a slight underestimation of the model simulations, whereas the negative PBIAS value found for h_c (-11.83%) showed a slight overestimation of this parameter. Nonetheless, the modelling efficiency (EF 0.87) was very high, thus indicating good model performance overall for all three crop growth parameters. During the 2015 validation period, the MOHID-Land simulations produced very similar goodness-of-fit indicators as those obtained for the 2014 calibration period (Table 4.1-4), proving that the crop parameters presented in Table 4.1-3 were properly calibrated.

Table 4.1-4 Results of the statistical analysis between measured and simulated soil water contents, leaf area index (LAI), canopy height, and aboveground dry biomass

Results of the statistical analysis between measured and simulated soil water contents, leaf area index (LAI), canopy height, and aboveground dry biomass.

Statistic	Water content (cm^3 cm^{-3})	LAI (m^2 m^{-2})	Canopy height (m)	Aboveground dry biomass (kg ha^{-1})
Calibration set (2014)				
R^2	0.73	0.97	0.93	0.94
RMSE	0.018	0.63	0.42	5128.3
NRMSE	0.061	0.16	0.22	0.39
PBIAS	−1.53	6.40	−11.83	19.20
EF	0.70	0.94	0.90	0.87
Validation set (2015)				
R^2	0.37	0.97	0.96	0.93
RMSE	0.019	0.61	0.33	4616.8
NRMSE	0.063	0.15	0.17	0.33
PBIAS	1.91	6.31	−11.00	15.27
EF	0.11	0.94	0.93	0.89

R^2, coeficient of determination; RMSE, root mean square error; NRMSE, normalized RMSE; PBIAS, percent bias; EF, modelling efficiency.

The simulated and observed crop yields were 14,670 and 16,093 kg ha^{-1}, respectively, during the 2014 calibration period, and 17,930 and 17,300 kg ha^{-1}, respectively, during the 2015 validation period. Hence, yield predictions expectably followed the same under- and overestimation tendencies observed in simulations of the aboveground dry biomass.

In our study, the sowing dates varied considerably between the two growing seasons (Table 4.1-2). The early start of the 2015 growing season meant less heat units accumulated during its first weeks than in 2014. Yet, the modelling results showed that crop parameters presented in Table 4.1-3 were conservative enough and only one year of data was sufficient for their calibration. This confirmed the adequateness and robustness of the modelling approach

implemented in the MOHID-Land model. Likewise, similar modified versions of the EPIC crop growth model have been successfully coupled with different state-of-the-art transient vadose zone models, and the heat unit theory has been tested as a reliable predictor in many modelling applications (Ficklin et al., 2010; Han et al., 2015; Steduto et al., 1995; Wang et al., 2014, 2015; Xu et al., 2015, 2013). Thus, based on Table 4.1-4 and Figure 4.1-5, it can be considered that the MOHID-Land could also simulate maize growth in the Sorraia Valley region.

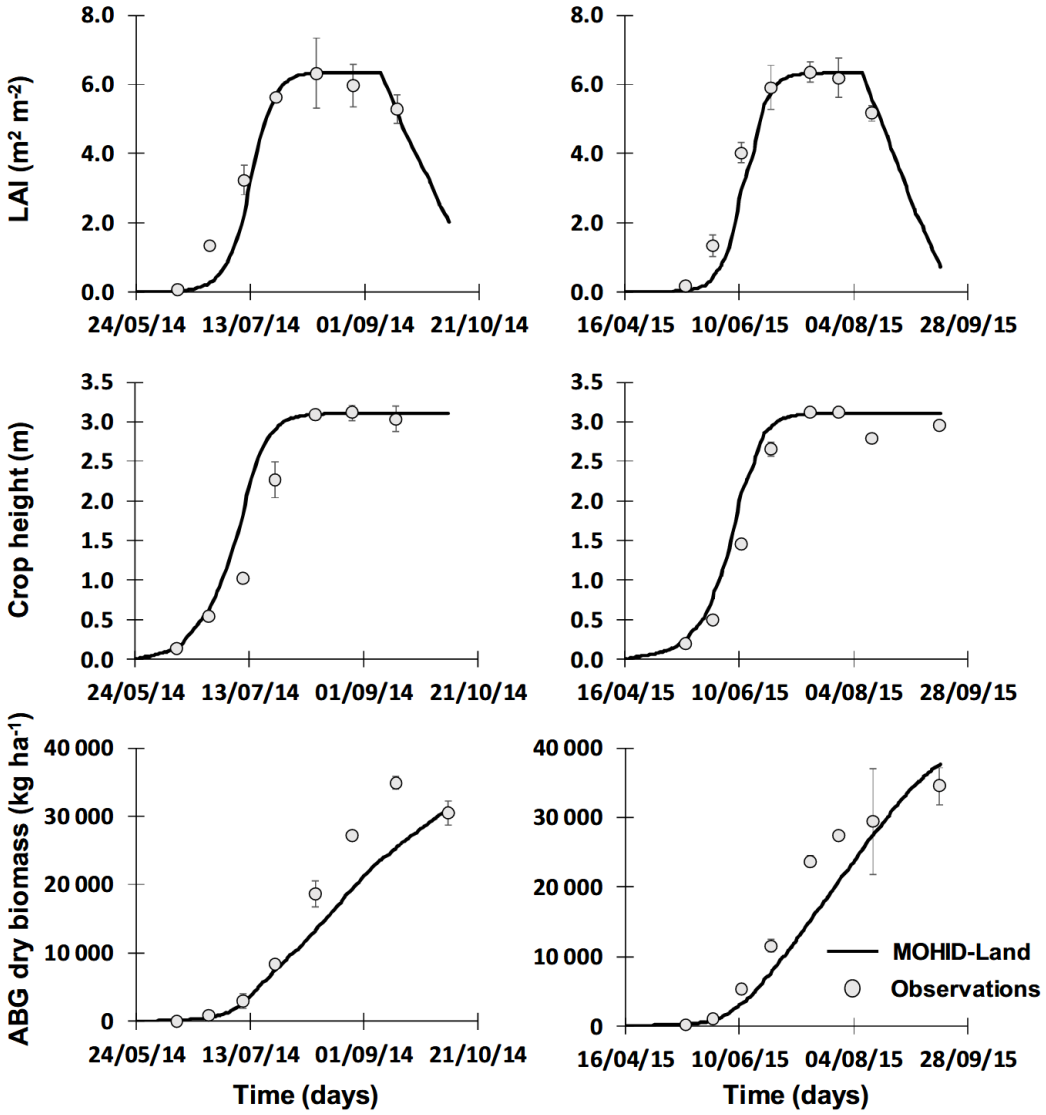

Figure 4.1-5 Measured and simulated leaf area index (top), canopy height (middle), and aboveground (ABG) dry biomass (bottom) during 2014 (left) and 2015 (right) crop seasons.

Table 4.1-5 Components of the soil water balance.

	Inputs				Outputs				
	P (mm)	I (mm)	CR (mm)	ΔSS (mm)	E_a (mm)	T_a (mm)	T_a/T_p (−)	DP (mm)	WP (kg m^{-3})
Farmer:									
2014	163	365	78	16	164	374	0.99	74	2.36
2015	12	620	94	11	181	481	1.00	75	2.43

4.1.3.3 Model inclusion in a DSS service

As previously mentioned, a properly calibrated/validated mechanistic model such as the MOHID-Land model can provide very accurate predictions of soil water contents and the components of the soil water balance, offering many solutions for improving irrigation water management at the plot scale. The new system- dependent boundary condition implemented in the model for automatically triggering irrigation when a certain threshold is reached at the root zone follows a physically-based approach and seems practical enough for operational use in an irrigation service like the FIGARO DSS since the threshold limits for most crops can be found in the literature (Wesseling et al., 1991). However, users should always consider that these threshold values usually represent averages for particular climates or crop varieties, meaning that some uncertainty should always be taken into account when applying it to different conditions.

However, the main challenge seems undoubtedly to be with the application of the new optimization tool to different soils since the model requires a detailed and accurate description of the soil hydraulic properties (i.e., the soil water retention and the unsaturated hydraulic conductivity curves). That information is usually not available as is the case of the Sorraia Valley irrigation district. Although alternatives are available today for the indirect estimation of the soil hydraulic parameters from basic soil properties using pedotransfer functions (Pachepsky and Rawls, 2004), these approaches also have their own limitations as most were never properly evaluated for describing soil water dynamics in the regions they intend to represent (i.e., a proper functional evaluation was mostly never done).

Crop season variability, particularly the length of crop seasons, may also have a direct influence on model results since shorter/longer crop seasons will necessary require adjustments in some crop parameters given in Table 4.1-3 (e.g., PHU). As model calibration/validation for every field assisted by a DSS is impractical, crop and soil databases are thus necessary to provide the necessary inputs for model simulations and complement the model running in operational mode. Hence, model recommendations should always be sustained by an agronomist service to assess model performance and uncertainties.

4.1.4 Conclusions

The MOHID-Land model could successfully simulate soil water dynamics and maize development in a plot located in the Sorraia Valley region, southern Portugal. Model estimates of the soil water content, LAI, canopy height, aboveground biomass, and maize yields showed a general good agreement with field data measured during the 2014 and 2015 growing seasons. Farmer's irrigation practices maintained soil water contents near field capacity, maximizing root water uptake and yields. Capillary rise was an important component of the soil water balance, contributing 14% of ET_c. However, deep percolation values showed an inefficient use of the water applied. Thus, the irrigation scheduling practices could be improved to better consider the soil's water holding capacity and the contribution of the shallow groundwater to the root zone. Future work should consider testing the new system-dependent boundary condition for different soils, particularly for soils with heavier textures, wherein the amount of water applied per irrigation event (I_{max}) needs to be also defined while considering soil infiltration constraints in order to prevent surface runoff and soil erosion.

4.2 Modeling soil water dynamics and pasture growth in the montado ecosystem using MOHID land

The material on which this chapter is based has been previously published in: Simionesei, L., Ramos, T.B., Oliveira, A.R., Jongen, M., Darouich, H., Weber, K., Proença, V., Domingos, T., Neves, R., 2018. Modeling soilwater dynamics and pasture growth in the montado ecosystem using MOHID land. Water (Switzerland) 10. https://doi.org/10.3390/w10040489

4.2.1 Introduction

The southern region of the Iberian Peninsula is characterized by a savanna-type agro-silvo-pastoral ecosystem, known as montado in Portugal (hereafter adopted) and dehesa in Spain (Aronson et al., 2012; Pinto-Correia et al., 2011). The montado system consists of an open formation of cork (Quercus suber L.) and holm oak (Quercus ilex rotundifolia L.) trees, presenting high levels of spatial variability in terms of density, combined with fallow land or pastures, which can be natural, improved, or cultivated (Pinto-Correia and Mascarenhas, 1999; Santos et al., 2015). The structural diversity of the system combines with the good overall habitat connectivity over its area of distribution, allowing animals to move around their territories, find mates, hunt, forage, and reproduce, resulting in high levels of biodiversity. As a result, the montado is considered as a High Natural Value system (Pinto-Correia et al., 2011), providing various ecosystem services (ES) that are perceived by farmers, stakeholders, and

society in general as being important for human welfare (Garrido et al., 2017; Guerra and Pinto-Correia, 2016; Pinto-Correia and Azeda, 2017).

In the last decades, the implementation of the European Common Agricultural Policy has led to an intensification of grazing, which has caused additional stress to the system, promoting the spread of tree diseases and preventing the natural regeneration of the ecosystem (Fragoso et al., 2011; Pinto-Correia and Mascarenhas, 1999; Santos et al., 2015). The most significant transformations have been (i) the increase of the stocking (or livestock) pressure (i.e., the replacement of sheep by cattle, the replacement of light indigenous breeds of cattle by heavier breeds, and the increase of livestock units per area); and (ii) the use of heavy machinery for shrub control (Pinto-Correia and Azeda, 2017). These changes have exhausted the natural pastures, decreased tree regeneration, and degraded water and soil quality (Pinto-Correia and Azeda, 2017; Pinto-Correia and Mascarenhas, 1999). Therefore, there is the need for the development of policy instruments that consider the specificities of the montado silvopastoral system; otherwise, its future will be severely threatened in the short term (Guerra and Pinto-Correia, 2016; Pinto-Correia and Azeda, 2017; Sandor et al., 2016).

One major challenge for improving system management is understanding soil water dynamics in the pasture component of the montado ecosystem, allowing for its improved management regarding grazing, and hence its capacity to withstand increased stocking pressure. Mediterranean grassland species have evolved adaptive strategies to avoid or endure severe summer droughts, adjusting their lifecycle to seasonal water availability (Tenhunen et al., 1990). The emergence of plants depends on the timing of the first autumn precipitations, and their active period is in winter and early spring, with senescence in May (Hussain et al., 2009; Jongen et al., 2013a, 2013b, 2011). In montado systems, the understory plays an important role in the functioning of the ecosystem (Jongen et al., 2011), having a variable productivity that responds to the temperature and precipitation (P) regimes. The relationship between soil water and biomass also influences whether these ecosystems act as CO_2 source or sink, with Jongen et al., 2011 suggesting that in dry years grasslands may act as a source of CO_2, while in more humid years they may act as a sink. With climate change scenarios suggesting a decrease in annual precipitation in mid-latitude temperate regions, accompanied by increasing temporal variability of precipitation and drought risks (Christiansen, 1942; IPCC, 2013; Jongen et al., 2013b), it is thus essential to develop tools for accurately quantifying the soil water balance and net primary production, and improving system management. The additional variability in precipitation also introduces the possibility of an additional

management alternative: the use of irrigated pastures. These both allow a smoothing of the effects of precipitation variability in rainfed pastures and provide a buffer of forage production, to release grazing pressure from rainfed pastures when that production is inadequately high.

Today, several process-based models, such as the BIOME–BGC (White et al., 2000), STICS (Brisson et al., 2003), SPACSYS (Wu et al., 2007), EPIC (Williams et al., 2008), ARMOSA (Perego et al., 2013), and PaSim (Ma et al., 2015) models, are available for simulating soil water dynamics and vegetation growth in grasslands. Most of these models provide an integrated perspective by taking into account the various vegetation, soil, and weather processes regulating energy and matter exchanges in agroecosystems. Some of these processes though, as in the cases of the EPIC (Williams et al., 2008) and PaSim (Ma et al., 2015) models, are described in a simplistic way. For example, soil water dynamics is usually defined based on the notion of field capacity and the wilting point, with soil water storage capacity being computed from atmospheric demands, while other outputs, such as capillary rise and percolation, are computed empirically. Other process-based models, such as SPACSYS (Wu et al., 2007), and ARMOSA (Perego et al., 2013), make use of the Richards equation for computing soil water dynamics, thereby providing a more physically-based approach for predicting soil water contents and fluxes. Another example is the MOHID-Land model (Trancoso et al., 2009), which is a distributed model based on primitive equations for surface runoff and flow in both the vadose zone and the aquifer. Flow in porous media is based on the Richards equation, while infiltration can be simulated using Darcy's equation and surface pressure, due to the surface runoff water column or by using empirical algorithms (e.g., Green and Ampt). The MOHID-Land model further includes a modified version of the EPIC model (Williams et al., 2008) for simulating crop development and biomass growth, which can potentially be used for estimating the stocking rates in the montado ecosystem and prevent soil degradation.

Hence, the objectives of this study were (i) to calibrate/validate the process-based MOHID-Land model (Trancoso et al., 2009) for estimating soil water dynamics and dry biomass growth in a rainfed and irrigated pasture during the 2010–2011 and 2011–2012 seasons; (ii) to estimate pasture irrigation (I) needs, using the calibrated model for the 1979–2009 seasons (30 years); and (iii) to compare the soil water balance and dry biomass estimates in rainfed and irrigated pastures during both wet and dry seasons, providing an insight on the influence of climate variability on model performance. The hypotheses addressed in this study were (i) that the MOHID-Land model could accurately estimate the soil water balance and

aboveground biomass growth in pastures under different management regimes; (ii) that the model could be used for irrigation scheduling; and (iii) that climate variability had a significant effect on model estimates. The results of this study will help to support the decision-making process regarding ecosystem management, by better accounting for the stocking rates and reducing the adverse impact of grazing in the montado ecosystem.

4.2.2 Material and Methods

4.2.2.1 Field Site Description and Data

The field data was collected at Herdade da Machoqueira do Grou, located near Coruche, southern Portugal (39º08′16" N, 08º20′03" W). The climate in the region is dry and sub-humid, with mild winters and hot, dry summers. The mean annual temperature is 15.9 ºC, with the mean daily temperatures at the coolest (December) and warmest (August) months being 10.4 and 23.8 ºC, respectively. The mean annual precipitation is 680 ± 210 mm, with 87% falling between October and May (over the 1955–2007 period). The weather variables (rainfall (mm), average temperature (ºC), wind speed (m s^{-1}), relative humidity (%), and solar radiation (W m^{-2}) were provided for the study area by the MM5 mesoscale model (http://meteo.tecnico.ulisboa.pt), forced by the initial conditions from the NCEP (National Centers for Environmental Prediction) Climate Forecast System Reanalysis, at a spatial resolution of 9 km.

The soil was classified as a Cambisol (FAO, n.d.). The main physical and chemical properties of the soil are presented in Table 4.2-1. The particle size distribution was determined using the pipette method (Staff, 2011) for particles with a diameter of <2 µm (clay fraction) and between 20 and 2 µm (silt), and by sieving for particles between 200 and 20 µm (fine sand) and between 2000 and 200 µm (coarse sand). These textural classes follow the Portuguese classification system (Gomes and Silva, 1962), and are based on international soil particle limits (Atterberg scale). The dry bulk density (eg, cm^{-3}) was obtained by the core method (Staff, 2011) (soil samples of 100 cm^3). The organic matter (OM, %) content was estimated from the organic carbon (OC, %) content determined by the Walkley–Black method, using the relation OM = 1.724 × OC (Nelson and Sommers, 1983).

Table 4.2-1 Main physical and chemical soil characteristics

Soil Properties	Soil Layers		
Depth (m)	0–0.2	0.2–0.8	>0.8
Coarse sand, 2000–200 µm (%)	65.83	56.18	63.43
Fine sand, 200–20 µm (%)	21.70	21.64	13.91

Soil Properties	Soil Layers		
Depth (m)	0–0.2	0.2–0.8	>0.8
Silt, 20–2 µm (%)	10.98	17.34	9.35
Clay, <2 µm (%)	1.49	9.35	13.30
Texture	Loamy-sand	Sandy-loam	Sandy-loam
Bulk density (g cm^{-3})	1.65	1.57	-
Organic matter (%)	1.39	0.32	0.02

Montado, with a density of Quercus suber (170 trees/ha), was the main land use at the field site. The understory vegetation and grassland was a mixture of C3 annual species, which emerged after the first rains in autumn and senesced in late spring. Initially, the dominant species were Agrostis pourretii Willd., Plantago coronopus L., Rumex acetosella L., Tolpis barbata (L.) Gaertn., Tuberaria guttata (L.) Fourr., Vulpia bromoides (L.) S.F. Gray, and Vulpia geniculata (L.) Link. In October 2009, the site was ploughed and seeded with a biodiverse mixture of legumes (Biserrula pelecinum L., Ornithopus compressus L., Ornithopus sativus Brot., Trifolium subterraneum L., Trifolium michelanium—balansae (Boiss.) Azn., Trifolium incarnatum L., Trifolium glanduliferum Boiss., Trifolium resupinatum L., and Trifolium vesiculosum Savi.), with one grass species (Lolium multiflorum L.) (Jongen et al., 2013a).

By the 2010–2012 seasons, the dominant species were Agrostis pourretii Willd., Bartsia trixago L., Ornithopus pinnatus (Mill.) Druce, Ornithopus sativus Brot., Rumex acetosella L., Spergula arvensis L., Tolpis barbata (L.) Gaertn., and Tuberaria guttata (L.) Fourr. The vegetation was therefore mostly dominated by non-sown species.

The MOHID-Land model was calibrated/validated using data from Jongen et al. (2013a), Jongen et al. (2013b). These authors carried out a rainfall manipulation experiment to study the resilience of montado understory to precipitation variability between October 2010 and June 2012. Eight rainfall manipulation shelters were constructed, each one covering an area of 6m x 5m ($30m^2$), within a fenced area of about $3500m^2$. The shelters were covered with a clear, 0.2mm, UV-transparent polyethylene greenhouse film. More details related to the shelter design can be found in (Jongen et al., 2013a).

During the 2010–2011 and 2011–2012 growing seasons, the pasture within four manipulation shelters was irrigated every three weeks, receiving 40mm per event, with this quantity being defined based on historical precipitation data (1955–2007). Hereafter, these plots will be referred to as “irrigated pasture”. Water was applied to the experimental plots using an irrigation system, consisting of four 18-VAN rotary sprinklers with 90◦ arc nozzles (Rainbird, Azusa, CA, USA), one in each corner of the experimental plots (Jongen et al., 2013b). In addition, four non-sheltered “control” plots receiving natural precipitation were

defined, referred to hereafter as rainfed pasture. All plots received an equal water input during the germination and seedling establishment (until the middle of November).

The soil volumetric water content was continuously measured (every 10min) in the middle of each experimental plot with an EC-5 soil moisture sensor (Decagon Devices, Pullman, WA, USA). In the irrigated and rainfed plots, measurements were taken at 10 and 5 cm depth, respectively. Aboveground (ABG) dry biomass was measured four times per season. Two 30cm × 30cm quadrats were defined in each experimental plot. All plants inside were harvested, oven-dried at 60ºC for 72h, and weighed. The maximum leaf area index (LAI_{max}, m^2 m^{-2}) was measured using a ceptometer (AccuPAR model LP-80, Decagon Devices, Pullman, USA), allowing an indirect determination of LAI by measuring the fraction of intercepted, photosynthetically-active radiation of the canopy. Maximum root depth was estimated at the end of the growing season (12 June). In each of the experimental plots, three soil cores of 8 cm diameter and a depth of up to 20cm were taken. Roots were washed out, with subsequent analysis of root length for determination of specific root length (SRL) using WinRhizo software (Regents Instruments Inc., Québec, QC, Canada), then oven dried at 60ºC for 72h, and weighed (Jongen et al., 2013b).

4.2.2.2 Model Setup, Calibration, and Validation

In the MOHID-Land model, the simulation period covered the 2010–2011 and 2011–2012 growing seasons, being set from emergence to senescence each year. The soil profile was specified with 4m depth and divided into three soil layers (Table 4.2-1). The soil domain was represented using an Arakawa C grid type (Purser and Leslie, 1988), defined by one vertical column discretized into 11 grid cells, 1m wide, 1 m long, and with variable thickness (0.05m on the top to 2.5m at the bottom).

The upper boundary condition was determined by the actual evaporation and transpiration rates, as well as the irrigation and precipitation fluxes. ET_c values were computed by multiplying the daily reference evapotranspiration (ET_0) values with crop coefficients (K_c) for the initial (0.3), mid-season (0.7), and late season (0.7) stages. These values were taken from Allen et al. (1998), and correspond to standard Kc values for pasture in the Mediterranean region. The K_c value for the initial stage was then adjusted for the frequency of the rainfall events and average infiltration depths, while the K_c values for mid-season and late season were adjusted for local climate conditions taking into consideration plant height, wind speed, and minimum relative humidity averages for the period under consideration (Allen et al., 1998).

Root water uptake reductions were computed by considering the following parameters: h_1 = −10, h_2 = −25, h_3 = −200 to −800, h_4 = −8000 cm (Wesseling et al., 1991).

Model calibration and validation were carried out during the 2010–2011 and 2011–2012 seasons, respectively, with procedures following Ramos et al. (2017). The soil hydraulic (Table 4.2-2) and the crop parameters (Table 4.2-3) were calibrated for both rainfed and irrigated plots (during the 2010–2011 growing season). A trial-and-error procedure was adopted. First, the parameters of the van Genuchten–Mualem equations (Equation 5 and 6) were defined according to the average values proposed by Carsel and Parrish (1988) for each soil texture class. The soil hydraulic parameters θ_s, α, η, and K_{sat} were then modified to reduce the deviation between the observed and the simulated soil water contents. The parameter θ_r was not modified, as it did not significantly influence soil moisture simulations. The l parameter was set to 0.5, as suggested by Mualem (1976). The crop parameters were calibrated by optimizing the default values of the EPIC model for pasture (Neitsch et al., 2011) until the deviation between the simulated and the observed ABG dry biomass was minimized. The values of the LAI_{max} and maximum root depth were taken directly from Jongen et al. (2013a). The calibrated model parameters were then validated during the 2011–2012 growing season and the statistical indicators (given below) computed.

Table 4.2-2 Van Genuchten–Mualem parameters in irrigated and rainfed plots.

Parameter	Soil Layers		
Depth (m)	0–0.2	0.2–0.8	>0.8
Irrigated Plots:			
θr (cm^3 cm^{-3})	0.035	0.035	0.067
θs (cm^3 cm^{-3})	0.300	0.300	0.450
α (cm^{-1})	0.015	0.015	0.020
η (-)	1.80	1.80	1.41
l (-)	0.50	0.50	0.50
Ksat (cm d^{-1})	62.4	27.8	4.5
Rainfed Plots:			
θr (cm^3 cm^{-3})	0.035	0.035	0.067
θs (cm^3 cm^{-3})	0.290	0.300	0.450
α (cm^{-1})	0.015	0.015	0.020
η (-)	1.85	1.80	1.41
l (-)	0.50	0.50	0.50
Ksat (cm d^{-1})	62.4	27.8	4.5

θ_r, residual water content; θ_s, saturated water content, α and η, empirical shape parameters; *l*, pore connectivity/tortuosity parameter; K_{sat}, saturated hydraulic conductivity.

The goodness-of-fit indicators adopted for comparing MOHID-Land model simulations with the observed values of θ and ABG dry biomass were the mean error (ME), the root mean square error (RMSE), the normalized RMSE (NRMSE), and the model efficiency (EF). ME

values close to zero indicate no bias. RMSE and NRMSE values close to zero indicate small estimation errors and good model predictions (Legates and McCabe, 1999; Moriasi et al., 2007; Wang et al., 2012). EF values close to one indicate that the residuals' variance is much smaller than the observed data variance, hence the model predictions are good. On the contrary, when EF is very close to 0 or negative, there is no gain in using the model (Nash and Sutcliffe, 1970).

Table 4.2-3 Optimized parameters of the crop growth model.

Crop Parameter	Irrigated Plot	Rainfed Plot
Optimal temperature for plant growth, T_{opt} (◦C)	20.0	20.0
Minimum temperature for plant growth, T_{base} (◦C)	5.0	5.0
Plant radiation-use efficiency, RUE [(kg ha^{-1}) (MJ m^{-2})$^{-1}$]	8.0	8.0
Total heat units required for plant maturity, PHU (◦C)	1800	1800
Fraction of PHU to reach the end of stage 1 (initial crop stage), $fr_{PHU,init}$ (-)	0.05	0.05
Fraction of PHU to reach the end of stage 2(canopy development stage), $fr_{PHU,dev}$ (-)	0.20	0.60
Fraction of PHU after which LAI starts to decline, $fr_{PHU,sen}$ (-)	0.70	0.70
Maximum leaf area index, LAI_{max} (m^2 m^{-2})	3.0	3.0
Fraction of LAI_{max} at the end of stage 1 (initial crop stage), $fr_{LAImax,ini}$ (-)	0.05	0.05
Fraction of LAI_{max} at the end of stage 2 (canopy development stage), $fr_{LAImax,dev}$ (-)	0.55	0.40
Maximum canopy height, $h_{c,max}$ (m)	0.30	0.30
Maximum root depth, $Z_{root,max}$ (m)	0.40	0.40

4.2.3 Results and Discussion

4.2.3.1 Soil Water Contents

Figure 4.2-1 presents the half-hourly θ measurements at 10 cm depth, and compares these values with the MOHID-Land model simulations during the 2010–2011 and 2011–2012 seasons. In the irrigated plots, θ showed a fast increase after rain or irrigation events, then decreased gradually due to redistribution, root water uptake, and soil evaporation. In the rainfed plots, soil water dynamics showed a similar behavior as in the irrigated plots. However, while θ was kept close to field capacity in the 2010–2011 season due to rainfall, in the 2011–2012 season θ was much lower, mainly due to the extended drought period that lasted from December 2011 to March 2012.

Table 4.2-4 presents the statistical indicators obtained after comparing measured values and model simulations. During calibration (2010–2011), the error of the estimates was small, producing an RMSE value of 0.018 and 0.015 cm^3 cm^{-3} and an NRMSE value of 0.030 and 0.039 for the rainfed and irrigated plots, respectively, while model efficiency was high (0.632–20.780). For the validation period (2011–2012), the errors of the estimates were kept small ($0.22 \leq RMSE \leq 0.26$ cm^3 cm^{-3}; $0.024 \leq NRMSE \leq 0.047$), while the model efficiency was

high (0.481 ≤ EF ≤ 0.863). According to Ramos et al. (2012b), Dabach et al. (2013), and Sándor et al. (2017), the deviation between measurements and model predictions may be attributed to several reasons, including model inputs, model structure, and field measurement errors, which can be considered also in this study. Nonetheless, the goodness-of-fit indicators were within the range of values reported in the literature for water content simulations using different process-based models (Hou et al., 2017; Ramos et al., 2017; Wang et al., 2015; Xu et al., 2013; Yu et al., 2006).

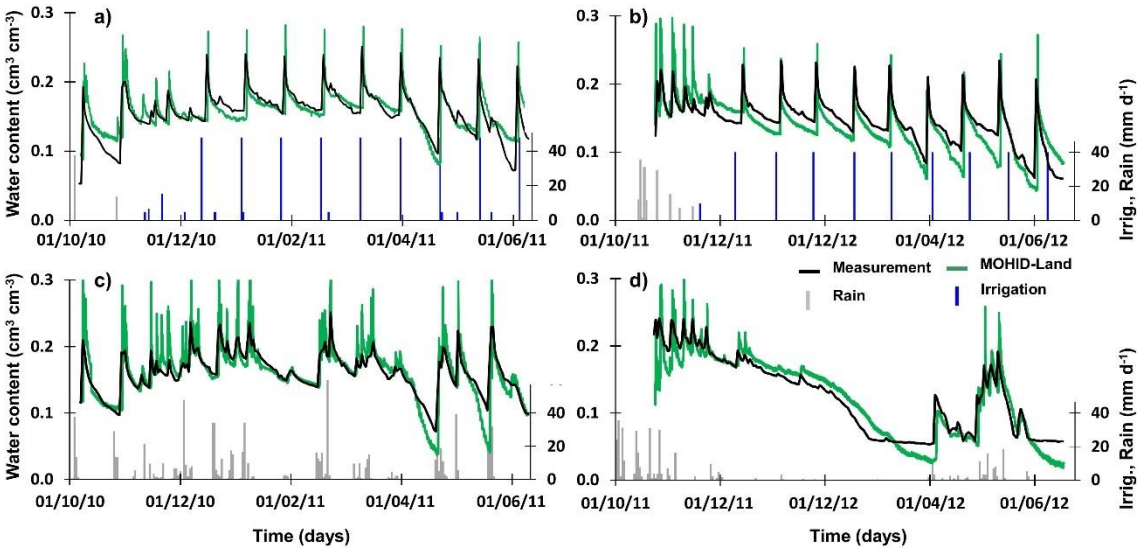

Figure 4.2-1 Measured and simulated soil water contents at 10 and 5 cm depth in irrigated and rainfed plots, respectively: (a) irrigated plot during the 2010–2011 season; (b) irrigated plot during the 2011–2012 season; (c) rainfed plot during the 2010–2011 season; and (**d**) rainfed plot during the 2011–2012 season.

Table 4.2-4 Results of the statistical analysis of measured and simulated soil water content and aboveground dry biomass.

Statistic	Irrigated Plot		Rainfed Plot	
	Water Content (cm^3 cm^{-3})	Aboveground Dry Biomass (kg ha^{-1})	Water Content (cm^3 cm^{-3})	Aboveground Dry Biomass (kg ha^{-1})
Calibration set (2010–2011)				
ME	0.001	−870.8	−0.002	−739.4
RMSE	0.015	1286.5	0.018	1125.5
NRMSE	0.039	0.210	0.030	0.372
EF	0.632	0.869	0.780	0.584
Validation set (2011–2012)				
ME	-0.010	-667.6	-0.003	120.9
RMSE	0.026	1088.1	0.022	279.8
NRMSE	0.047	0.375	0.024	0.243
EF	0.481	0.718	0.863	0.882

ME, mean error; RMSE, root mean square error; NRMSE, normalized RMSE; EF, model efficiency.

4.2.3.2 Pasture Growth

Pasture growth parameters were calibrated/validated for the irrigated and rainfed plots separately, based on the observed dynamics under the different regimes. However, only two parameters differed between the irrigation and rainfed regimes (Table 4.2-3): the fraction of PHU to reach the end of the canopy development stage ($fr_{PHU,dev}$), and the fraction of LAI_{max} at the end of the canopy development stage ($fr_{LAImax,dev}$). These parameters influenced the time needed for pasture to reach the mid-season stage, with irrigated pasture reaching it faster due to higher water availability, and also presenting a higher LAI value at the beginning of that stage (i.e., higher transpiration rates).

Regarding the aboveground dry biomass, the MOHID-Land simulations were in agreement with the measured values (Figure 4.2-2; Table 4.2-4). For the calibration period, the RMSE values were 1286.5 and 1125.5 kg ha^{-1} in the irrigated and rainfed plots, respectively. The NRMSE values were 0.210 and 0.372, and model efficiency were 0.584 and 0.869. For the validation period, RMSE, NRMSE, and EF values were within the same order of magnitude of those values.

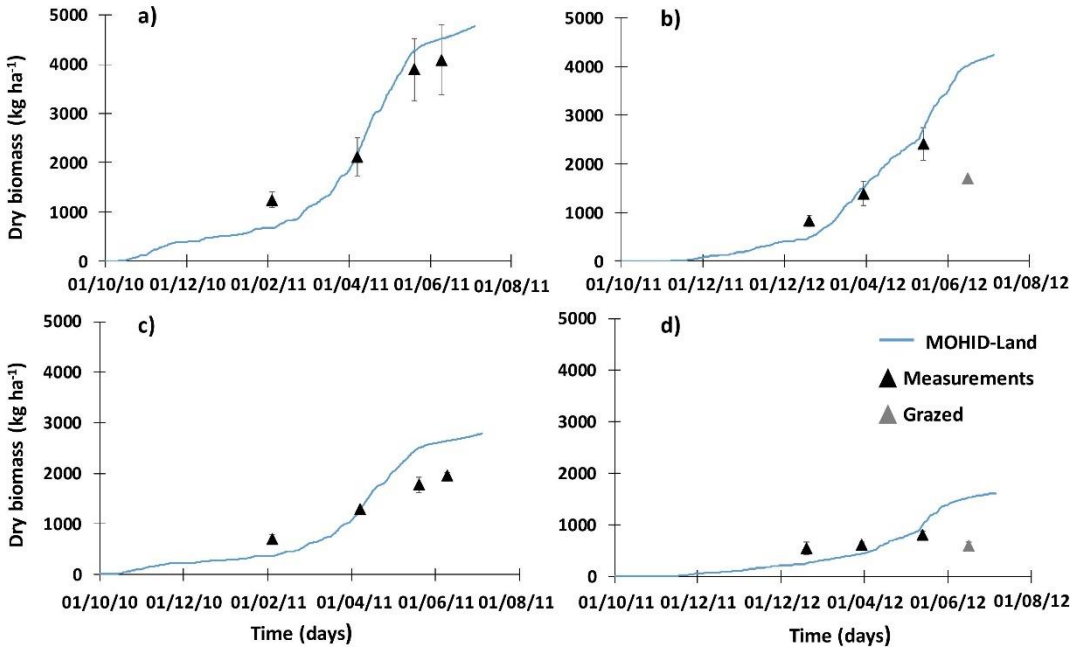

Figure 4.2-2 Measured and simulated aboveground dry biomass in irrigated and rainfed plots. (a) irrigated plot during the 2010–2011 season; (b) irrigated plot during the 2011–2012 season; (c) rainfed plot during the 2010–2011 season; and (d) rainfed plot during the 2011–2012 season (marks in grey were not considered in the statistical analysis as measurements showed that sites were grazed).

The general agreement between the simulated and measured data suggested that the calibrated parameters resulted in an adequate estimate of θ and aboveground dry biomass for both the calibration and validation seasons. Thus, it can be concluded that the model performance was generally good, and the model was properly calibrated for simulating soil water dynamics and crop growth in Herdade da Machoqueira do Grou.

4.2.3.3 Soil Water Balance

Table 4.2-5 presents the water balance for the irrigated and rainfed plots during the 2010–2011 and 2011–2012 seasons. Precipitation varied considerably between seasons, amounting to 873 mm during the 2010–2011 season and 413 mm during the 2011–2012 season, constituting the sole water input in the rainfed plots. The irrigated plots received natural precipitation until mid-November during the earlier plant stages (134 mm in 2010 and 152 mm in 2011). From that date on, plots were sheltered from rainfall, and an additional 370–454 mm were applied as irrigation (Jongen et al., 2013a, 2013b) (Figure 4.2-1).

Figure 4.2-3 shows the evolution of the T_p, T_a, and E_a values in the irrigated and rainfed plots during the 2010–2011 and 2011–2012 seasons. Ta varied between 143–166 mm in the irrigated plots, and between 56–65 mm in the rainfed plots (Table 4.2-5). These values corresponded to a water stress (given by the T_a/T_p ratio) between 0.86–0.95 in the irrigated plots, and between 0.60–0.94 in the rainfed plots.

The largest water stress was obviously registered in the rainfed plot during the 2011–2012 season due to the extended drought period observed between December 2011 and March 2012. The E_a values varied between 128–155 mm in the irrigated plots, and between 182–198 mm in the rainfed plots. E_a values were thus notoriously higher than T_a values in the rainfed plots. As discussed by Allen et al., 2011, when revising the various methods for field ET estimation, combined approaches of accurate θ observations and water balance simulation modeling provide for appropriate accuracy in ET estimates. Nonetheless, those results are further consistent with Huxman et al. (2005) and Kurc and Small (2007), who referred to the fact that in semi-arid ecosystems E_a may account for more than half of ET due to the near-surface source of E (the top 20cm), and because small rainstorms only wet the top few cm of soil. Also, Graham et al. (2016) reported pasture losing more water to soil evaporation when compared to ryegrass.

Table 4.2-5 Components of the simulated soil water balance.

Season	Inputs			Outputs			
	P (mm)	I (mm)	ΔSS (mm)	Ea (mm)	Ta (mm)	Ta/Tp (-)	DP (mm)
Irrigated plot							

2010–2011	134	454	-31	128	143	0.95	296
2011–2012	152	370	56	155	166	0.86	257
Rainfed plot:							
2010–2011	873	0	-263	182	65	0.94	362
2011–2012	413	0	65	198	53	0.60	226

Precipitation; I, irrigation; E_a, actual soil evaporation; T_a, actual crop transpiration; T_p, potential. crop transpiration; DP, deep percolation; ΔSS, soil moisture variation.

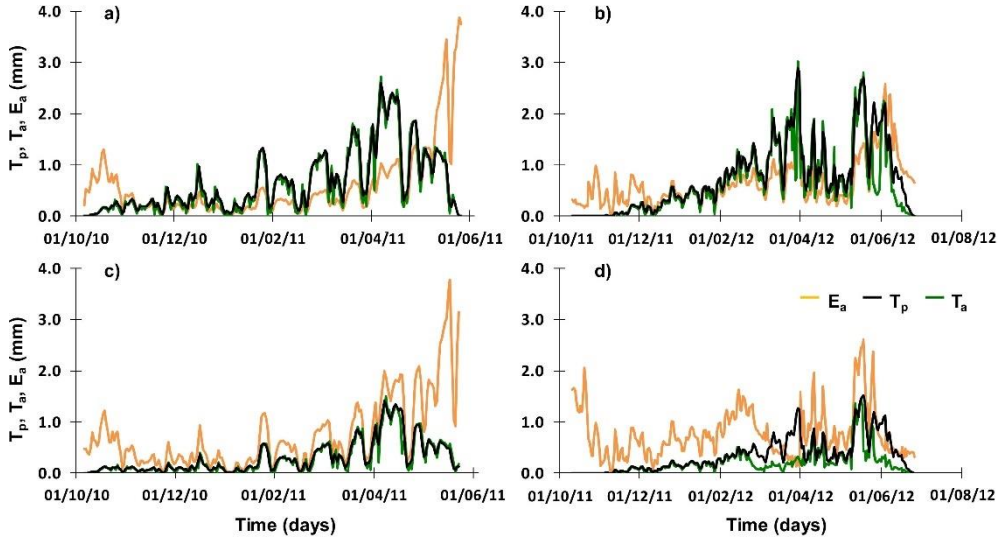

Figure 4.2-3 Estimates of water fluxes in irrigated and rainfed plots: (a) irrigated plot during the 2010–2011 season; (b) irrigated plot during the 2011–2012 season; (c) rainfed plot during the 2010–2011 season; and (d) rainfed plot during the 2011–2012 season.

As the rainfall manipulation experiments were carried out between autumn and spring, most of the water applied was lost through deep percolation (226–362 mm), which was to be expected (Table 4.2-5), providing natural recharge to the existing aquifers.

4.2.3.4 Future Research Needs Direction

Although the MOHID-Land model results were relatively good, the modeling approach followed in this study was relatively simple, presenting still many limitations that need to be considered in future applications while addressing the complexity of the montado ecosystem.

Firstly, there is the need to simulate the carbon and nutrient fluxes, in order to better unveil uncertainties related to whether and when grasslands act as sinks or sources of ecosystem carbon, providing further insight into the effects of stocking pressures on soil quality. The current model formulation already includes a biochemical module to conduct those studies, and will be the focus of future simulations.

Secondly, there is the need to consider grazing removals during growing seasons, as the system should be seen as dynamic, and interactions with pasturing herds should always be

taken into account in a proper management tool. Managing short-term variability in plant growth is considered to present a greater challenge in grazing systems than in cropping systems, which need to be tackled when developing a proper forecasting tool for accurately assessing daily/weekly pasture production (Chapman et al., 2020). However, for this study grazing was not considered, as the objective was to show the capability of the MOHID-Land model in simulating the main processes related to soil water dynamics and dry biomass growth in the montado ecosystem.

Thirdly, the model currently considers grasslands as a single species, while in fact they should be treated as a mixture of plants with different strategic properties, as suggested by van der Molen et al. (2011). Thus, the model needs to be able to simulate different species within the same cell domain. This approach also needs to be adopted for modeling the rest of the montado ecosystem, namely the niche located directly beneath the tree canopy, and the inter-relationships between the understory and trees for soil water and nutrients (Hussain et al., 2009). Only by addressing this will it be possible to further understand the ecosystem decline observed in different regions of the southern Iberian Peninsula over the last few decades (Garrido et al., 2017; Pinto-Correia and Azeda, 2017), namely the competition and synergies for water resources and nutrients.

Lastly, the MOHID-Land model is a process-based model that simulates variably saturated water flow using the Richards equation. This means that model simulations require reliable information on soil hydraulic properties for computing water flows, which are usually not easily available, as direct measurements are expensive, difficult, and time-consuming (Dane and Topp, 2020). While there is the need to adopt indirect approaches, including pedotransfer functions (Ramos et al., 2013), in order to provide the necessary inputs to process-based models, the approach followed in this study seems preferable to any of the existing simplifications, including those adopted by water-balance models. For example, Sándor et al., (2017) compared nine simulation models for predicting θ in the topsoil and biomass production. These authors found that some of the main drivers and results of the grassland processes, particularly θ and yield, were not represented well by common grassland models, attributing deviations between observations and simulations to model formulations rather than structural uncertainties within the models.

4.2.4 Conclusions

The MOHID-Land model was able to successfully simulate soil water dynamics and pasture development in a plot located in southern Alentejo, Portugal. Model estimates of θ and

aboveground dry biomass showed a general good agreement with field data collected during the 2010–2011 and 2011–2012 seasons. The RMSE, NRMSE, and model efficiency values were lower than 0.026 cm^3 cm^{-3}, lower than 0.047 cm^3 cm^{-3}, and higher than 0.481 cm^3 cm^{-3} for θ, respectively, and lower than 1286.5 kg ha^{-1}, lower than 0.450, and higher than 0.60 for the aboveground dry biomass.

As precise quantification of water fluxes over the pasture is essential for accurately quantifying ecosystem carbon and assessing uncertainties related to the source or sink behavior of pastures, the MOHID-Land model can be considered as a valuable tool for farmers to take the stocking rates into account and reduce the adverse impact of grazing in the pastures.

4.3 Modeling deficit irrigation in vineyards with MOHID-Land

The material on which this chapter is based has been previously published in: Simionesei, L., Ramos, T., Oliveira, A., Neves, R., 2019b. Modelação da rega deficitária em vinha com o MOHID-Land. Servicio de Publicaciones Universidad. https://doi.org/10.26754/c_agroing.2019.com.3373

4.3.1 Introduction

Once considered a dryland culture, irrigation of vineyards has become indispensable today to meet the water needs of the plants, especially during their most sensitive phases such as pre-maturation and grape ripening. This practice leads to an improved quantity and quality of the grapes produced (COTR, 2009). Deficit irrigation strategies are commonly adopted, considering the higher tolerance of certain stages of crop development to water stress. This promotes the development of a greater number of fruits as well as higher sugar and phenolic compound levels. However, these strategies depend on the desired product characteristics (Fandiño et al., 2012).

On the other hand, efficient irrigation management requires detailed monitoring of the soil water balance. Mechanistic models such as MOHID-Land (Trancoso et al., 2009) are now used in various irrigation decision support systems (Ramos et al., 2017; Simionesei et al., 2019b), along with information provided by soil moisture sensors, to increase water use efficiency. However, these models are more complex than the semi-empirical models traditionally used in irrigation management. The dynamics of water in the soil are described using the Richards equation. Therefore, a detailed knowledge of the hydraulic properties of the soil, specifically the soil water retention curve ($\theta_{(h)}$) and hydraulic conductivity curve ($K_{(h)}$), is essential but not always feasible. For this reason, it is imperative that these models undergo a calibration and validation process prior to their use to ensure reliable predictions.

This study describes an application of the MOHID-Land model for calculating the soil water balance in an irrigated vineyard in the Ribatejo region. The results of the calibration process will then be used in the IrrigaSys system (Simionesei et al., 2019b) to support vineyard irrigation in the region.

4.3.2 Materials and Methods

4.3.2.1 Study Area Description

This study was conducted in the vineyard of Adega do Catapereiro, Companhia das Lezírias, Samora Correia, Portugal (38.808044º N, 8.899858º W) between January 2017 and October 2018. The climate in the region is classified as sub-humid dry, with hot and dry summers and mild winters with irregular rainfall. The average annual temperature is 16.8°C, while the average annual precipitation reaches 669mm, mainly concentrated between October and April. The soil is classified as Haplic Fluvisol (FAO, n.d.), with a sandy loam texture.

The study plot, known as the "vinha do mel," occupies approximately 14 ha out of a total of 130ha covered by vineyards. The "vinha do mel" has a row spacing of 2.8m and a plant spacing of 1.0m, irrigated by a drip irrigation system. Management practices, including fertilization and irrigation, were carried out according to the practices followed by Companhia das Lezírias. In 2017, the total irrigation applied amounted to 358mm, while net precipitation reached 527 mm. In 2018, the irrigation applied totaled 242mm, while net precipitation reached 370 mm. The irrigation applied per event ranged from 3 to 5 mm.

Soil water content was continuously measured at depths of 10, 20, 30, 40, 50, 60, 70, and 80 cm using two EnviroPro MT capacitance probes (MAIT Industries, Australia). The irrigation applied in each event was monitored with a flowmeter installed in the irrigation pipe. Meteorological information was obtained from the Figueirinha station located nearby and included hourly values of precipitation (mm), air temperature (ºC), global radiation (W m^{-2}), relative humidity (%), and wind speed (m s^{-1}). Leaf area index (LAI, m^2 m^{-2}) was monitored using Landsat 8 satellite images. In 2017, a total of 16 images were extracted between January and November, with cloud coverage below 10%. In 2018, only 10 images were extracted. The reflectance values of each image were first corrected to eliminate atmospheric effects and solar angle variations. The LAI was then obtained using the following function (Richter and Schläpfer, n.d.):

$$LAI = -\frac{1}{a_2} ln\left(\frac{a_0 - SAVI}{a_1}\right) \quad \text{Equation 32}$$

Where SAVI corresponds to "Soil Adjusted Vegetation Index":

$$SAVI = \frac{(\rho_{850}-\rho_{650})*1.5}{\rho_{850}+\rho_{650}+0.5}$$ Equation 33

And a_0=0.82, a_1=0.82, a_2=0.6 are empirical parameters.

4.3.2.2 Model implementation, calibration, and validation

The simulation took place from January 2017 to October 2018. The soil profile was defined with a depth of 2m, divided into 2 soil layers according to the limits presented in Table 4.3-1. The simulation domain was represented by a vertical column discretized into 20 cells, each with a width and length of 1 m and a variable thickness (0.05 m in the upper cell to 0.3 m in the lower cell). The upper boundary condition was defined by E_p and T_p as well as irrigation and precipitation fluxes. The ET_c values were calculated by multiplying the ET_o values by the respective K_c for each crop development phase. K_c values of 0.3, 0.7, and 0.45 were considered for the initial, middle, and final phases of crop development, respectively. These values were taken from Allen et al. (1998) and represent the standard K_c values for vineyards in Mediterranean climate regions. The K_c value for the initial phase was then adjusted for the frequency of precipitation events and irrigation application, while the K_c values for the middle and final phases of the crop were adjusted for local weather conditions (average wind speed and relative humidity) and plant height (Allen et al., 1998). The lower boundary condition was defined as free drainage. Reductions in water extraction by roots were calculated considering the following parameters: h_1 = -10, h_2 = -25, h_3 = -1000, h_4 = -18000 cm (Wesseling et al., 1991).

Table 4.3-1 Soil hydraulic parameters

Depth (m)	0-0.25	0.25-0.45
Residual water content θr (m^3 m^{-3})	0.065	0.065
Saturation water content θs (m^3 m^{-3})	0.500	0.450
Empirical parameter α (m^{-1})	38	25
Empirical parameter η (-)	1.35	1.35
Pore connectivity/tortuosity parameter l (-)	-1	-1
Saturated hydraulic conductivity K_{sat} (m s^{-1})	8.23E^{-05}	3.23E^{-05}

The calibration and validation of the model were carried out during the years 2017 and 2018, respectively, following the procedure described in Ramos et al. (2017). The soil hydraulic properties (Table 4.3-1) and crop parameters (Table 4.3-2) were adjusted through trial and error to reduce the discrepancies between the model simulations and the observed values of soil water content and LAI.

Initially, the soil hydraulic parameters were set according to the average values proposed by Carsel and Parrish (1988) for each soil texture class. The parameters θ_s, α, η, and K_{sat} were

then modified to minimize the deviation between the observed and simulated soil water content. The parameter θ_r was not modified given its low influence on the simulations of soil water content. The parameter l was set to -1.0, as proposed by Schaap and Leij (2000b).

Subsequently, the crop parameters were adjusted based on the model's default values for the vineyard (Neitsch et al., 2011) until the deviation between the simulated LAI and the remotely sensed LAI was minimized. The calibrated parameters were then validated during the year 2018.

Table 4.3-2 Crop development parameters.

Crop Parameter	Value
Optimal temperature for plant growth, T_{opt} (°C)	20.0
Minimum temperature for plant growth, T_{base} (°C)	11.0
Plant radiation-use efficiency, RUE [(kg ha^{-1}) (MJ m^{-2})$^{-1}$]	30.0
Total heat units required for plant maturity, PHU (°C)	2800
Fraction of PHU to reach the end of stage 1 (initial crop stage), $fr_{PHU,init}$ (-)	0.05
Fraction of PHU to reach the end of stage 2 (canopy development stage), $fr_{PHU,dev}$ (-)	0.10
Fraction of PHU after which LAI starts to decline, $fr_{PHU,sen}$ (-)	0.20
Maximum leaf area index, LAI_{max} (m^2 m^{-2})	1.1
Leaf Area Index during dormancy phase, LAI_{dorm} (m^2 m^{-2})	0.5
Fraction of LAI_{max} at the end of stage 1 (initial crop stage), $fr_{LAImax,ini}$ (-)	0.35
Fraction of LAI_{max} at the end of stage 2 (canopy development stage), $fr_{LAImax,dev}$ (-)	0.55
Maximum canopy height, $h_{c,max}$ (m)	1.5
Maximum root depth, $Z_{root,max}$ (m)	0.8
Net radiation coefficient (-).	0.463
Photosynthetically active radiation coefficient (-).	0.650

The statistical indicators adopted to compare the results of MOHID-Land simulations with observed values of soil water content and LAI were: mean error (ME), root mean square error (RMSE), normalized RMSE (NRMSE), and model efficiency (EF). ME values close to zero indicate no bias. RMSE and NRMSE values close to zero indicate small estimation errors and good model predictions (Legates and McCabe, 1999; Moriasi et al., 2007). EF values close to one indicate that the variance of the residuals is much smaller than the variance of the observed data, indicating good model predictions. Conversely, when EF is close to zero or negative, there is no improvement in model performance (Nash and Sutcliffe, 1970).

4.3.3 Results and Discussion

4.3.3.1 Soil Water Content

Figure 4.3-1 presents the measurements of soil water content at depths ranging from 10 to 80 cm and compares these values with the simulations of the MOHID-Land model during the years 2017 and 2018. Precipitation events, more than irrigation, generally led to a rapid increase in soil water content in the surface layers, followed by a gradual decrease due to water

redistribution, plant water uptake, and soil evaporation. In the deeper layers, the effect of irrigation was less noticeable, with soil water content varying primarily due to precipitation, although to a lesser extent than in the surface layers.

Table 4.3-3 presents the statistical indicators obtained after comparing the measured and simulated values by the model. During the calibration period (2017), the estimation errors were relatively small, resulting in an RMSE of 0.033 m^3 m^{-3} and an NRMSE of 0.016. The model overestimated the observed values by 11.25%, while the EF was acceptable (0.425). For the validation period (2018), the estimation errors remained within the same order of magnitude as those obtained during model calibration (RMSE = 0.029 m^3 m^{-3}; NRMSE = 0.012), the model underestimated the observed data by 3.25%, while the EF increased considerably (EF = 0.706). It was considered that the MOHID-Land model successfully reproduced the observed soil water content values in vineyard irrigation for two years, presenting similar statistical indicators to those obtained in other similar applications (Ramos et al., 2018, 2017; Simionesei et al., 2018).

Table 4.3-3 statistical indicators during model calibration (2017) and validation (2018).

Indicator	Soil water content		Leaf Area Index	
	2017	2018	2017	2018
R^2	0.800	0.853	0.846	0.896
RMSE	0.033	0.029	0.139	0.125
NRMSE	0.016	0.012	0.206	0.210
PBIAS (%)	-11.25	3.25	-4.22	7.10
NSE	0.425	0.706	0.365	0.602

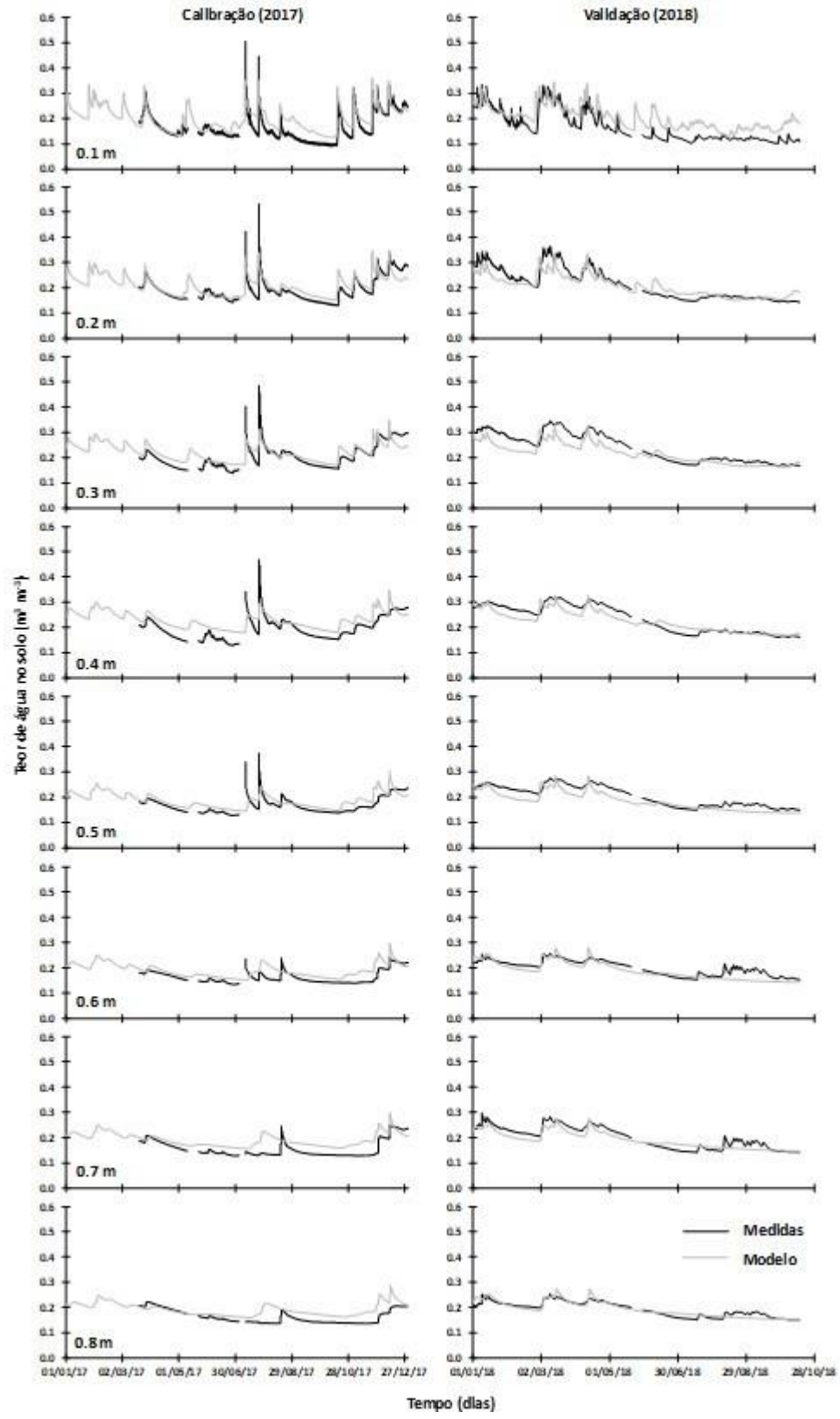

Figure 4.3-1 Soil water content evolution

4.3.3.2 Leaf Area Index (LAI) evolution

In the MOHID-Land model, the partitioning of ET_c into T_p and E_p is based on LAI, so its evaluation should be as accurate as possible to ensure reliable estimates of the soil water balance. According to values derived from satellite images, the LAI of the crop began to increase from March/April, reaching a maximum of around 1.0-1.2 m^2 m^{-2} in late May or early June. From there, LAI values gradually declined until complete leaf loss in October/November. During the calibration phase (2017), the RMSE and NRMSE obtained by comparing the simulated values with those obtained from remote sensing were 0.139 m^2 m^{-2} and 0.206, respectively (

Table 4.3-3). The model overestimated LAI by 4.22%, while the EF was 0.365. During the validation phase (2018), the RMSE was 0.125 m^2 m^{-2}, NRMSE was 0.210, PBIAS was 7.098%, indicating some underestimation of values obtained from remote sensing, and the EF was 0.602. The model adjustment was therefore acceptable, although the statistical indicators were lower than those obtained by Ramos et al. (2017,2018) for maize crop. In that case, LAI values were directly measured in the field, not derived from satellite images, which may explain the lower adjustment achieved here.

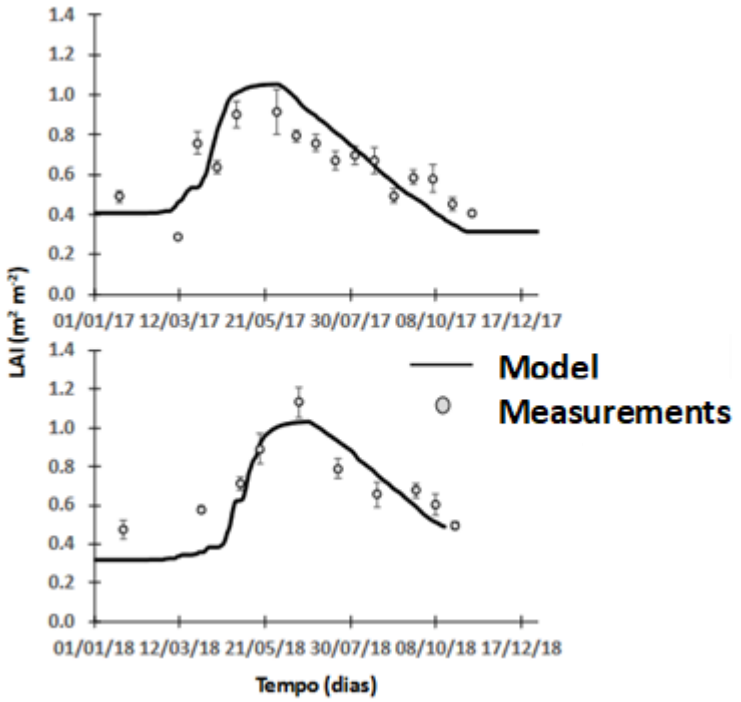

Figure 4.3-2 Leaf Area Index evolution

4.3.3.3 Soil water balance

Table 4.3-4 presents the water balance for the years 2017 and 2018, with T_a accumulating 166 mm and 112 mm, respectively. The water stress, given by 1 - T_a/T_p, ranged between 5% and 8% during the irrigation months (April to October), indicating a relatively moderate water deficit. On the other hand, the values of E_a (actual evapotranspiration) amounted to 453 mm and 295mm for the years 2017 and 2018, respectively. These values can be considered quite high, partly explained by the fact that soil evaporation can account for a significant fraction of ET_c in permanent crops, where a large portion of the soil surface is exposed to solar radiation (Testi et al., 2004; Villalobos et al., 2000). Furthermore, in MOHID-Land, E_a is calculated based on a threshold soil water pressure imposed on the values of E_p (potential evaporation). Therefore, it is a simplified version based on the two-phase method used by Allen et al. (1998) for E_a calculation, which may also lead to some overestimation of this component of the water balance. Table 4.3-4 also shows considerably high values of percolation, totaling 287mm and 330mm, respectively, mainly occurring during the periods following precipitation events.

Table 4.3-4 Soil Water Balance

Componentes (mm)	2017	2018
Inputs:		
Precipitation	527	370
Irrigation	358	242
Capillary Rise	0	0
Δ storage	21	125
Outputs:		
RunOff	0	0
Actual evaporation	453	295
Actual transpiration	166	112
Percolation	287	330

4.3.4 Conclusions

The MOHID-Land model successfully reproduced the measured soil water content values throughout the years 2017 and 2018. The actual transpiration values in the vineyard ranged from 112 to 166 mm, with irrigation inducing a water stress of 5% to 8%. The values of actual evaporation amounted to 453 mm and 295 mm in the years 2017 and 2018, respectively, which may be slightly overestimated due to the simplified formulation of the model in calculating this parameter. However, overall, the performance of MOHID-Land in modeling soil water dynamics in a permanent crop such as vineyard can be considered quite acceptable. This work serves as a reference for the IrrigaSys decision support system, which

provides weekly irrigation recommendations to various farmers in the region regarding how much and when to irrigate.

5. The use of remote sense data as a tool to improve the quality of the system

In this chapter, we explore the utilization of remote sensing data as a tool within the Decision Support System (DSS) aimed at enhancing system quality. The outcomes of this calibration process have been documented in two scientific papers. The following succinctly presents the objectives of these articles/applications:

Chapter 5.1: This section focuses on assessing the impact of LAI (Leaf Area Index) Data Assimilation on simulations related to Soil Water Balance and Maize Development using the MOHID-Land model.

Chapter 5.2: The primary objective of this segment is to explore the use of vegetation indices for validating computed crop transpiration fluxes with the MOHID-Land Model, particularly applied to vineyards.

Collectively, these chapters contribute to the enhancement of the Decision Support System by integrating remote sensing data, thereby improving modelling accuracy and validation techniques.

5.1 Assessing the Impact of LAI Data Assimilation on Simulations of the Soil Water Balance and Maize Development Using MOHID-Land

The material on which this chapter is based has been previously published in: Ramos, T.B., Simionesei, L., Oliveira, A.R., Darouich, H., Neves, R., 2018. Assessing the impact of LAI data assimilation on simulations of the soil water balance and maize development using MOHID-Land. Water (Switzerland) 10. https://doi.org/10.3390/w10101367

5.1.1 Introduction

In recent decades, modeling has become an essential part of the decision-making process for improving irrigation water use (González et al., 2015; Paço et al., 2014; Paredes et al., 2018; Ramos et al., 2017), optimizing fertilization practices (Cameira et al., 2005; Ramos et al., 2012), predicting crop yields (Ashraf Vaghefi et al., 2017; Jiang et al., 2015) and coping with climate change (Fraga et al., 2018; Valverde et al., 2015) at the field and regional scales. However, modeling tools require first a considerable time investment in calibration to provide feasible results to their users. This is often accomplished at the plot scale, where most variables influencing crop development (soil properties, plant physiology, groundwater levels and weather conditions) can be more easily monitored. The problem often arises when upscaling to the field or regional scales due to the difficulties in portraying landscape heterogeneity, including soil, land use and climate variability.

Remote sensing technology offers a potential solution for accurately and reliably describing the spatial distribution of soil properties and canopy state variables (leaf area index, canopy height, biomass) at the field and regional scales (Mulla, 2013). A vast number of new satellite sensors (Landsat 8, Sentinel-2, Spot-6, RapidEye, Huanjing-1) together with versatile, light-weighted and low-cost sensors mounted in farm tractors or unmanned aerial vehicles are now available for providing information with high spatial and temporal resolution to farmers and technicians. This information can potentially be also assimilated into field or regional scale models, overcoming many constraints in terms of input parameterization.

The purpose of assimilation is to optimize model input parameters by integrating, both in space and time, soil or canopy state variables derived from remote sensing methods (Jin et al., 2018). Accurate and up-to-date information has been increasingly available at low cost, which has led to numerous research studies focusing on assimilation of remote sensing measurements (Ines et al., 2013; Li et al., 2014; Linker and Ioslovich, 2017; Nearing et al., 2012; Thorp et al., 2010; Tripathy et al., 2013; Vazifedoust et al., 2009). Some of these have estimated leaf area index (LAI) using different remote sensing data sources, then assimilating those values by directly replacing the simulated LAI to improve model estimates of the aboveground dry biomass, yield and crop transpiration (Thorp et al., 2010; Tripathy et al., 2013). Other studies have used more advanced assimilation techniques, usually based on the Extended Kalman Filter (Evensen, 1994) and Ensemble Kalman Filter (Evensen, 2003) assimilation methods, for integrating remote sensing LAI into model simulations (Ines et al., 2013; Linker and Ioslovich, 2017; Nearing et al., 2012). Overall, regardless of the technique used, most of those studies concluded that remote sensing provides useful measurements which can then be used for improving model simulations.

While a wide variety of models exist capable of simulating crop growth processes at the regional scale, thus portraying landscape heterogeneity at some extent (Basso et al., 2016; Guzmán et al., 2018; Zhang et al., 2018), fully distributed process-based models such as MIKE SHE (Butts et al., 2014), SHETRAN (Ewen et al., 2000) and MOHID-Land (Trancoso et al., 2009) are often considered ideal for further studying distributed state variables (the spatiotemporal variability of soil moisture) and flow paths (sediment and nutrient transport) (Fatichi et al., 2016). These fully distributed process-based models consider interactions between multiple components of the soil-water-atmosphere continuum, with fundamental process being formulated at fine spatial (plot) and temporal scales, contributing to the overall dynamics at a higher organizational level, such as the watershed (Fatichi et al., 2016). For the

case of MOHID-Land, the model has been used for improving irrigation practices at the plot and field scales (Ramos et al., 2017; Simionesei et al., 2018, 2016), understanding the contribution of flood events to the eutrophication of water reservoirs (Brito et al., 2018, 2017) and forecasting fresh water quantity and quality in coastal rivers (Brito et al., 2015). Extensive calibration has been normally required for characterizing soil, groundwater, crop and river flow properties. Thus, data assimilation may have here a decisive contribution for more accurately describing the spatial and temporal variability of many of the required input parameters. However, the impact of data assimilation on final model outputs needs to be first assessed.

The main objective of this study was thus to understand the impact of LAI assimilation on MOHID-Land's estimates of the soil water balance and crop state variables (LAI, canopy height, aboveground dry biomass and yield). The hypothesis addressed were that (i) the MOHID-Land model could accurately estimate the soil water balance and aboveground biomass growth in a one-dimensional domain; (ii) LAI assimilation could improve simulations of crop development and (iii) the related uncertainties could be assessed. Results from this study will help to improve hydrological modeling at the field and regional scales by quantifying the uncertainty related to data assimilation using the MOHID-Land model.

5.1.2 Materials and Methods

5.1.2.1 Field Site Description and Data

Field data used in this study was collected at Herdade do Zambujeiro (22ha), Benavente, southern Portugal (38◦58′0.97″ N, 8◦44′46.63″ W, 6m a.s.l.) (Figure 5.1-1). The climate in the region is semi-arid to dry sub-humid, with hot dry summers and mild winters with irregular rainfall. The mean annual temperature is 16.8 ºC, with the mean daily temperatures at the coolest (January) and warmest (August) months reaching 11.4 and 22.7ºC, respectively. The mean annual precipitation is 668 mm, mostly occurring between October and May. The soil was a Haplic Fluvisol (IUSS Working Group WRB, 2014), with the main soil physical and chemical properties presented in Table 5.1-1. The bottom layers exhibited higher dry bulk density and lower measured saturated hydraulic conductivity values than the topsoil layers (Ramos et al., 2017), evidencing some soil compaction due to tillage operations carried out throughout the years and the relatively high soil moisture that was constant along the seasons because of the shallow groundwater levels.

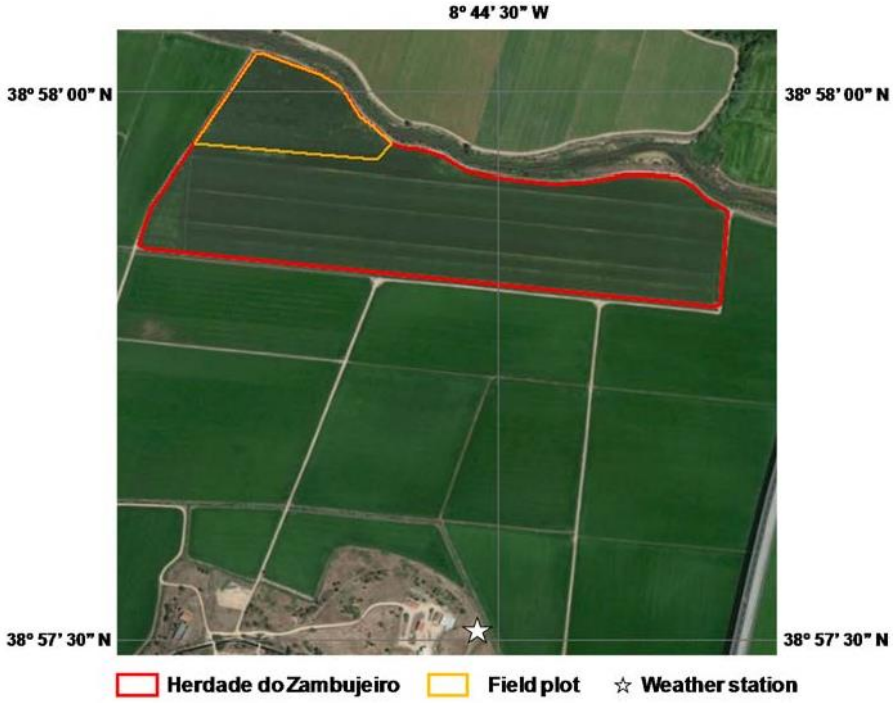

Figure 5.1-1 Location of the study site.

The MOHID-Land model was previously implemented in the area by Ramos et al. (2017). These authors evaluated the model's capacity in predicting soil water contents and fluxes and the evolution of different crop growth parameters, including the leaf area index (LAI), canopy height, aboveground dry biomass and yields during the 2014 and 2015 maize growing seasons. Details on the calibration/validation approach can be found in the cited reference. For that, the field was cropped with maize hybrid P1574 (FAO 600) with a density of approximately 89,000 plants ha^{-1}. Management practices, including fertilization and irrigation, were performed according to the standard practices in the region and were decided by the farmer. During 2014, maize was sown on May 24 and harvested on October 8; the net rainfall reached 163mm, while the net irrigation amounted 365 mm (Figure 5.1-2). During 2015, maize was sown on April 16 and harvested on September 20; the net rainfall reached only 12mm, while the net irrigation summed 620mm (Figure 5.1-2). Irrigation was applied with the farmer's stationary sprinkler system. Groundwater depth (GWD) varied between approximately 1.5m depth at the beginning of the growing season to 1.0m depth during irrigation, further reaching 0.3m depth during September 2014 after successive rain events (Figure 5.1-2). Crop stages were set as in Table 5.1-2 based on field observations.

One SM1 capacitance probe (Adcon Telemetry, Klosterneuburg, Austria) and one ECH2O-5 capacitance probe (Decagon Devices, Pullman, WA, USA) were installed at depths of 10, 30 and 50 cm to continuously measure soil water contents. One LEV1 level sensor

(Adcon Telemetry, Klosterneuburg, Austria) was used to continuously monitor the groundwater level (Figure 5.1-2). One RG1 (Adcon Telemetry, Klosterneuburg, Austria) and two QMR101 (Vaisala, Helsinki, Finland) rain gauges were used to measure the amount of water applied per irrigation event.

LAI, canopy height and the aboveground dry biomass were further monitored by harvesting 3 random plants in four locations distributed randomly throughout the field plot, every 15 days, between May and September, during the 2014 and 2015 maize growing seasons (Table 5.1-3). The same crop parameters were measured at the end of each crop season, but by harvesting all plants in random areas of 1.5 m^2 (corresponding to approximately 12 plants). The length and width of crop leaves were measured in every harvested plant and then converted to LAI values as documented in Ramos et al. (2017). The aboveground dry biomass was determined by oven drying maize stems, leaves and grain at 70 ºC to a constant weight. Maize yield was obtained from the grain's dry biomass measured at the end of each crop season.

Table 5.1-1 Main physical and chemical soil characteristics.

Depth (m)	Soil Layers			
	0-0.2	0.2-0.4	0.4-0.6	0.6-0.8
Coarse Sand, 2000–200 µm (%)	3.4	6.8	11.5	14.7
Fine Sand, 200–20 µm (%)	44.6	47.8	53.6	48.4
Silt, 20–2 µm (%)	33.3	28.1	20.6	23.2
Clay, <2 µm (%)	18.8	17.3	14.3	13.7
Texture	Silty Loam	Loam	Loam	Loam
Bulk Density (g cm^{-3})	1.57	1.52	1.66	1.66
Organic Matter (%)	1.73	0.96	0.57	0.59
θ_{FC} (cm^3 cm^{-3})	0.321	0.293	0.311	0.311
θ_{WP} (cm^3 cm^{-3})	0.209	0.235	0.223	0.223
Van Genuchten-Mualem Parameters:				
θ_r (cm^3 cm^{-3})	0.078	0.067	0.065	0.065
θ_S (cm^3 cm^{-3})	0.393	0.356	0.340	0.340
α (cm^{-1})	0.009	0.016	0.005	0.005
η (-)	1.75	1.31	1.80	1.80
l (-)	−1.0	−1.0	−1.0	−1.0
K_{sat} (cm d^{-1})	500.3	22.6	0.7	0.7

θ_{FC}, soil water content at field capacity; θ_{WP}, soil water content at the wilting point, θ_r, residual water content; θ_s, saturated water content; α and η, empirical shape parameters; l, pore connectivity/tortuosity parameter; K_{sat}, saturated hydraulic conductivity.

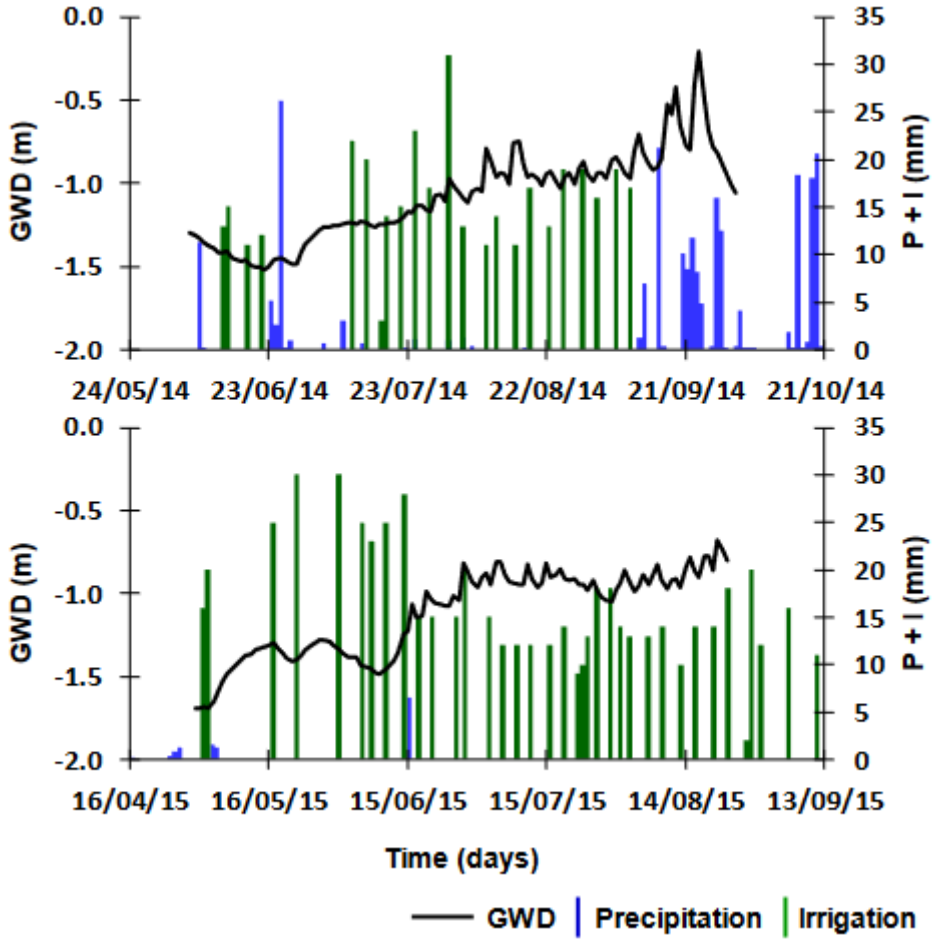

Figure 5.1-2 Daily values of precipitation, irrigation and groundwater depth (GWD) during the 2014 (top) and 2015 (bottom) crop seasons.

Table 5.1-2 Dates of crop growth stages.

Stage	2014		2015	
	Days	Date	Days	Date
Initial	31	24 May	37	16 April
Canopy Development	30	24 June	32	23 May
Mid-Season	52	24 July	53	24 June
Late Season	27	14 September	26	16 August
Harvest	-	8 October	-	20 September

Table 5.1-3 Measured values of Leaf Area Index (LAI), canopy height (hc) and aboveground dry biomass during the 2014 and 2015 crop seasons.

Date	LAI (m^2 m^{-2})		h_c (m)		Biomass (kg ha^{-1})	
	Mean	Standard Deviation	Mean	Standard Deviation	Mean	Standard Deviation
11/06/2014	0.1	0.0	0.14	0.02	48.3	15.3
25/06/2014	1.3	0.1	0.54	0.04	826.7	56.6
10/07/2014	3.2	0.4	1.02	0.10	2906.7	1083.2
24/07/2014	5.6	0.1	2.27	0.23	8279.4	339.2

Date	LAI (m^2 m^{-2})		h_c (m)		Biomass (kg ha^{-1})	
	Mean	Standard Deviation	Mean	Standard Deviation	Mean	Standard Deviation
11/08/2014	6.3	1.0	3.08	0.03	18,593.8	1881.7
27/08/2014	6.0	0.6	3.11	0.10	27,228.2	594.8
15/09/2014	5.3	0.4	3.03	0.15	34,945.6	982.8
08/10/2014	-		-	-	30,423.2	1735.6
15/05/2015	0.2	0.0	0.19	0.03	80.0	16.8
28/05/2015	1.3	0.3	0.49	0.01	1090.1	61.8
11/06/2015	4.0	0.3	1.45	0.06	5309.5	280.6
25/06/2015	5.9	0.6	2.65	0.09	11,550.0	958.9
14/07/2015	6.4	0.3	3.12	0.02	23,711.2	812.9
28/07/2015	6.2	0.6	3.12	0.01	27,373.9	229.2
13/08/2015	5.2	0.2	2.78	0.06	29,434.4	7624.1
14/09/2015	-	-	-	-	34,540.3	2670.5

5.1.2.2 Model Setup and Data Assimilation

The assimilation of LAI data into MOHID-Land simulations has a direct influence on the water balance through the partition of ET_c values into T_p (Equation 8) and E_p (Equation 9) and on the computation of the aboveground dry biomass (Equation 13) Three distinct approaches were thus considered for better understanding the impact of LAI assimilation on model simulations:

A—The model was run as in T.B. Ramos et al., 2017, which simulations of soil water contents, LAI, h_c, aboveground dry biomass and yields served as baseline for this study (Calibrated model). These authors followed a traditional calibration/validation approach, where a trial-and-error procedure was carried out to adjust soil hydraulic (Table 5.1-1) and crop parameters (Table 5.1-4) until deviations between the measured 2014 dataset and simulated values were minimized. The calibrated parameters were then validated using the 2015 dataset, with model simulations being compared to measured data.

B—The model was run using LAI values extracted from satellite data as inputs (LAI assimilation). LAI values were derived from the normalized difference vegetation index (NDVI) using the relationship shown in Figure 5.1-3. This relationship was found by comparing NDVI values computed from Landsat 8 satellite images (band 4 and 5) with LAI values measured in the study site, at multiple locations and over the 2014 and 2015 growing seasons. The calibrated soil hydraulic parameters were here also adopted (Table 5.1-1). However, the default crop parameters from the MOHID-Land's database (Table 5.1-4) were considered instead so that model performance in the absence of a calibrated dataset could be assessed.

C—The model was again run using LAI values extracted from satellite data as inputs. However, Ramos et al. (2017) calibrated crop parameters (Table 5.1-4) were here considered

(Calibration + LAI assimilation), as well as the calibrated soil hydraulic parameters (Table 5.1-1).

Table 5.1-4 Parameters of the crop growth model.

Crop Parameter	Default	Calibrated
Optimal Temperature for Plant Growth, T_{opt} (°C)	25.0	25.0
Minimum Temperature for Plant Growth, T_{base} (°C)	8.0	8.0
Plant Radiation-Use Efficiency, RUE [(kg ha^{-1}) (MJ $m^{-2})^{-1}$]	45.0	39.0
Total Heat Units Required for Plant Maturity, PHU (°C)	1700	1900
Fraction of PHU to Reach the End of Stage 1 (Initial Crop Stage), $fr_{PHU,init}$ (-)	0.15	0.20
Fraction of PHU to Reach the End of Stage 2 (Canopy Development Stage), $fr_{PHU,dev}$ (-)	0.50	0.43
Fraction of PHU after which LAI Starts to Decline, $fr_{PHU,sen}$ (-)	0.70	0.73
Maximum Leaf Area Index, LAI_{max} (m^2 m^{-2})	6.0	6.5
Fraction of LAI_{max} at the End of Stage 1 (Initial Crop Stage), $fr_{LAImax,ini}$ (-)	0.05	0.05
Fraction of LAI_{max} at the end of Stage 2 (Canopy Development Stage), $fr_{LAImax,dev}$ (-)	0.95	0.95
Maximum Canopy Height, $h_{c,max}$ (m)	2.5	3.1
Maximum Root Depth, $Z_{root,max}$ (m)	2.0	0.6
Potential Harvest Index for the Crop at Maturity, HI_{opt} (-)	0.50	0.49
Minimum Harvest Index Allowed, HI_{min} (-)	0.30	0.30

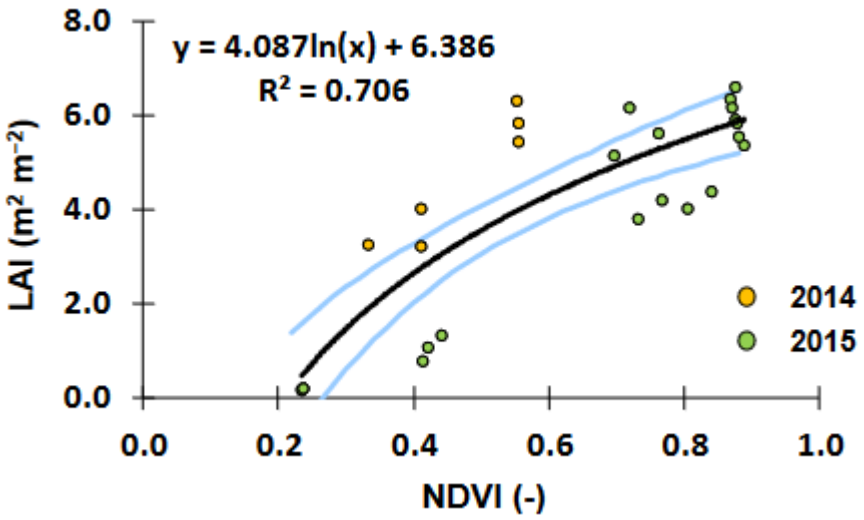

Figure 5.1-3 Relationship between measured Leaf Area Index (LAI) and the Normalized Difference Vegetation Index (NDVI). The blue lines correspond to the 95% confidence interval.

Landsat 8 images were first corrected to convert the TOA (Top of Atmosphere) planetary reflectance using reflectance rescaling coefficients provided in the Landsat 8 OLI metadata file and to correct the reflectance value with the sun angle. Two images were available from sowing to harvest during the 2014 growing season, while eight images were used during the 2015 growing season (Table 5.1-5). These images were used to extract the NDVI values corresponding to the multiple locations where LAI field observations were carried out, in a total of 26 measurements (Figure 5.1-3). LAI and NDVI values ranged from 0.41–5.85 and 0.23–0.88, respectively, in line with Pôças et al. (2015).

Table 5.1-5 Leaf Area Index (LAI) assimilation data.

Date	Assimilated LAI (m^2 m^{-2})	NDVI (-)	LAI 95% Confidence Interval	
			Lower	Upper
09/07/2014	2.75	0.41	-	-
10/08/2014	3.97	0.55	-	-
23/04/2015	0.41	0.23	0.00	1.53
09/05/2015	0.48	0.24	0.00	1.58
25/05/2015	3.04	0.44	2.47	3.61
10/06/2015	5.50	0.81	4.89	6.11
26/06/2015	5.85	0.88	5.17	6.53
12/07/2015	5.79	0.86	5.12	6.46
28/07/2015	5.82	0.87	5.15	6.49
29/08/2015	5.31	0.77	4.73	5.89

Data assimilation in MOHID-Land was carried out using the forcing method (Jin et al., 2018). The approach is relatively straightforward, with the model simply replacing the predicted value by a new input when an image becomes available, updating then fr_{LAImax} to account for what still needs to be reached during a specific crop stage and more interestingly, the water balance and the aboveground dry biomass estimates. From that date on and until another image becomes available model simulations follow the parameterization given in Table 5.1-4. Table 5.1-5 lists the assimilated LAI values and dates.

In all simulations (Approach A–C), the soil profile was specified with 2m depth, divided into four soil layers according to observations (Table 5.1-1). The soil domain was represented using an Arakawa C-grid type (Purser and Leslie, 1988), defined by one vertical column (one-dimensional domain) discretized into 100 grid cells with 1 m wide, 1 m long and 0.02 m thickness each (i.e., $1 \times 1 \times 0.02$ m^3). The simulation periods covered from sowing to harvest. The upper boundary condition was determined by the actual evaporation and transpiration rates and the irrigation and precipitation fluxes (Figure 5.1-2). Weather data used in this study was taken from a meteorological station located 950 m from the study site (38◦57′30.25″ N, 8◦44′31.70″ W, 7 m a.s.l.; Figure 5.1-1) and included the average temperature (ºC), wind speed (m s^{-1}), relative humidity (%), global solar radiation (W m^{-2}) and precipitation (mm). ET_c values were computed from hourly ET_0 values and K_c values of 0.30, 1.20 and 0.35 for the initial, mid-season and late season crop stages, respectively (Brito et al., 2017). The K_c value for the initial crop stage was then adjusted for the frequency of the wetting events (precipitation and irrigation) and average infiltration depths, while the K_c values for mid-season and late season crop stages were adjusted for local climate conditions taking into consideration canopy height, wind speed and minimum relative humidity averages for the periods under consideration (Allen et al., 1998). The following parameters of the Feddes et al. (1978) model

were used to compute T_p reductions due to water stress: $h_1 = -15$, $h_2 = -30$, $h_3 = -325$ to -600, $h_4 = -8000$ cm (Wesseling et al., 1991). The bottom boundary condition was specified using the observed GWD (Figure 5.1-2). The initial soil water content conditions were set to field capacity.

5.1.2.3 Statistical and Uncertainty Analysis

Model calibration and validation was performed by comparing field measured values of soil water contents, LAI, hc and aboveground dry biomass with the MOHID-Land simulations (Approaches A–C) using various quantitative measures of the uncertainty, such as, the coefficient of determination (R^2), the root mean square error (RMSE), the ratio of the RMSE to the standard deviation of observed data (NRMSE), the percent bias (PBIAS) and the model efficiency (EF). R^2 values close to 1 indicate that the model explains well the variance of observations. RMSE, NRMSE and PBIAS values close to zero indicate small errors of estimate and good model predictions (Legates and McCabe, 1999; Moriasi et al., 2007; Wang et al., 2012). Positive or negative PBIAS values refer to the occurrence of under- or over-estimation bias, respectively. Nash and Sutcliff (Nash and Sutcliffe, 1970) modelling efficiency EF values close to 1 indicate that the residuals variance is much smaller than the observed data variance, hence the model predictions are good; contrarily, when EF is very close to 0 or negative there is no gain in using the model.

Data assimilation is much dependent on the empirical relationship (Figure 5.1-3) established to derive LAI values from the NDVI measurements (Li et al., 2014; Thorp et al., 2010). As such, the uncertainty related to that conversion was quantified on final model estimates of T_a, E_a and aboveground dry biomass using a Monte Carlo method. This evaluation was performed on modeling Approach C (Calibration + LAI assimilation) as the objective here was to assess if remote sensing data assimilation could further correct for simulation errors that result from model parameter uncertainty. The 2015 dataset was also considered as more satellite images were available during this season. A randomly population of 10,000 LAI values was first created for each available image date following a normal distribution with mean equal to the estimated parameter given by the LAI-NDVI regression equation and range defined by the 95% confidence intervals (Figure 5.1-3, Table 5.1-5). The model was then run following Approach C settings until reaching the dates of each of the eight available images (8 × 1 simulation). Afterwards, the 10,000 LAI randomly generated values were assimilated by the model, which then proceeded with simulations until the end season following Approach C settings again (8 × 10,000 simulations). In the end, the uncertainty of final model estimates of

T_a, E_a and aboveground dry biomass were assessed for each assimilation date (8 dates) from 10,000 simulations (80,000 simulations in total). The Monte Carlo simulations were performed with a Python script.

5.1.3 Results and Discussion

5.1.3.1 LAI Evolution

Figure 5.1-4 shows the evolution of LAI estimated values using the calibrated model in Ramos et al. (2017) (Approach A), direct LAI assimilation (Approach B) and the combination of the calibrated model and LAI assimilation (Approach C). Table 5.1-6 presents the statistical indicators used to evaluate the agreement between model simulations and measured values. Ramos et al. (2017) showed that the MOHID-Land model could reasonably well simulate LAI evolution during the 2014 and 2015 growing seasons. In their study, the values of R^2 were very high (0.97), showing that the model could explain well the variability of the observed data. The errors of the estimates were quite small, resulting in RMSE values lower than 0.63 m^2 m^{-2} and NRMSE values lower than 0.16. The PBIAS values were lower than 6.40%, indicating some underestimation of the measured data. The modelling efficiency EF were also high (≥0.93), meaning that the residual variance was much smaller than the measured data variance.

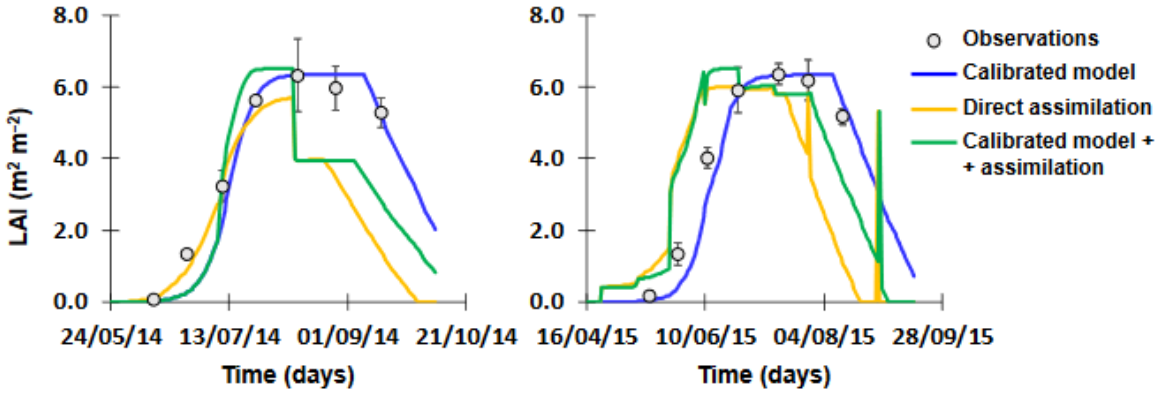

Figure 5.1-4 Measured and simulated leaf area index during 2014 (left) and 2015 (right) crop seasons. Vertical bars correspond to the standard deviation of measured data.

Table 5.1-6 Results of the statistical analysis between measured and simulated soil water contents, leaf area index (LAI), canopy height and aboveground dry biomass.

Statistic	R^2	RMSE	NRMSE	PBIAS	EF
2014					
Water Content (cm^3 cm^{-3})					
Calibrated Model	0.73	0.018	0.061	-1.53	0.70
Direct Assimilation	0.85	0.012	0.041	-1.16	0.87
Calibrated Model + Assimilation	0.89	0.012	0.039	-0.95	0.88
LAI (m^2 m^{-2})					
Calibrated Model	0.97	0.63	0.16	6.40	0.94
Direct Assimilation	0.60	2.13	0.54	33.82	0.26

Statistic	R^2	RMSE	NRMSE	PBIAS	EF
Calibrated Model + Assimilation	0.70	1.73	0.43	24.39	0.51
Canopy Height (m)					
Calibrated Model	0.93	0.42	0.22	-11.83	0.90
Direct Assimilation	0.86	0.58	0.31	0.96	0.80
Calibrated Model + Assimilation	0.90	0.50	0.26	-13.87	0.85
Dry Biomass (kg ha^{-1})					
Calibrated Model	0.94	5128.3	0.39	19.20	0.87
Direct Assimilation	0.94	2183.7	0.24	4.60	0.95
Calibrated Model + Assimilation	0.96	2518.9	0.32	14.20	0.91
2015					
Water Content (cm^3 cm^{-3})					
Calibrated Model	0.37	0.019	0.063	1.91	0.11
Direct Assimilation	0.40	0.017	0.057	0.90	0.28
Calibrated Model + Assimilation	0.39	0.018	0.060	1.58	0.18
LAI (m^2 m^{-2})					
Calibrated Model	0.97	0.61	0.15	6.31	0.94
Direct Assimilation	0.35	2.16	0.52	-1.18	0.24
Calibrated Model + Assimilation	0.63	1.58	0.38	-10.34	0.59
Canopy Height (m)					
Calibrated Model	0.96	0.33	0.17	-11.00	0.93
Direct Assimilation	0.85	0.65	0.33	-2.57	0.73
Calibrated Model + Assimilation	0.88	0.60	0.30	-19.13	0.77
Dry Biomass (kg ha^{-1})					
Calibrated Model	0.93	4616.8	0.33	15.27	0.89
Direct Assimilation	0.98	6211.4	0.44	-31.49	0.80
Calibrated Model + Assimilation	0.96	6237.8	0.44	-28.52	0.79

R^2, coeficient of determination; RMSE, root mean square error; NRMSE, normalized RMSE; PBIAS, percent bias; EF,modeling efficiency.

The direct assimilation of LAI values into model simulations (Approach B) produced worse statistical indicators than when using the calibrated model (Approach A), with the R^2 values decreasing down to 0.35 and the RMSE and NRMSE values increasing up to 2.16 m^2 m^{-2} and 0.53, respectively. The PBIAS showed contrasting results, while the EF values also decreased down to 0.24, indicating nonetheless that the model was still able to describe field measurements with relative success. The direct assimilation approach made that MOHID-Land's LAI simulated results were directly replaced by the remote sensing LAI values in the dates when satellite images were available. From that date on and until another image was available model simulations followed the default parameterization of the MOHID-Land crop database given in Table 5.1-4. As a result, assimilation of remote sensing LAI values using the forcing method available in the MOHID-Land model resulted in several unrealistic discontinuities in simulated LAI (Figure 5.1-4), a common feature when using this assimilation approach (Thorp et al., 2010). Also, LAI increased at a much faster pace during the initial and development crop stages, with maize also reaching senescence earlier. The difference of 200

◦C in the total heat units required for plant maturity (PHU) considered between the default and calibrated crop parameters (Table 5.1-4) showed here to be critical for model performance. LAI assimilation was able to correct model simulations during the earlier crop stages but failed to counteract the end of the crop cycle as observed in the 2015 simulations (Figure 5.1-4). Here, despite assimilating higher LAI values, the model was obviously never able to extend the crop lifecycle longer than the allowed by the default PHU parameter.

The previous results show the importance of considering Approach C, where data assimilation forced simulations of the local calibrated model. Contrarily to the expected, LAI assimilation did not further improve Approach A results. The R^2 values still decreased down to 0.63, while the RMSE and NRMSE values increased up to 1.73 m^2 m^{-2} and 0.43, respectively. The EF values also decreased to 0.51. However, these statistics were better than those obtained using only direct LAI assimilation (Approach B), showing the importance of local model calibration. Model simulations fully covered maize's lifecycle this time since no constraints in the PHU existed. However, results were still dependent on the quality of the assimilated data, with LAI evolution at the end of the 2015 season suggesting that some filtering would be needed during the assimilation process (Figure 5.1-4).

Despite the lower statistical indicators found when compared to those using only the calibrated model (Approach A), LAI evolution was also considered to be well represented when LAI data assimilation was included in the MOHID-Land model simulations (Approaches B and C), particularly during the earlier crop stages. Results further suggested that a higher time resolution of assimilated data would improve the agreement between model simulations and measured data. Nonetheless, more important than accurately predicting LAI evolution was to understand how data assimilation impacted the soil water balance, aboveground dry biomass and yield estimates during the 2014 and 2015 growing seasons, as shown below.

5.1.3.2 Soil Water Balance

Figure 5.1-5 presents the measured soil water contents at depths of 10, 30 and 50cm during the 2014 and 2015 growing seasons and compares these values with model simulations following the approaches referred above. Contrarily to LAI results, forcing remote sensing LAI data into model simulations reduced deviations between measured and simulated soil water content values. During the 2014 growing season, the RMSE values decreased from 0.018 to 0.012 cm^3 cm^{-3}, while the NRMSE values reduced from 0.061 to 0.039 when considering LAI assimilation (Approaches B and C). Inversely, the EF values increased from 0.70 to 0.88 (Table 5.1-6). During the 2015 growing season, the positive impact of LAI data assimilation on soil

water content simulation was more modest with only the EF values showing a relative improvement from 0.11 to 0.28. No noticeable differences were found between Approach B and Approach C statistical indicators. All simulations shared the same soil hydraulic parameters (Table 5.1-1) to better assess the actual impact of LAI assimilation on soil water content simulations, explaining thus the similarity of model results.

As LAI evolution was used in the partition of ET_c values into T_p (Equation 8) and E_p (Equation 9) (Ritchie, 1972), these two soil water balance components showed the greatest variation when considering LAI data assimilation (Table 5.1-7). The calibrated model (Approach A) produced estimates of T_a, E_a, capillary rise (CR) and deep percolation (DP), in line with other studies carried out in the region (Cameira et al., 2003; Paredes et al., 2014c, 2014a), some of which highlighting the importance of CR to the soil water balance in the Sorraia Valley region. Direct LAI assimilation produced always the lowest T_p and T_a values ($T_a/T_p = 1$), and, naturally, the highest E_p and E_a values during both seasons. The LAI data forcing on the calibrated model (Approach C) produced contrasting results when compared to Approach A, with T_p values decreasing in 2014 when LAI evolution was underestimated (PBIAS = 24.39%) and increasing in 2015 when the opposite occurred (PBIAS = −10.34%). Accurate LAI predictions were thus essential for simulating crop transpiration and soil evaporation, even though other important soil water balance components such as deep percolation and capillary rise were not significantly affected by less accurate LAI predictions. As a result, LAI assimilation in MOHID-Land may thus have a direct influence on biomass development, while estimates of groundwater recharge or solute leaching from the root zone may be impacted less significantly.

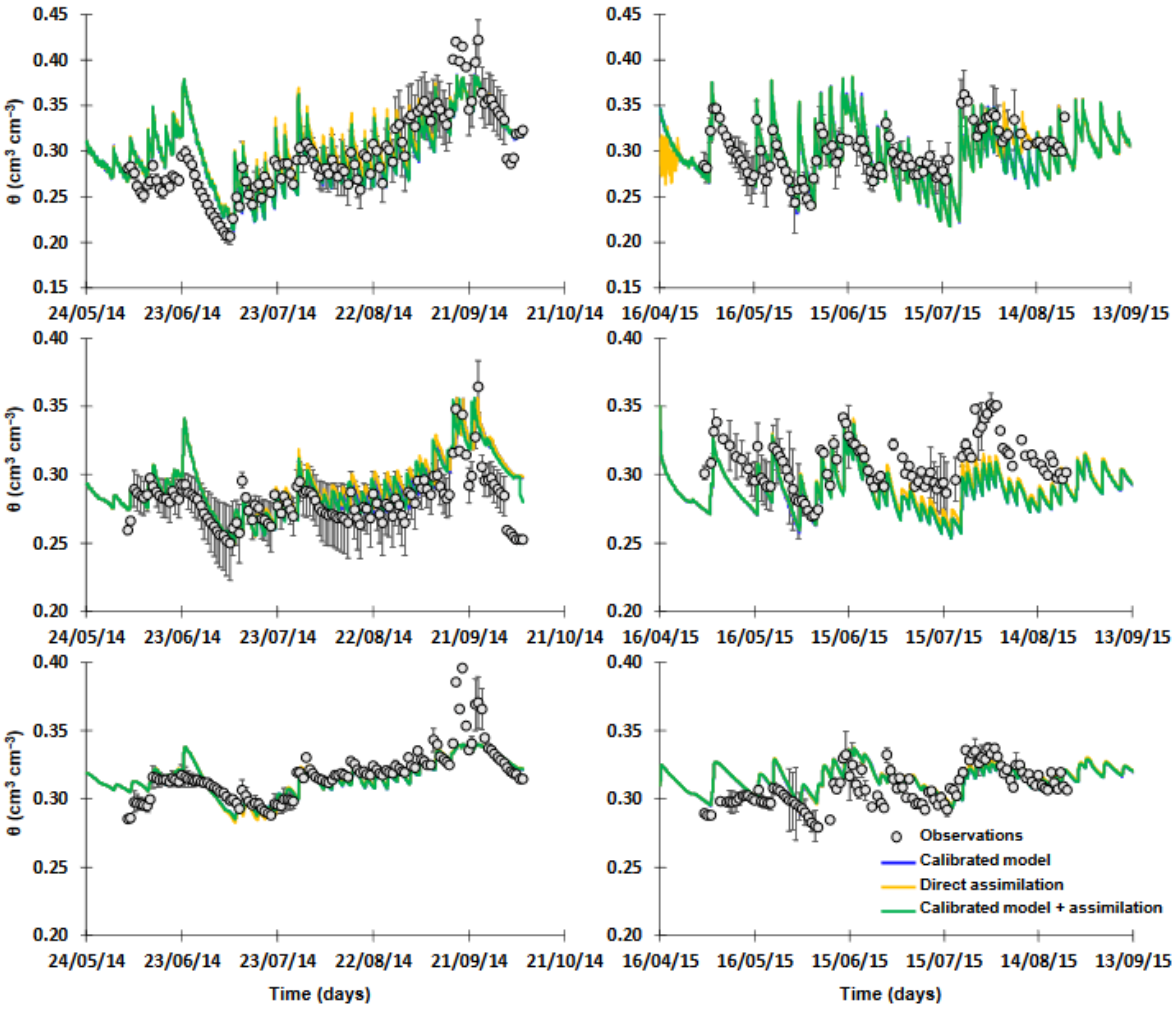

Figure 5.1-5 Measured and simulated soil water contents (θ) at depths of 10 (top), 30 (middle) and 50 cm (bottom) during 2014 (left) and 2015 (right) crop seasons. Vertical bars correspond to the standard deviation of measured data.

Table 5.1-7 Components of the soil water balance.

Approach	Inputs				Outputs			
	P (mm)	I (mm)	CR (mm)	ΔSS (mm)	E_a (mm)	T_a (mm)	T_a/T_p (-)	DP (mm)
2014								
Calibrated model	163	365	78	16	164	374	0.99	74
Direct assimilation	163	365	70	2	191	345	1.00	90
Calibrated model + Assimilation	163	365	78	2	183	355	1.00	84
2015								
Calibrated model	12	620	94	11	181	481	1.00	75
Direct assimilation	12	620	84	3	199	461	1.00	82
Calibrated model + Assimilation	12	620	95	3	150	512	1.00	75

P, precipitation; I, irrigation; CR, capillary rise; E_a, actual soil evaporation; T_a, actual crop transpiration; T_p, potential crop transpiration; DP, deep percolation.

5.1.3.3 Crop Height

The direct assimilation of LAI (Approach B) showed the maize canopy growing faster than that measured in the field or simulated by Ramos et al. (2017) (Approach A), similarly to LAI predictions (Figure 5.2-6). Canopy height then assumed a default maximum value ($h_{c,max}$) of 2.5 m when the mid-season crop stage was reached (default value in Table 5.1-4), underestimating field values from that date onward and producing worse statistical indicators than those computed using the calibrated model (Table 5.1-6). The main problem here was thus the lack of a local calibrated dataset with the impact of LAI assimilation on canopy height simulations being only marginal as shown by the good indicators again obtained in Approach C.

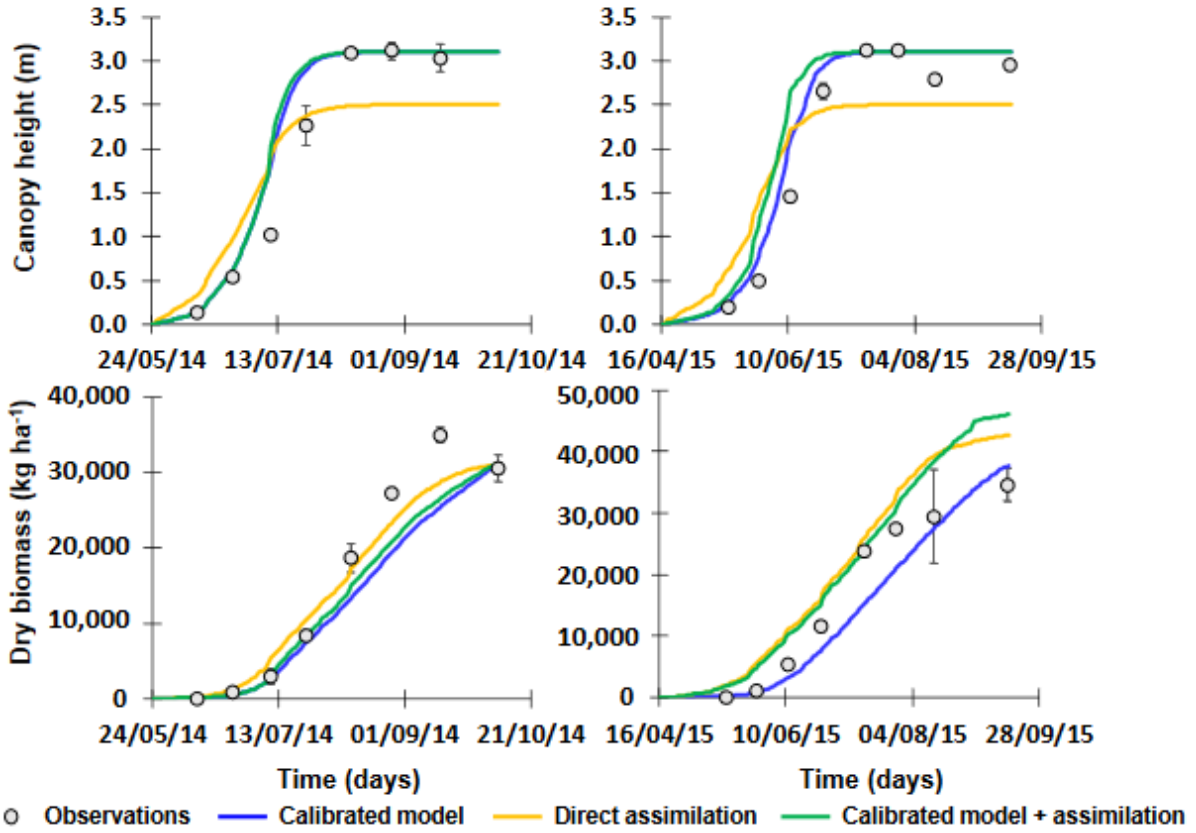

Figure 5.1-6 Measured and simulated canopy height (top) and aboveground dry biomass (bottom) during 2014 (left) and 2015 (right) crop seasons. Vertical bars correspond to the standard deviation of measured data.

5.1.3.4 Dry Biomass and Yields

Simulations of the aboveground dry biomass were concordant with the estimated LAI values during the 2014 and 2015 growing seasons. In 2014, the underestimation of LAI values led also to lower aboveground dry biomass estimates following the direct LAI assimilation approach (Approach B), with these being further closer to field measurements than the earlier results from the calibrated model (Approach A). As a result, the RMSE values decreased from

5128.3 to 2183.7 kg ha^{-1}, the NRMSE values reduced from 0.39 to 0.24 and the EF values increased from 0.87 to 0.95 when direct LAI assimilation was considered. Contrarily, the overestimation of LAI values produced larger errors in 2015 when compared to field measurements, with the RMSE values increasing from 4616.8 to 6211.4 kg ha^{-1}, the NRMSE values increasing from 0.33 to 0.44 and the EF values decreasing from 0.89 to 0.79. The local calibrated crop dataset (Approach C) did not improve aboveground dry biomass estimates.

Measured crop yields reached 16,093 and 17,300 kg ha^{-1} during the 2014 and 2015 seasons, respectively (Table 5.1-8). Yield predictions were in line with the same under- and overestimation tendencies observed in simulations of the aboveground dry biomass. Yield estimated from the three modeling approaches were relatively close (14,670–15,518 kg ha^{-1}) during the 2014 season, with Approach C producing the best estimates. On the other hand, during the 2015 season, yield estimates from that same approach produced the worse results (23,016 kg ha^{-1}), with all models diverging substantially from the measured value.

Table 5.1-8 Yield (kg ha^{-1}) estimates.

Season	Measured	Approach A	Approach B	Approach C
2014	16,093	14,670	15,196	15,518
2015	17,300	17,930	20,916	23,016

While many studies throughout the literature reported that precise knowledge of light interception and hence LAI, was critical for predicting biomass and yield accurately (Jin et al., 2018; Tripathy et al., 2013; Yuping et al., 2008), results presented here were more in line with Linker and Ioslovich (2017), who found that assimilation of easy-to-obtain canopy cover measurements did not always improve the predictions of biomass. They explained that by model choice, which in their case was a purely water-driven model in which solar radiation and light interception were not considered explicitly, likely resulting in underestimating the overall impact of canopy cover on crop development. A similar reasoning can be considered here. Ines et al. (2013) also found that LAI assimilation could not always improve simulated aboveground dry biomass and yield predictions, particularly during dry conditions as the root zone soil moisture could not meet the increased water demand that resulted from improved canopy growth. Likewise, Nearing et al. (2012) referred to the failure of LAI and soil moisture data assimilation in improving yield estimates, especially in water-limited environments, pointing out similar reasons as Ines et al. (2013). From a different perspective, Trombetta et al., 2016 made use of remote sensed LAI data derived from the MODIS satellite images for calibrating/validating a hydrological model at the plot scale. Remote sensing LAI data, after

being converted into canopy cover, was used as an alternative to field measurements during the calibration/validation process, with results suggesting this approach as a viable alternative for characterizing landscape heterogeneity (crop variability) at larger scales.

5.1.3.5 Uncertainty of Model Estimates

The previous sections showed that the impacts of LAI assimilation on MOHID-Land final estimates of T_a, E_a and aboveground biomass were substantial and that some filtering would be eventually needed for improving the quality of assimilated data. The uncertainty analysis carried out using a Monte Carlo method confirmed these early findings, with Figure 5.1-7 showing a relatively large uncertainty of final model estimates when LAI assimilation was performed during the first two dates (23/04/2015, 09/05/2015) of 2015 crop growing season. In these dates, Ta values ranged from 460 to 527mm, while E_a values varied between 102 and 184mm. Likewise, the aboveground dry biomass showed also considerable variation, ranging from 37,978 to 47,347 kg ha^{-1}. From those dates onwards, the uncertainty of final model estimates decreased, being relatively small when LAI assimilation was carried out at the end of the crop cycle. Filtering of the assimilation data would thus be important during the earlier crop stages, becoming irrelevant as the crop reaches the end of its life cycle.

The large uncertainty observed on model final estimates was already expected when LAI assimilation was performed during the earlier dates since the crop was still at the initial and development stages and thus is growth cycle was not yet well defined. Yet, the Monte Carlos simulation results showed that the assimilation of too low LAI values could lead the model to greatly underestimate crop transpiration and aboveground dry biomass, while soil evapotranspiration would be greatly overestimated. Hence, this can be quite problematic in the absence of additional information to update model simulations throughout the crop season if new satellite images are no longer available (e.g., due to cloud cover). In this case, the model will never be able to further update simulations of T_a, E_a and aboveground dry biomass, producing quite substantial errors.

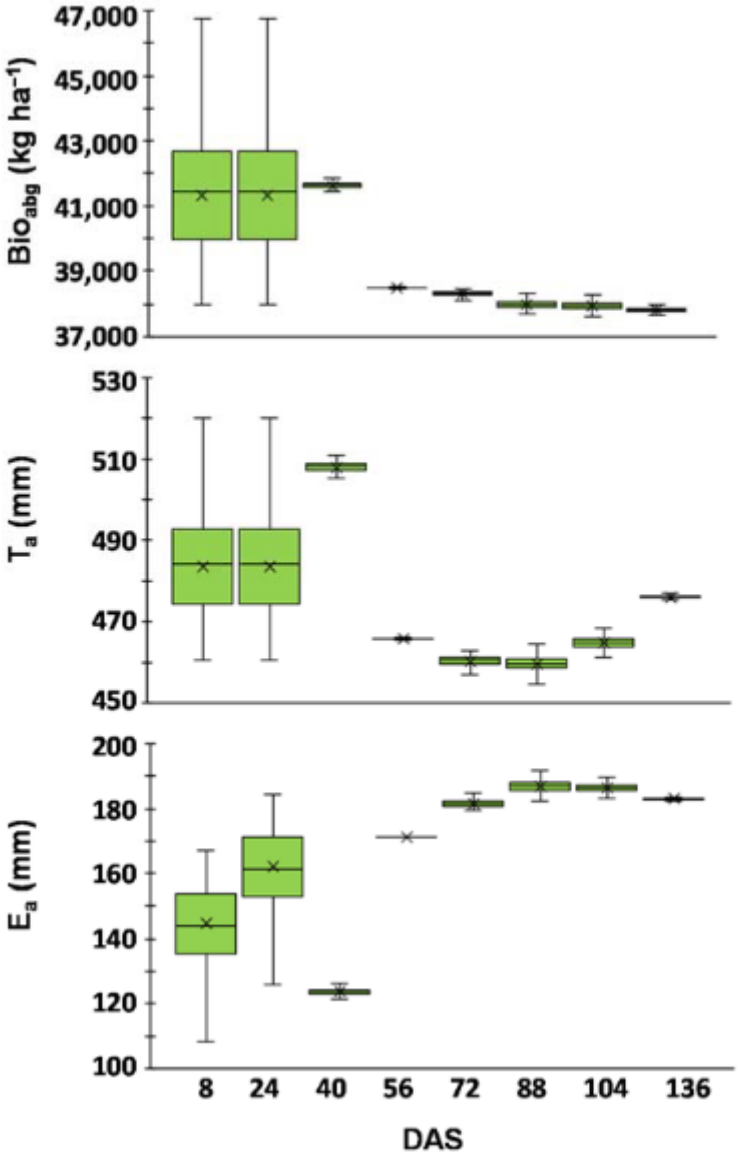

Figure 5.1-7 Uncertainty of data assimilation on aboveground dry biomass (top), actual transpiration Ta (middle) and actual soil evaporation Ea (bottom) final model estimates for the 2015 crop season on different dates (DAS, days after sowing). Box-plots indicate maximum and minimum values, median (–), first and third quartiles and average (×) of 10,000 Monte Carlo simulations.

5.1.4 Conclusions

Remote sensing technology can provide valuable information for hydrological modeling at the field and regional scales by better characterizing the spatial and temporal variability of soils, land uses and climate, which otherwise are difficult to portray. This study showed that LAI assimilation from NDVI derived satellite data improved MOHID-Land estimates of the soil water balance and simulations of crop height and aboveground dry biomass during the early stages of the crop growing period. However, data assimilation was never sufficient to improve model simulations in the absence of a crop calibrated dataset, failing to simulate the

entire growing season when calibrated potential heat units (PHU) were missing or even crop maximum height when crop parameterization was misadjusted. LAI data assimilation led also to great uncertainty on final estimates of crop transpiration, soil evaporation and the aboveground dry biomass when solely performed during the initial stages of the crop growing period. Although model uncertainty then decreased as LAI assimilation was being carried out closer to the end of the crop cycle, results showed that this approach may lead to complete erroneous estimates of the soil water balance and crop yields even when local calibrated soil and crop datasets are used. Therefore, while LAI remote sensing data can help defining MOHID-Land's input parameters, additional data sources should be accessed for complementing such characterization. The implementation of the MOHID-Land model at the regional scale cannot depend solely on inputs from the LAI data assimilation as estimates may diverge substantially from reality.

5.2 Exploring the Use of Vegetation Indices for Validating Crop Transpiration Fluxes Computed with the MOHID-Land Model. Application to Vineyard

The material on which this chapter is based has been previously published in: Ramos, T.B., Simionesei, L., Oliveira, A.R., Neves, R., Darouich, H., 2021. Exploring the use of vegetation indices for validating crop transpiration fluxes computed with the MOHID-land model. Application to vineyard. Agronomy 11. https://doi.org/10.3390/agronomy11061228

5.2.1 Introduction

Irrigation is fundamental to fulfill crop water requirements in many regions of the world. Yet, inefficient practices often lead to the degradation of soil and water resources by promoting nutrient leaching, surface runoff and soil erosion, salt accumulation in the rootzone, and the eutrophication of water bodies with associated biodiversity loss. There is thus the need for minimizing environmental risks through the accurate estimate of crop water requirements and the definition of irrigation schedules (irrigation timing, duration, and quantity) that maximize agricultural water productivity and farmers' income (Pereira et al., 2002).

Several decision support systems (DSS) were developed over the last few decades to aid farmers in the decision-making of irrigation. One example is the IrrigaSys DSS developed by academics and stakeholders to support farmers in the Sorraia valley irrigation district, in southern Portugal (Simionesei et al., 2020). When running in operational mode this DSS computes the weekly soil water balance based on hindcast and forecast weather data as well as inputs from farmers. It then suggests an optimized irrigation schedule for the week that follows.

Assuring the reliability of predictions has been fundamental for the success of the DSS. It has also been its most challenging issue considering that the core engine of the system is the MOHID-Land model (Ramos et al., 2017), which is highly complex in terms of parametrization of soil and crop state variables. The current support of the DSS to 103 agricultural fields distributed throughout the region only further presses the need for correctly accounting for a wide variety of crop management and soil conditions to guarantee the quality of the service.

Remote sensing, with the ability to cover large remote areas at different spatial and temporal resolutions, compatible with the characterization of the state and dynamics of several meteorological, vegetation growth, and hydrological variables, has been a preferential approach for evaluating the performance of the DSS (Ramos et al., 2018; Simionesei et al., 2018). Ramos et al. (2018) analyzed the impact of assimilation of leaf area index (LAI) data derived from Landsat 8 imagery on model simulations. The relevancy of this study was because MOHID-Land computes the soil water balance using mass and momentum conservation equations, with LAI being critical to the correct partition of crop evapotranspiration (ET_c) rates into crop transpiration and soil evaporation. Their main conclusion was that modeling vegetation growth and the partition of the ET_c components at the plot scale could not depend solely on inputs from LAI data assimilation because estimates of the soil water balance could diverge substantially from the reality, thus confirming the need to use a proper crop dataset for model calibration. On the other hand, Simionesei et al. (2018) used LAI data derived from the same satellite sensor for simply adjusting crop growth parameters to calibrate/validate model results, providing a more feasible solution for rapidly developing a large database of crop variability at the regional scale. This would, however, depend on the availability of a relationship to be established between field LAI data and that estimated from the satellite sensor.

This paper now focuses on an alternative solution for evaluating the performance of the DSS, in this case by comparing MOHID-Land estimates of the transpiration component in ET_c with those derived from remote sensing-based vegetation indices (VI). Several procedures already exist that make use of spectral VI for estimating crop evapotranspiration fluxes and irrigation needs in agricultural fields (Pôças et al., 2020). Although in most of these procedures the soil water balance is computed according to the FAO56 approach (Allen et al., 1998), they can eventually be adapted for obtaining calibrated relations between the VI and fluxes from a complex mechanistic model such as MOHID-Land, providing a scalable solution for assessing model behavior in fields with similar management.

Hence, the objectives of this study are (i) to simulate soil water contents in an irrigated vineyard (Vitis vinifera L.) using the MOHID-Land model during the 2018–2020 growing seasons; (ii) to compute the soil water balance for the study period; (iii) to establish relationships between actual transpiration rates computed by the MOHID-Land model and those derived from the normalized difference vegetation index (NDVI) and Sentinel-2 satellite (European Space Agency, European Union) imagery. Results of this study can thus help define better management practices to be implemented in IrrigaSys and improve its performance in the Sorraia Valley region.

5.2.2 Materials and Methods

5.2.2.1 Description of the Study Area

This study was carried out at Companhia das Lezírias, Samora Correia, Portugal (38.808◦ N, 8.900◦ W, 45 m a.s.l.) from January 2018 to October 2020. The climate in the region is dry subhumid, with mild winters and hot, dry summers. The mean annual precipitation is 669 mm, mainly concentrated between October and May, while the mean annual temperature is 16.8 ◦C. The weather data (Figure 5.2-1) for the study area was obtained from the local weather station (Figueirinha) and included daily precipitation (P; mm); maximum (T_{max}; ◦C) and minimum (T_{min}; ◦C) surface air temperatures; maximum (RH_{max};%), mean (RH_{avg}; %), and minimum (RH_{min}; %) relative humidity; solar radiation (Rs; MJ m^{-2} d^{-1}); wind speed measured at 2m height (u_2; m s^{-1}). This information was then used to compute the reference evapotranspiration (ET_o, mm) following the FAO Penman– Monteith method (Allen et al., 1998). The soil was classified as a Haplic Fluvisol (IUSS Working Group WRB, 2014), with loamy-sand texture in the top 60cm layer and sandy texture in the bottom 60–100cm layer.

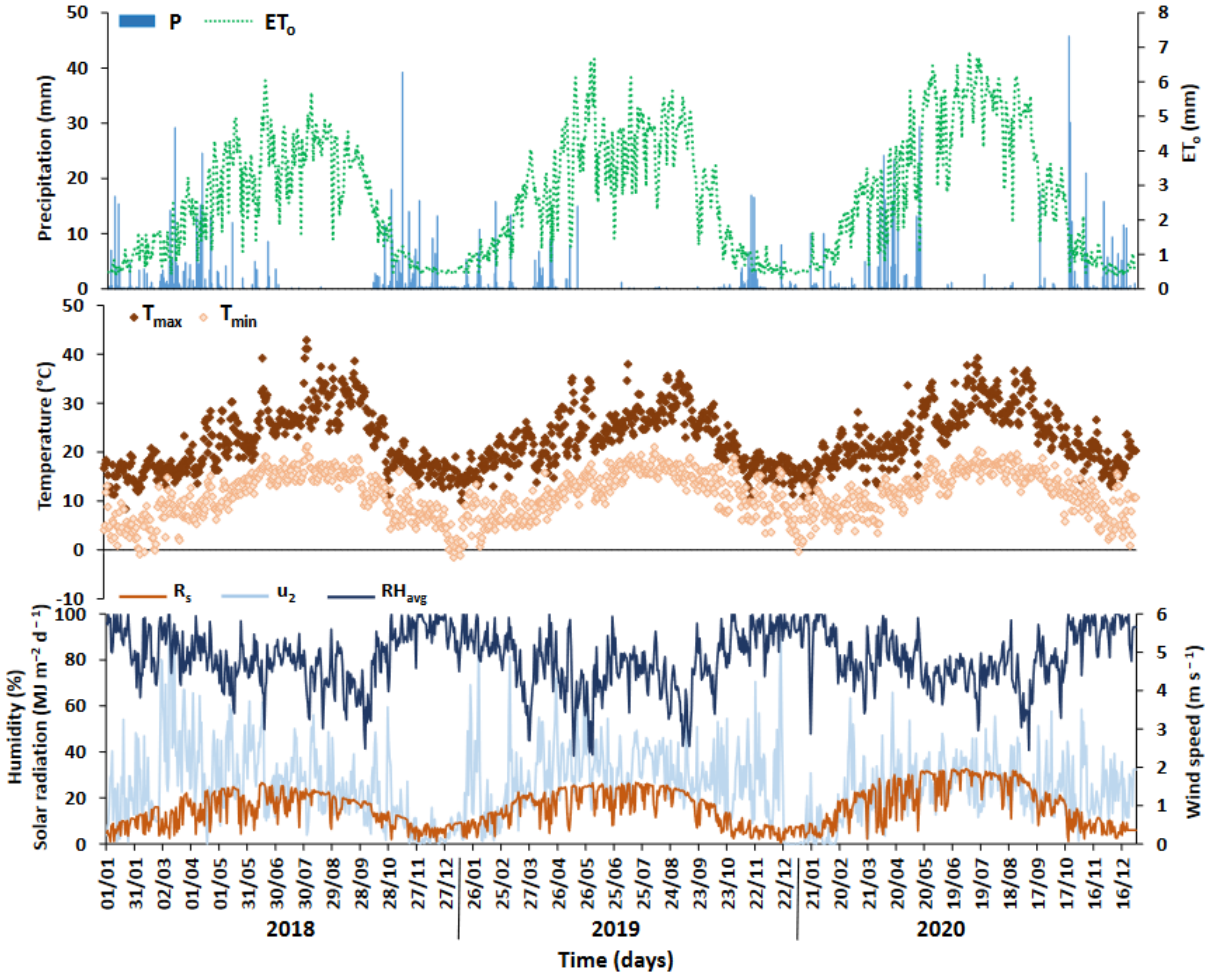

Figure 5.2-1 Weather data for the study period (P, precipitation, ET_0, reference evapotranspiration; T_{max} and T_{min}, maximum and minimum surface air temperatures, respectively; RH_{avg}, mean relative humidity; Rs, solar radiation, u2, wind speed at 2 m height).

The selected field, planted in 2008, was relatively flat (slope < 2‰), and part of a larger (130 ha) vineyard area. The field was a drip-irrigated plot, 5 ha in size, planted with different varieties of wine grapes, with Touriga Nacional being dominant and Castelão, Moreto, and Alicante Bouschet in smaller proportions. The plants were grown on vertical shoot positioned trellis, with wood pruning during the dormant period. Plants presented a row distance of 1.0m and a row spacing of 2.8m, thus a plant density of approximately 3571 plants ha^{-1}, with an orientation in the east–west direction. Irrigation was delivered through a drip system, with management practices performed according to the standard practices in the region and decided by the farmer. Drippers were spaced 1m apart, and the drip line was placed on the trellis 0.5 m above the soil surface. The total water applied through irrigation summed 470, 625, and 465 mm in 2018, 2019, and 2020 growing seasons, respectively. The application depth during irrigation events varied from 1 to 12 mm. Soil water contents were continuously monitored in

two locations at depths of 10, 20, 30, 40, 50, 60, 70, and 80 cm using EnviroPro MT (MAIT Industries, Bayswater North, Australia) capacitance probes.

5.2.2.2 Model Setup, Calibration, Validation

The simulation period covered the 2018–2020 growing seasons. The soil profile was represented by one vertical column discretized into 20 grid cells, 1 m wide, 1 m long, and with variable thickness (0.025m on the top to 0.625m at the bottom) considering the depth of the simulation domain, the root zone, and the measured soil moisture data. ET_c rates were computed by multiplying daily ET_o values with the respective crop coefficients (K_c) for the initial, mid-season, and late-season stages. The K_c values for wine grapes listed in Allen et al. (1998) were used as default. The upper boundary condition was then determined by $E_{a\ model}$ and $T_{c\ model}$ rates, and net irrigation and precipitation fluxes. The soil hydraulic parameters were initially set according to the texture classes of the soil horizons/layers following the class pedotransfer functions in Ramos et al. (2014, 2013). The crop growth parameters in Neitsch et al., (2011) crop database were also used as default settings. Root water uptake reductions were computed by considering the following parameters: $h_1 = -10$, $h_2 = -25$, $h_3 = -1000$, $h_4 = -18{,}000$ cm (Wesseling et al., 1991). Free drainage was used as the bottom boundary condition.

Model calibration was performed during the 2018 growing season following Ramos et al. (2017). The trial-and-error procedure was first used to calibrate the crop growth parameters by making them vary within reasonable ranges until deviations between modeled and field LAI data were minimized. The Copernicus Global Land Service LAI dataset derived from the Sentinel-3 sensor at 300 m resolution was assumed here to represent field conditions ("Copernicus Global Land Service. Available online: https://land.copernicus.eu/global/index.html (accessed on 17 March 2021).," n.d.). Only pixels covering the vineyard area and not affected by adjacent vegetation were used to extract LAI data. LAI values were also compared to the existing literature to evaluate their adequacy (Fraga et al., 2016; Orlando et al., 2016). LAI data corresponding to the non-growing season were simply ignored since it represented grass growth covering the vine's interrow during the rainfall period, but which dynamics could not be considered in this application. The interrow crop had also little influence on soil moisture data as the capacitance probes were installed in the vine rows. Then, the same trial-and-error procedure was adopted for calibrating the K_c values for the different crop stages as well as the soil hydraulic parameters for the different soil layers. These parameters were also made to vary within reasonable ranges until deviations between observed and simulated soil water contents were minimized. The connectivity/tortuosity

parameter l was not adjusted, being set to 0.5 following Mualem (1976). The parameters θ_s, α, η, K_{sat}, and the maximum value of LAI (LAI_{max}) are identified as the most sensitive parameters during model calibration (Ramos et al., 2017). The calibrated crop growth parameters, K_c values, and soil hydraulic parameters were then used to validate model simulations of crop growth and soil water contents during the 2019 and 2020 growing seasons. Seasons were run separately, with end results from one season being updated at the beginning of the following according to measured data of soil water contents.

The goodness-of-fit indicators adopted for comparing field and simulated LAI values and soil water contents were the coefficient of determination (R^2), the root mean square error (RMSE), the normalized RMSE (NRMSE), the percentage bias (PBIAS), and the model efficiency (NSE). R^2 values close to 1 indicate that the model explains well the variance of observations. RMSE and NRMSE values close to zero indicate small estimation errors and good model predictions (Moriasi et al., 2007). PBIAS values close to zero indicate that model simulations are accurate, while positive or negative values indicate under- or over-estimation bias, respectively. NSE values close to 1 indicate that the residuals' variance is much smaller than the observed data variance, hence the model predictions are good. On the contrary, if NSE is less than zero the model-predicted values are worse than simply using the observed mean (Nash and Sutcliffe, 1970).

5.2.2.3 Data Processing of Sentinel-2 Imagery

$T_{c\ act\ model}$ rates, and respective actual basal crop coefficients ($K_{cb\ act\ model} = T_{c\ act\ model}/ET_o$ ratio), computed by the MOHID-Land model were compared with those derived using a second approach, where those variables were estimated from a vegetation index (VI). Satellite sensors have been extensively used for estimating crop evapotranspiration with real-time single (K_c) or basal crop coefficients (K_{cb}) estimated from VI data. Pôças et al. (2020) provided a comprehensive listing of the many types of K_c -VI and K_{cb}-VI relationships developed for annual and perennial crops. Examples of applications in vineyards can be found in Campos et al. (2016, 2010) and Er-Raki et al. (2013). Landsat imagery (National Aeronautics and Space Administration Agency, Washington, DC, USA) has been the most frequently used satellite data to generate VIs to estimate those crop coefficients. However, its revisiting period of 16 days, which is often extended due to high levels of cloud cover, and the relatively coarse resolution (30m) of its multispectral imagery has limited the use of that sensor for irrigation water management at the field scale. In this sense, the launch of the Sentinel-2 mission (European Space Agency, European Union) in 2017 represented a major step forward on the

use of satellite data for remotely monitoring crop irrigation needs by offering a revisiting time of 5 days under the same viewing angle, and multispectral imagery at 10 m (visible and broad near-infrared spectrum), 20m (red edge and narrow and short-wave infrared), and 60 m (atmospheric bands) resolution.

In this study, the red (Red; band 4) and near infra-red (NIR, band 8) bands from Sentinel-2 image tiles having less than 10% cloud cover were downloaded from the Copernicus Open Access Hub ("Copernicus Open Access Hub. Available online: https://scihub.copernicus.eu/ (accessed on 17 March 2021).," n.d.) for the study period. The images were subjected to atmospheric correction of the downloaded scenes using the Sen2cor software ("European Space Agency. Available online: https://step.esa.int/main/third-party-plugins-2/sen2cor/ (accessed on 17 March 2021)," n.d.), which is a processor for Sentinel-2 Level 2A product generation and formatting, performing the atmospheric, terrain and cirrus correction of top-of-atmosphere Level 1C input data, and creating bottom- of-atmosphere corrected reflectance images. A total of 65 images were available during the 2018–2020 growing seasons. The NDVI was then computed for all available images with the Equation 26 (Rouse et al., 1974).

This VI was chosen as it is the most used for establishing K_c-VI and K_{cb}-VI relationships for annual and perennial crops in the literature (Pôças et al., 2020). Following Campos et al. (2010), the NDVI was calculated on a pixel-by-pixel basis and averaged for the area surrounding the location of soil moisture probes (100 m long 60 m width), avoiding field edge pixels (Figure 5.2-2).

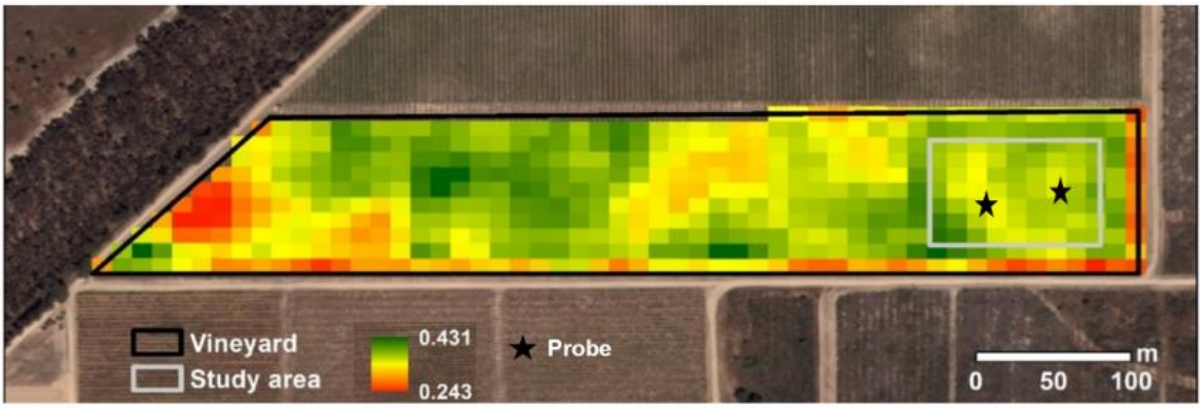

Figure 5.2-2 NDVI image for the study area on 7 July 2020.

The NDVI data were used to derive values of the basal crop coefficients and actual transpiration rates for each available image date as follows (González-Dugo and Mateos, 2008; Pôças et al., 2020):

$$K_{cb\ act\ NDVI} = \min\left[K_{cb\ max}, K_{cb\ max}/f_{c\ max}\ (NDVI - NDVI_{min})/(NDVI_{max} - NDVI_{min})\right] \quad \text{Equation 34}$$

$$T_{c\ act\ NDVI} = K_{cb\ act\ NDVI}\ ET_o \quad \text{Equation 35}$$

where $K_{cb\ act\ NDVI}$ is the actual basal crop coefficient computed from the NDVI (-), $T_{c\ act\ NDVI}$ is the actual transpiration rate computed from the NDVI (L T^{-1}), $K_{cb\ max}$ is the maximum value of basal crop coefficient (-), $f_{c\ max}$ is the fraction of ground cover corresponding to the maximum K_{cb} (-), and $NDVI_{min}$ and $NDVI_{max}$ represent the maximum and minimum values of NDVI corresponding to bare soil and effective full cover, respectively (-). Thus, in this study, the subscript NDVI identifies the variables computed from satellite imagery. The $K_{cb\ act\ NDVI}$ represents primarily plant transpiration as well as a residual diffusive evaporation component supplied by soil water below the dry surface (Allen et al., 2005; Allen et al., 1998). As the VI reflects the actual vegetation cover conditions, the estimated values represent actual rather than standard conditions (Pereira et al., 2015). For each growing season, the $K_{cb\ max}$ (0.48) was defined according to Rallo et al. (2021). The fc max was obtained from the maximum LAI value (LAI_{max}) and crop height following Allen and Pereira (2009). The $NDVI_{min}$ and $NDVI_{max}$ values were specified based on the evolution of the NDVI over the growing seasons, being set to 0.10 (assumed to represent bare soil conditions) and 0.58 (corresponding to a 10% increase of the maximum observed NDVI value), respectively, in each season.

The $K_{cb\ act\ model}$ and $T_{c\ act\ model}$ values computed using the MOHID-Land model were thus compared with the corresponding values derived from satellite imagery ($K_{cb\ act\ NDVI}$ and $T_{c\ act\ NDVI}$) by linear regression analysis. The estimates from the MOHID-Land model were considered the dependent variables since they were the objective of validation. The resulting linear regression models were analyzed using a cross-validation technique, in which data from two years were used as the training subset and data from the remaining year was used as the validation subset. As data from only three growing seasons was used, this procedure was repeated three times to include all possible combinations as calibration and validation subsets. For each validation test, the performance of regression models was assessed using the same goodness-of-fit tests referred to earlier except for the NSE.

5.2.3 Results and Discussion

5.2.3.1 Model Parametrization

Table 5.2-1 presents the calibrated crop growth parameters for the vine. Like in previous applications of the MOHID-Land model (Ramos et al., 2017; Simionesei et al., 2018), most default settings used for simulating crop growth needed to be modified to accurately describe field data. In this case study, LAI_{max} was set according to the maximum value extracted from the Copernicus Global Land Service LAI dataset ("Copernicus Global Land Service. Available

online: https://land.copernicus.eu/global/index.html (accessed on 17 March 2021).," n.d.) during the three growing seasons. The remaining parameters of the LAI curve were then modified using the data available in the calibration period. The maximum canopy height ($h_{c,max}$) was defined according to field observations while the maximum root depth ($Z_{root,max}$) was adjusted based on measured soil moisture profiles using the capacitance probes installed at the field plot. Lastly, the base temperature for vine growth (T_{base}), i.e., the minimum temperature required for crop development, was calibrated to 8◦C, which is slightly lower than the minimum threshold of 10◦C generally considered for vineyard in the literature (Santos et al., 2020). The optimal temperature was set to 20◦C, in accordance with the existing literature.

Table 5.2-1 Calibrated crop growth parameters.

Crop Parameter	Value
Optimal temperature for plant growth, T_{opt} (°C)	20.0
Minimum temperature for plant growth, T_{base} (°C)	8.0
Plant radiation-use efficiency, RUE [(kg ha^{-1}) (MJ m^{-2})$^{-1}$]	30
Total heat units required for plant maturity, PHU (°C)	3500
Fraction of PHU to reach the end of stage 1 (initial crop stage), $fr_{PHU,init}$ (-)	0.05
Fraction of PHU to reach the end of stage 2 (canopy development stage), $fr_{PHU,dev}$ (-)	0.15
Fraction of PHU after which LAI starts to decline, $fr_{PHU,sen}$ (-)	0.55
Maximum leaf area index, LAI_{max} (m^2 m^{-2})	1.4
Fraction of LAI_{max} at the end of stage 1 (initial crop stage), $fr_{LAImax,ini}$ (-)	0.35
Fraction of LAI_{max} at the end of stage 2 (canopy development stage), $fr_{LAImax,dev}$ (-)	0.85
Maximum canopy height, $h_{c,max}$ (m)	1.5
Maximum root depth, $Z_{root,max}$ (m)	0.8
Net radiation coefficient (-)	0.463
Photosynthetically active radiation coefficient (-)	0.650

Table 5.2-2 presents the calibrated van Genuchten-Mualem parameters for different soil layers. Most parameters showed little variation with depth, with α and η reflecting as expected the characteristically relatively high values of coarse-textured soils (Ramos et al., 2014, 2013). The exception was the K_{sat}, which values increased with depth on several orders of magnitude. On the other hand, the calibrated K_c values for the initial ($K_{c\ ini}$ = 0.30), mid-season ($K_{c\ mid}$ = 0.70), and late-season ($K_{c\ end}$ = 0.45) crop stages agreed well with Allen et al. (1998). The K_c value for the initial stage was then adjusted for the frequency of the rainfall events and average infiltration depths, varying between 0.3 and 0.5. The K_c values for mid-season and late-season were adjusted for local climate conditions taking into consideration plant height, mean u_2, and mean RH_{min} for the period under consideration, varying from 0.69 to 0.71 and 0.44 to 0.46, respectively, during the different growing seasons.

Table 5.2-2 Calibrated soil hydraulic parameters.

Depth (m)	0–0.15	0.15–0.25	0.25–0.35	0.35–0.45	0.45–0.55	0.55–0.65	0.65–0.75	0.75–2.0
θ_r ($m^3\ m^{-3}$)	0.057	0.057	0.057	0.057	0.057	0.057	0.037	0.037
θ_s ($m^3\ m^{-3}$)	0.410	0.410	0.410	0.410	0.410	0.410	0.410	0.410
α (cm^{-1})	0.184	0.184	0.194	0.194	0.184	0.184	0.184	0.164
η (-)	2.0	1.9	1.8	1.8	1.8	1.8	1.8	1.8
l (-)	0.5	0.5	0.5	0.5	0.5	0.5	0.5	0.5
K_{sat} ($cm\ d^{-1}$)	90.7	90.7	1339.2	907.2	565.9	565.9	907.2	1339.2

θ_r, residual water content; θ_s, saturated water content; α and η, empirical shape parameters; l, pore connectivity/tortuosity parameter; K_{sat}, saturated hydraulic conductivity.

5.2.3.2 Model Performance

Figure 5.2-3 shows the daily averages of the soil water contents measured at depths of 10, 40, and 80 cm during the 2018–2020 growing seasons and compares these values with the MOHID-Land simulations. Although measured and simulated data were compared for all monitored depths, results are presented graphically only for the depths mentioned above to limit the number of figures. Measured soil water contents increased sharply with precipitation to values close to saturation to then decrease also rapidly to lower levels due to the dominance of the gravitational gradient near saturation which promoted percolation, but also due to crop evapotranspiration. Irrigation was usually applied at small depths (1–12 mm) to maintain soil water contents relatively controlled during the growing seasons. Yet, large variations of soil moisture levels were still noticed during these periods, particularly at shallower depths.

Table 5.2-3 presents the statistical indicators used for evaluating the level of agreement between measured and simulated values. The MOHID-Land model performed reasonably well when simulating soil water contents during the 2018 calibration period. The value of R^2 was relatively high (0.671), showing that the model could explain most of the variability of the observed data. The errors of the estimates were quite small, resulting in a RMSE value of 0.014 $m^3\ m^{-3}$ and a NRMSE value of 0.102. The PBIAS value was 0.51%, indicating no under or overestimation trend when simulating the measured data. The NSE value was also high (0.653), indicating that the residual variance was much smaller than the measured data variance. The parameters calibrated in 2018 were then validated during the 2019 and 2020 growing seasons, producing similar goodness-of-fit indicators. These were also within the range of values reported in the literature for soil water content simulations using the MOHID-Land model (Ramos et al., 2017; Simionesei et al., 2018). As such, the model was considered adequate to simulate soil water dynamics during the three growing seasons.

Figure 5.2-4 presents the simulated LAI using the MOHID-Land model as well as the Copernicus Global Land Service dataset used for representing field LAI data during the

growing seasons ("Copernicus Global Land Service. Available online: https://land.copernicus.eu/global/index.html (accessed on 17 March 2021).," n.d.). As referred earlier, only satellite data corresponding to the vine growing seasons is shown, with data from the non-growing period being ignored since the development of the interrow plants could not be considered in this application. Table 5.2-3 describes the goodness-of-fit indicators obtained when comparing the simulated and field datasets during the three growing seasons. The correspondence between those datasets was quite satisfactory during the 2018 calibration period, resulting in relatively high R^2 (0.680) and NSE (0.639) values, and relatively low RMSE (0.155 m^2 m^{-2}) and NRMSE (0.186) values. However, model simulations failed to reproduce crop growth during the 2019 validation season, with the main stressor affecting crop development during that year not being identified. This may have been the fire occurrence that affected the area west of the study vineyard at the end of the 2018 growing season, with effects on the 300 m resolution LAI product being then particularly noticed during the following year. Nevertheless, as satellite data in 2019 revealed an uncharacteristic trend of the LAI curve the model was also considered to be calibrated for simulating vine growth in the study area since the goodness-of-fit indicators were again satisfactory in 2020.

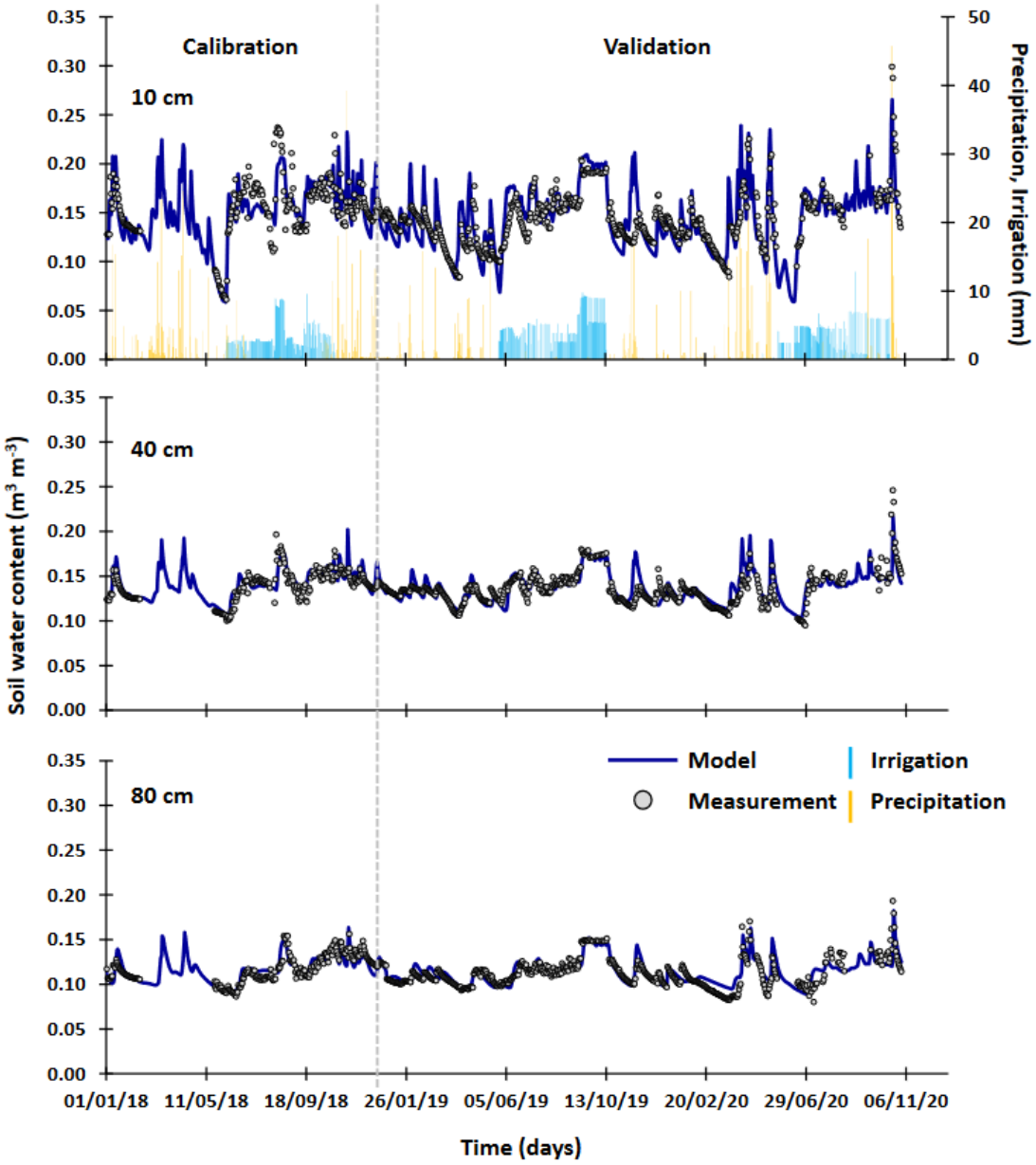

Figure 5.2-3 Measured and simulated soil water contents at 10, 40, and 80 cm depths during the 2018, 2019, and 2020 seasons.

Table 5.2-3 Statistical parameters for the agreement between model simulations and observed data.

Statistical Indicator	Soil Water Contents			LAI		
	Validation 2018	Validation 2019	Validation 2020	Validation 2018	Validation 2019	Validation 2020
R^2	0.671	0.683	0.676	0.680	0.445	0.842
RMSE (L L^{-1})	0.014	0.012	0.015	0.155	0.462	0.191
NRMSE	0.102	0.097	0.115	0.186	0.794	0.246
PBIAS (%)	0.508	−1.550	−0.614	−6.035	−67.403	14.667
NSE	0.653	0.615	0.658	0.639	−9.311	0.513

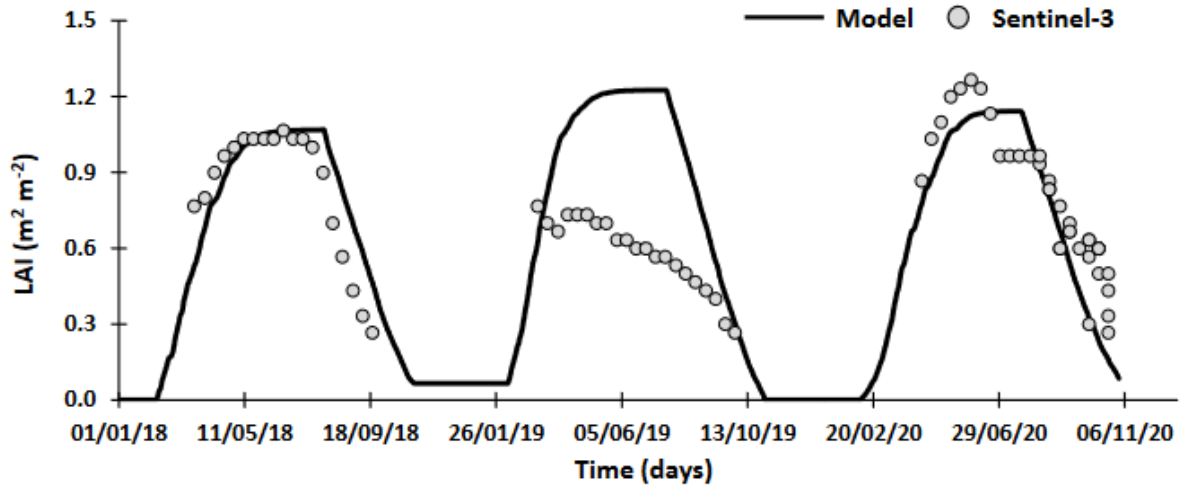

Figure 5.2-4 Satellite and simulated leaf area index (LAI) data during the 2018, 2019, and 2020 growing seasons.

5.2.3.3 Soil Water Balance

Table 5.2-4 shows the components of the soil water balance for each growing season. Figure 5.2-5 also presents the daily fluxes of ET_c, $T_{c\ model}$, $T_{c\ act\ model}$, Es act model computed with the MOHID-Land as well as the daily irrigation and precipitation depths during the 2018–2020 growing seasons. The seasonal ET_c values ranged from 445mm in 2018 to 555mm in 2020. The seasonal $ET_{c\ act\ model}$ values were smaller due to the impact of water stress on T_c model, varying from 293 to 320mm in the same years. Although these values depended on the seasonal atmospheric demand as well as soil moisture conditions, they were found to be comparable to estimates of 321mm in Campos et al. (2010), 274–354 mm in Cancela et al. (2015), and even 395–567mm in Fandiño et al. (2012) for different regions in Spain, 239–382 mm in Phogat et al. (2017) for South Australia, and 320–480mm in Wilson et al. (2020) for California, USA.

In terms of ET_c partitioning, $T_{c\ model}$ and $E_{s\ model}$ rates varied from 130 to 177mm and 315–378mm, respectively, throughout the different seasons, being mostly dependent of the quality of the adjustment of the LAI curve to the LAI dataset derived from Sentinel-3. On the other hand, $T_{c\ act\ model}$ and $E_{s\ act\ model}$ rates ranged from 82 to 117mm and 203–210mm, respectively. Thus, the $T_{c\ act\ model}$ accounted for only 28–37% of the $ET_{c\ act\ model}$. The $T_{c\ act\ model}$ values were also comparably smaller than the range of 137–278mm estimated in Fandiño et al. (2012) or to the 183–263mm reported in Cancela et al. (2015) for vines subjected to different irrigation treatments. To refer that besides the obvious differences in climate conditions during different growing seasons, irrigation management, cultivars, soil textures, and soil water storage capabilities, the soil water balance in these latter studies was computed using the FAO56 dual-K_c approach (Allen et al., 2005; Allen et al., 1998), which estimation of the individual

components of the ET_c generally results more precise as commonly recognized in the literature (Pereira et al., 2020, 2015). Nevertheless, the small $T_{c\ act\ model}$ values estimated by the MOHID-Land model find some explanation in the coarse textures (loamy-sand to sandy) and limited water holding capacity of the study soil as well as irrigation management. The reduction of $T_{c\ model}$ values was relatively large due to water stress (34–37%) and was usually observed from mid-June onwards (Figure 5.2-5) as the farmer attempted to improve berry and wine quality while controlling shoot vigor and ripening through deficit irrigation.

While $T_{c\ act\ model}$ values were relatively small and crop stress was significant, the amount of water applied through irrigation was relatively high, varying from 465mm in 2020 to 625mm in 2019 (Table 5.2-4). Irrigation was used to compensate for the deficit in precipitation during the dry period, with seasonal values increasing when annual precipitation was less. However, due to limited soil water storage capacity percolation losses were quite high, ranging from 544mm in 2020 to 688mm in 2018. From these, 39–61% occurred during the irrigation period, corresponding to 45–58% of the total irrigation water applied. The occurrence of high percolation losses with the simultaneous observation of crop water stress only evidenced the imperative need for better irrigation protocols that duly consider the physical characteristics of the study soil.

Table 5.2-4 Soil water balance in the studied vineyard.

	Farmer's Schedule			Optimized Schedule		
	2018	**2019**	**2020**	**2018**	**2019**	**2020**
Inputs (mm):						
P	512	241	399	512	241	399
I	470	625	465	55	98	105
CR_{model}	0	0	0	0	0	0
ΔSS_{model}	-1	9	1	−2	9	1
Outputs (mm):						
$T_{c\ act\ model}$	82	105	117	115	139	146
$T_{c\ model}$	130	164	177	130	164	177
$1-T_{c\ act\ model}/T_{c\ model}$	0.37	0.36	0.34	0.11	0.15	0.17
$E_{s\ act\ model}$	210	210	203	68	44	49
$E_{s\ model}$	315	333	378	315	333	379
DP_{model}	688	560	544	382	166	309
$Runoff_{model}$	0	0	0	0	0	0
Error (%)	0	0	0	0	0	0

P, precipitation; I, irrigation; CR_{model}, capillary rise; ΔSS_{model}, soil water storage variation; $T_{a\ act\ model}$, actual transpiration; $T_{c\ model}$, potential transpiration; $E_{a\ act\ model}$, actual soil evaporation; $E_{s\ model}$, potential soil evaporation; DP_{model}, deep percolation. The subscript model corresponds to results computed with the MOHID-Land model. Model error = 100 ($\sum$inputs − $\sum$outputs)/$\sum$inputs.

Table 5.2-4 further shows the soil water balance in the studied vineyard following an optimized irrigation schedule using the MOHID-Land model. The threshold pressure head (h_t) for triggering irrigation was set at 1200 cm, i.e., slightly below the h_3 value in the Feddes (1982) model to induce some water stress to the plant. The target pressure head (h_0) was set at 100cm, here assumed to represent field capacity. The maximum irrigation pulse (I_{max}) was set to 5mm, with a minimum irrigation interval (I_{int}) of 1 day. Following these settings, the model proposed the net application of only 55, 98, and 105 mm in 2018, 2019, and 2020, respectively, which compared to farmer's inputs are considerably lower. This inevitably led to lower percolation, with values ranging now from 166 mm in 2019 to 382 mm in 2018, resulting mostly from precipitation events. Additionally, the $E_{s\ act\ model}$ decreased considerably since the soil surface was less moistened with the absence of successive irrigation events. On the other hand, $T_{c\ act\ model}$ values increased between 25 and 40%, corresponding to a less pronounced, more controlled water stress (11–17%). Hence, this exercise exposed the advantages of using a modeling tool for optimizing irrigation schedules, helping to save substantial amounts of water in the process. Those low irrigation depths were only possible because the model was not subjected to constraints that usually occur in the decision-making of irrigation, being hard to match in field conditions. Additionally, model estimates much depended on how well soil hydraulic properties were able to represent actual flow conditions in the vineyard soil, how well the three-dimensional flow from the drip irrigation system was represented by a simple one-dimensional modeling approach as the one used here, how representative were the Feddes, 1982 pressure head threshold values for describing the response of this particular variety to water stress, and how reliable was the partitioning of the ET_c and the computation of the soil water balance based on LAI evolution.

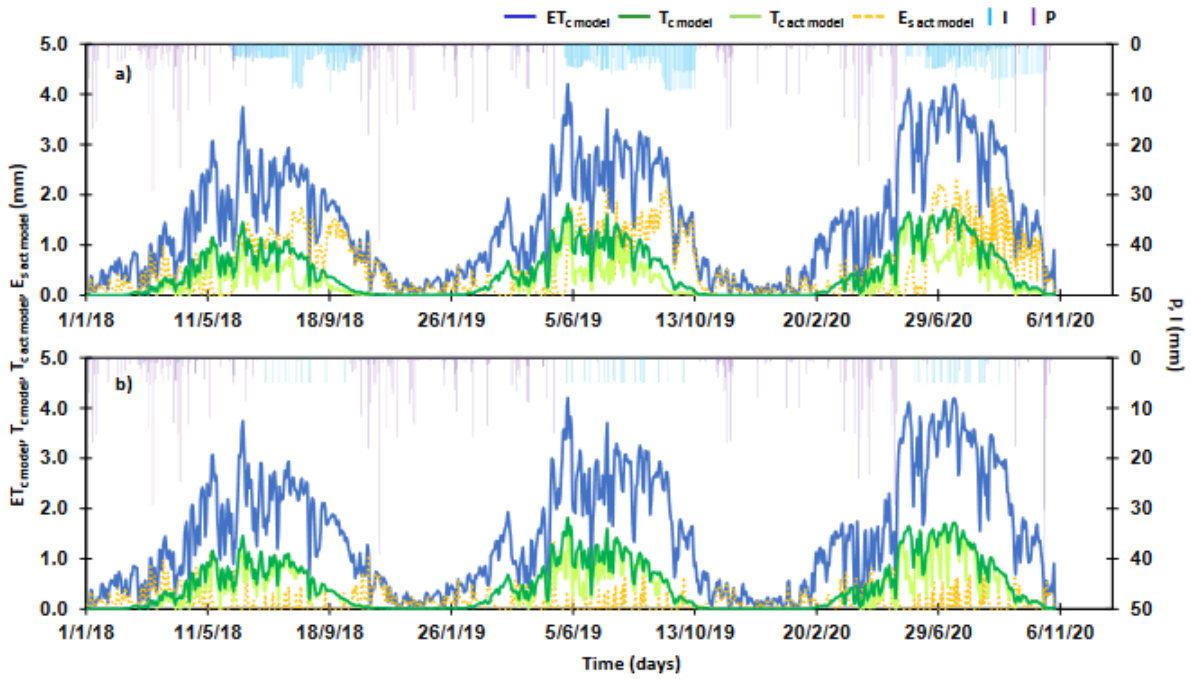

Figure 5.2-5 Crop evapotranspiration (ET_c), potential ($T_{c\ model}$) and actual ($T_{c\ act\ model}$) crop transpiration, actual soil evaporation ($E_{s\ act\ model}$), irrigation (I), and precipitation (P) fluxes following (a) irrigation applied by the farmer and (b) an optimized irrigation schedule computed by the model (the subscript model corresponds to results computed with the MOHID-Land model).

5.2.3.4 MOHID-Land vs. Remote Sensing

Table 5.2-5 presents the regression models obtained after relating the MOHID-Land outputs with the corresponding ones derived from Sentinel-2 imagery. Figure 5.2-6 shows the scatterplots of those relations. Considering the mismatch between the simulated LAI curve and the field LAI dataset derived from the Sentinel-3 sensor during the 2019 growing season (Figure 5.2-4), the simulated LAI values were first correlated to the NDVI values computed from Sentinel-2 imagery to evaluate the quality of both datasets and whether the same disagreement was observed here. This was not verified as the comparison resulted in Pearson correlation coefficient (r) values of 0.80, 0.84, and 0.92 for 2018, 2019, and 2020 growing seasons (r = 0.65 for total data), with the correlation significant at the 0.01 level.

Table 5.2-5 Regression models between the MOHID-Land model and satellite sensor estimates of crop coefficients and transpiration fluxes (values in brackets correspond to the standard deviation of errors) a.

Model	Equation	R^2 (-)	RMSE ([b])	NRMSE (-)	PBIAS(%)
1	$K_{cb\ act\ model} = 1.006\ NDVI - 0.258$	0.534	0.050	0.421	-0.555
		(0.050)	(0.008)	(0.113)	(39.96)
2	$K_{cb\ act\ model} = 0.875\ K_{cb\ act\ NDVI} - 0.168$	0.550	0.049	0.414	0.041
		(0.054)	(0.007)	(0.097)	(39.84)
3	$T_{c\ act\ model} = 2.216\ NDVI - 0.612$	0.365	0.432	0.839	57.057
		(0.066)	(0.102)	(0.182)	(10.55)
4	$T_{c\ act\ model} = 0.718\ T_{c\ act\ NDVI} - 0.443$	0.782	0.174	0.339	0.065
		(0.069)	(0.022)	(0.119)	(10.07)

[a] $K_{cb\ act\ model}$ and $K_{cb\ act\ NDVI}$, actual basal crop coefficient computed, respectively, from the MOHID-Land and satellite imagery; NDVI, normalized difference vegetation index; $T_{a\ act\ model}$ and $T_{a\ act\ NDVI,}$ actual transpiration computed, respectively, from the MOHID-Land andsatellite imagery; R^2, coefficient of determination; RMSE, root mean square error; NRMSE, normalized RMSE; PBIAS, percentage bias.[b] Units are the same as the variable units.

The direct relationships between the NDVI and the estimated $K_{cb\ act\ model}$ or $T_{c\ act\ model}$ values generally resulted in poor regression models (models 1 and 3). On the other hand, the scaling of the NDVI values between minimum and maximum values defined based on observed data improved the agreement between the MOHID-Land outputs and those derived from the satellite sensor. This improvement was only minor for $K_{cb\ act\ model}$ (model 2), with the resulting R^2 value (0.55) remaining relatively low. This was attributed to the fact that the lowest NDVI value (0.232), computed at the end of the 2020 growing season (11/10/2020), corresponded to a $K_{cb\ act\ NDVI}$ value of 0.16, which is close to the minimum K_{cb} value (0.15) to be expected for bare soils in the FAO56 procedure. However, in mechanistic models such as the MOHID-Land model where LAI is used for the partition of ET_c rates, this does not occur. At the beginning or close to the end of the crop growing season, when LAI values are null or very small, the corresponding $T_{c\ model}/ET_o$ ratio (or K_{cb}) is equally null or very small. For that, the $K_{cb\ act\ model}$ values varied from 0 to 0.27 in MOHID-Land simulations while the range of variation for the $K_{cb\ act\ NDVI}$ was from 0.16 to 0.48. This conceptual difference also affected the relationship between $T_{c\ act\ model}$ and the $T_{c\ act\ NDVI}$, with the latter values being slightly higher than the former. Yet, the regression model obtained between these two parameters (model 4) was quite good, with the R^2 value (0.782) showing the ability of the model to explain most of the variability observed in the MOHID-Land dataset while the RMSE of 0.174 mm d^{-1} showed the low error of the estimate. On the other hand, the large variation in the PBIAS revealed the conceptual differences in the two approaches that need to be considered in the IrrigaSys decision support system. Nevertheless, the relatively low RMSE suggested that the satellite approach if duly calibrated could be considered as a reliable approach for validating transpiration fluxes from the MOHID-Land model and assuring the reliability of the weekly recommendations issued by IrrigaSys to farmers. The assimilation of these independent predictions into IrrigaSys may, however, be dependent on the plot location as the number of Sentinel-2 images available in this case study was much lower compared to Ramos et al. (2020), who had twice as many images for a study carried out 15 km north during the 2017–2019 growing seasons.

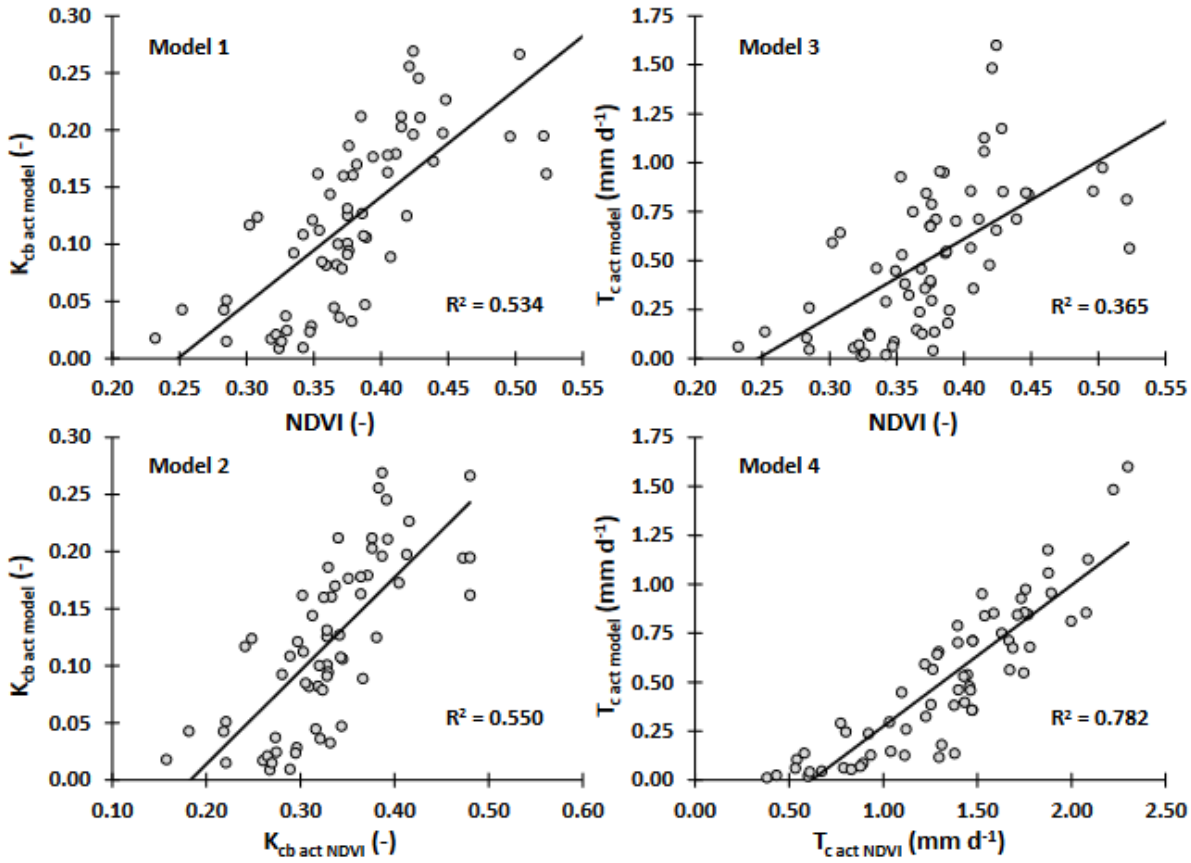

Figure 5.2-6 Scatterplots of the relationships between the actual basal crop coefficients ($K_{cb\ act\ model}$) and actual transpiration rates ($T_{c\ act\ model}$) computed using the MOHID-Land model (subscript model) and the corresponding indicators ($K_{cb\ act\ NDVI}$ and $T_{c\ act\ NDVI}$) derived from the normalized difference vegetation index (subscript NDVI).

5.2.4 Conclusions

In this study, the MOHID-Land model was able to successfully estimate the soil water balance in an irrigated vineyard located in southern Portugal. Estimated actual transpiration rates were relatively low, revealing considerable water stress during the three monitored growing seasons. At the same time, percolation losses were high, showing the need for improved agricultural water use. Precise irrigation scheduling tools such as the one in MOHID-Land may thus contribute to ensuring optimum soil moisture levels for vine growth. Yet, the particularity of vine irrigation management is difficult to scale up in a decision support system such as IrrigaSys, much influenced by the characteristics of crop variety and fruit quality. Expert knowledge on these issues seems thus fundamental for setting up the model correctly and ensuring the accuracy of the irrigation schedules provided by the DSS. While model support can be validated by remote sensing data, the established relationships between model outputs and the NDVI were much dependent on experimental conditions, including irrigation management and climate conditions. This should be always considered when generalizing these products to other vineyards in the region. Nonetheless, taking the necessary precautions,

Sentinel-2 data can well provide important information to validate model outputs during the decision-making of irrigation on a regular basis. In the absence of calibration datasets, the regression models developed in this study can be further helpful to rapidly identify fields covered by the DSS where the hydrological model may be acting poorly.

6. Irrigation scheduling

6.1 Introduction

In this chapter, we introduce the MOHID Land Irrigation Module, highlighting its capabilities and functionalities. Based on previously calibrated and validated models, we explore the practical applications of the MOHID Land Irrigation Module in optimizing irrigation management for maize and pasture crops and we present the methodology used. The chapter ends with conclusions about the use of this module.

6.2 Material and Methods

6.2.1 MOHID Irrigation scheduling

MOHID-Land was extended with a system-dependent boundary condition that triggered irrigation when a certain threshold pressure head (h_t) was obtained in different grid cells of the root zone domain. Irrigation then ceased after a second target pressure head (h_0) was obtained in the same grid cells. Since the root zone domain is typically defined by a large and variable number of grid cells MOHID-Land further included a series of constraints that prevented the application of meaningless irrigation amounts and countess irrigation events, namely a minimum irrigation pulse (I_{min}), a maximum irrigation pulse (I_{max}), and a minimum irrigation interval (I_{int}). The model was thus automatized for triggering irrigation whenever soil pressure heads dropped below h_t in different cells of the root zone domain, supplying them sufficient water to reach h_0 in those same cells based on a pre-defined irrigation strategy.

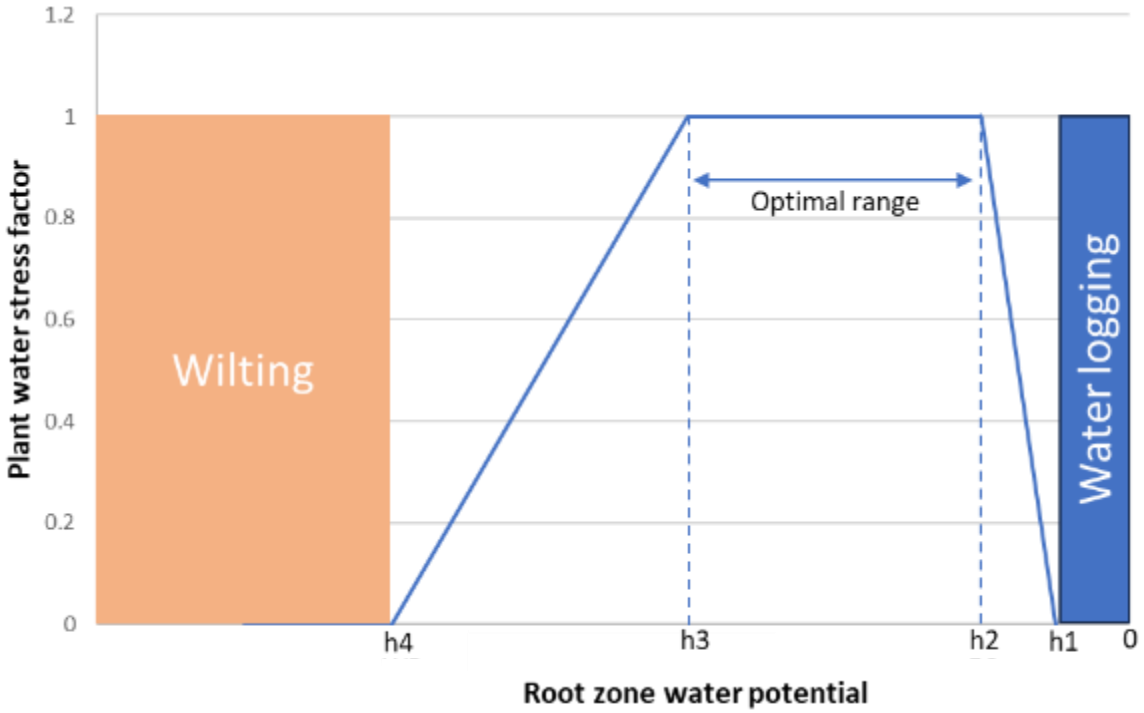

Figure 6.2-1Feddes plant water stress function. Root water uptake commences with the onset of desaturation at h1 (anoxic moisture conditions), optimum root water uptake is given between h2 (field capacity, FC) and h3 (onset of drought-stress). From optimum root water uptake towards h4 (permanent wilting point, WP) the plants experience increasing drought stress.

MOHID-Land's irrigation parameters should be specified as follows:

- h_t should be defined based on crop characteristics and irrigation strategy. For full irrigation strategies, h_t should be set between h_2 and h_3 to prevent T_p reductions (Feddes and Zaradny, 1978), while for deficit irrigation strategies h_t should drop below h_3, thus inducing some water stress;
- h_0 should be defined based on soil characteristics and irrigation strategy. h_0 should be set: (i) at field capacity to fulfil soil storage capacity; (ii) at higher heads than field capacity to promote percolation (e.g., for saline conditions); or (iii) at lower heads than field capacity to induce deficit conditions in the root zone domain;
- I_{min}, I_{max}, and I_{int} should consider the constraints of the irrigation system (application rates, number of irrigation blocks, water availability, energy costs, etc.).

6.2.2 Model setup maize scenario

The soil profile consisted of four layers with a total depth of 2 meters, represented using a one-dimensional Arkawa C-grid (Purser and Leslie, 1988) with 100 grid cells. Each cell has dimensions of 1 meter wide, 1 meter long, and 0.02 meters thick (Figure 4.1-3). The state

variables such as water content were calculated at the center of each cell, with fluxes computed on the faces of the cells. Only vertical fluxes are considered.

The upper boundary condition was determined by actual evaporation, transpiration rates, and precipitation fluxes. Crop evapotranspiration (ET_c) was calculated from hourly reference evapotranspiration (ET_0) values multiplied with crop coefficients (K_c) for different crop stages. These K_c values were adjusted based on local climate conditions and crop characteristics. The bottom boundary condition was specified using observed groundwater depth, and initial soil water content conditions were set to field capacity.

Datasets relative to 2014 and 2015 were used to calibrate and validate the model, respectively. Details about the calibration and the validation of the model for the maize scenario, as well as the model setup, can be found in Chapter 4 - Section 4.1.

6.2.3 Model setup pasture scenario

The soil profile consisted of three layers with a total depth of 4 meters, represented using a one-dimensional Arkawa C-grid (Purser and Leslie, 1988) with 11 grid cells. Each cell has dimensions of 1 meter wide, 1 meter long, and with variable thickness (0.05 m on the top to 2.5 m at the bottom). The upper boundary condition was determined by actual evaporation, transpiration rates, irrigation and precipitation fluxes. Crop evapotranspiration (ET_c) was calculated by multiplying hourly reference evapotranspiration (ET_0) values with crop coefficients (K_c) for different crop stages. These K_c values correspond to standard K_c values for pasture in the Mediterranean region, and were adjusted based on local climate conditions and crop characteristics. The bottom boundary condition was specified using observed groundwater depth, and initial soil water content conditions were set to field capacity.

Model calibration and validation were carried out during the 2010–2011 and 2011–2012 seasons, respectively, with procedures following Ramos et al. (2017). Details about the calibration and the validation of the model for the pasture scenario, as well as the model setup, can be found in the Chapter 4 – Section 4.2

6.2.4 Maize irrigation scenario

Different irrigation scenarios were set to help demonstrate the new system-dependent boundary condition implemented in the MOHID-Land model and improve irrigation scheduling performed by the farmer. In this study, the experimental field was limited north by the Sorraia river, whereas rice (Oryza sativa L.) fields bordered the area in all remaining directions. These field boundary conditions, particularly the large irrigation pulses applied in neighboring rice fields partially explain the shallow groundwater levels monitored during each

season. The contribution of the shallow groundwater table to the soil-water balance was thus high under the local climate conditions, but was significantly influenced by the GWD. For each growing season, and after model calibration and validation, two hypotheses related to GWD were analyzed: (i) a constant GWD was set based on the average depth monitored in each season (-1.08 m in 2014, and 1.12 m in 2015), thus considering the current field conditions; (ii) a constant GWD was set to 1.50 m, corresponding to the initial depth monitored before the beginning of each growing season, thus assuming land use changes in the vicinity of the experimental field (i.e., no rice fields in the vicinity of the study area). Irrigation scheduling in each of the above scenarios should expectably reduce irrigation needs, promote capillary rise, and eventually increase water use efficiency in the study area. Each of these GWD scenarios, was further extended by setting ht to different irrigation trigger thresholds (-500, -1000, -1500, and -2000 cm) in order to assess model performance under increasing water stress conditions. For all 16 scenarios (2 GWD × 4 ht × 2 seasons), h_0 was always set close to field capacity (h_0 = -300 cm; I_{min} was set to 5 mm; I_{max} was set to 24 mm after considering the limitations of the local irrigation system (application rate of 8 mm d^{-1}; 6 irrigation blocks; maximum irrigation duration per block of 3 h); and I_{int} was set to 3 days. The same climatic data of 2014 and 2015 were used for the hypothetical scenarios.

Water productivity (WP) was computed for both monitored irrigation seasons and irrigation scenarios, being here defined as the ratio between actual crop yields (kg ha^{-1}) and the total water use (m^3), including the net precipitation, the seasonal net irrigation depth, CR, and soil storage .

6.2.5 Pasture Irrigation Scenario

After model calibration/validation, the MOHID-Land model was used to compute the water balance and dry biomass yields in rainfed and irrigated pastures, hypothetically grown in the studied area during the 1979–2009 seasons (30 years). Climatic data was also provided by the same numerical mesoscale MM5 used earlier (http://meteo.tecnico.ulisboa.pt), and expresses the typical climatic variability found in the Mediterranean region (Figure 6.2-2), with annual precipitation amounting to between 68 and 805 mm.

In irrigated pastures, irrigation needs were further computed with a system-dependent boundary condition that automatically triggered irrigation when a certain threshold pressure head (h_t) was obtained in different grid cells of the root zone domain. Irrigation then ceased after a second target pressure head (h_0) was obtained in the same grid cells. This system-dependent boundary condition further included a series of constraints that prevented the

application of meaningless irrigation amounts and countless irrigation events, namely a minimum irrigation pulse (I_{min}), a maximum irrigation pulse (I_{max}), and a minimum irrigation interval (I_{int}). The model was thus capable of automatizing irrigation whenever soil pressure heads dropped below h_t in different cells of the root zone domain, supplying them sufficient water to reach h0 in those same cells based on a pre-defined irrigation strategy (Ramos et al., 2017). Simulations for irrigation pastures were thus run with the following settings: $h_t = -800$ cm, corresponding to h_3 in the Feddes et al. (1978) model (i.e., no water stress was allowed); $h_0 = -200$ cm, corresponding to field capacity; $I_{min} = 5$ mm; $I_{max} = 20$ mm; and $I_{int} = 1$ day.

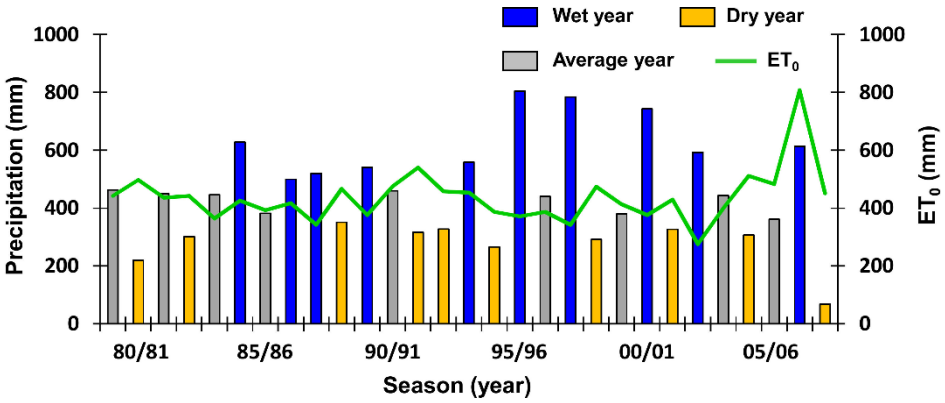

Figure 6.2-2 Annual precipitation and reference evapotranspiration (ET0) between the 1979–980 and 2007–2008 seasons.

Results of the soil water balance components (E_a, T_p, and T_a), LAI, and dry biomass yields in rainfed and irrigated pastures were then compared for the 30-year period (1979–2019) and for the 10 driest and 10 wettest years (Figure 6.2-2). Averages were compared using a paired, double-tailed Student t-test, in which a p value of <0.05 was considered significant.

6.3 Results and discussion

6.3.1 Maize scenario

Table 6.3-1 Components of the soil water balance.

	Inputs				Outputs				
	P (mm)	I (mm)	CR (mm)	ΔSS (mm)	E_a (mm)	T_a (mm)	T_a/T_p (−)	DP (mm)	WP (kg m^{-3})
Farmer:									
2014	163	365	78	16	164	374	0.99	74	2.36
2015	12	620	94	11	181	481	1.00	75	2.43
Scenarios:									
2014, GWD −1.08 m, h_t = −500 cm	163	218	191	−4	164	373	1.00	30	2.58
2014, GWD −1.08 m, h_t = −1000 cm	163	136	248	−2	167	356	0.96	22	2.60
2014, GWD −1.08 m, h_t = −1500 cm	163	68	269	−2	170	314	0.85	15	2.56
2014, GWD −1.08 m, h_t = −2000 cm	163	23	275	−2	172	272	0.75	14	2.47
2014, GWD −1.50 m, h_t = −500 cm	163	286	101	11	164	373	1.00	23	2.61
2014, GWD −1.50 m, h_t = −1000 cm	163	226	141	13	165	361	0.97	17	2.64
2014, GWD −1.50 m, h_t = −1500 cm	163	181	153	14	169	327	0.89	15	2.58
2014, GWD −1.50 m, h_t = −2000 cm	163	159	154	13	172	299	0.82	18	2.51
2015, GWD −1.12 m, h_t = −500 cm	12	377	243	37	181	480	1.00	9	2.68
2015, GWD −1.12 m, h_t = −1000 cm	12	249	323	50	183	441	0.93	9	2.65
2015, GWD −1.12 m, h_t = −1500 cm	12	181	340	47	191	381	0.81	9	2.57
2015, GWD −1.12 m, h_t = −2000 cm	12	113	354	58	193	336	0.72	9	2.50
2015, GWD −1.50 m, h_t = −500 cm	12	499	117	47	181	480	1.00	15	2.65
2015, GWD −1.50 m, h_t = −1000 cm	12	385	183	68	184	450	0.94	15	2.63
2015, GWD −1.50 m, h_t = −1500 cm	12	317	201	76	188	405	0.86	15	2.57
2015, GWD −1.50 m, h_t = −2000 cm	12	272	207	74	191	359	0.77	15	2.51

P, precipitation; I, irrigation; CR, capillary rise; E_a, actual soil evaporation; T_a, actual crop transpiration; T_p, potential crop transpiration; DP, deep percolation; WP, water productivity.

6.3.1.1 Soil water balance

Table 6.3-1 shows the components of the soil water balance during the 2014 and 2015 growing seasons. Precipitation amounts varied substantially between years. Irrigation needs consequently differed, with September's 2014 precipitation events making irrigation even unnecessary during that period. The 2014 growing season further registered lower average daily temperatures and higher relative humidity conditions than in 2015. These differences were obviously reflected in the irrigation requirements, with ET_c estimates summating to 542 and 662 mm in 2014 and 2015, respectively, while T_p values amounted to 378 and 481 mm in the same respective years. The MOHID-Land model estimated no ET_c and T_p reductions due to water stress during both seasons, i.e., ET_a /ET_c and T_a/T_p were always 1.0 (Table 6.3-1). As discussed by Allen et al. (2011) when revising the various methods for field ET estimation, combined approaches of accurate soil water observations and water balance simulation modelling provide for appropriate accuracy in ET estimates. Figure 6.3-6 presents the seasonal variation of T_p, T_a, and E_a during the 2014 and 2015 growing seasons. These values were in line with those estimated for the same region and for maize by Paredes et al. (2014a) using a simpler soil water balance model. Also, Cameira et al. (2003) estimated similar ET_c values for maize by measuring the upward fluxes in different soils in the region.

The seasonal variation of GWD was significantly affected by irrigation applied to the maize, but also by irrigation practices in neighboring rice fields. Thus, GWD became progressively shallower, rising from 1.50 m in the beginning of each season to an average depth of 1.10 m during most parts of both growing periods. Hence, the shallow GWD conditions ended up favoring capillary rise (CR), depending on the farmer's irrigation scheduling, root water uptake, and the established hydraulic head gradients. CR became an important component of the soil water balance, reaching 14% of ET_c in both seasons (Table 6.3-1). Cameira et al. (2003) had already highlighted the importance of CR to the soil water balance in the Sorraia Valley region, with this component contributing up to 45% of ET_c in their case studies.

Deep percolation (DP) values amounted to 12% (2014) and 10% (2015) of the water inputs (precipitation, net irrigation, and CR), explaining most of the GWD variations monitored after excessive irrigation or precipitation events (Figure 4.1-2).

Based on model estimates, WP reached 2.36 and 2.43 kg m^{-3} in the 2014 and 2015 growing seasons, respectively (Table 6.3-1). Although these values can be considered relatively satisfactory, and were perfectly within the range of WP values reported by Paredes et al. (2014b) for different irrigation management strategies studied in the same region (1.48-3.15 kg m^{-3}), model results showed still an opportunity for improving WP in the study area, namely by optimizing irrigation scheduling and groundwater contribution to the root zone.

6.3.1.2 *Improving irrigation scheduling in the Sorraia valley region*

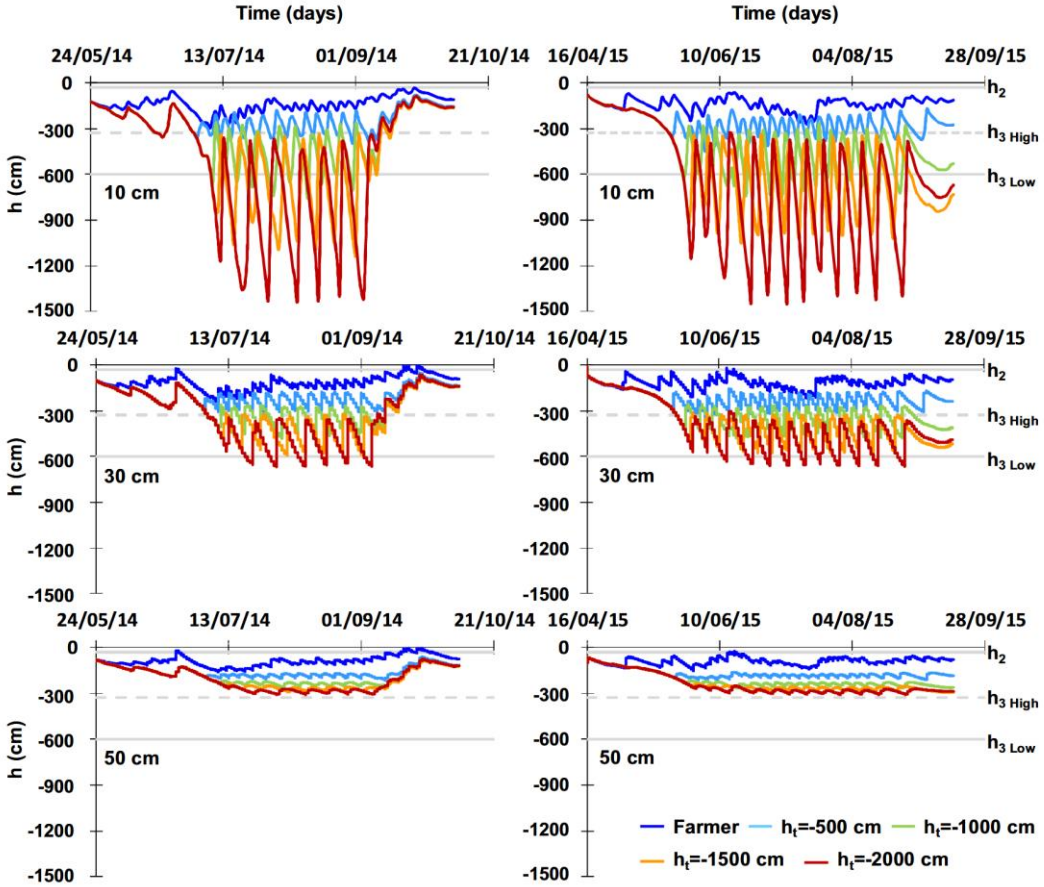

Figure 6.3-1 Monitored and simulated soil pressure heads (h) at depths of 10 (top), 30 (middle), and 50 cm (bottom) during 2014 (left) and 2015 (right) crop seasons. Irrigation scenarios with groundwater depth at −1.50 m, and trigger thresholds (h_t) at different pressure heads.

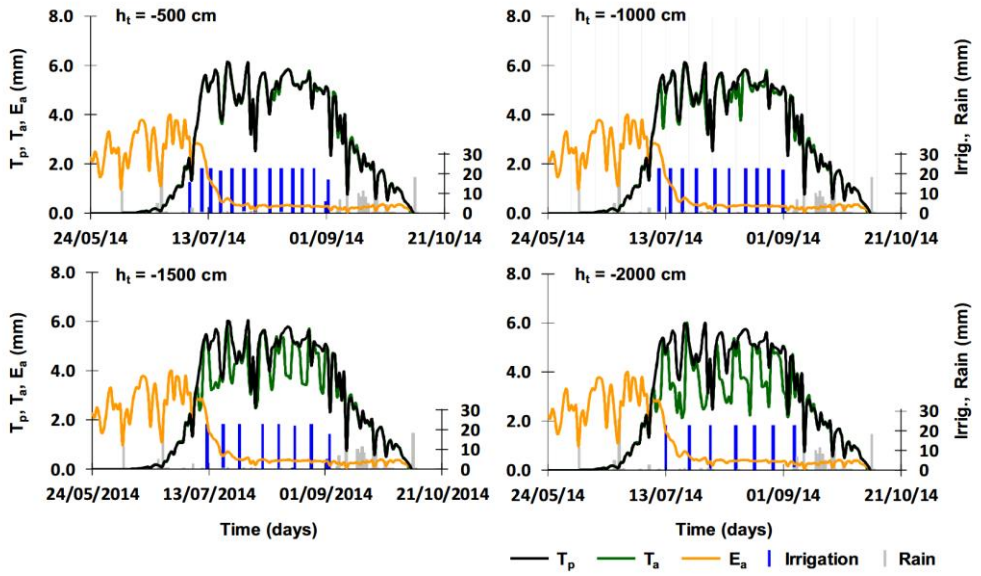

Figure 6.3-2 Seasonal variation of potential crop transpiration (T_p), actual crop transpiration (T_a), and actual soil evaporation (E_a) during 2014 crop season. Irrigation scenarios with groundwater depth at −1.50 m, and trigger thresholds (h_t) at different pressure heads.

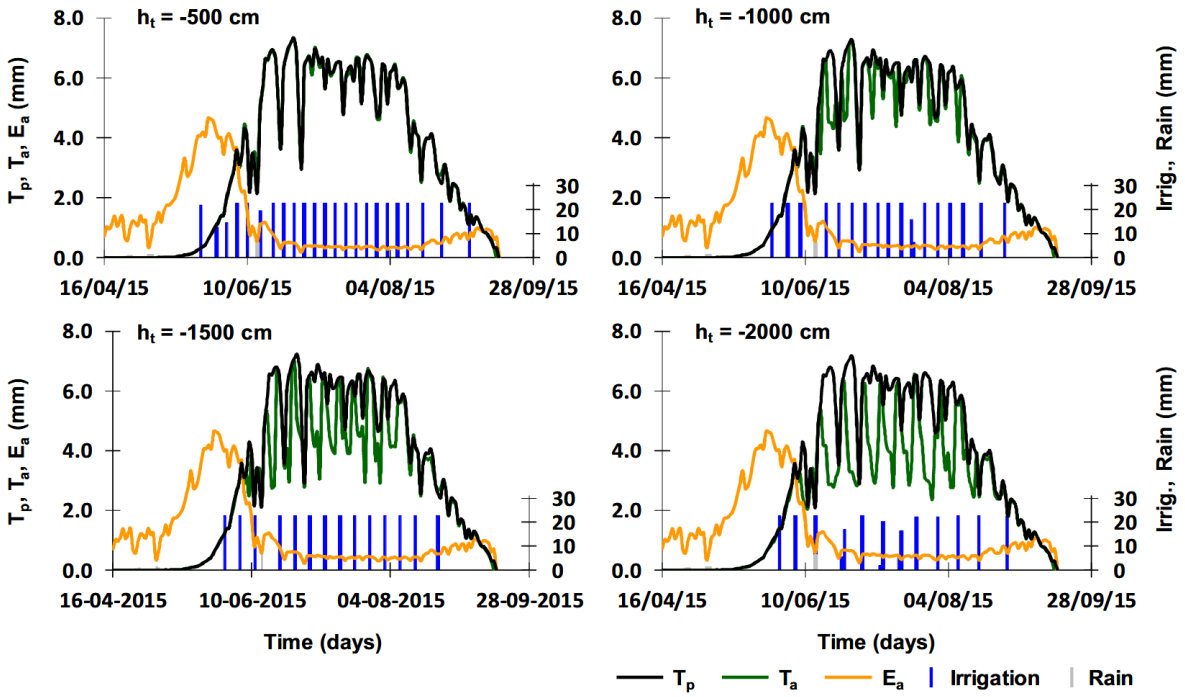

Figure 6.3-3 Seasonal variation of potential crop transpiration (T_p), actual crop transpiration (T_a), and actual soil evaporation (E_a) during 2015 crop season. Irrigation scenarios with groundwater depth at −1.50 m, and trigger thresholds (h_t) at different pressure heads.

Figure 6.3-1 shows the simulated soil pressure heads for the 2015 irrigation scenarios with GWD at 1.50 m, and h_t at different pressure heads. The simulations of the remaining irrigation scenarios are not presented graphically in order to limit the number of figures, and because Figure 6.3-1 illustrates well the functioning of the new system- dependent boundary condition implemented in the MOHID-Land model. Soil pressure heads became increasingly lower, with the rate decrease depending on the transpiration rate. Naturally, the lower the h_t value considered in the irrigation scenarios, the lower the simulated soil pressure heads in the soil profile. Irrigation was then triggered when h_t was reached in the grid cells located closer to the soil surface, where root water uptake and soil evaporation were more pronounced. However, at 10 cm depth, soil pressure heads approached but never dropped below h_t. At lower depths, soil pressure heads were even mostly within the range where no water stress occurs (between h_2 and h_3). After the model triggered irrigation, soil pressure heads increased back to h_0 = –300 cm in all layers of the soil profile, meaning that I_{max} was enough to increase soil water contents of the different layers close to field capacity.

Since h_t was reached faster in the cells closer to the soil surface, the MOHID-Land model further included a constraint to trigger irrigation only when the amount of water required to increase soil pressure heads from h_t to h_0 was higher than I_{min} (5

mm), thus taking into account the deficit of water in multiple cells, and avoiding countless irrigation events. Following a different approach, Dabach et al. (2013), implemented a system-dependent boundary condition which initiated irrigation whenever the soil pressure head at a predetermined location dropped below ht. In their simulations, that specific location corresponded to the position of tensiometers, and h_t was defined based on the average of their readings. Depending on the position of the tensiometers, this approach would likely better assess the soil moisture condition in the root zone domain than that implemented in the MOHID-Land model. However, these authors had to set ht empirically based on experimental data, while in the MOHID-Land model ht was fixed directly based on the pressure head parameters of the Feddes et al. (1978) model used for computing T_p reductions due to water stress, thus simplifying its use in an irrigation service like FIGARO DSS.

The soil water balances of the monitored 2014 and 2015 irrigation practices showed that the maize crop was well supplied with water (Table 6.3-1). Simulated soil pressure heads were always within the range where water uptake was at the potential rate (Figure 6.3-1). Farmer's irrigation scheduling maintained soil water contents near field capacity, maximizing crop production and preventing water shortages caused by unforeseen problems in the irrigation system or water distribution. However, the analyses of the full irrigation scenarios (Table 6.3-1; h_t = –500 cm) showed that it could have been still possible to reduce the amount of water applied to the crop and maintain root water uptake at the maximum rates. All scenarios with h_t values at 500 cm showed a reduction of the irrigation needs between 20 and 40% while still maintaining a T_a/T_p = 1 ratio. In these scenarios, irrigation needs decreased from 365 to 218–286 mm in 2014, and from 620 mm to 377–499 mm in 2015, depending on the GWD. Higher water savings were obviously obtained when considering GWD at shallower depths (1.08 m in 2014, and 1.12 m in 2015) since groundwater contribution to the root zone was higher. Irrigation reductions were compensated by the increase of CR, with groundwater contributing for 17.7-36.8% of ET_c. For the $h_t = -$ 500 cm scenarios, CR increased from 78 to 191–101 mm in 2014, and from 94 to 243–117 mm in 2014, again depending on the level of the GWD. Also, WP increased from 2.36 to 2.60-2.64 kg m^{-3} in 2014, and from 2.43 to 2.65-2.68 kg m^{-3} in 2015, demonstrating the importance of adjusting irrigation scheduling practices to the soil's water holding capacity and groundwater conditions.

In the deficit irrigation scenarios ($h_t < h_3$), the lower the h_t value, the longer it took for the matric head to reach it and initiate irrigation, resulting in a smaller number of irrigation pulses (Figure 6.3-1). For example, irrigation events decreased from 13 to 7 and from 23 to 15 in the 2014 and 2015 scenarios (GWD at −1.50 mm), respectively, after h_t was modified from 500 to 2000 cm (Table 6.3-1). Irrigation amounts also decreased from 286 to 159 mm, and from 499 to 272 mm in the same corresponding years. In all deficit scenarios, groundwater contribution increased to 47.4-66.9% and 26.8-37.6% of ET_a when considering the current average and hypothetical GWDs, respectively. The former values very much approximated those computed by Cameira et al., 2003 for maize grown in a similar silty loam Fluvisol of the Sorraia Valley region (45% of ET_c; 200 mm). Percolation was practically irrelevant, resulting mostly from water drained below the root zone after larger precipitation events.

All deficit irrigation scenarios further showed reductions of the T_p values due to water stress. The lower the h_t value, the lower the T_a/T_p ratio (Table 4.1-5), decreasing from 1.0 in the h_t = –500 cm scenarios to a minimum of 0.72 in one of the h_t = −2000 scenarios (GWD = −1.12 m; 2015). Figure 6.3-2 and Figure 6.3-3 describe the seasonal variation of T_p and T_a following the hypothetical irrigation scheduling scenarios considered for the 2014 and 2015 crop seasons (GWD at 1.50 m), respectively. The T_a values gradually dropped as the soil dried up, increasing again to the potential values with irrigation, whereas CR was never able to fully compensate the soil water deficit caused by increasingly lower h_t values. This was certainly because no root water uptake compensation mechanism was considered in the MOHID-Land model. For example, Šimůnek and Hopmans (2009b) described a compensation mechanism where water uptake is increased in non-stressed soil layers, compensating for reductions in soil layers where pressure heads are below the wilting point or above the anaerobiosis point (González et al., 2015; Rosa et al., 2016). Since the MOHID-Land model grid cells reaching h_t were mostly located close to the soil surface, and as mentioned earlier soil pressure heads at deeper soil layers were mostly within the range where no water stress occurs (Figure 6.3-1), a similar procedure in the MOHID-Land model as that documented by Šimůnek and Hopmans (2009b) would certainly increase root water uptake in deeper soil layers, eliminating much of the predicted water stress. Irrigation reductions and the corresponding increase of CR in the deficit scenarios did not result in a direct increase of the WP values when compared to the full irrigation

scenarios (h_t values at -500 cm). Generally, the lower the h_t value defined for triggering irrigation, the lower the computed WP value. The 2014 scenarios with h_t at 1000 cm were the exception. These were mostly explained by the effect of the water stress on LAI development and the aboveground biomass simulated with the MOHID-Land model (Figure 6.3-4). Thus, yields were also reduced up to 25% depending on the GWD and the h_t value. Nonetheless, WP values in the deficit irrigation scenarios were always higher than those computed from the farmer's irrigation practices.

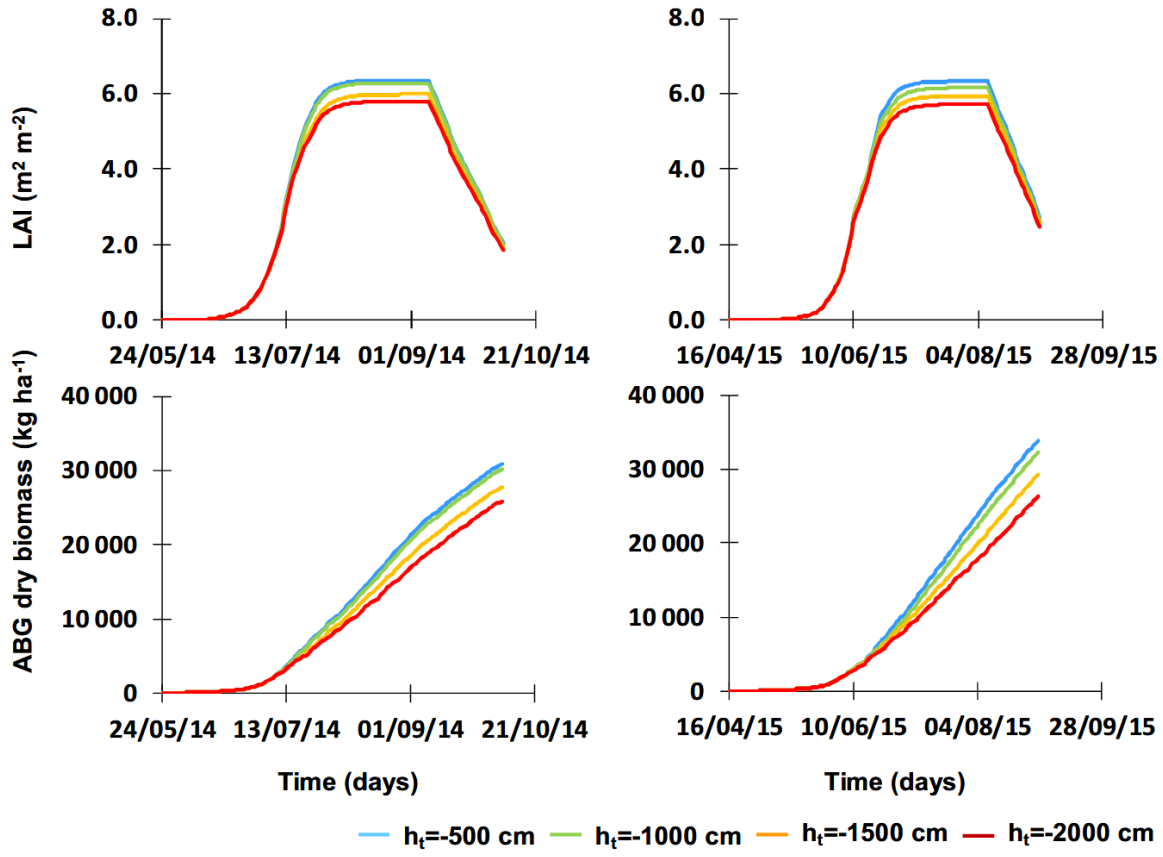

Figure 6.3-4 Simulated leaf area index (top), and aboveground (ABG) dry biomass (bottom) during 2014 (left) and 2015 (right) crop seasons. Irrigation scenarios with groundwater depth at −1.50 m, and trigger thresholds (ht) at different pressure heads.

6.3.2 Pasture scenario

Dry Biomass and Water Balance Estimates in Wet and Dry Seasons

Model estimates of aboveground dry biomass ranged from 1331 to 2681 kg ha^{-1} and from 2778 to 5092 kg ha^{-1} in rainfed and irrigated pasture, respectively, for the period 1979–2009 (Figure 6.3-5). Mean differences between the two pasture regimes were found to be statistically different. Likewise, model estimates of the aboveground dry biomass for the 10

driest and the 10 wettest seasons were found to be statistically different. Mean values reached 2055 (1340–2469) and 4395 (3675–5092) kg ha^{-1} in the rainfed and irrigated regimes, respectively, during the 10 driest seasons, and 2132 (1476–2681) and 3802 (2778–4653) kg ha^{-1} in the same regimes during the 10 wettest seasons (Figure 6.3-5). While mean values in the rainfed regime were relatively close, dry biomass estimates during the wet seasons were more regular, with the first (2067 kg ha^{-1}) and third (2293 kg ha^{-1}) quartiles being relatively close when compared with the dry seasons (Figure 6.3-5). Note that simulations of dry biomass values started to differ between pasture regimes during spring when water became a limiting factor. In these simulations, and based on the field data used for calibrating the model, irrigated pasture was modelled only until June/July, when plants reached their PHU. Therefore, pastures with longer life cycles—namely permanently irrigated pastures—will reach higher dry biomass values, since they are not limited by temperature and water stresses during spring and summer months.

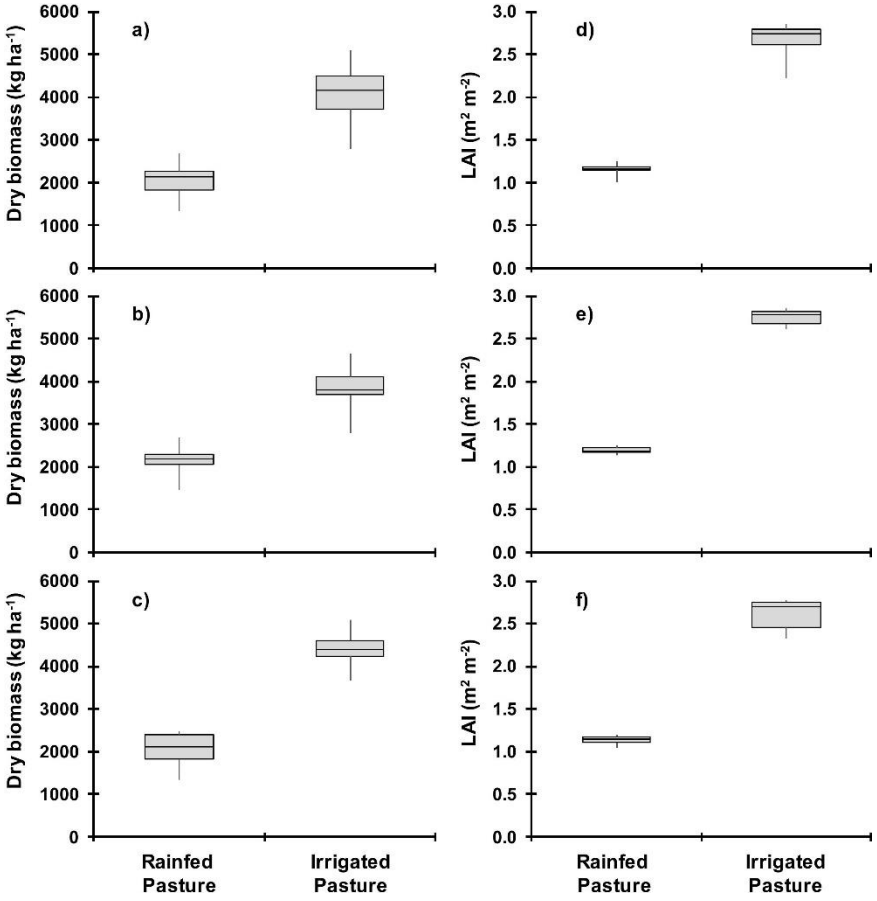

Figure 6.3-5 Aboveground dry biomass and leaf area index (LAI) values estimated in rainfed and irrigated pastures between the 1979–1980 and 2007–2008 seasons: (a,d) average years; (b,e) 10 wettest years; and (c,f) 10 driest years.

Irrigation was thus a determining factor for pasture's dry biomass increase. Irrigation needs varied between 20 and 360 mm, being higher during the dry seasons (220–360 mm) than during the wet seasons (20–200 mm). Irrigation needs were obviously dependent of rainfall (R^2 = 0.513), with the model trying to maintain soil water contents within the predefined threshold (h_t) and target (h_0) pressure heads. Figure 6.3-6 gives, as an example, the irrigation scheduling estimated by MOHID-Land for the 1980–1981 (P = 220 mm; I = 360 mm), 1995–1996 (P = 805 mm; I = 140 mm), and 2002–2003 (P = 592 mm; I = 20 mm) seasons. Results showed that rainfall amount and distribution had a notorious influence when computing the soil–water balance and irrigation scheduling with MOHID-Land.

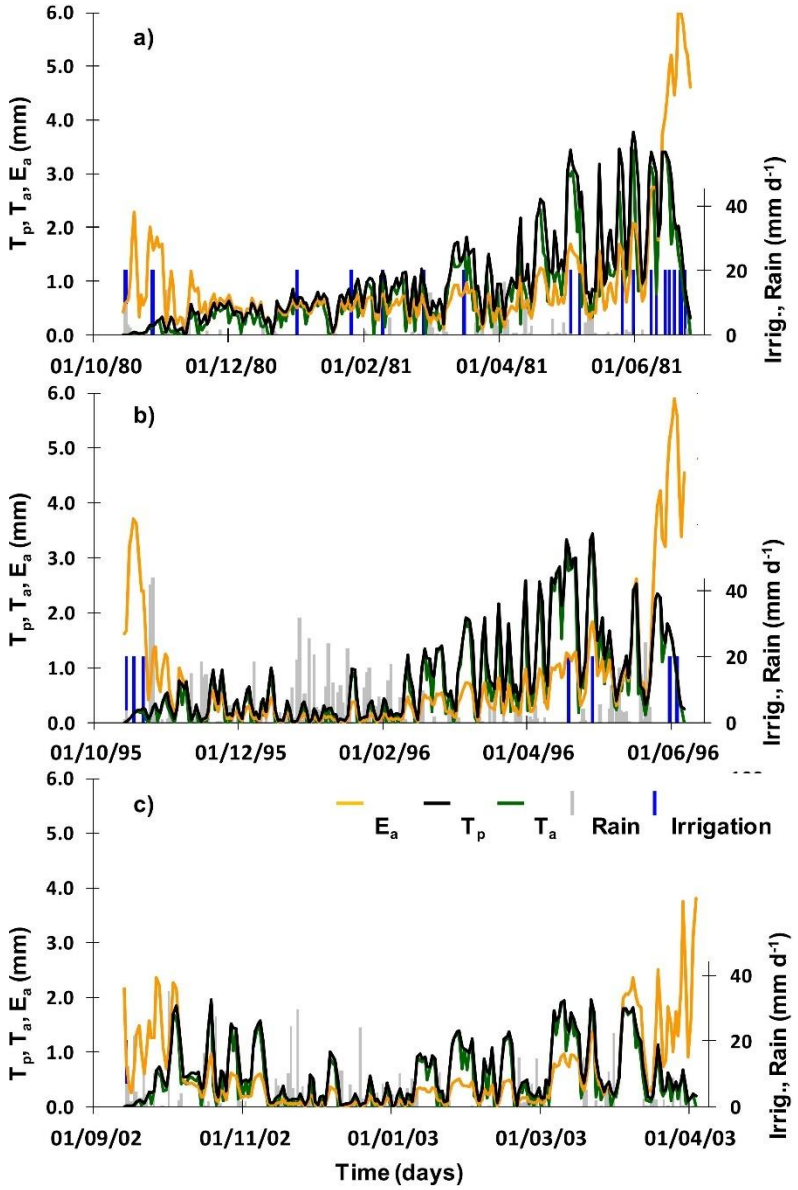

Figure 6.3-6 Seasonal variation of actual evaporation (Ea), potential transpiration (Tp), and actual transpiration (Ea) values during the 1980–1981 (a), 1995–1996 (b), and 2002–2003 (c) seasons.

T_p values were also found to be statistically different between rainfed and irrigated pastures. The difference was justified by the LAI values found in each pasture regime (Figure 6.3-5), these also being statistically different. As explained earlier, LAI had a direct influence on the partition of ET_c values into E_p and T_p. Similarly, T_a values ranged between 32–73 mm and 128–266 mm in rainfed and irrigated pastures Figure 6.3-7, respectively, indicating a water stress that varied between 0.71–5.88% and 0.47–1.97% in the same plots. Water stress was generally higher during the 10 driest seasons, ranging from 1.42 to 5.88% in rainfed pasture and from 0.54–1.97% in irrigated pasture. During the 10 wettest seasons, these values tended to decrease (0.71–2.44% in rainfed pasture, and 0.55–0.99% in irrigated pasture).

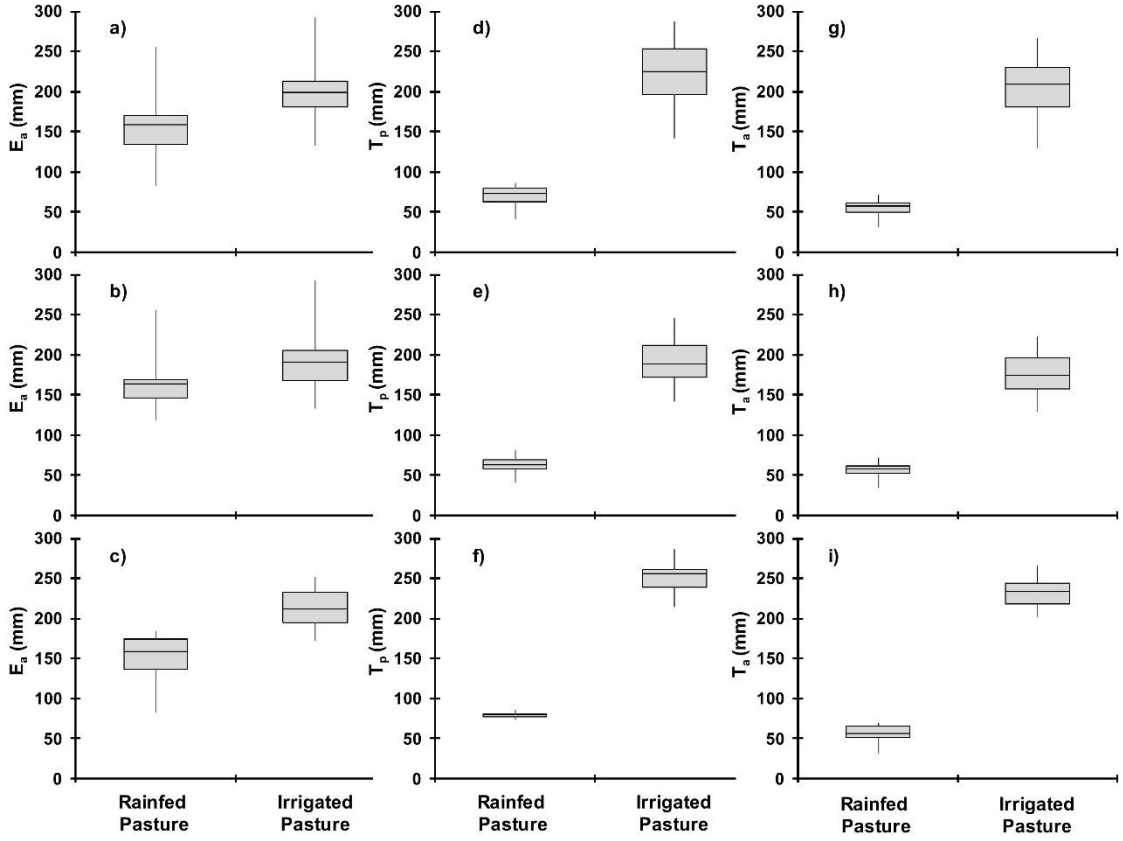

Figure 6.3-7 Actual evaporation (Ea), potential transpiration (Tp), and actual transpiration (Ea) values estimated in rainfed and irrigated pastures between the 1979–1980 and 2007–2008 seasons: (a,d,g) average years; (b,e,h) 10 wettest years; and (c,f,i) 10 driest years.

As in model calibration/validation, in rainfed pasture, E_a values were always higher than T_a values (83–256 mm). In irrigated pasture, E_a values (133–293 mm) tended to be more similar to T_a values (128–266 mm)(Figure 6.3-7), as plants' canopy considerably increased with the temperature increase during the final stages of pasture development (spring), covering the soil and decreasing the fraction of the soil surface exposed to radiation. During the wet seasons, E_a values estimated for rainfed (118–156 mm) and irrigated (133–293 mm) pasture were more similar to one another than during the 10 driest seasons when the former decreased (83–185 mm) and the latter increased (172–252 mm).

6.4 Conclusions

A system-dependent boundary condition was implemented in the MOHID-Land model to automatically trigger irrigation when a certain threshold pressure head was reached in the grid cells of the root zone domain. The lower the h_t value, the longer it took for the matric head to attain it and initiate irrigation, resulting in smaller number of irrigation pulses and less water applied.

The irrigation scheduling tool was then tested in two scenarios on previously calibrated and validated models for maize and pasture crops.

In the case of the maize scenario, the new irrigation scheduling tool was thus able to improve water productivity up to 12% when compared with the farmer's standard irrigation practices. The CR contribution also increased between 17.7 and 66.9% of ET_a.

The second case, where the MOHID-Land was applied in a pasture, the model was able to successfully simulate soil water dynamics and pasture development in a plot located in southern Alentejo, Portugal. The MOHID-Land model was further shown to take into account climate variability when estimating the soil water balance and biomass growth in two different pasture regimes (rainfed and irrigated). Irrigation played a decisive role in the production of dry biomass, with irrigation amounts varying between 20 and 360 mm. As a result, actual transpiration values (128–266 mm) increased considerably when compared with the corresponding values estimated for rainfed pasture (32–73 mm), being closer to the actual evaporation values observed in both regimes (83–256 mm in rainfed pasture; 133–293 mm in irrigated pasture). However, the higher actual evaporation values show the inefficiency of the system, where most soil water is consumed through a non-beneficial use instead of being converted into biomass.

As precise quantification of water fluxes over the pasture is essential for accurately quantifying ecosystem carbon and assessing uncertainties related to the source or sink behavior of pastures, the MOHID-Land model can be considered as a valuable tool for farmers to take the stocking rates into account and reduce the adverse impact of grazing in the pastures.

The MOHID-Land model may thus be considered a useful tool for establishing sound irrigation policies and improving irrigation water management at the plot scale in the Sorraia Valley region. Future work should consider testing the new system-dependent boundary condition for different soils, particularly for soils with heavier textures, wherein the amount of water applied per irrigation event (I_{max}) needs to be also defined while considering soil infiltration constraints in order to prevent surface runoff and soil erosion.

7. Assessing the impact of IrrigaSys decision support system on farmers' irrigation practices in Southern Portugal: A post-evaluation

7.1 Introduction

The development of decision support systems (DSS) was driven by the imperative need to assure the sustainability of agricultural systems, focusing on improving irrigation water management at both the field and irrigation district scales.

DSS are interactive software-based tools employed to gather valuable information from various raw data sources (e.g., soil moisture sensors, proximal and remote sensing platforms, soil water balance models) and deliver optimized solutions (e.g., irrigation scheduling), aiding farmers in the decision-making process (Rinaldi and He, 2014).

The IrrigaSys Decision Support System (DSS) has supported farmers' decision-making regarding irrigation scheduling in the Sorraia Valley irrigation district in Southern Portugal over a span of six years (2017-2022). The IrrigaSys DSS (Simionesei et al., 2020) uses a complex model as a core engine. The MOHID-Land model (Ramos et al., 2017), adopts a mechanistic approach wherein the Richards' equation is used for computing soil water storage and fluxes in the root zone, meaning that a full description of soil hydraulic functions is required, i.e., the soil water retention and soil hydraulic conductivity curves from saturation to oven dryness. Moreover, the model includes the simulation of crop growth, considering factors such as intercepted light, conversion of intercepted light into biomass, crop stress, and the number of heat units defining the crop season (Neitsch et al., 2011; Williams et al., 1989). The model includes a system dependent boundary condition based on soil pressure heads for irrigation scheduling (Ramos et al., 2017).

Despite the complexity of the model, the DSS requires only a limited set of inputs from farmers, which include the location of the agricultural field, crop type, sowing and harvest dates, soil texture, and characteristics of the irrigation system (Simionesei et al., 2020). Since the DSS is not connected remotely to sensors, information regarding applied daily or weekly irrigation depths is gathered through weekly surveys conducted by the technical staff from the local Water Board. This information is critical for the reliability of outputs. Furthermore, a series of demonstrative case studies have been implemented over the years to gain farmers' confidence in the system (Ramos et al., 2021, 2018, 2017; Simionesei et al., 2018). However, there is still uncertainty regarding the willingness of farmers to adhere to the recommended irrigation schedules generated by IrrigaSys. Multicriteria analysis (MCA) may provide insights into the extent to which farmers follow the IrrigaSys recommendations by comparing their

performance with irrigation schedules generated by the DSS using a range of environmental and economic indicators.

MCA emerged in the 1960s as a decision-making tool, facilitating a comparative evaluation of diverse alternatives or heterogeneous scenarios, considering multiple criteria simultaneously within complex situations. Its structure is designed to yield conclusions based on the preferences and priorities of multiple decision-makers, or to generate single synthetic conclusions at the end of the evaluation (e Costa, 2012). This method aids integrating various options, incorporating the perspectives of involved decision-makers within a prospective or retrospective framework. Additionally, MCA aims to organize and merge diverse evaluations considered by decision-makers to find conclusions based on multiple choices. Ultimately, this process provides operational suggestions or recommendations for future activities (Keen and Scott Morton, 1978; Linkov et al., 2006). MCA finds application across various fields such as hydrology, environment, and agronomy. In irrigation agriculture, MCA improves the understanding of impacts, allowing for a satisfactory compromise between conflicting decision-maker objectives (Hajkowicz and Collins, 2007; Huang and Chen, 2005; Ishizaka and Nemery, 2013). MCA is further considered as a valuable tool for addressing water management issues, highlighting social, economic, environmental, and water-related aspects that require careful consideration to meet sustainability objectives in the irrigated agriculture sector. As such, MCA has been extensively applied in irrigation scheduling, design, and management, aiding in finding suitable solutions for specific environmental conditions (Darouich et al., 2017, 2012, 2014; Gonçalves et al., 2009; Pedras and Pereira, 2009).

Therefore, the primary objective of this chapter is to gain insights into farmers' adherence to IrrigaSys recommendations using MCA. The specific aim is to compare different sets of farmers' and model applications from both water-saving and economic perspectives. The ultimate goal is to assess how closely farmers' performance aligns with an optimized irrigation schedule provided by IrrigaSys.

7.2 Materials and methods

7.2.1 Study area description

The plots selected for this study are located in the Sorraia Valley irrigation district, in southern Portugal (38.95 N, 8.54 W). IrrigaSys supported 30 farmers in managing 103 plots ranging from 0.03 to 75 ha, covering a total area of 2080 ha, between 2017 and 2022. The climate in the region is semi-arid to dry sub-humid, with hot dry summers and mild winters with irregular rainfall. The mean annual rainfall is close to 500 mm, varying from 200 to 900

mm along the years. The annual surface air temperature averages 15 ºC, ranging from ~9 ºC in January to ~22 ºC in July. The mean annual reference evapotranspiration (ET_o), calculated using the FAO56 Penman-Monteith (PM) equation (Allen et al., 1998), is close to 900 mm. The dominant soils are Fluvisols, Planosols, Cambisols, Luvisols, and Regosols (IUSS Working Group WRB, 2014). Maize (Zea mays L.) is one of the main crops in the region, after rice (Oryza sativa) and most recently olives (Olea europaea), occupying 21% from the cultivated area, and 24% of the total irrigated area from 2013 to 2022 (Figure 7.2-1). Surface irrigation and center pivots were used in 36.7-39.9% and 30.0-36.1% of the total irrigated area during the same period (2017-2022). IrrigaSys only supported irrigation management of plots equipped with pressurized systems. The district is overseen by a local water board, the Associação de Regantes e Beneficiários do Vale do Sorraia (ARBVS, 2022). Water access is on demand.

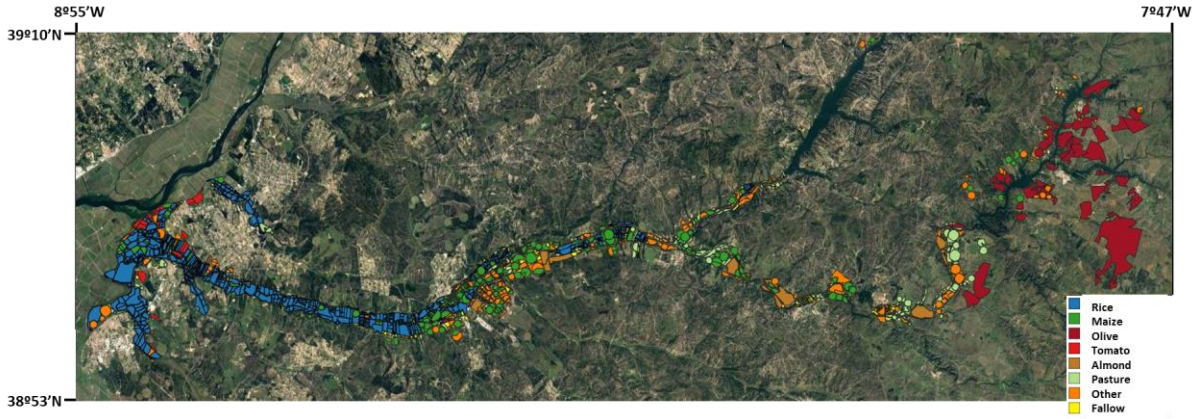

Figure 7.2-1 Maize cultivated plots in Sorraia Valey, 2022

7.2.2 Data selection

For each plot, IrrigaSys generated weekly reports with the irrigation schedule for the upcoming week. During its operation, the system retrieved daily weather data from the closest weather station in the local network, which was subsequently used to compute the ET_o using the FAO-PM equation. Crop evapotranspiration (ET_c) rates were then determined following the single crop coefficient (K_c) approach (Allen et al., 1998), and were used for defining the atmospheric boundary conditions in MOHID-Land. Following this, the model calculated the soil water balance for both the preceding and forthcoming week using irrigation data provided by farmers through ARBVS technicians. In instances, where irrigation data from farmers were not inputted promptly, the system incorporated a set of procedures, as elaborated in Simionesei et al. (2020). Most of these procedures assumed that farmers had adhered to the irrigation schedule outlined in the previous report. Upon receiving the delayed data, the system proceeded

to update the soil water balance, incorporating all information from the time of sowing up to the provided date using farmers data. When issuing recommendations, irrigation scheduling aimed to maximize crop yields by equalizing actual evapotranspiration (ET_a) rates with potential values.

Twenty plots were selected for conducting the MCA based on the following criteria: (i) maize was chosen as the most representative crop in IrrigaSys, and (ii) center pivot was selected as the most represented pressurized irrigation system in the region. The selected plots included the same crop grown in both the driest year (2019) and the average year (2022) served by IrrigaSys for seasonal comparison. Data extracted for each plot included the seasonal gross irrigation amount, the seasonal ET_a, and crop yield (Y)(Table 7.2-1, Table 7.2-2). For each plot, the data from farmers was compared to the corresponding optimized values generated by the MOHID-Land model. Model estimates of gross irrigation amounts assumed an application efficiency of center pivot of 85% (Keller and Bliesner, 1990). Farmers data on ET_a and crop yields was estimated by the model following farmers' irrigation data instead of the optimized schedules. In both scenarios (farmers *vs.* model), ET_a values were computed from the soil water balance by following a macroscopic approach proposed by Feddes et al. (1978), where potential transpiration rates are linearly distributed over the rootzone and eventually reduced due to water stress when soil pressure heads fall outside predefined threshold limits. On the other hand, soil evaporation rates are limited by a pressure head threshold value (American Society of Civil Engineers (ASCE), 1996.). Yields were obtained as the product of the aboveground biomass and a harvest index (Ramos et al., 2017). This procedure can be found in many other modeling applications (e.g., Han et al., 2015; Vanuytrecht et al., 2014; Xu et al., 2013).

Table 7.2-1 Maximum and minimum values Actual Evapotranspiration, Total irrigation, Yield and Precipitation for 2019

2019		ET_a (mm)	Total irrigation (mm)	Yield (kg/ha)	P (mm)
Farmer	Max	622.9	954.1	20062	114.9
	Min	244.3	343.4	8018	14.2
Model	Max	657.4	834.1	20338	114.9
	Min	396.0	623.4	15499	14.2

Table 7.2-2 Maximum and minimum values Actual Evapotranspiration, Total irrigation, Yield and Precipitation for 2022

2022		ET_a (mm)	Total irrigation (mm)	Yield (kg/ha)	P (mm)
Farmer	Max	731.8	771.6	16902	102.4
	Min	402.0	547.6	14337	32.3
Model	Max	590.1	766.5	25387	119.9
	Min	402.0	619.6	14339	32.3

7.2.3 Multicriteria Analysis (MCA)

The MCA was organized into five phases, as depicted in Figure 7.2-2. Phase 1 involved defining the study objectives, specifically comparing farmers' performance in each plot against irrigation schedules recommended by the model using a set of environmental and economic indicators.

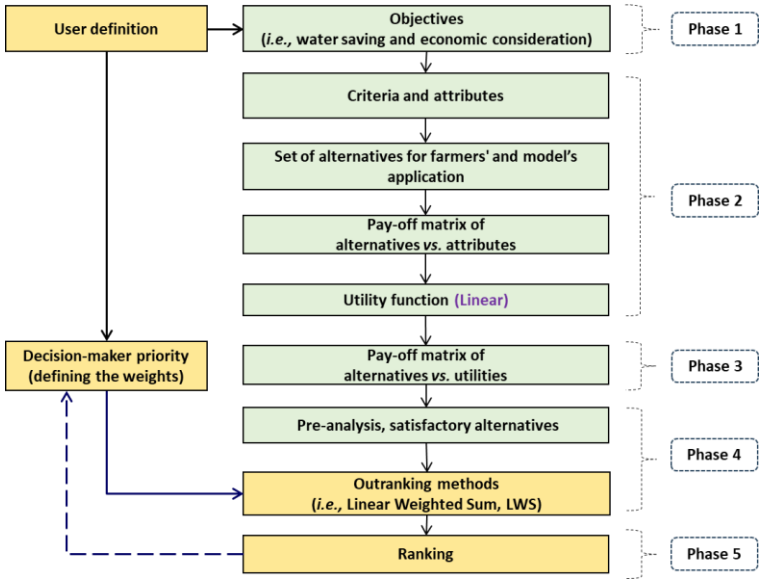

Figure 7.2-2 Functional diagram of MCA model

Phase 2 involved a sequence of steps. The first step referred to the definition of the criteria attributes, which were applicable to two scenarios: Scenario 1 (S1), focusing on environmental and water-saving assessment in relation to irrigation performance, and Scenario 2 (S2), addressing the benefit and economic assessment associated with farmers' economic perspectives. For S1, the following criteria attributes were considered (Fernández et al., 2020; Pereira et al., 2012):

- Irrigation water use (IWU, m^3 ha^{-1}), representing to the total or gross irrigation applied each season.
- Water use efficiency (WUE, dimensionless), calculated as the ratio of ET_a to the sum of IWU and precipitation (P).

- Crop water productivity (WP_c, kg m^{-3}), given by the ratio of the actual marketable yield (Y) to ET_a.
- Irrigation water productivity (WP_i, kg m^{-3}), calculated as the ratio of Y to IWU.

For S2, the criteria attributes were the following (Fernández et al., 2020; Pereira et al., 2012):

- Land productivity (LP, kg ha^{-1}), corresponding to Y.
- Economic land productivity (ELP, € ha^{-1}), representing the value of Y in current prices. In this study, maize yield was 0.26 € kg^{-1} following market prices in 2022.
- Economic crop water productivity (EWP_c, € m^{-3}), given by the ratio of ELP and ET_a.
- Economic irrigation water productivity (EWP_i, € m^{-3}), calculated by the ratio between the ELP and IWU.

The second and third steps in Phase 2 involved creating a payoff matrix that put together alternatives (total of 40 results from both farmers and models for each season) against attributes (environmental and economic indicators). The last step in Phase 2 involved defining the utility function (U_j) for each attribute value (x_j) considered in criterion j using a linear model (Darouich et al., 2012; Gonçalves et al., 2011a; Saaty, 1977), as follows:

$$U_j(x_j) = \alpha_j x_j + \beta_j \quad \text{Equation 36}$$

where α is the slope's function, and β is the utility value of $U_j(x_j)$ for a null value of the attribute. In this function, U_j is normalized from 0 to 1; 0 corresponds to the most adverse condition, while 1 signifies the most advantageous result. As commonly observed in irrigation studies (Darouich et al., 2017; Miao et al., 2018) the slope α is negative (Figure 7.2-3b) for criteria associated with water savings (IWU) and positive (Figure 7.2-3a) for the water productivities, WUE, and economic criteria.

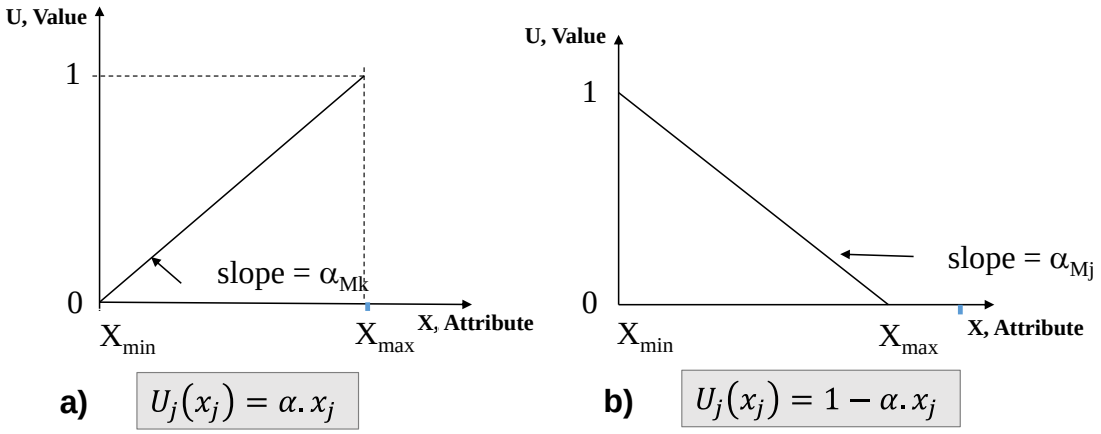

Figure 7.2-3 Linear utility functions relating two points of type a) “more is better” and b) “more is worst”

In Phase 3, a pay-off matrix of the alternatives verse utilities of each criterion (normalized environmental and economic indicators) was established. Phase 4 started by pre-analyzing all set of alternatives to eliminate unsatisfactory results. The viable alternatives were then subjected to outranking. Outranking methods are based on multiple comparisons of the type: "does Measure A outrank Measure B from the point of view of the environmental or economic criterion?” (Roy and Vincke, 1981; Simpson, 1996; Vetschera, 1986; Vincke, 1992). Among various available methods, the Linear Weighted Sum (LWS) (Pomerol and Barba-Romero, 2000) was used. LWS has the advantage of simplicity, facilitating a clearer understanding of the procedures and results. However, a drawback lies in the full compensatory assumption of the LWS method, meaning any criterion with lower results can be compensated by another one with better results.

In this method, a global utility value (U) is computed for each alternative by integrating the utilities of the different criteria attributes using weights that are assigned to reflect users’ priorities (Darouich et al., 2017, 2012, 2014; Gonçalves et al., 2011a, 2011b; Saaty, 1977), as follows:

$$U = \sum_{j=1}^{n} \lambda_j U_j(x_j) \qquad \text{Equation 37}$$

where U is the global utility (scaled from 0 to 1), n is the number of criteria attributes (n=8), and λ_j is the corresponding attribute weight. In this study, criterion weights aimed to emphasize the environmental and economic perspectives. Table 7.2-3 presents the weights assigned to attributes for water saving and economic result priorities. These were used in Phase 5 to compare global utilities and rank alternatives by building the prioritization scenarios. S1

assumed a 90% weight for water saving results and 10% for farm economic results. S2 was the opposite, assuming 10% weight for water saving results and 90% for farm economic results.

Table 7.2-3 Criteria attributes, utility functions, and criteria weights

Criteria attributes (x)	Symbol	Units	Weights (λ_j) assigned to two scenarios		Utility functions
			S1	S2	
Economic productivity			**10**	**90**	
Land productivity	LP	kg ha^{-1}	3	30	**U(x) =5.75E^{-5} – 0.46**
Economic land productivity	ELP	€ ha^{-1}	3	30	**U(x) = 1.1E^{-4} x – 0.22**
Economic crop water productivity	EWPc	€ m^{-3}	2	15	**U(x) = 0.690 x – 0.41**
Economic irrigation water productivity	EWPi	€ m^{-3}	2	15	**U(x) = 0.769 – 0.31**
Water saving			**90**	**10**	
Irrigation water use	IWU	m^3 ha^{-1}	25	3	**U(x) = 1– (1.4E^{-4} x – 0.42)**
WUE (ETa/(IWU+P))	WUE	Ratio	25	3	**U(x) = 1.18 x – 0.29**
Crop water productivity	WPc	kg m^{-3}	20	2	**U(x) = 0.263 x – 0.63**
Irrigation water productivity	WPi	kg m^{-3}	20	2	**U(x) = 0.53 x – 0.89**

7.3 Results and discussion

7.3.1 Environmental and economic indicators

Figure 7.3-1 presents the environmental and economic indicators computed for each plot based on the outputs derived from irrigation schedules adopted by farmers or recommended by the MOHID-Land model for the 2019 and 2022 growing seasons. Plots are designated from P1 to P20, with the letters F and M representing results from farmers and the model, respectively.

Figure 7.3-1a shows model alternatives for WUE ranging from 0.60 to 0.73 in 2019 and 0.53 to 0.74 in 2022. Correspondingly, the results from farmers showed a wider dispersion in both seasons, varying from 0.46 to 0.84 in 2019 and 0.42 to 0.86 in 2022. Moreover, except for a few plots (P2, P3, and P17), WUE values computed from farmers results were generally lower during the average (wetter) season of 2022 than the drier season of 2019. They were also generally lower than the WUE values computed from model results. Therefore, despite relatively high and comparable WUE values during the dry season, Figure 7.3-1a highlights some challenges farmers face in incorporating precipitation forecasts, whether provided by IrrigaSys or other sources, into their irrigation scheduling during the wetter season.

Figure 7.3-1b indicates that IWU values from both farmers and the model were relatively close, averaging 7800 and 8650 m^3 ha^{-1} in 2019 and 7940 and 7800 m^3 ha^{-1} in 2022, respectively. IWU values from farmers being higher than those recommended by the model during the average (wetter) season aligns with the earlier observation regarding the challenges

of assimilating weather forecasts into irrigation schedules. Larger differences between IWU values from farmers schedules and those recommended by the model were noticed in P2, P3, and P16 in 2019, and P2 and P3 in 2022. Because WUE values in these plots are comparable to others, these differences may be explained by the contribution of upward water fluxes from a shallow groundwater table to the soil water balance. As reported by Cameira et al. (2003) and Ramos et al. (2017), capillary fluxes may constitute a significant component of the soil water balance in certain locations of the Vale Sorraia irrigation district, contributing up to 45% of crop evapotranspiration. However, IrrigaSys does not consider such fluxes because modelling the groundwater table requires a regional approach, while the service uses a one-dimensional plot-scale model for computation of the soil water balance. Therefore, farmers' performance, for example in plots P2 and P16, appears to outperform the IrrigaSys service.

Figure 7.3-1b further shows the WP_c and WP_i values computed from farmers and model results. It should be noted that yields were estimated in both cases using the MOHID-Land model while assuming the irrigation schedules defined by farmers or those recommended by the model. Therefore, farmers' results reflect solely the impact of the irrigation schedule on crop yields and do not account for the effect of pests and diseases on crop yields that eventually occurred during the two studied seasons. Farmers' consumptive WP_c values ranged from 2.75 to 4.08 kg m^{-3} in 2019 and 2.47 to 4.22 kg m^{-3} in 2022. These values are comparable to those reported in Ramos et al. (2017) for maize grown in the same region (2.71-2.73 kg m^{-3}). Model's optimized schedules returned similar values, ranging from 2.71 to 4.08 kg m^{-3} in 2019 and 2.74 to 6.12 kg m^{-3} in 2022. However, average WP_c values notably differed in the average (wetter) season, with farmers' results averaging 3.66 kg m^{-3}, while the model reached an average of 4.19 kg m^{-3}. Similar findings were observed for WP_i (1.71-3.34 kg m^{-3}), despite yielding smaller values than WP_c. Nonetheless, values were within the WP_i range reported by Paredes et al. (2014c)) for the same crop and region.

Lastly, Figure 7.3-1c presents the land productivity and economic indicators computed for the study plots. In 2019, LP values in farmers' results varied from 8 to 20 Mg ha^{-1}. However, only results from P16 stand out from the others, being abnormally low. As previously hypothesized, this low LP may have resulted from not considering the contribution of groundwater flows to the root zone when computing the soil water balance, with actual yield values being substantially higher than estimated here. In this case, model parametrization in this plot should be reevaluated. Alternatively, the lower LP value could reflect some mismanagement of irrigation water during that season, as the same was not observed in 2022.

In this year, farmers' LP values were found to be within the 16 to 20 Mg ha^{-1} range. The same was observed for the model's LP values in both seasons, despite some high values (>23.5 Mg ha^{-1}) estimated in five plots for 2022. These higher yields can be attributed to farmers choosing longer crop cycle, and more productive varieties of maize in that year.

EWP_c and EWP_i trends naturally aligned with the yield variations observed between plots and seasons (Figure 7.3-1c). EWP_c values computed from farmers' results ranged from 0.72 to 1.06 € m^{-3} in 2019 and 0.64 to 1.10 € m^{-3} in 2022. The corresponding values computed from model results were similar for 2019, and again higher for 2022 (0.71-1.59 € m^{-3}). Similar findings and interpretations can be applied to the EWP_i values, with farmers' values ranging from 0.48 to 0.78 € m^{-3} in 2019 and 0.44 € m^{-3} to 0.71 in 2022. Nonetheless, all reported values were found to be higher than the EWP_c (0.29-0.51 € m^{-3}) and EWP_i (0.31-0.69 € m^{-3}) values reported in Paredes et al. (2014c)) for the same crop and region, which can be explained by the lower commodity price of maize (0.21 € m^{-3}) at the time of that study compared to today's prices (0.26 € m^{-3}).

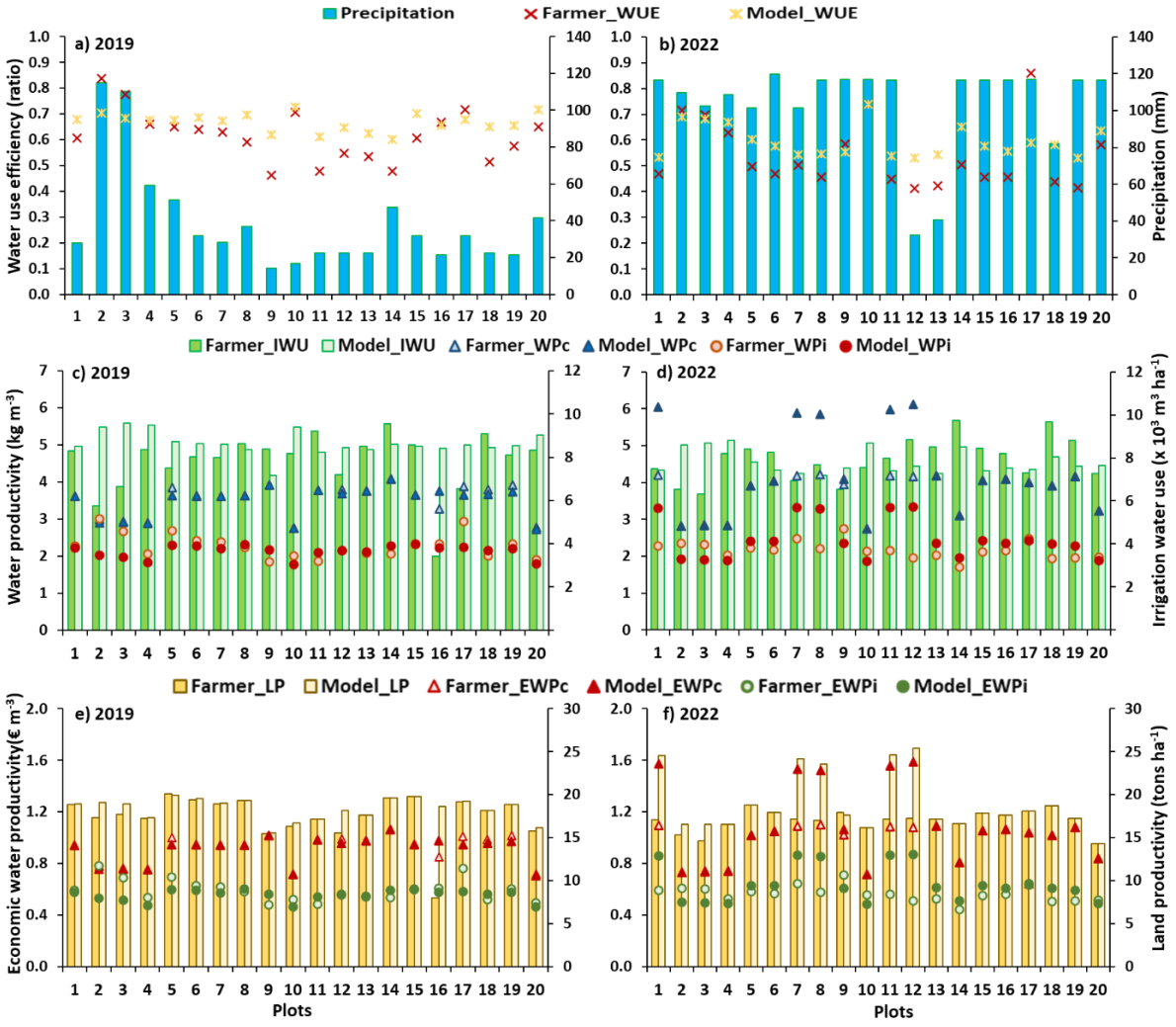

Figure 7.3-1 Farmers versus model alternatives during the growing seasons of 2019 and 2022 relative to: a,b) water use efficiency (WUE, ratio); c,d) gross irrigation water use (IWU, m^3 ha^{-1}), and crop and irrigation water productivities (WPc, WPi, kg m^{-3}); and e,f) land productivity (LP, €·ha^{-1}), economic crop. and irrigation water productivities (EWP_c, EWP_i, € m^{-3}).

7.3.2 Results of multicriteria analysis

The global utilities (U) characterizing farmers and model alternatives when priorities are assigned to water saving (S1) or farm economic returns (S2) during 2019 and 2022 are presented in Figure 7.3-2. In the water-saving S1 scenario, farmers' U values varied from 0.21 to 0.55 in 2019 and from 0.16 to 0.45 in 2022. The corresponding model U values ranged from 0.23 to 0.38 in 2019 and from 0.26 to 0.55 in 2022. The results clearly indicate that farmers' performance during the dry season (2019) approached or even surpassed model performance in most fields. This means that, during the dry season, farmers, in general, adopted irrigation schedules deemed comparable to those optimized by the physically based model. The reasons for surpassing model results in some plots were previously discussed and refer to challenges

associated with incorporating upward fluxes from the groundwater table in the one-dimensional modeling of the soil water balance, as implemented in IrrigaSys.

During the wetter season of 2022, farmers' U values consistently fell below those of the model, highlighting the difficulties in integrating dependable information from precipitation forecasts into decision-making processes. The relevance of this information for computing the soil water balance increases with the earlier sowing dates, which, depending on the farmer and season, may vary in the region from April to July. Hence, it appears that the most crucial factor for increasing the efficient use of water in the region is reliable precipitation forecast information. Regarding other factors considered in this analysis, farmers demonstrate an acceptable level of knowledge in terms of irrigation scheduling and irrigation water management. However, as demonstrated by Linker et al. (2018), who assessed the quality of current weather forecasts, including those for the Sorraia Valley region, precipitation forecasts exhibited significant shortcomings at the locations studied by those authors. This inadequacy was observed not only in terms of predicting rain amounts but also in predicting rain/no rain events.

Relative to farmers' economic returns S2 scenario, farmers' U values varied from 0.12 to 0.43 in 2019 and from 0.24 to 0.38 in 2022. The corresponding model U values ranged from 0.26 to 0.41 in 2019 and from 0.24 to 0.65 in 2022. The results were highly consistent in both years, indicating that farmers achieved economic returns comparable to those obtained by following the model's recommendations. It is crucial to reiterate that yield estimates in farmers' applications do not incorporate the impacts of pests, diseases, or other transient stresses. These estimates solely reflect the effects of water stresses resulting from non-optimal irrigation schedules on transpiration rates and, consequently, on yields. The actual yield values undoubtedly varied from the estimates considered here, which are contingent solely upon irrigation schedules. Economic indicators also did not account for variable costs (e.g., operation, maintenance, labor, energy) that certainly differed from one plot to the other. However, from a water management perspective, both farmers and the model exhibited equivalent performances.

Lastly, Table 7.3-1 ranks the first best 20 alternatives based on water-saving and economic returns priorities. The table confirms that in the dry year of 2019, farmers' applications proved to be feasible and effective solutions concerning water conservation and economic considerations. Additionally, model solutions exhibited progress in ranking, securing the 6th and 3rd positions for S1 and S2, respectively. The top common applications for farmers

in both S1 and S2, ranked among the best 10, were P17, P5, and P6. Conversely, for model applications, P15 emerged as the most common choice.

In 2022, model solutions took the lead in the rankings showing superiority in both scenarios S1 and S2, having P1, P7, P8, P11, and P12 in the first top rank order when the priority is assigned to water saving, while a set of plots of P1, P5, P7, P8, P11 and P12 shows high ranking order when the priority is assigned to economic return. Some of these best common applications show up as good options for both S1 and S2. However, farmers also present viable and satisfactory solutions, such as P9, which is applicable in both scenarios. In general in S2, without including the abnormal values of yield (>23.5 Mg ha^{-1}) simulated in 5 plots in 2022, farmers and models applications show very similar results for both seasons, and the differences in ranking are very small. In S1, the difference is larger, with farmers' solutions showing superiority compared to model applications in some plots.

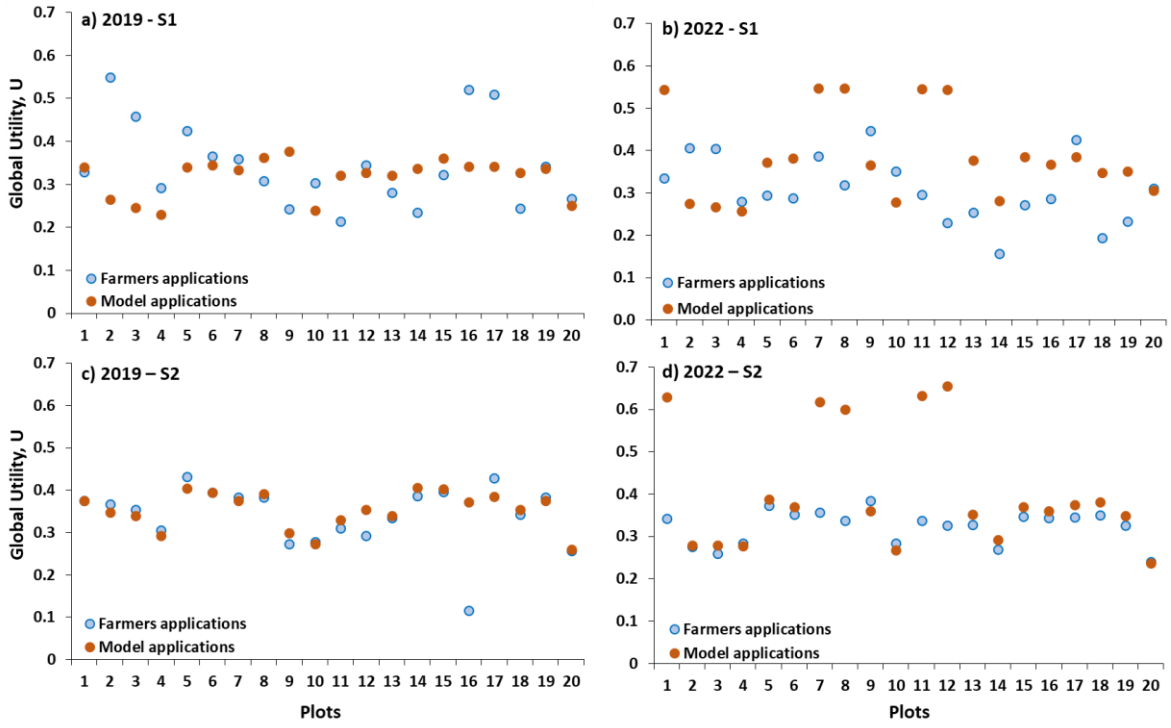

Figure 7.3-2 Global utilities, U, for farmers versus model alternatives, when prioritizing water conservation (a, b) or economic returns (c, d) during the growing seasons of 2019 and 2022.

Table 7.3-1 . Ranking of the best 20 alternative solutions for water saving and economic priorities in 2019 and 2022.

Alternatives	2019		2022	
	Water priority (S1)	Economic priority (S2)	Water priority (S1)	Economic priority (S2)
1	F_P2	F_P5	M_P7	M_P12
2	F_P16	F_P17	M_P8	M_P11

Alternatives	2019		2022	
	Water priority (S1)	Economic priority (S2)	Water priority (S1)	Economic priority (S2)
3	F_P17	M_P14	M_P11	M_P1
4	F_P3	M_P5	M_P12	M_P7
5	F_P5	M_P15	M_P1	M_P8
6	M_P9	F_P15	F_P9	M_P5
7	F_P6	F_P6	F_P17	F_P9
8	M_P8	M_P6	F_P2	M_P18
9	M_P15	M_P8	F_P3	M_P17
10	F_P7	F_P14	F_P7	F_P5
11	M_P6	M_P17	M_P17	M_P6
12	F_P12	F_P8	M_P15	M_P15
13	F_P19	F_P7	M_P6	M_P16
14	M_P17	F_P19	M_P13	M_P9
15	M_P16	M_P7	M_P5	F_P7
16	M_P1	M_P1	M_P16	M_P13
17	M_P5	M_P19	M_P9	F_P6
18	M_P14	F_P1	M_P19	F_P18
19	M_P19	M_P16	F_P10	M_P19
20	M_P7	F_P2	M_P18	F_P15

7.4 Conclusions

This study aimed to conduct a post-evaluation of IrrigaSys, a DSS that facilitated farmers' decision-making regarding irrigation scheduling in the Sorraia Valley irrigation district in Southern Portugal from 2017 to 2022. This post-evaluation primarily focused on comparing farmers' performance with recommendations generated by the model running the DSS. The comparison was conducted using a set of environmental and economic indicators, employing a multicriteria analysis approach.

Although it cannot be directly assumed that farmers strictly adhered to the system, the results of the MCA unequivocally demonstrate that farmers demonstrated a commendable level of expertise in irrigation scheduling, closely aligning with the environmental and economic indicators derived from model's recommendations, particularly during the dry season. However, in a wetter season, a noticeable disparity emerged between farmers and model indicators, primarily due to the difficulties associated with incorporating reliable information from precipitation forecasts into the decision-making process. Addressing this challenge appears to be the key factor for enhancing the future utilization of IrrigaSys.

8. General conclusions

The primary objective of this thesis was to develop a tool aimed at assisting decision-makers in enhancing water use efficiency at the plot scale, particularly focusing on irrigated agro-ecosystems in southern Portugal. This goal was achieved through the creation of the IrrigaSys Decision Support System (DSS).

Additionally, another key objective was the calibration of the MOHID Land model for various crops. This objective was accomplished by calibrating the main crops of the Sorraia Valley region, which included maize, pasture, and vine.

Furthermore, the thesis aimed to assess the utilization and impact of remote sensing, specifically LAI (Leaf Area Index) data, on model simulations. This was accomplished by evaluating the effects of LAI data assimilation on simulations related to soil water balance and maize development. Additionally, the study explored the potential of using vegetation indices to validate crop transpiration fluxes, with a specific application to vineyards.

The final chapter of the thesis also aimed to conduct a post-evaluation of IrrigaSys, a DSS that facilitated farmers' decision-making regarding irrigation scheduling.

In summary, the thesis addressed the following objectives:

Development of the IrrigaSys DSS to improve water use efficiency in irrigated agro-ecosystems.

Calibration of the MOHID Land model for key crops in the Sorraia Valley.

Assessment of the impact of remote sensing data (LAI) on model simulations, including LAI data assimilation effects and vegetation index utilization for validating crop transpiration fluxes, applied to vineyards.

These analyses allowed, therefore, answering the following questions:

Can a distributed model like the MOHID-Land model be used for irrigation water management?

The MOHID-Land model has been utilized for various aspects of irrigation water management in different agricultural scenarios. The model demonstrates its capability to simulate soil water dynamics, biomass growth, and plant development in different types of ecosystems, including maize, pastures, and vineyards, located in different regions of Portugal.

In the Sorraia Valley region, the MOHID-Land model was used to simulate soil water dynamics and maize development. The model's estimations of soil water content, leaf area

index (LAI), canopy height, aboveground biomass, and maize yields were found to be in good agreement with field data. The study indicated that the irrigation scheduling practices could be improved by considering soil water holding capacity and groundwater contributions, leading to increased water productivity and more efficient irrigation practices.

Similarly, in southern Alentejo, the model simulated soil water dynamics and pasture development. The model took into account climate variability and demonstrated the impact of irrigation on biomass production. Irrigation was shown to play a significant role in biomass growth, with transpiration values increasing considerably under irrigation. However, it also highlighted the inefficiencies in water use, where a significant portion of soil water was lost to non-beneficial evaporation instead of being converted into biomass.

Furthermore, the MOHID-Land model was applied to a vineyard ecosystem, replicating measured soil water content values and providing insights into irrigation-induced water stress and evaporation dynamics. Although the model's calculation of actual evaporation is a simplified formulation, its overall performance in modeling soil water dynamics for a permanent crop like a vineyard was considered acceptable.

The MOHID-Land model's capabilities extend to providing valuable information for decision support systems like IrrigaSys, aiding farmers in making informed irrigation choices. These instances collectively demonstrate the model's potential as a useful tool for establishing irrigation policies, optimizing irrigation practices, and improving water management in various agricultural settings.

However, it's important to note that the model's success is largely contextual and dependent on the specific characteristics of the ecosystems and regions being studied. Different soils, climates, and crops may require adjustments and validations to ensure accurate results.

Can a decision support system (DSS) function with the MOHID-Land model as its core system?

Irrigasys decision support system (DSS), was designed to support irrigation water management at the field plot scale. The system relies on various inputs such as location, crop type, soil texture, irrigation system characteristics, and more, to generate optimized irrigation schedules and provide additional information like soil water balance, weather forecasts, and satellite images.

The DSS works with the MOHID-Land model as its core system. IrrigaSys DSS is integrated with the MOHID-Land model, and integrating a DSS with a specific model like

MOHID-Land depends on various factors like: compatibility, data-exchange, calibration and validation, user experience, performance and reliability, and maintenance. IrrigaSys and the MOHID-Land model and their data inputs, outputs, and processing methods of both systems are compatible. IrrigaSys and MOHID-Land work with similar data types or share common data. The interface is designed to facilitate data exchange between the two systems. MOHID-Land was calibrated and validated for several crops and scenarios. Other crops and locations might need to require adapting or recalibrating to ensure accurate results within the context of irrigation management. Irrigasys offers an attractive interface to deal with the input data to MOHID-Land but also to visualize the model results. In terms of performance and reliability, the integration was thoroughly tested to ensure that the combined system performs reliably and provides accurate recommendations to users. Both IrrigaSys and MOHID-Land receive regular updates and improvements over time, and the integrated system has been designed to accommodate these updates seamlessly.

Can remote sensing products be used for scaling up the DSS to plots with limited data availability?

The use of remote sensing products in Decision Support Systems (DSS) for scaling up to plots with limited data availability can provide valuable information to improve model estimates and validate outputs. However, it's important to note that the effectiveness of using remote sensing data for such purposes is context-dependent and has its limitations.

In the first study, the assimilation of Leaf Area Index (LAI) data from NDVI-derived satellite data improved certain aspects of the MOHID-Land model's performance, particularly during the early stages of the crop growing period. This indicates that incorporating remote sensing data can enhance the accuracy of model simulations, especially when there's limited ground-based calibration data available. However, the study also pointed out several limitations:

Calibration Data Requirement: Remote sensing data assimilation was insufficient to improve model simulations when a crop calibrated dataset was absent. This suggests that while remote sensing data can enhance model performance, it cannot entirely replace the need for ground-based calibration data.

Temporal Considerations: The timing of remote sensing data assimilation is crucial. While model uncertainty decreased when LAI assimilation was carried out closer to the end of the crop cycle, using remote sensing data solely during the initial stages of the crop growing

period led to erroneous estimates. This emphasizes the importance of selecting appropriate timeframes for assimilation.

Model Complexity: The study highlights that using remote sensing data for LAI assimilation doesn't guarantee accurate simulations of all model outputs, such as crop transpiration, soil evaporation, and aboveground dry biomass. The complexity of the model and its various components can affect the success of data assimilation.

The second study suggests that while remote sensing data, particularly Sentinel-2 data, can validate model outputs, there are nuances to consider:

Dependence on Conditions: The relationships established between model outputs and NDVI were found to be dependent on experimental conditions like irrigation management and climate conditions. This implies that the effectiveness of using remote sensing data for validation can vary based on specific circumstances.

Generalization Limitations: The study warns against generalizing the results to other vineyards without considering the local conditions. Variability in environmental factors can influence the applicability of remote sensing-based relationships across different regions.

Use in Decision-Making: Despite the limitations, Sentinel-2 data proved useful for validating model outputs during irrigation decision-making. This demonstrates that remote sensing data can provide timely information to guide operational choices, even without extensive calibration datasets.

In both studies, it's evident that while remote sensing data can be a valuable tool for improving and validating models within a DSS framework, they are not a standalone solution. They need to be used in conjunction with other data sources and considerations, and their application must be tailored to the specific context and conditions of the study area. Additionally, model calibration and validation remain crucial components of ensuring accurate and reliable DSS outcomes.

A post-evaluation of IrrigaSys was conducted, primarily focused on comparing farmers' performance with recommendations generated by the model running the DSS. The comparison used a set of environmental and economic indicators, employing a multicriteria analysis approach. The results of the MCA demonstrate that farmers demonstrated a commendable level of expertise in irrigation scheduling, closely aligning with the environmental and economic indicators derived from the model's recommendations, particularly during the dry season. However, in a wetter season, a noticeable disparity emerged between farmers and model

indicators, primarily due to the difficulties associated with incorporating reliable information from precipitation forecasts into the decision-making process.

All the investigation done here for this thesis shows the usefulness and versatility of using a DSS and more specifically, using Irrigasys DSS as a water management tool at a plot scale in order to respond to the increase of water demand and withdrawals that have been building up the pressure on freshwater resources.

Taking into account the results, these kinds of tools are essential for water management at plot scale and can also be in the future used in other scales and in a water basin management tool. The major strength results from the close cooperation between the academy and a local Water Board during its development. On the other hand, the complexity of the DSS core engine as well as the inherent difficulties in calibrating/validating model parameters for all case scenarios constitutes a major weakness. IrrigaSys needs thus to continue being developed to overcome such limitations and become a more trustworthy tool in irrigation water management.

Related to the use of remote sensing, this technology can provide valuable information for hydrological modeling at the field and regional scales by better characterizing the spatial and temporal variability of soils, land uses, and climate, which otherwise are difficult to portray. The studies showed that data derived from satellites can provide valuable information to improve model estimates and validate outputs. However, it's important to note that the effectiveness of using remote sensing data for such purposes is context-dependent and has its limitations.

Also, it is important to mention the importance of taking into consideration the uncertainties that may be associated with the models, data, and implementation of DSS's it's not always an easy task to quantify. Besides that, this tool remains quite effective given its simplified and integrative approach in the study of complex processes of nature such as those occurring in soils related water balance leaching, among others.

Some specific recommendations for improving the use of DSSs for irrigation water management can include making DSSs more user-friendly and easier to use, developing DSSs that are tailored to the specific needs of farmers in different regions, improving the accuracy of DSS outputs by using better quality input data and conducting more research on the use of DSSs for irrigation water management. This can make DSSs a more effective tool for irrigation water management and help to improve water productivity and sustainability in agriculture.

Further advancements are needed for the reimplementation of IrrigaSys in the Sorraia Valley region. Specifically, attention should be directed toward addressing the outdated process

of gathering information on irrigation applications in different plots through surveys. Numerous solutions, particularly those utilizing remote sensing data, are now accessible for automatically collecting this information. This use of remote sensing automatically should be tested, validated, and integrated into the system.

Big data analytics can revolutionize agriculture by empowering farmers to make well-informed irrigation decisions. Through the analysis of vast datasets comprising historical weather patterns combined with past irrigation behaviors, yearly reports generated from this data can highlight the significant water conservation achieved. This tangible evidence underscores the benefits of data-driven decision-making. Moreover, by comparing these outcomes with traditional methods, the effectiveness of the analytics model becomes apparent, fostering the adoption of more sustainable farming practices.

Future research into the integration of machine learning in agriculture should focus on the integration of ensemble models and machine learning techniques can bring a significant advancement in irrigation services. Ensemble models, which combine multiple predictive models to improve accuracy, can be particularly effective in forecasting water demand and availability, thus optimizing irrigation schedules. Machine learning algorithms can analyze vast amounts of data from sensors and weather stations to predict optimal irrigation times and quantities, leading to more efficient water use and potentially higher crop yields. Together, these technologies can revolutionize irrigation practices, making them more responsive to environmental conditions and reducing waste.

These research directions have the potential to advance the field, resulting in agricultural systems that are more sustainable, efficient, and resilient.

The research presented in this thesis has the potential to contribute to the improvement of irrigation water management in agricultural settings. The findings of this research can be used to develop more accurate and reliable DSS for irrigation water management. This can help farmers to make more informed irrigation decisions, leading to increased water productivity and improved water management practices.

Abi Saab, M.T., Jomaa, I., Skaf, S., Fahed, S., Todorovic, M., 2019. Assessment of a smartphone application for real-time irrigation scheduling in Mediterranean environments. Water 11, 252.

Allen, R., Wright, J.L., Pruitt, W.O., Pereira, L., Jensen, M., 1998. Water Requirements. Design and Operation of Farm Irrigation Systems 29. https://doi.org/10.1007/978-94-011-5131-3_2

Allen, R.G., Pereira, L.S., 2009. Estimating crop coefficients from fraction of ground cover and height. Irrigation Science 28, 17–34.

Allen, R.G., Pereira, L.S., Howell, T.A., Jensen, M.E., 2011. Evapotranspiration information reporting: I. Factors governing measurement accuracy. Agricultural Water Management 98, 899–920. https://doi.org/10.1016/j.agwat.2010.12.015

Allen, R.G., Pereira, L.S., Raes, D., Smith, M., 1998. Crop evapotranspiration-Guidelines for computing crop water requirements-FAO Irrigation and drainage paper 56. Fao, Rome 300, D05109.

Allen, R.G., Pereira, L.S., Smith, M., Raes, D., Wright, J.L., 2005. *FAO-56* Dual Crop Coefficient Method for Estimating Evaporation from Soil and Application Extensions. Journal of Irrigation and Drainage Engineering.

American Society of Civil Engineers (ASCE), n.d. Hydrology Handbook Task Committee on Hydrology Handbook, II Series. GB 661.2. H93.1996.

Andales, A.A., Bauder, T.A., Arabi, M., 2014. A mobile irrigation water management system using a collaborative GIS and weather station networks. Practical applications of agricultural system models to optimize the use of limited water 5, 53–84.

Annandale, J.G., Jovanovic, N.Z., Campbell, G.S., Du Sautoy, N., Benade, N., 2003. A two-dimensional water balance model for micro-irrigated hedgerow tree crops. Irrigation Science 22, 157–170.

ARBVS, 2015. Evolução Da área Cultivada, http://www.arbvs.pt/areacultivada#. VmreI0qLQdU (last Accessed 12 November 2015).

Aronson, J., Pereira, J.S., Pausas, J.G., 2012. Cork oak woodlands on the edge: ecology, adaptive management, and restoration. Island Press.

Ashraf Vaghefi, S., Abbaspour, K.C., Faramarzi, M., Srinivasan, R., Arnold, J.G., 2017. Modeling crop water productivity using a coupled SWAT–MODSIM model. Water 9, 157.

Azevedo, A.S., Kanwar, R.S., Pereira, L.S., 2000. Atrazine Transport in Irrigated Heavy- and Coarse-Textured Soils, Part II: simulations with the Root Zone Water Quality Model. Journal of Agricultural Engineering Research 76, 341–354. https://doi.org/10.1006/jaer.2000.0544

Basso, B., Liu, L., Ritchie, J.T., 2016. A comprehensive review of the CERES-wheat,-maize and-rice models' performances. Advances in agronomy 136, 27–132.

Belfiore, O.R., Castagna, A., Longo-Minnolo, G., Ippolito, M., Bavieri, A., Comegna, A., D'Urso, G., 2022. Monitoring of Irrigation Water Use in Italy by Using IRRISAT Methodology: The INCIPIT Project, in: Conference of the Italian Society of Agricultural Engineering. Springer, pp. 41–49.

Bender, E.A., 2000. An Introduction to Mathematical Modeling. Dover Publications.

Bernard-Jannin, L., Brito, D., Sun, X., Jauch, E., Neves, R., Sauvage, S., Sánchez-Pérez, J.-M., 2016. Spatially distributed modelling of surface water-groundwater exchanges during overbank flood events – a case study at the Garonne River. Advances in Water Resources 94, 146–159. https://doi.org/10.1016/j.advwatres.2016.05.008

Boegh, E., Poulsen, R.N., Butts, M., Abrahamsen, P., Dellwik, E., Hansen, S., Hasager, C.B., Ibrom, A., Loerup, J.-K., Pilegaard, K., 2009. Remote sensing based evapotranspiration and runoff modeling of agricultural, forest and urban flux sites in Denmark: From field to macro-scale. Journal of Hydrology 377, 300–316.

Brisson, N., Gary, C., Justes, E., Roche, R., Mary, B., Ripoche, D., Zimmer, D., Sierra, J., Bertuzzi, P., Burger, P., Bussière, F., Cabidoche, Y.M., Cellier, P., Debaeke, P., Gaudillère, J.P., Hénault, C., Maraux, F., Seguin, B., Sinoquet, H., 2003. An overview of the crop model stics. European Journal of Agronomy 18, 309–332. https://doi.org/10.1016/S1161-0301(02)00110-7

Brito, D., Campuzano, F.J., Sobrinho, J., Fernandes, R., Neves, R., 2015. Integrating operational watershed and coastal models for the Iberian Coast: Watershed model implementation – A first approach. Estuarine, Coastal and Shelf Science 167, 138–146. https://doi.org/10.1016/j.ecss.2015.10.022

Brito, D., Neves, R., Branco, M.A., Gonçalves, M.C., Ramos, T.B., 2017. Modeling flood dynamics in a temporary river draining to an eutrophic reservoir in southeast Portugal. Environmental Earth Sciences 76, 1–15.

Brito, D., Ramos, T.B., Gonçalves, M.C., Morais, M., Neves, R., 2018. Integrated modelling for water quality management in a eutrophic reservoir in south-eastern Portugal. Environmental earth sciences 77, 1–20.

Butts, M., Drews, M., Larsen, M.A., Lerer, S., Rasmussen, S.H., Grooss, J., Overgaard, J., Refsgaard, J.C., Christensen, O.B., Christensen, J.H., 2014. Embedding complex hydrology in the regional climate system–Dynamic coupling across different modelling domains. Advances in Water Resources 74, 166–184.

Calera, A., Campos, I., Osann, A., D'Urso, G., Menenti, M., 2017. Remote sensing for crop water management: From ET modelling to services for the end users. Sensors 17, 1104.

Cameira, M.R., Fernando, R.M., Ahuja, L., Pereira, L., 2005. Simulating the fate of water in field soil–crop environment. Journal of Hydrology 315, 1–24.

Cameira, M.R., Fernando, R.M., Ahuja, L.R., Ma, L., 2007. Using RZWQM to simulate the fate of nitrogen in field soil–crop environment in the Mediterranean region. Agricultural Water Management 90, 121–136. https://doi.org/10.1016/j.agwat.2007.03.002

Cameira, M.R., Fernando, R.M., Pereira, L.S., 2003. Monitoring water and NO3-N in irrigated maize fields in the Sorraia Watershed, Portugal. Agricultural Water Management 60, 199–216.

Campos, I., Balbontín, C., González-Piqueras, J., González-Dugo, M.P., Neale, C.M., Calera, A., 2016. Combining a water balance model with evapotranspiration measurements to estimate total available soil water in irrigated and rainfed vineyards. Agricultural Water Management 165, 141–152.

Campos, I., Neale, C.M., Calera, A., Balbontín, C., González-Piqueras, J., 2010. Assessing satellite-based basal crop coefficients for irrigated grapes (Vitis vinifera L.). Agricultural Water Management 98, 45–54.

Cancela, J.J., Fandiño, M., Rey, B.J., Martínez, E.M., 2015. Automatic irrigation system based on dual crop coefficient, soil and plant water status for Vitis vinifera (cv Godello and cv Mencía). Agricultural Water Management 151, 52–63.

Car, N.J., 2018. USING decision models to enable better irrigation Decision Support Systems. Computers and Electronics in Agriculture 152, 290–301.

Carsel, R.F., Parrish, R.S., 1988. Developing joint probability distributions of soil water retention characteristics. Water Resources Research 24, 755–769. https://doi.org/10.1029/WR024i005p00755

Chapman, D.F., Rawnsley, R.P., Cullen, B.R., Clark, D.A., 2020. Inter-annual variability in pasture herbage accumulation in temperate dairy regions: causes, consequences, and management tools.

Chauhan, Y.S., Wright, G.C., Holzworth, D., Rachaputi, R.C.N., Payero, J.O., 2013. AQUAMAN: a web-based decision support system for irrigation scheduling in peanuts. Irrigation Science 31, 271–283. https://doi.org/10.1007/s00271-011-0296-y

Christiansen, J.E., 1942. IRRIGATION BY SPRINKLING.

Comission, European, n.d. The common agricultural policy: 2023-27.

Copernicus, E.S.A., 2022. Copernicus open access hub.

Copernicus Global Land Service. Available online: https://land.copernicus.eu/global/index.html (accessed on 17 March 2021)., n.d.

Copernicus Open Access Hub. Available online: https://scihub.copernicus.eu/ (accessed on 17 March 2021)., n.d.

COTR, 2009. "Benchmarking" na Rega e Boas Praticas de Gestão da Rega da Vinha. Centro Operativo e Tecnológico do Regadio.

Dabach, S., Lazarovitch, N., Šimůnek, J., Shani, U., 2013. Numerical investigation of irrigation scheduling based on soil water status. Irrigation Science 31, 27–36. https://doi.org/10.1007/s00271-011-0289-x

Dane, J.H., Topp, C.G., 2020. Methods of soil analysis, Part 4: Physical methods. John Wiley & Sons.

Darouich, H., Cameira, M.R., Gonçalves, J.M., Paredes, P., Pereira, L.S., 2017. Comparing sprinkler and surface irrigation for wheat using multi-criteria analysis: water saving vs. economic returns. Water 9, 50.

Darouich, H., Goncalves, J.M., Muga, A., Pereira, L.S., 2012. Water saving vs. farm economics in cotton surface irrigation: An application of multicriteria analysis. Agricultural water management 115, 223–231.

Darouich, H.M., Pedras, C.M.G., Gonçalves, J.M., Pereira, L.S., 2014. Drip vs. surface irrigation: A comparison focussing on water saving and economic returns using multicriteria analysis applied to cotton. Biosystems Engineering 122, 74–90. https://doi.org/10.1016/j.biosystemseng.2014.03.010

Dige, G., De Paoli, G., Strosser, P., Anzaldua, G., Ayres, A., Lange, M., Lago, M., Oosterhuis, F.H., Hrabar, M., Navrud, S., 2013. Assessment of cost recovery through water pricing. EEA Technical Report.

e Costa, C.A.B., 2012. Readings in multiple criteria decision aid. Springer Science & Business Media.

Eching, S., Frame, K., Snyder, L., 2002. Role of technology in irrigation advisory services: The CIMIS experience, in: 18th Congress and 53rd IEC Meeting of the International Commission on Irrigation and Drainage (ICID). FAO/ICID International Workshop on Irrigation Advisory Services and Participatory Extension Management.

EEA, 2009. Water Resources Across Europe -Confronting Water Scarcity and Drought. Report No. 2/2009. European Environment Agency (EEA), Luxembourg (55pp).

Epelde, A.M., Antiguedad, I., Brito, D., Jauch, E., Neves, R., Garneau, C., Sauvage, S., Sánchez-Pérez, J.M., 2016. Different modelling approaches to evaluate nitrogen transport and turnover at the watershed scale. Journal of Hydrology 539, 478–494. https://doi.org/10.1016/j.jhydrol.2016.05.066

Er-Raki, S., Rodriguez, J.C., Garatuza-Payan, J., Watts, C.J., Chehbouni, A., 2013. Determination of crop evapotranspiration of table grapes in a semi-arid region of Northwest Mexico using multi-spectral vegetation index. Agricultural water management 122, 12–19.

European Commission, 2012. A Blueprint to Safeguard Europe's Water Resources, 2012. Communication from the Commission to the European Parliament, the Council, the European Economic and Social Committee and the Committee of the Regions, COM, Brussels, pp. 673.

European Commission, 2011. A Resource-efficient Europe –Flagship Initiative Under the Europe 2020 Strategy, 2011. Communication from the Commission to the European Parliament, the Council, the European Economic and Social Committee and the Committee of the Regions, COM, Brussels, pp. 21.

European Space Agency. Available online: https://step.esa.int/main/third-party-plugins-2/sen2cor/ (accessed on 17 March 2021), n.d.

Evensen, G., 2003. The ensemble Kalman filter: Theoretical formulation and practical implementation. Ocean dynamics 53, 343–367.

Evensen, G., 1994. Sequential data assimilation with a nonlinear quasi-geostrophic model using Monte Carlo methods to forecast error statistics. Journal of Geophysical Research: Oceans 99, 10143–10162.

Ewen, J., Parkin, G., O'Connell, P.E., 2000. SHETRAN: distributed river basin flow and transport modeling system. Journal of hydrologic engineering 5, 250–258.

Fandiño, M., Cancela, J.J., Rey, B.J., Martínez, E.M., Rosa, R.G., Pereira, L.S., 2012. Using the dual-Kc approach to model evapotranspiration of Albariño vineyards (Vitis vinifera L. cv. Albariño)

with consideration of active ground cover. Agricultural Water Management 112, 75–87. https://doi.org/10.1016/j.agwat.2012.06.008
FAO, I., n.d. ISRIC 2006. World Reference Base for Soil Resources. A Framework for International Classification, Correlation and Communication. World soil resources reports NO 103, 67–97.
FAO's Director-General on How to Feed the World in 2050, 2009. . Population and Development Review 35, 837–839. https://doi.org/10.1111/j.1728-4457.2009.00312.x
Farré, I., Faci, J.M., 2009. Deficit irrigation in maize for reducing agricultural water use in a Mediterranean environment. Agricultural Water Management 96, 383–394. https://doi.org/10.1016/j.agwat.2008.07.002
Fatichi, S., Vivoni, E.R., Ogden, F.L., Ivanov, V.Y., Mirus, B., Gochis, D., Downer, C.W., Camporese, M., Davison, J.H., Ebel, B., 2016. An overview of current applications, challenges, and future trends in distributed process-based models in hydrology. Journal of Hydrology 537, 45–60.
Feddes, R.A., 1982. Simulation of field water use and crop yield, in: Simulation of Plant Growth and Crop Production. Pudoc, pp. 194–209.
Feddes, R.A., Zaradny, H., 1978. Model for simulating soil-water content considering evapotranspiration — Comments. Journal of Hydrology 37, 393–397. https://doi.org/10.1016/0022-1694(78)90030-6
Fernández, J.E., Alcon, F., Diaz-Espejo, A., Hernandez-Santana, V., Cuevas, M.V., 2020. Water use indicators and economic analysis for on-farm irrigation decision: A case study of a super high density olive tree orchard. Agricultural water management 237, 106074.
Ficklin, D.L., Luedeling, E., Zhang, M., 2010. Sensitivity of groundwater recharge under irrigated agriculture to changes in climate, CO2 concentrations and canopy structure. Agricultural Water Management 97, 1039–1050. https://doi.org/10.1016/j.agwat.2010.02.009
Fraga, H., de Cortázar Atauri, I.G., Santos, J.A., 2018. Viticultural irrigation demands under climate change scenarios in Portugal. Agricultural water management 196, 66–74.
Fraga, H., García de Cortázar Atauri, I., Malheiro, A.C., Santos, J.A., 2016. Modelling climate change impacts on viticultural yield, phenology and stress conditions in Europe. Global change biology 22, 3774–3788.
Fragoso, R., Marques, C., Lucas, M.R., Martins, M. de B., Jorge, R., 2011. The economic effects of common agricultural policy on Mediterranean montado/dehesa ecosystem. Journal of Policy Modeling 33, 311–327.
Gan, Y., Siddique, K.H.M., Turner, N.C., Li, X.-G., Niu, J.-Y., Yang, C., Liu, L., Chai, Q., 2013. Ridge-Furrow Mulching Systems—An Innovative Technique for Boosting Crop Productivity in Semiarid Rain-Fed Environments. pp. 429–476. https://doi.org/10.1016/B978-0-12-405942-9.00007-4
Garrido, P., Elbakidze, M., Angelstam, P., Plieninger, T., Pulido, F., Moreno, G., 2017. Stakeholder perspectives of wood-pasture ecosystem services: A case study from Iberian dehesas. Land Use Policy 60, 324–333.
Goap, A., Sharma, D., Shukla, A.K., Krishna, C.R., 2018. An IoT based smart irrigation management system using Machine learning and open source technologies. Computers and electronics in agriculture 155, 41–49.
Gomes, M.P., Silva, A.A., 1962. Um novo diagrama triangular para a classificação básica da textura do solo. Garcia da Orta 10, 171–179.
Gonçalves, J.M., Muga, A.P., Horst, M.G., Pereira, L.S., 2011a. Furrow irrigation design with multicriteria analysis. Biosystems Engineering 109, 266–275.
Gonçalves, J.M., Muga, A.P., Pereira, L.S., 2011b. A Web-based decision support system for surface irrigation design. Efficient Decision Support Systems-Practice and Challenges in Multidisciplinary Domains 291–318.
Gonçalves, J.M.M., Muga, A.P., Pereira, L.S., 2009. A Web-based Decision Support System for Surface Irrigation Design. Sofware Development, in: 7th World Congress on Computers in Agriculture

Conference Proceedings, 22-24 June 2009, Reno, Nevada. American Society of Agricultural and Biological Engineers, p. 1.

González, M.G., Ramos, T.B., Carlesso, R., Paredes, P., Petry, M.T., Martins, J.D., Aires, N.P., Pereira, L.S., 2015. Modelling soil water dynamics of full and deficit drip irrigated maize cultivated under a rain shelter. Biosystems Engineering 132, 1–18. https://doi.org/10.1016/j.biosystemseng.2015.02.001

González-Dugo, M.P., Mateos, L., 2008. Spectral vegetation indices for benchmarking water productivity of irrigated cotton and sugarbeet crops. Agricultural water management 95, 48–58.

Graham, S.L., Kochendorfer, J., McMillan, A.M.S., Duncan, M.J., Srinivasan, M.S., Hertzog, G., 2016. Effects of agricultural management on measurements, prediction, and partitioning of evapotranspiration in irrigated grasslands. Agricultural Water Management 177, 340–347. https://doi.org/10.1016/j.agwat.2016.08.015

Gu, Z., Qi, Z., Burghate, R., Yuan, S., Jiao, X., Xu, J., 2020. Irrigation Scheduling Approaches and Applications: A Review. Journal of Irrigation and Drainage Engineering 146, 04020007–1~15. https://doi.org/10.1061/(ASCE)IR.1943-4774.0001464

Guerra, C.A., Pinto-Correia, T., 2016. Linking farm management and ecosystem service provision: Challenges and opportunities for soil erosion prevention in Mediterranean silvo-pastoral systems. Land Use Policy 51, 54–65.

Guzmán, S.M., Paz, J.O., Tagert, M.L.M., Mercer, A.E., Pote, J.W., 2018. An integrated SVR and crop model to estimate the impacts of irrigation on daily groundwater levels. Agricultural systems 159, 248–259.

Hajkowicz, S., Collins, K., 2007. A review of multiple criteria analysis for water resource planning and management. Water resources management 21, 1553–1566.

Han, M., Zhao, C., Šimůnek, J., Feng, G., 2015. Evaluating the impact of groundwater on cotton growth and root zone water balance using Hydrus-1D coupled with a crop growth model. Agricultural Water Management 160, 64–75. https://doi.org/10.1016/j.agwat.2015.06.028

Hanson, J.D., Rojas, K.W., Shaffer, M.J., 1999. Calibrating the root zone water quality model. Agronomy Journal 91, 171–177.

Harbaugh, A.W., Banta2, E.R., Hill3, M.C., Mcdonald4, M.G., n.d. MODFLOW-2000, THE U.S. GEOLOGICAL SURVEY MODULAR GROUND-WATER MODEL USER GUIDE TO MODULARIZATION CONCEPTS AND THE GROUND-WATER FLOW PROCESS, Geological Survey. CO 4 McDonald Morrissey Associates.

Hatfield, J.L., Boote, K.J., Kimball, B.A., Ziska, L.H., Izaurralde, R.C., Ort, D., Thomson, A.M., Wolfe, D., 2011. Climate impacts on agriculture: Implications for crop production. Agronomy Journal 103, 351–370. https://doi.org/10.2134/agronj2010.0303

Hornbuckle, J.W., Car, N.J., Christen, E.W., Stein, T.M., Williamson, B., 2009. IrriSatSMS. Irrigation water management by satellite and SMS-A utilisation framework.

Hou, L., Zhou, Y., Bao, H., Wenninger, J., 2017. Simulation of maize (Zea mays L.) water use with the HYDRUS-1D model in the semi-arid Hailiutu River catchment, Northwest China. Hydrological Sciences Journal 62, 93–103.

Huang, W.-C., Chen, C.-H., 2005. Using the ELECTRE II method to apply and analyze the differentiation theory, in: Proceedings of the Eastern Asia Society for Transportation Studies. Citeseer, pp. 2237–2249.

Hussain, M.Z., Otieno, D.O., Mirzae, H., Li, Y.L., Schmidt, M.W.T., Siebicke, L., Foken, T., Ribeiro, N.A., Pereira, J.S., Tenhunen, J.D., 2009. CO2 exchange and biomass development of the herbaceous vegetation in the Portuguese montado ecosystem during spring. Agriculture, ecosystems & environment 132, 143–152.

Huxman, T.E., Wilcox, B.P., Breshears, D.D., Scott, R.L., Snyder, K.A., Small, E.E., Hultine, K., Pockman, W.T., Jackson, R.B., 2005. ECOHYDROLOGICAL IMPLICATIONS OF WOODY PLANT ENCROACHMENT. Ecology 86, 308–319. https://doi.org/10.1890/03-0583

Ines, A.V., Das, N.N., Hansen, J.W., Njoku, E.G., 2013. Assimilation of remotely sensed soil moisture and vegetation with a crop simulation model for maize yield prediction. Remote Sensing of Environment 138, 149–164.

Inthavong, T., Tsubo, M., Fukai, dan S., 2011. A water balance model for characterization of length of growing period and water stress development for rainfed lowland rice. Field crops research 121, 291–301.

IPCC, A., 2013. Climate change 2013: the physical science basis. Contribution of working group I to the fifth assessment report of the intergovernmental panel on climate change 1535.

Ishizaka, A., Nemery, P., 2013. Multi-criteria decision analysis: methods and software. John Wiley & Sons.

IUSS Working Group WRB, 2014. World Reference Base for Soil Resources 2014. International Soil Classification System for Naming Soils and Creating Legends for Soil Maps. World Soil Resources Reports No. 106.

Jacques, D., Šimůnek, J., Timmerman, A., Feyen, J., 2002. Calibration of Richards' and convection–dispersion equations to field-scale water flow and solute transport under rainfall conditions. Journal of Hydrology 259, 15–31. https://doi.org/10.1016/S0022-1694(01)00591-1

Jiang, Y., Xu, X., Huang, Q., Huo, Z., Huang, G., 2015. Assessment of irrigation performance and water productivity in irrigated areas of the middle Heihe River basin using a distributed agro-hydrological model. Agricultural water management 147, 67–81.

Jin, X., Kumar, L., Li, Z., Feng, H., Xu, X., Yang, G., Wang, J., 2018. A review of data assimilation of remote sensing and crop models. European Journal of Agronomy 92, 141–152.

Johnson, L.F., Trout, T.J., 2012. Satellite NDVI assisted monitoring of vegetable crop evapotranspiration in California's San Joaquin Valley. Remote Sensing 4, 439–455.

Jongen, M., Lecomte, X., Unger, S., Pintó-Marijuan, M., Pereira, J.S., 2013a. The impact of changes in the timing of precipitation on the herbaceous understorey of Mediterranean evergreen oak woodlands. Agricultural and Forest Meteorology 171, 163–173.

Jongen, M., Pereira, J.S., Aires, L.M.I., Pio, C.A., 2011. The effects of drought and timing of precipitation on the inter-annual variation in ecosystem-atmosphere exchange in a Mediterranean grassland. Agricultural and Forest Meteorology 151, 595–606.

Jongen, M., Unger, S., Fangueiro, D., Cerasoli, S., Silva, J.M., Pereira, J.S., 2013b. Resilience of montado understorey to experimental precipitation variability fails under severe natural drought. Agriculture, ecosystems & environment 178, 18–30.

Keen, P.G., Scott Morton, M.S., 1978. Decision support systems: an organizational perspective. (No Title).

Keller, J., Bliesner, R.D., 1990. Sprinkle and trickle irrigation. Springer.

Kovats, R.S., 2014. Europe. In: Climate Change 2014: Impacts, Adaptation, and Vulnerability. Part B: Regional Aspects. Contribution of Working Group II to the Fifth Assessment Report of the Intergovernmental Panel on Climate Change.

Kröbel, R., Sun, Q., Ingwersen, J., Chen, X., Zhang, F., Müller, T., Römheld, V., 2010. Modelling water dynamics with DNDC and DAISY in a soil of the North China Plain: A comparative study. Environmental Modelling & Software 25, 583–601. https://doi.org/10.1016/J.ENVSOFT.2009.09.003

Kroes, J.G., Van Dam, J.C., 2003. Reference manual SWAP version 3.03. Alterra Rep. 773. Alterra, Wageningen, the Netherlands.

Kurc, S.A., Small, E.E., 2007. Soil moisture variations and ecosystem-scale fluxes of water and carbon in semiarid grassland and shrubland. Water Resources Research 43. https://doi.org/10.1029/2006WR005011

Legates, D.R., McCabe, G.J., 1999. Evaluating the use of "goodness-of-fit" Measures in hydrologic and hydroclimatic model validation. Water Resources Research 35, 233–241. https://doi.org/10.1029/1998WR900018

Li, H., Li, J., Shen, Y., Zhang, X., Lei, Y., 2018. Web-based irrigation decision support system with limited inputs for farmers. Agricultural Water Management 210, 279–285.
Li, Y., Zhou, Q., Zhou, J., Zhang, G., Chen, C., Wang, J., 2014. Assimilating remote sensing information into a coupled hydrology-crop growth model to estimate regional maize yield in arid regions. Ecological modelling 291, 15–27.
Linker, R., Ioslovich, I., 2017. Assimilation of canopy cover and biomass measurements in the crop model AquaCrop. Biosystems engineering 162, 57–66.
Linker, R., Ioslovich, I., Sylaios, G., Plauborg, F., Battilani, A., 2016. Optimal model-based deficit irrigation scheduling using AquaCrop: A simulation study with cotton, potato and tomato. Agricultural Water Management 163, 236–243. https://doi.org/10.1016/J.AGWAT.2015.09.011
Linker, R., Sylaios, G., Tsakmakis, I., Ramos, T., Simionesei, L., Plauborg, F., Battilani, A., 2018. Sub-optimal model-based deficit irrigation scheduling with realistic weather forecasts. Irrigation Science 36. https://doi.org/10.1007/s00271-018-0592-x
Linkov, I., Satterstrom, F.K., Kiker, G., Batchelor, C., Bridges, T., Ferguson, E., 2006. From comparative risk assessment to multi-criteria decision analysis and adaptive management: Recent developments and applications. Environment international 32, 1072–1093.
Liu, Y., Pereira, L.S., Fernando, R.M., 2006. Fluxes through the bottom boundary of the root zone in silty soils: Parametric approaches to estimate groundwater contribution and percolation. Agricultural Water Management 84, 27–40.
Loucks, D.P., van Beek, E., Stedinger, J.R., Dijkman, J.P.M., Villars, M.T., 2005. Water Resources Systems Planning and Management: An Introduction to Methods, Models and Applications. UNESCO.
Ma, S., Lardy, R., Graux, A.I., Touhami, H.B., Klumpp, K., Martin, R., Bellocchi, G., 2015. Regional-scale analysis of carbon and water cycles on managed grassland systems. Environmental Modelling & Software 72, 356–371. https://doi.org/10.1016/J.ENVSOFT.2015.03.007
Mannini, P., Genovesi, R., Letterio, T., 2013. IRRINET: Large Scale DSS Application for On-farm Irrigation Scheduling. Procedia Environmental Sciences 19, 823–829. https://doi.org/10.1016/j.proenv.2013.06.091
Miao, Q., Shi, H., Gonçalves, J.M., Pereira, L.S., 2018. Basin irrigation design with multi-criteria analysis focusing on water saving and economic returns: Application to wheat in Hetao, Yellow River Basin. Water 10, 67.
Monsi, M., 1953. Uber den Lichtfaktor in den Pflanzengesellschaften und seine Bedeutung fur die Stoffproduktion. Jap. J. Bot. 14, 22–52.
Moriasi, D.N., Arnold, J.G., Van Liew, M.W., Bingner, R.L., Harmel, R.D., Veith, T.L., 2007. Model evaluation guidelines for systematic quantification of accuracy in watershed simulations. Transactions of the ASABE 50, 885–900.
Mualem, Y., 1976. A new model for predicting the hydraulic conductivity of unsaturated porous media. Water Resources Research 12, 513–522. https://doi.org/10.1029/WR012i003p00513
Mulla, D.J., 2013. Twenty five years of remote sensing in precision agriculture: Key advances and remaining knowledge gaps. Biosystems engineering 114, 358–371.
Nash, J.E., Sutcliffe, J.V., 1970. River flow forecasting through conceptual models part I — A discussion of principles. Journal of Hydrology 10, 282–290. https://doi.org/10.1016/0022-1694(70)90255-6
Navarro-Hellín, H., Martinez-del-Rincon, J., Domingo-Miguel, R., Soto-Valles, F., Torres-Sánchez, R., 2016. A decision support system for managing irrigation in agriculture. Computers and Electronics in Agriculture 124, 121–131.
Nawandar, N.K., Satpute, V.R., 2019. IoT based low cost and intelligent module for smart irrigation system. Computers and electronics in agriculture 162, 979–990.
Nearing, G.S., Crow, W.T., Thorp, K.R., Moran, M.S., Reichle, R.H., Gupta, H.V., 2012. Assimilating remote sensing observations of leaf area index and soil moisture for wheat yield estimates: An observing system simulation experiment. Water Resources Research 48.
Neitsch, S.L., Arnold, J.G., Kiniry, J.R., Williams, J.R., 2011. Soil and water assessment tool theoretical documentation version 2009. Texas Water Resources Institute.

Nelson, D. a, Sommers, L., 1983. Total carbon, organic carbon, and organic matter. Methods of soil analysis: Part 2 chemical and microbiological properties 9, 539–579.

Orlando, F., Movedi, E., Coduto, D., Parisi, S., Brancadoro, L., Pagani, V., Guarneri, T., Confalonieri, R., 2016. Estimating leaf area index (LAI) in vineyards using the PocketLAI smart-app. Sensors 16, 2004.

Pachepsky, Y., Rawls, W.J., 2004. Development of pedotransfer functions in soil hydrology. Elsevier.

Paço, T.A., Pôças, I., Cunha, M., Silvestre, J.C., Santos, F.L., Paredes, P., Pereira, L.S., 2014. Evapotranspiration and crop coefficients for a super intensive olive orchard. An application of SIMDualKc and METRIC models using ground and satellite observations. Journal of Hydrology 519, 2067–2080.

Paredes, P., de Melo-Abreu, J.P., Alves, I., Pereira, L.S., 2014a. Assessing the performance of the FAO AquaCrop model to estimate maize yields and water use under full and deficit irrigation with focus on model parameterization. Agricultural Water Management 144, 81–97. https://doi.org/10.1016/J.AGWAT.2014.06.002

Paredes, P., Rodrigues, G.C., Alves, I., Pereira, L.S., 2014b. Corrigendum to "Partitioning evapotranspiration, yield prediction and economic returns of maize under various irrigation management strategies" [Agric. Water Manage. 135 (2014) 27–39]. Agricultural Water Management 141, 84. https://doi.org/10.1016/J.AGWAT.2014.04.001

Paredes, P., Rodrigues, G.C., Alves, I., Pereira, L.S., 2014c. Partitioning evapotranspiration, yield prediction and economic returns of maize under various irrigation management strategies. Agricultural water management 135, 27–39.

Paredes, P., Rodrigues, G.J., Petry, M.T., Severo, P.O., Carlesso, R., Santos Pereira, L., 2018. Evapotranspiration partition and crop coefficients of Tifton 85 bermudagrass as affected by the frequency of cuttings. Application of the FAO56 dual Kc model. Water 10, 558.

Pedras, C.M., Pereira, L.S., 2009. Multicriteria analysis for design of microirrigation systems. Application and sensitivity analysis. agricultural water management 96, 702–710.

Perego, A., Giussani, A., Sanna, M., Fumagalli, M., Carozzi, M., Alfieri, L., Brenna, S., Acutis, M., 2013. The ARMOSA simulation crop model: overall features, calibration and validation results. Italian Journal of Agrometeorology 3, 23–38.

Pereira, L.S., Allen, R.G., Smith, M., Raes, D., 2015. Crop evapotranspiration estimation with FAO56: Past and future. Agricultural Water Management 147, 4–20.

Pereira, L.S., Cordery, I., Iacovides, I., 2012. Improved indicators of water use performance and productivity for sustainable water conservation and saving. Agricultural Water Management 108, 39–51. https://doi.org/10.1016/J.AGWAT.2011.08.022

Pereira, L.S., Cordery, I., Iacovides, I., 2009. Coping with water scarcity: Addressing the challenges. Springer Science & Business Media.

Pereira, L.S., Oweis, T., Zairi, A., 2002. Irrigation management under water scarcity. Agricultural water management 57, 175–206.

Pereira, L.S., Paredes, P., Jovanovic, N., 2020. Soil water balance models for determining crop water and irrigation requirements and irrigation scheduling focusing on the FAO56 method and the dual Kc approach. Agricultural water management 241, 106357.

Phogat, V., Skewes, M.A., Cox, J.W., Sanderson, G., Alam, J., Šimůnek, J., 2014. Seasonal simulation of water, salinity and nitrate dynamics under drip irrigated mandarin (Citrus reticulata) and assessing management options for drainage and nitrate leaching. Journal of Hydrology 513, 504–516. https://doi.org/10.1016/J.JHYDROL.2014.04.008

Phogat, V., Skewes, M.A., McCarthy, M.G., Cox, J.W., Šimůnek, J., Petrie, P.R., 2017. Evaluation of crop coefficients, water productivity, and water balance components for wine grapes irrigated at different deficit levels by a sub-surface drip. Agricultural Water Management 180, 22–34.

Pinto-Correia, T., Azeda, C., 2017. Public policies creating tensions in Montado management models: Insights from farmers' representations. Land Use Policy 64, 76–82.

Pinto-Correia, T., Mascarenhas, J., 1999. Contribution to the extensification/intensification debate: new trends in the Portuguese montado. Landscape and Urban Planning 46, 125–131.

Pinto-Correia, T., Ribeiro, N., Sá-Sousa, P., 2011. Introducing the montado, the cork and holm oak agroforestry system of Southern Portugal. Agroforestry Systems 82, 99–104.

Pôças, I., Calera, A., Campos, I., Cunha, M., 2020. Remote sensing for estimating and mapping single and basal crop coefficientes: A review on spectral vegetation indices approaches. Agricultural Water Management 233, 106081.

Pôças, I., Paço, T.A., Paredes, P., Cunha, M., Pereira, L.S., 2015. Estimation of actual crop coefficients using remotely sensed vegetation indices and soil water balance modelled data. Remote Sensing 7, 2373–2400.

Pomerol, J.-C., Barba-Romero, S., 2000. Multicriterion decision in management: principles and practice. Springer Science & Business Media.

Portaria n.502015, n.d.

Portaria n.542023, n.d.

Purser, R.J., Leslie, L.M., 1988. A Semi-Implicit, Semi-Lagrangian Finite-Difference Scheme Using Hligh-Order Spatial Differencing on a Nonstaggered Grid. Monthly Weather Review 116, 2069–2080. https://doi.org/10.1175/1520-0493(1988)116<2069:ASISLF>2.0.CO;2

Raes, D., 2002. BUDGET: a soil water and salt balance model. Reference manual, version 5.

Raes, D., Steduto, P., Hsiao, T.C., Fereres, E., 2009. AquaCrop—The FAO Crop Model to Simulate Yield Response to Water: II. Main Algorithms and Software Description. Agronomy Journal 101, 438–447. https://doi.org/10.2134/agronj2008.0140s

Raij, I., Šimůnek, J., Ben-Gal, A., Lazarovitch, N., 2016. Water flow and multicomponent solute transport in drip-irrigated lysimeters. Water Resources Research 52, 6557–6574. https://doi.org/10.1002/2016WR018930

Rallo, G., Paço, T.A., Paredes, P., Puig-Sirera, À., Massai, R., Provenzano, G., Pereira, L.S., 2021. Updated single and dual crop coefficients for tree and vine fruit crops. Agricultural Water Management 250, 106645.

Ramos, T.B., Castanheira, N., Oliveira, A.R., Paz, A.M., Darouich, H., Simionesei, L., Farzamian, M., Gonçalves, M.C., 2020. Soil salinity assessment using vegetation indices derived from Sentinel-2 multispectral data. application to Lezíria Grande, Portugal. Agricultural Water Management 241. https://doi.org/10.1016/j.agwat.2020.106387

Ramos, T.B., Gonçalves, M.C., Brito, D., Martins, J.C., Pereira, L.S., 2013. Development of class pedotransfer functions for integrating water retention properties into Portuguese soil maps. Soil Research 51, 262. https://doi.org/10.1071/SR12347

Ramos, T.B., Horta, A., Gonçalves, M.C., Martins, J.C., Pereira, L.S., 2014. Development of ternary diagrams for estimating water retention properties using geostatistical approaches. Geoderma 230, 229–242.

Ramos, T.B., Simionesei, L., Jauch, E., Almeida, C., Neves, R., 2017. Modelling soil water and maize growth dynamics influenced by shallow groundwater conditions in the Sorraia Valley region, Portugal. Agricultural Water Management 185. https://doi.org/10.1016/j.agwat.2017.02.007

Ramos, T.B., Simionesei, L., Oliveira, A.R., Darouich, H., Neves, R., 2018. Assessing the impact of LAI data assimilation on simulations of the soil water balance and maize development using MOHID-Land. Water (Switzerland) 10. https://doi.org/10.3390/w10101367

Ramos, T.B., Simionesei, L., Oliveira, A.R., Neves, R., Darouich, H., 2021. Exploring the use of vegetation indices for validating crop transpiration fluxes computed with the MOHID-land model. Application to vineyard. Agronomy 11. https://doi.org/10.3390/agronomy11061228

Ramos, T.B., Šimůnek, J., Gonçalves, M.C., Martins, J.C., Prazeres, A., Castanheira, N.L., Pereira, L.S., 2011. Field evaluation of a multicomponent solute transport model in soils irrigated with saline waters. Journal of Hydrology 407, 129–144. https://doi.org/10.1016/J.JHYDROL.2011.07.016

Ramos, T.B., Šimůnek, J., Gonçalves, M.C., Martins, J.C., Prazeres, A., Pereira, L.S., 2012. Two-dimensional modeling of water and nitrogen fate from sweet sorghum irrigated with fresh and

blended saline waters. Agricultural Water Management 111, 87–104. https://doi.org/10.1016/J.AGWAT.2012.05.007

Ren, D., Xu, X., Hao, Y., Huang, G., 2016. Modeling and assessing field irrigation water use in a canal system of Hetao, upper Yellow River basin: Application to maize, sunflower and watermelon. Journal of Hydrology 532, 122–139. https://doi.org/10.1016/J.JHYDROL.2015.11.040

Richter, R., Schläpfer, D., n.d. Atmospheric/Topographic Correction for Satellite Imagery (ATCOR-2/3, Version 9.1. 1, February 2017) Theoretical Background Document.

Rinaldi, M., He, Z., 2014. Decision support systems to manage irrigation in agriculture. Advances in agronomy 123, 229–279.

Ritchie, J.T., 1972. Model for predicting evaporation from a row crop with incomplete cover. Water Resources Research 8, 1204–1213. https://doi.org/10.1029/WR008i005p01204

Romano, N., Hopmans, J.W., Dane, J.H., 2002. 3.3. 2.6 Suction table. Methods of soil analysis. Part 4, 692–698.

Rosa, R.D., Paredes, P., Rodrigues, G.C., Alves, I., Fernando, R.M., Pereira, L.S., Allen, R.G., 2012. Implementing the dual crop coefficient approach in interactive software. 1. Background and computational strategy. Agricultural Water Management 103, 8–24. https://doi.org/10.1016/J.AGWAT.2011.10.013

Rosa, R.D., Ramos, T.B., Pereira, L.S., 2016. The dual Kc approach to assess maize and sweet sorghum transpiration and soil evaporation under saline conditions: Application of the SIMDualKc model. Agricultural Water Management 177, 77–94. https://doi.org/10.1016/J.AGWAT.2016.06.028

Rouse, J.W., Haas, R.H., Schell, J.A., Deering, D.W., 1974. Monitoring vegetation systems in the Great Plains with ERTS. NASA Spec. Publ 351, 309.

Roy, B., Vincke, P., 1981. Multicriteria analysis: survey and new directions. European journal of operational research 8, 207–218.

Saaty, T.L., 1977. A scaling method for priorities in hierarchical structures. Journal of mathematical psychology 15, 234–281.

Salmon, J.M., Friedl, M.A., Frolking, S., Wisser, D., Douglas, E.M., 2015. Global rain-fed, irrigated, and paddy croplands: A new high resolution map derived from remote sensing, crop inventories and climate data. International Journal of Applied Earth Observation and Geoinformation 38, 321–334. https://doi.org/10.1016/j.jag.2015.01.014

Sándor, R., Barcza, Z., Acutis, M., Doro, L., Hidy, D., Köchy, M., Minet, J., Lellei-Kovács, E., Ma, S., Perego, A., Rolinski, S., Ruget, F., Sanna, M., Seddaiu, G., Wu, L., Bellocchi, G., 2017. Multi-model simulation of soil temperature, soil water content and biomass in Euro-Mediterranean grasslands: Uncertainties and ensemble performance. European Journal of Agronomy 88, 22–40. https://doi.org/10.1016/j.eja.2016.06.006

Sandor, R., Barcza, Z., Hidy, D., Lellei-Kovács, E., Ma, S., Bellocchi, G., 2016. Modelling of grassland fluxes in Europe: evaluation of two biogeochemical models. Agriculture, Ecosystems & Environment 215, 1–19.

Santos, J.A., Fraga, H., Malheiro, A.C., Moutinho-Pereira, J., Dinis, L.-T., Correia, C., Moriondo, M., Leolini, L., Dibari, C., Costafreda-Aumedes, S., 2020. A review of the potential climate change impacts and adaptation options for European viticulture. Applied Sciences 10, 3092.

Santos, R., Clemente, P., Brouwer, R., Antunes, P., Pinto, R., 2015. Landowner preferences for agri-environmental agreements to conserve the montado ecosystem in Portugal. Ecological Economics 118, 159–167.

Schaap, M.G., Leij, F.J., 2000. Improved Prediction of Unsaturated Hydraulic Conductivity with the Mualem-van Genuchten Model. Soil Science Society of America Journal 64, 843–851. https://doi.org/10.2136/sssaj2000.643843x

Simionesei, L., Oliveira, A., Ramos, T., Neves, R., 2019a. Modelação da rega deficitária em vinha com o MOHID-Land.

Simionesei, L., Ramos, T.B., Brito, D., Jauch, E., Leitão, P.C., Almeida, C., Neves, R., 2016. Numerical Simulation of Soil Water Dynamics Under Stationary Sprinkler Irrigation With Mohid-Land. Irrigation and Drainage 65. https://doi.org/10.1002/ird.1944

Simionesei, L., Ramos, T.B., Oliveira, A.R., Jongen, M., Darouich, H., Weber, K., Proença, V., Domingos, T., Neves, R., 2018. Modeling soilwater dynamics and pasture growth in the montado ecosystem using MOHID land. Water (Switzerland) 10. https://doi.org/10.3390/w10040489

Simionesei, L., Ramos, T.B., Palma, J., Oliveira, A.R., Neves, R., 2020. IrrigaSys: A web-based irrigation decision support system based on open source data and technology. Computers and Electronics in Agriculture 178. https://doi.org/10.1016/j.compag.2020.105822

Simionesei, L., Ramos, T.B., Palma, J., Oliveira, A.R., Neves, R., 2019b. O sistema IrrigaSys de apoio à gestão da rega no Vale do Sorraia.

Simpson, L., 1996. Do decision makers know what they prefer?: MAVT and ELECTRE II. Journal of the Operational Research Society 47, 919–929.

Šimůnek, J., Angulo-Jaramillo, R., Schaap, M.G., Vandervaere, J.-P., van Genuchten, M.Th., 1998. Using an inverse method to estimate the hydraulic properties of crusted soils from tension-disc infiltrometer data. Geoderma 86, 61–81. https://doi.org/10.1016/S0016-7061(98)00035-4

Šimůnek, J., Genuchten, M.Th., Šejna, M., 2016. Recent Developments and Applications of the HYDRUS Computer Software Packages. Vadose Zone Journal 15, 1–25. https://doi.org/10.2136/vzj2016.04.0033

Šimůnek, J., Hopmans, J.W., 2009. Modeling compensated root water and nutrient uptake. Ecological Modelling 220, 505–521. https://doi.org/10.1016/j.ecolmodel.2008.11.004

Skaggs, T.H., van Genuchten, M.T., Shouse, P.J., Poss, J.A., 2006. Macroscopic approaches to root water uptake as a function of water and salinity stress. Agricultural Water Management 86, 140–149. https://doi.org/10.1016/J.AGWAT.2006.06.005

Smith, M., 1989. Manual for Cropwat: A Computer Program for IBM-PC Or Compatibles. AGLW, FAO, Rome.

Staff, S., 2011. Soil survey laboratory information manual. Soil survey investigations report No. 45, Version.

Steduto, P., Pocuca, V., Caliandro, A., Debaeke, P., 1995. An evaluation of the crop-growth simulation submodel of EPIC for wheat grown in a Mediterranean climate with variable soil-water regimes. European Journal of Agronomy 4, 335–345. https://doi.org/10.1016/S1161-0301(14)80034-8

Stockle, C.O., Williams, J.R., Rosenberg, N.J., Jones, C.A., 1992. A method for estimating the direct and climatic effects of rising atmospheric carbon dioxide on growth and yield of crops: Part I—Modification of the EPIC model for climate change analysis. Agricultural Systems 38, 225–238. https://doi.org/10.1016/0308-521X(92)90067-X

Stolte, J., 1997. Determination of the saturated hydraulic conductivity using the constant head method. Manual for soil physical measurements. Tech. Doc 37, 27–32.

Teixeira, J.L., Pereira, L.S., 1992. ISAREG, an irrigation scheduling model. ICID bulletin 41, 29–48.

Tenhunen, J.D., Serra, A.S., Harley, P.C., Dougherty, R.L., Reynolds, J.F., 1990. Factors influencing carbon fixation and water use by Mediterranean sclerophyll shrubs during summer drought. Oecologia 82, 381–393.

Testi, L., Villalobos, F.J., Orgaz, F., 2004. Evapotranspiration of a young irrigated olive orchard in southern Spain. Agricultural and Forest Meteorology 121, 1–18.

Thorp, K.R., Hunsaker, D.J., French, A.N., 2010. Assimilating leaf area index estimates from remote sensing into the simulations of a cropping systems model. Transactions of the ASABE 53, 251–262.

Todorovic, M., Lamaddalena, N., Jovanovic, N., Pereira, L.S., 2014. Agricultural water management: Priorities and challenges (Preface).

Todorovic, M., Riezzo, E.E., Buono, V., Zippitelli, M., Galiano, A., Cantore, V., 2016. Hydro-tech: An automated smart-tech decision support tool for eco-efficient irrigation management. Int. Agric. Eng. J 25, 44–45.

Trancoso, A.R., Braunschweig, F., Chambel Leitão, P., Obermann, M., Neves, R., 2009. An advanced modelling tool for simulating complex river systems. Science of The Total Environment 407, 3004–3016. https://doi.org/10.1016/J.SCITOTENV.2009.01.015

Tripathy, R., Chaudhari, K.N., Mukherjee, J., Ray, S.S., Patel, N.K., Panigrahy, S., Parihar, J.S., 2013. Forecasting wheat yield in Punjab state of India by combining crop simulation model WOFOST and remotely sensed inputs. Remote sensing letters 4, 19–28.

Trombetta, A., Iacobellis, V., Tarantino, E., Gentile, F., 2016. Calibration of the AquaCrop model for winter wheat using MODIS LAI images. Agricultural Water Management 164, 304–316.

Twarakavi, N.K.C., Šimůnek, J., Seo, S., 2008. Evaluating Interactions between Groundwater and Vadose Zone Using the HYDRUS-Based Flow Package for MODFLOW. Vadose Zone Journal 7, 757–768. https://doi.org/10.2136/vzj2007.0082

Valverde, P., Serralheiro, R., de Carvalho, M., Maia, R., Oliveira, B., Ramos, V., 2015. Climate change impacts on irrigated agriculture in the Guadiana river basin (Portugal). Agricultural Water Management 152, 17–30.

van der Molen, M.K., Dolman, A.J., Ciais, P., Eglin, T., Gobron, N., Law, B.E., Meir, P., Peters, W., Phillips, O.L., Reichstein, M., Chen, T., Dekker, S.C., Doubková, M., Friedl, M.A., Jung, M., van den Hurk, B.J.J.M., de Jeu, R.A.M., Kruijt, B., Ohta, T., Rebel, K.T., Plummer, S., Seneviratne, S.I., Sitch, S., Teuling, A.J., van der Werf, G.R., Wang, G., 2011. Drought and ecosystem carbon cycling. Agricultural and Forest Meteorology 151, 765–773. https://doi.org/10.1016/j.agrformet.2011.01.018

van Genuchten, M.T., 1980. A Closed-form Equation for Predicting the Hydraulic Conductivity of Unsaturated Soils. Soil Science Society of America Journal 44, 892–898. https://doi.org/10.2136/sssaj1980.03615995004400050002x

Van Genuchten, M. van, Leij, F.J., Yates, S.R., 1991. The RETC code for quantifying the hydraulic functions of unsaturated soils.

Van Looy, K., Bouma, J., Herbst, M., Koestel, J., Minasny, B., Mishra, U., Montzka, C., Nemes, A., Pachepsky, Y.A., Padarian, J., 2017. Pedotransfer functions in Earth system science: Challenges and perspectives. Reviews of Geophysics 55, 1199–1256.

Vanuytrecht, E., Raes, D., Steduto, P., Hsiao, T.C., Fereres, E., Heng, L.K., Garcia Vila, M., Mejias Moreno, P., 2014. AquaCrop: FAO's crop water productivity and yield response model. Environmental Modelling & Software 62, 351–360. https://doi.org/10.1016/J.ENVSOFT.2014.08.005

Vazifedoust, M., Van Dam, J.C., Bastiaanssen, W.G.M., Feddes, R.A., 2009. Assimilation of satellite data into agrohydrological models to improve crop yield forecasts. International Journal of Remote Sensing 30, 2523–2545.

Vazifedoust, M., Van Dam, J.C., Feddes, R.A., Feizi, M., 2008. Increasing water productivity of irrigated crops under limited water supply at field scale. Agricultural water management 95, 89–102.

Vetschera, R., 1986. Sensitivity analysis for the ELECTRE multicriteria method. Zeitschrift für Operations Research 30, B99–B117.

Villalobos, F.J., Orgaz, F., Testi, L., Fereres, E., 2000. Measurement and modeling of evapotranspiration of olive (Olea europaea L.) orchards. European Journal of Agronomy 13, 155–163.

Vincke, P., 1992. Multicriteria decision-aid. John Wiley & Sons.

Vories, E., Tacker, P., Hall, S., 2009. The Arkansas irrigation scheduler, in: World Environmental and Water Resources Congress 2009: Great Rivers. pp. 1–10.

Wang, J., Huang, G., Zhan, H., Mohanty, B.P., Zheng, J., Huang, Q., Xu, X., 2014. Evaluation of soil water dynamics and crop yield under furrow irrigation with a two-dimensional flow and crop growth coupled model. Agricultural Water Management 141, 10–22.

Wang, X., Huang, G., Yang, J., Huang, Q., Liu, H., Yu, L., 2015. An assessment of irrigation practices: Sprinkler irrigation of winter wheat in the North China Plain. Agricultural Water Management 159, 197–208. https://doi.org/10.1016/J.AGWAT.2015.06.011

Wang, X., Williams, J.R., Gassman, P.W., Baffaut, C., Izaurralde, R.C., Jeong, J., Kiniry, J.R., 2012. EPIC and APEX: Model use, calibration, and validation. Transactions of the ASABE 55, 1447–1462.

Water, U.N., 2020. Water and climate change. The United Nations World Water Development Report.

Wesseling, J.G., Elbers, J.A., Kabat, P., Van den Broek, B.J., 1991. SWATRE: Instructions for input. Internal Note, Winand Staring Centre, Wageningen, the Netherlands 1991.

White, M.A., Thornton, P.E., Running, S.W., Nemani, R.R., 2000. Parameterization and sensitivity analysis of the BIOME–BGC terrestrial ecosystem model: Net primary production controls. Earth interactions 4, 1–85.

Whytock, G., 2020. Water resources across Europe : confronting water stress: an updated assessment, EEA report;No 12/2021. European Environment Agency, Copenhagen.

Williams, J.R., Izaurralde, R.C., Steglich, E.M., 2008. Agricultural Policy/Environmental eXtender Model: Theoretical Documentation Version 0604; Texas AgriLIFE Research, Available online: http://epicapex.brc.tamus.edu (accessed on 15 January 2018).

Williams, J.R., Jones, C.A., Kiniry, J.R., Spanel, D.A., 1989. EPIC crop growth model. Transactions of the American Society of Agricultural Engineers 32, 497–511.

Wilson, T.G., Kustas, W.P., Alfieri, J.G., Anderson, M.C., Gao, F., Prueger, J.H., McKee, L.G., Alsina, M.M., Sanchez, L.A., Alstad, K.P., 2020. Relationships between soil water content, evapotranspiration, and irrigation measurements in a California drip-irrigated Pinot noir vineyard. Agricultural Water Management 237, 106186.

Wu, L., McGechan, M.B., McRoberts, N., Baddeley, J.A., Watson, C.A., 2007. SPACSYS: Integration of a 3D root architecture component to carbon, nitrogen and water cycling—Model description. Ecological Modelling 200, 343–359. https://doi.org/10.1016/J.ECOLMODEL.2006.08.010

Xu, X., Huang, G., Sun, C., Pereira, L.S., Ramos, T.B., Huang, Q., Hao, Y., 2013. Assessing the effects of water table depth on water use, soil salinity and wheat yield: Searching for a target depth for irrigated areas in the upper Yellow River basin. Agricultural Water Management 125, 46–60. https://doi.org/10.1016/j.agwat.2013.04.004

Xu, X., Huang, G., Zhan, H., Qu, Z., Huang, Q., 2012. Integration of SWAP and MODFLOW-2000 for modeling groundwater dynamics in shallow water table areas. Journal of Hydrology 412–413, 170–181. https://doi.org/10.1016/J.JHYDROL.2011.07.002

Xu, X., Sun, C., Qu, Z., Huang, Q., Ramos, T.B., Huang, G., 2015. Groundwater Recharge and Capillary Rise in Irrigated Areas of the Upper Yellow River Basin Assessed by an Agro-Hydrological Model. Irrigation and Drainage 64, 587–599. https://doi.org/10.1002/ird.1928

Yang, G., Liu, L., Guo, P., Li, M., 2017. A flexible decision support system for irrigation scheduling in an irrigation district in China. Agricultural water management 179, 378–389.

Yu, Q., Saseendran, S.A., Ma, L., Flerchinger, G.N., Green, T.R., Ahuja, L.R., 2006. Modeling a wheat–maize double cropping system in China using two plant growth modules in RZWQM. Agricultural Systems 89, 457–477. https://doi.org/10.1016/J.AGSY.2005.10.009

Yuping, M., Shili, W., Li, Z., Yingyu, H., Liwei, Z., Yanbo, H., Futang, W., 2008. Monitoring winter wheat growth in North China by combining a crop model and remote sensing data. International Journal of Applied Earth Observation and Geoinformation 10, 426–437.

Zhang, B., Feng, G., Ahuja, L.R., Kong, X., Ouyang, Y., Adeli, A., Jenkins, J.N., 2018. Soybean crop-water production functions in a humid region across years and soils determined with APEX model. Agricultural Water Management 204, 180–191.

Zhang, Y., Feng, L., 2010. CropIrri: A Decision Support System for Crop Irrigation Management, in: Li, D., Zhao, C. (Eds.), Computer and Computing Technologies in Agriculture III, IFIP Advances in Information and Communication Technology. Springer, Berlin, Heidelberg, pp. 90–97. https://doi.org/10.1007/978-3-642-12220-0_14